CVR JOURNAL OF SCIENCE & TECHNOLOGY

Vol.No. 14, June 2018 ISSN 2277-3916

CVR COLLEGE OF ENGINEERING

In Pursuit of Excellence

PATRONS

Dr. Raghava V. Cherabuddi, President & Chairman

Dr. K. Rama Sastri, Director

Dr. K.S. Nayanathara, Principal

Editor : **Dr. K. Lal Kishore, Professor and Dean- Research, CVRCE**

Associate Editor : **Dr. S. Venkateshwarlu, Professor & Head, Dept. of EEE**

Editorial Board :

Dr. K.V. Chalapati Rao	Professor Emeritus, Dept. of CSE, CVRCE
Dr.M.V. Seshagiri Rao	Professor & Dean-Planning & Coordination, CVRCE
Prof. L.C. Siva Reddy	Professor & Vice-Principal, CVRCE
Dr. Rameshwar Rao	Professor & Dean- Projects & Consultancy, CVRCE
Dr. N.V. Rao	Professor & Dean-Academics, CVRCE
Dr. T. Muralidhara Rao	Professor & Head, Dept. of Civil Engg., CVRCE
Dr. K. Venkateswara Rao	Professor & Head, Dept. of CSE, CVRCE
Dr.K. Lalithendra	Professor & Head, Dept. of ECE, CVRCE
Dr. M.S. Bhat	Professor & Head, Dept. of EIE, CVRCE
Dr. Bipin Bihari Jayasingh	Professor & Head, Dept. of IT, CVRCE
Dr. M. Venkata Ramana	Professor & Head, Dept. of Mech. Engg., CVRCE
Dr. G. Bikshamaiah	Professor & Head, Dept. of H&S, CVRCE

CVR JOURNAL OF SCIENCE & TECHNOLOGY

Indexed by

- Google Scholar
- Directory of Research Journals Indexing (DRJI)
- Scientific Indexing Services (SIS)
- International Institute of Organised Research (I2OR)
- Scholar Impact - Journal Index
- Citefactor

Ranked in the 101-150 band by NIRF (MHRD) for the II Consecutive Time

Accredited by NAAC with 'A' GRADE

CVR COLLEGE OF ENGINEERING

(UGC Autonomous - Affiliated to JNTU Hyderabad)
Mangalpalli (V), Ibrahimpatnam (M),
R.R. District, Telangana. – 501510
http://cvr.ac.in

EDITORIAL

It is with immense pride that we bring out the Volume – 14 of the Biannual journal of our college, CVR Journal of Science and Technology. This Volume is brought out in the first week of June 2018 itself, with the co-operation of all the contributors and the editorial team. We are thankful to the Management for supporting this activity, by encouraging us to publish the journal in colour print. This will enable to decipher the graphs, pictorial representations etc with more clarity. We are sure that researchers will appreciate this.

The first article in this issue is on prediction of multipath interference for static GNSS applications. Based on the data collected from SHAR, ISRD, this article is written. Another article on colour recognition device for visually impaired persons is also published. Another interesting article on estimating the % of degradation of rooftop solar PV plant is also presented. Other research articles on high blood pressure prediction using algorithms and modeling of potassium chloride sensor with two-dimensional optical nanostructure are also published. Based on six-sigma, a case study on investigating the cause of poor efficiency in thermal power plants is also presented. Breakup of number of research articles published, disciplines is given below, in the following lines.

We are very happy to share with our readers that CVR College of Engineering is **one among the TOP 3 institutions**, **in the State of Telangana**, as per the **NIRF MHRD rankings**. It is ranked in the **101-150 band** of rankings by the **NIRF,** consecutively for the II time. For a college which is about 17 years old, it is remarkable achievement. This made the management of the college to launch Mission 100, to be among the top 100 institutions in the country. Research activity plays an important role in this aspect. Hope the Journal and the contributors will help in improving the ranking of the institution. We are also happy to share with the readers that the college is **Accredited by NAAC with 'A' grade.** It is expected that the contributors will further enhance the reputation of the college through this Journal.

We have received good number of research papers for review, from our own faculty and from outside our institution also. A rigorous filtration process is done, anti plagiarism check using software, and review by experts are done. Finally, research papers were selected for publication in the present volume.

This volume covers research articles in the branches of engineering, Humanities and Social Sciences. The breakup of the papers among the various branches is:

ECE – 5, EEE – 4, EIE – 1, CSE– 2, IT - 2, MECH- 5, CIVIL-1, H & S-2.

The management is supporting the research and Ph.D Programmes by liberally sanctioning study leave for the faculty of this college. Faculty members working for Ph.D and on research projects are expected to contribute for the journal. Management is also encouraging the authors of research papers with incentives, based on merit. Some of the research articles accepted for publication in the forth coming Volume 15 are listed in Page No. 117.

I am thankful to all the members of the Editorial Board for their help in reviewing and short listing the research papers for inclusion in the current Volume of the journal. I wish to thank **Dr.S.Venkateshwarlu, HOD, EEE and Associate Editor**, for the effort made in bringing out this Volume. Thanks are due to **HOD, H & S, Dr. G. Bhikshamaiah** and the staff of English Department for reviewing the papers to see that grammatical and typographical errors are corrected. I am also thankful to **Smt. A. Sreedevi**, **DTP Operator** in the Office of Dean Research for the effort put in the preparation of the papers in Camera Ready form.

For further clarity on waveforms, graphs, circuit diagrams and figures, readers are requested to browse the soft copy of the journal, available on the college website **www.cvr.ac.in**, wherein a link is provided.

Prof. K. Lal Kishore
Editor

CONTENTS

Page No

Prediction of Multipath Interference for Static GNSS Applications

Yedukondalu Kamatham
Professor, CVR College Engineering/ECE Department, Hyderabad, India
Email: kyedukondalu@gmail.com

Abstract: **Positional accuracy of Global Navigation Satellite System (GNSS) is limited by several error sources like troposphere, ionosphere, instrumental bias, clock, multipath etc. Among these error sources, multipath is quite significant, since it should be dynamically modeled with respect to user GNSS receiver environment. In this paper, multipath error is estimated based on both code and carrier phase measurements using CMC (code minus carrier) technique. It is quantified with experimental static dual frequency Global Positioning System (GPS) receiver data. The time series of multipath data is analyzed with other satellite parameters like elevation and azimuth angles of satellite vehicle (SV). Multipath error is estimated for all SVs and is analyzed for sequential days to predict the multipath error of any SV during the forthcoming days. The results are very much encouraging and significant in prediction of multipath error for GPS/GNSS static applications such as atmospheric research using GNSS satellites data and during site selection phase for installing base stations for continuous monitoring of satellites' data.**

Index Terms: **GNSS; GPS; Multipath Error; Code minus Carrier technique; Multipath Repeatability**

I. Introduction

Multipath is a phenomenon in which, a signal arrives at a receiving antenna via various directions after signal reflection and/ or diffraction interfering with the direct signal. In the receiver, multipath is analyzed relative to the direct signal by various parameters such as: (1) The amplitude of the reflected or indirect signal, (2) Path delay, (3) Amount of phase from the reflected signal and (4) Phase rate [1]. Various methods were proposed to reduce multipath effects such as hardware, software (data processing) and hybrid approaches. Multipath can be estimated by the code and carrier phase differences between L1 and L2 observations [2]. The Global Navigation Satellite System (GNSS) measurements are biased due to several error sources such as ionospheric and tropospheric errors, satellite and receiver clock errors, ephemeris errors, receiver noise etc. In addition to these, the range estimation experiences a problem of multipath leading to inaccurate estimation of user position in navigation applications. Initially the fundamental analysis of GPS code and carrier multipath was reported by Hagerman (1973) [3]. Multipath is very difficult to model due to its user receiver-satellite geometry dependence and its non-correlation even in very close distances. Consequently, it has received great attention in the literature [4-6]. Better understanding of the multipath environment with respect to the elevation of satellite and distance to reflecting objects, is very important for predicting the multipath error for Global Positioning System (GPS) or GNSS static applications such as atmospheric research and also during the site selection phase in installing base stations for either Differential GPS (DGPS) or Local Area Augmentation Systems (LASS). Here, experimental estimation of multipath and its analysis for static applications is presented.

II. Multipath Error Estimation

Direct and indirect signals received at the GPS receiver have phase differences and relative phase offsets, which are proportional to their differences in path lengths. Multipath error can be estimated by using a combination of carrier phase and code measurements. Extensive work on multipath estimation was reported in literature based on carrier phase and code measurements [7].

MP_{L1} and MP_{L2} can be quantified and detected using a dual frequency receiver and is given as [8]:

$$MP_{L1} \cong \rho_{L1} - \frac{9529}{2329}.\phi_{L1} + \frac{7200}{2329}.\phi_{L2} + K_1 \qquad (1)$$

$$MP_{L2} \cong \rho_{L2} - \frac{11858}{2329}.\phi_{L1} + \frac{9529}{2329}.\phi_{L2} + K_2 \qquad (2)$$

Where ρ_{L1} and ρ_{L2} are pseudo ranges (in meters) on L1 and L2; Φ_{L1} and Φ_{L2} are carrier phase measurement (in meters). Using Eqs. (1) and (2), the multipath error on L_1 and L_2 in meters can be estimated for all epochs of dual frequency GPS data. K_1 and K_2 are functions of unknown integer ambiguities which can be assumed constant [9].

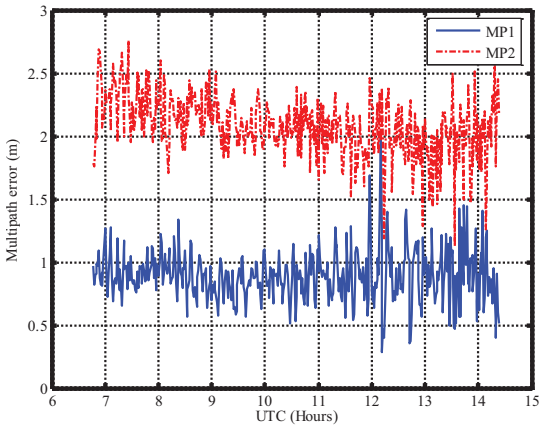

Figure 1. Multipath error on L_1 (MP_1) and L2 (MP_2) carrier frequencies

Various experiments were conducted at NERTU (Research & Training Unit for Navigational Electronics),

Osmania University (OU), Hyderabad, India, to analyze the effects of multipath for various static stations. For analysis, dual frequency GPS data was recorded on 8th August 2010 at 60 s intervals. The estimated multipath error for Satellite Vehicle 17 (SV 17) on L_1 (MP_1) and L_2 (MP_2) frequencies is shown in Fig. 1. The mean multipath error on L_1 and L_2 are 0.79 m and 2.01 m respectively. L_1 signal consists of C/A code and P-code with minimum received power of -160 dBW and -163 dBW respectively. But, L_2 signal consists of either C/A code or P-code (-166 dBW). i.e., L_1 signal's power is 3 dB more than L_2 [10]. Hence the error on L_2 is more than on L_1.

III. Analysis of Multipath Error

For any static GNSS base station, the multipath pattern of any SV is highly repeated with a constant phase shift during the successive days. When the SV is in the same position during each orbital pass, the multipath error is same. GPS satellites are semi synchronous, with a period of one half of a sidereal day. Ground track geometry of each SV at a reference station repeats with a fixed time shift of 236 s every day. This time shift is due to the difference between mean sun day and sidereal day [11]. Fig. 2 shows that the multipath error pattern (both on L_1 and L_2) is repeated for two successive days i.e., on 8th and 9th March, 2010 for SV 8.

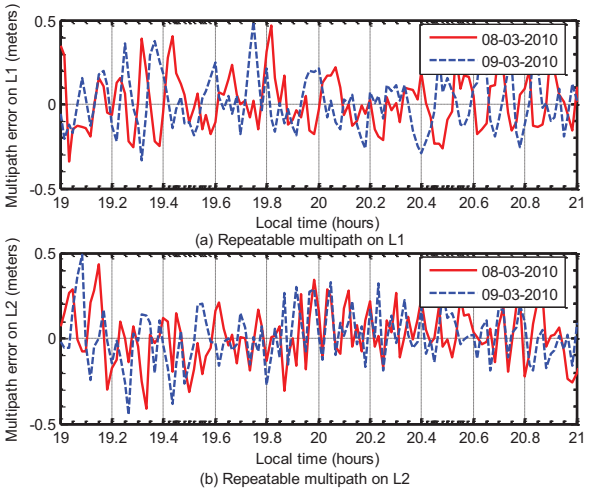

Figure 2. Repeatability of multipath pattern on L_1 and L_2 for SV8

Multipath is due to reflection of signals from physical surface. The multipath effects can be correlated with satellite elevation angle. Most of the obstructions produce reflected and / or diffracted signals with low elevations. Therefore, both real-time kinematic and static GNSS applications, multipath error is more at lower elevations, which is shown in Fig. 3.

IV. Analysis of Multipath Error using TEQC

GPS data are recorded and stored as binary digits (bits) in the receiver (i.e., raw data). It is downloaded and converted to ASCII (American Standard Code for Information Interchange) for exchange and archive. This conversion and other processing can be done by non-interactive TEQC software developed by UNAVCO (University Navstar Consortium), Colorado Springs. TEQC software can be used to Translate, Edit and Quality check (TEQC) of GPS raw data. It can take any of the Receiver Independent Exchange (RINEX) files such as Observation, Navigation and Meteorological files as input and can process them. It can handle RINEX version 1.0 and 2.0 files.

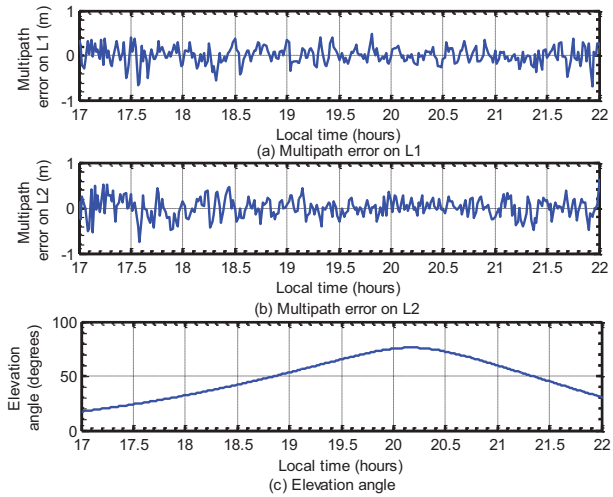

Figure 3. Multipath error dependency on elevation angle (SV 8)

For many common GPS native receiver formats, the TEQC, a freeware program allows the user to translate from the binary receiver format to the standard RINEX format and to quality-check the data before post processing. The TEQC software is widely used by many universities and agencies around the globe for generating RINEX files from GPS data collected during survey or by continuously operating stations [12], [13]. For Quality check of GPS data, a set of RINEX observation and navigation files are used namely "080310.10O", "08030660.10N" of dated 8 March 2010, which is acquired from a dual frequency GPS receiver (Model: Novatel DL 4 *plus*) located at NERTU, OU, Hyderabad. The navigation and observation files obtained from the receiver are quality checked with TEQC software using *qc lite* mode and *qc full* mode commands and further processed as shown in Fig. 4.

The multipath and SNR report files are important to assess the site specific (environmental and instrumental) errors that have repercussions on the accuracy of site position. In some scenarios, where GPS antennas are installed on building rooftops the multipath needs to be detected so that it is not mistaken for building or antenna phase center variations due to local vibrations, wind or even sharp temperature changes [11]. Identification of which satellite(s) is/are causing the multipath is an important assignment for understanding of their geometry at GPS receiver site. Identification of which satellite(s) is/are causing the multipath is an important assignment for understanding of their geometry at GPS receiver site.

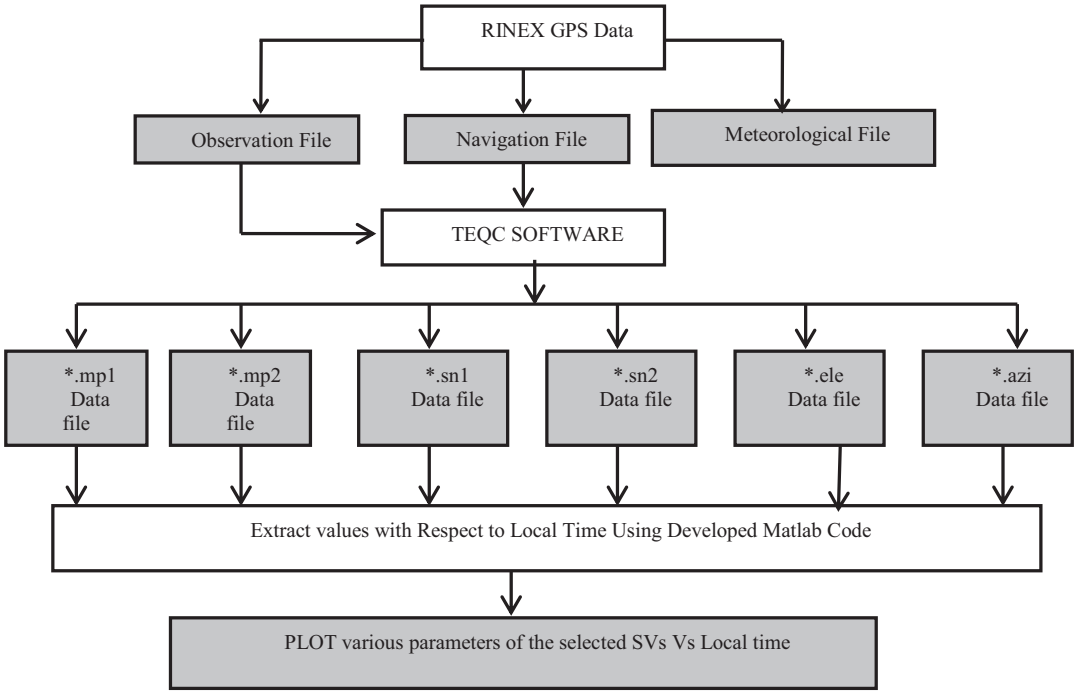

Figure 4. Multipath analysis using TEQC processed files

The GPS antenna at this station (NERTU) is located on a concrete pillar on the terrace of the building. This site is surrounded by Department of ECE building and vegetation. Multipath error variations are caused by a variety of factors such as buildings, nearby reflectors, antenna phase center variations and antenna pole movements etc. Hence, it is important to detect and separate multipath error to precisely estimate the receiver position at this site. The RINEX observation file "090310.10O" and navigation file "09030660.10N" (9th March 2010) is applied to non-interactive post processing TEQC software. The Quality check process generates six report files corresponding to the multipath error (mp1 and mp2), SNR (sn1 and sn2), elevation and azimuth angle files. The GPS receiver antenna position is calculated by using QC, which matches with the pre-surveyed position of the site (Table I). The processed QC files are used to compute Root Mean Square (RMS) multipath error on L_1 and L_2 carrier frequencies. The RMS multipath error obtained from QC results is summarized in Table II. The errors are less than a meter. Fig. 5 shows L_1 and L_2 pseudorange (code) multipath error (in meters) for SV 6 (9 March 2010) during 13:00:00 to 17:00:00 hours. The analysis has been carried out with an elevation mask of 10^0 to avoid higher multipath oscillations at lower elevations. Here, the data are recorded at 60 sec intervals. From Fig. 5, it is observed that multipath error (mean) on L_1 carrier frequency is 0.0148 m where as on L_2, it is 0.0273 m. This shows that multipath error on L_2 carrier frequency is more than on L_1 (Table III).

Fig. 6 shows the Signal to Noise Density Ratio (SNR) variations on L_1 and L_2 carrier frequencies. The peak value of SNR on L_1 is 47dB-Hz where as on L_2, it is 41dB-Hz during the local time 15:00:00 to 15:50:00 hours. The SNR on L_1 is more than L_2 which is clearly given in Table III. Fig. 7 shows the corresponding elevation and azimuth angles of SV 6. For better understanding of multipath geometry, the three plots namely multipath error (m), SNR (dB-Hz) and their elevation angle are compared. From Figs 5, 6 and 7, it is observed that the SNR and elevation angles are directly proportional, whereas SNR and multipath error are inversely proportional. It is also observed that, for a peak value of elevation angle (37^0) attains maximum SNR values of 46 dB-Hz on L_1 and 40.7097 dB-Hz on L_2. At this elevation angle value, the multipath error reaches minimum value (0.0454m on L_1 and 0.0573m on L_2) during local time 15:00:00 to 15:50:00 hours.

TABLE I.
NERTU RECEIVER ANTENNA POSITION (WGS-84)

Coordinate	Value of the parameter
X (m)	1211896.6729
Y (m)	5966440.3357
Z (m)	1896110.0680
Φ (deg)	17.408037
λ (deg)	78.518345
h (m)	465.1588

TABLE II.
SUMMARY OF MULTIPATH ERROR

Carrier Measurement	**L1**	0.325264 (m)
	L2	0.402367 (m)
Code Measurement	**P1**	0.50 (m)
	P2	0.65 (m)

TABLE III.
MEAN AND STANDARD DEVIATION OF MULTIPATH ERROR (M) AND SIGNAL TO NOISE DENSITY RATIO (dB-Hz)

S No	Parameter	L_1 carrier		L_2 carrier	
		Mean	Std	Mean	Std
1.	Multipath error (m)	0.0148	0.2343	0.0273	0.3005
2.	Signal to noise density ratio (dB-Hz)	43.7214	2.3799	37.7679	2.7435

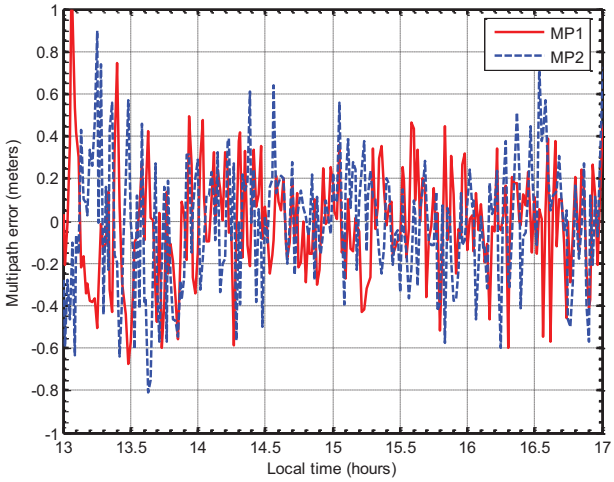

Figure 5. Multipath error (m) on L_1 and L_2 for SV 6

At lower elevation angles (say 15^0) SNR attains minimum value (38.2 dB-Hz on L_1 and 32.5 dB-Hz on L_2) whereas, the multipath error attains a maximum value (0.0687 m on L_1 and 0.3017m on L_2). The results show that multipath error is more at lower elevations and less at higher elevations because the satellite signal at lower elevations enters the antenna at a point where the gain is relatively low, and the reflected signals enter the antenna where the gain is relatively high. Therefore, the multipath effect at low elevation angles can be reduced by setting an elevation mask to the receiver.

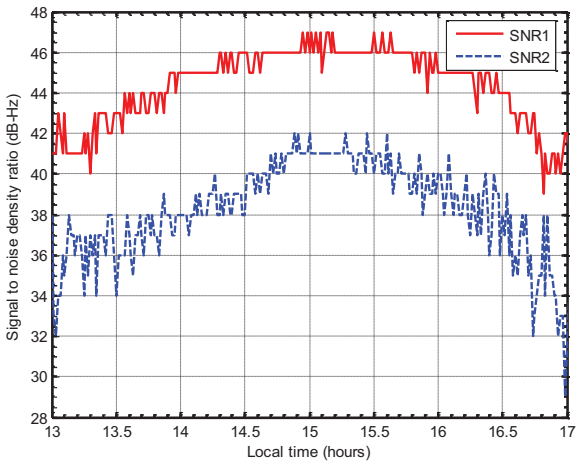

Figure 6. Signal to noise density ratio (dB-Hz) on L_1 and L_2 for SV 6

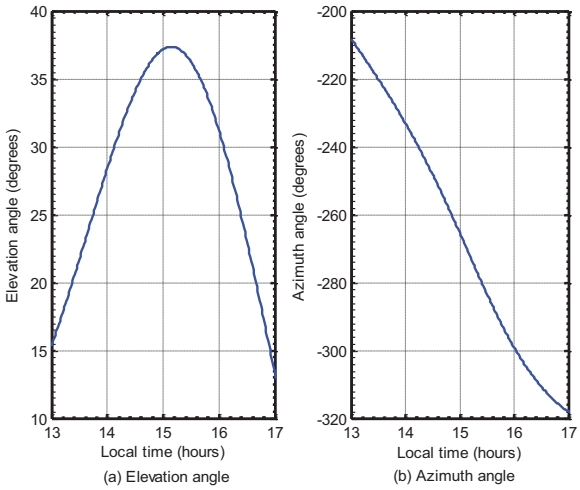

Figure 7. Elevation and Azimuth angle (degrees) variations for SV 6

V. CONCLUSIONS

In this paper, the multipath error (time series) on both L_1 and L_2 is precisely estimated by a prominent method known as CMC technique. The multipath errors (mean) estimated with experimental GPS data on L_1 and L_2 are 0.79 m and 2.01 m respectively. The CMC technique is very useful for both real-time kinematic and static applications. Various characteristics such as magnitude and repeatability of GNSS multipath plays a major role in installing base stations for DGPS and LAAS applications. The maximum carrier phase multipath error for L_1 and L_2 is 4.75 cm and 6.0 cm respectively. But, the maximum pseudorange (code) multipath error can reach up to (one chip wavelength) 293.05 m for the C/A-code and 29.305 m for P-code measurements. Therefore, the magnitude of multipath error is more on the pseudorange measurements than on the carrier phase measurements. For any static GNSS base station, the multipath pattern of any SV is highly repetitive with a constant phase (time) shift (approximately 236 s) during the successive days. Hence by creating such multipath time series patterns for couple of days at the static station, multipath error can be predicted for the forthcoming days by shifting the time by 236 s for everyday.

REFERENCES

[1] Braasch M. S., Van Dierendonck A. J., "GPS receiver architectures and measurements", Proceedings of the IEEE, Vol. 87, No.1, January, 1999, pp: 48-64.

[2] Georgiadou Y., Kleusberg A., "On carrier signal multipath effects in relative GPS positioning", Manuscript Geodetics, 1988, Vol. 13, pp: 172-179.

[3] Hagerman L., "Effects of multipath on Coherent and Non coherent PRN Ranging Receiver", Aerospace Rep. TOR-0073 (3020-03)-3, Development Planning Division, the Aerospace Corporation, May 15, 1973.

[4] Braasch, M. S., "Multipath effects, in Global Positioning System: Theory and Applications", Vol. 1, edited by B. W. Parkinson et al., chap. 14, Am. Inst. of Aeronaut. And Astronaut., Reston, 1996.

[5] Satirapod, C. and Rizos, C., "Multipath mitigation by wavelet analysis for GPS base station applications," Survey Review. CASLE. London, Vol.38, pp.2-10, May 2005.

[6] Bilich, A., and K. M. Larson, “Mapping the GPS multipath environment using the Signal-to-Noise Ratio (SNR)”, Radio Science, Vol.42, RS6003, 2007.

[7] K Yedukondalu, A D Sarma, and V S Srinivas, "Estimation and Mitigation of GPS Multipath Interference using Adaptive Filtering", Progress in Electromagnetics Research M (PIER-M), Vol. 21, pp: 133-148, 2011, USA, ISSN: 1937-8726.

[8] K Yedukondalu, A D Sarma, Ashwani Kumar and K Satyanarayana, “Spectral Analysis and Mitigation of GPS Multipath Error Using Digital Filtering for Static Applications”, IETE Journal of Research, Vol. 59, Issue 2, March-April 2013, pp: 156-166, Medknow publishers, ISSN: 0377-2063.

[9] LinLin G E, Shaowei Han and Chris Rizos, “Multipath mitigation of continuous GPS measurements using an adaptive filter”, GPS solutions, Vol. 4, No: 2, pp. 19-30, 2000.

[10] Kaplan D., “Understanding GPS: Principles and Applications”, Artech House, Boston, London, 1996.

[11] Ogaja, C and C. Satirapod, “Analysis of high-frequency multipath in 1-Hz GPS kinematic solutions”, GPS Solutions-Springer Verlag, Vol.11, No.4, pp.269-280, 2007.

[12] Estey and Meertens, “TEQC: The multipurpose tool kit for GPS/GLONASS data”, Journal GPS Solutions, Vol. 3, No.1, pp. 42-49, 1999.

[13] Gurtner, W., “RINEX: The Receiver-Independent Exchange Format”, GPS World, Volume 5, Number 7, pp.48-52, 2000.

Distinctiveness of Manet and its Security Issues: A Review

P. Tamilselvi[1], C. Ganeshbabu[2] and V. Arthi[3]
[1]Asst. Professor, Sri Eshwar College of Engineering/ECE Department, Coimbatore, India
Email: ttamil_p@yahoo.com
[2]Professor, Bannari Amman Institute of Technology/ECE Department, Sathyamangalam, India
Email: bits_babu@yahoo.co.in
[3] Assoc. Professor, CVR College of Engineering/ECE Department, Hyderabad, India
Email: arthi.psv@gmail.com

Abstract: **Manet is a wireless network that has a group of nodes that can move in any direction. Manets do not have a particular infrastructure. So, they are not controlled by a central system. The autonomous nodes have arbitrary movement inside the network which can create momentary dynamic network. Because of this, the topology of the network often changes. Manets are nowadays used for commercial purposes due to their distinguishing properties. But these networks have to face a lot of security related issues. Also Manet has restricted bandwidth, dynamic topology and has to share the wireless medium. Because of the usage of shared medium, security challenges has become a primary concern to provide secure communication. The aim of the paper is to provide a complete knowledge about the various routing protocols used, characteristics of Manet and security issues the network has. To achieve our aim, literature survey is done and the related information is collected. In order to provide a secure communication in manet, attacks should be recognized and prevented.**

Index Terms**: Black hole, Routing protocol, Manet, Security attack**

I. INTRODUCTION

A mobile adhoc network is a group of mobile nodes that do not have an access point or any infrastructure for proper opertion. Ad hoc networks are to be used in tactical networks for Military communication and operations, Automated battlefields. In sensor networks to automate everyday functions like earth and weather activities. Manets are also used in emergency situations like earthquakes, disaster recovery and commando operations. One of the main security threats is that nodes may become malicious. Black hole and Gray hole attacks are major types of malicious attacks.

A. Black hole attack

A Black hole attack is an active attack where the nodes captures all the data packets and drop them, Black hole attack is depicted in Fig.1. In this attack the malicious node broadcasts to all its neighboring nodes that it has shortest route to destination without checking the routing table. Receiving this information, the source node will transmit its data packet to the malicious node. The malicious node will receive the data packets and drop all the data without forwarding them to destination. This is the black hole attack in MANETs.

B. Gray hole attack

A Gray hole attack is an extension of black hole attack. Attackers drop data packets from selected nodes while forwarding the data from other nodes. The behavior of malicious nodes is unpredictable. The attack cannot be easily detected. The Gray hole may behave maliciously for some time and return to normal behavior later.

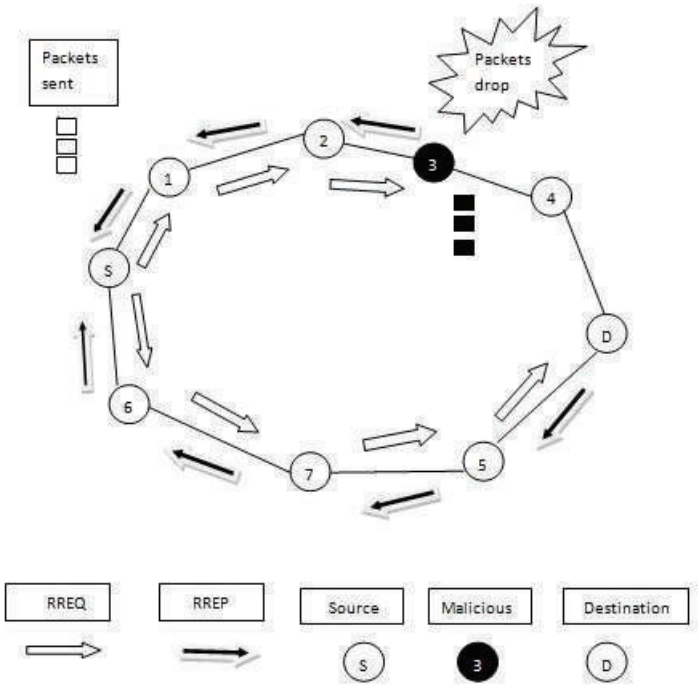

Figure1. Manet with black hole

II. CHARACTERISTICS

2.1. Multi-hop transmission

Multi-hop transmission is applied to transmit messages when the source and destination are not closer and they are apart. So, the MANETs use multi-hop transmission when the network size is large and one-hop transmission is not possible. One or more intermediate nodes are used to forward the message packets when the source and destination are not directly connected.

2.2. Distributed nature of operation

There is no centralized control system to monitor and control the functions of the network. So the nodes present in the network takes the responsibility and collaborates to implement the functions such as routing and security.

2.3. Self directed

In MANET, the role of host and router are done by the same mobile node. It means that a node has ability to work both as host and router. Nodes perform switching functions as router and so endpoints and switches are same.

2.4. Dynamically varying topology

The topology of the Manets is dynamic as the nodes in the network are mobile. As time goes on, nodes move in random manner and so routes are established dynamically.

2.5. Poor link capacity

Compared to wired links, the reliability, scalability, efficiency and capacity of wireless links are often less. The communication channel is subject to noise, fading, interference and has less bandwidth than a wired network.

2.6. Absence of Infrastructure

Nodes in ad-hoc networks are able to operate independently without any fixed infrastructure.

III. ROUTING PROTOCOLS

Routing protocols are a set of rules used for connecting a source and destination for transmission of message packets in a network. There are different types of routing protocols used in MANETs. The appropriate routing protocols are chosen according to the network circumstances and requirements. The routing protocol's classification are:

3.1. Proactive Routing Protocols

The other name of Proactive routing protocols is table-driven routing protocols. The contents present in the routing table are used for routing. In this protocol, each node maintains a routing table that stores all the updates related to the changes in the structure of the network. Data renewal is done every time network structure changes. Proactive protocols are not suitable for large networks because for each node, entries should be made in the routing table which is complex. DSDV, OLSR, WRP etc are some of the proactive routing protocols.

3.2. Reactive Routing Protocols

In reactive routing protocol, whenever necessary the routes are discovered. So this protocol is called on demand routing protocol. Whenever there is a need for new route, route discovery is initiated by the nodes. Nodes with appropriate routes reply to the source. DSR, AODV, TORA and LMR are some of the reactive routing protocols. There are two mechanisms in this protocol:

3.2.1. Route discovery

In this phase source node initiates route discovery on demand basis. Source node checks its route cache for the available route from source to destination. If the required route is not available, the route discovery is initiated. The source generates a request message. The request message contains the address of the intermediate nodes in the path and the destination node.

3.2.2. Route maintenance

The happenings like link breakage cause route failure whenever the topology of the network changes. Acknowledgement mechanism is used in reactive protocols for checking the reliability and to maintain the routes.

3.3. Hybrid Routing Protocol

Both proactive and reactive protocols have some advantages and disadvantages. Hybrid protocol combines the advantage of both proactive and reactive protocols. The overhead is high in proactive routing protocols compared to reactive routing protocols. The latency is less in proactive routing protocols compared to reactive routing protocols. Hybrid protocol is appropriate for large networks where lots of nodes are present. Both the 'on- demand technique' and 'routing- table maintenance' are used in hybrid routing protocol. It avoids latency and overhead problems in the network. In large networks, the network is divided into a set of zones. Proactive approach is used for routing inside the zone. Reactive approach for routing outside the zone routing. MANET like ZRP, SHRP etc is some of the types of hybrid routing protocol.

IV. CHALLENGES

The MANET has to face several challenges that must be analyzed.

4.1. Routing

Routing the packets between any pair of nodes is not easy as the topology of the network changes. The protocols chosen may be reactive routing or proactive routing. The nodes have a random motion in the network and so multicast routing is another challenge. Routes between the nodes may have single hop or multiple hops. Multi hop communication is more complex than the single hop communication.

4.2. Quality of Service

The environment for Manet is constantly changing and so achieving necessary quality of service levels will be a challenge. Appropriate routing methods are selected so as to provide good quality of service.

4.3 Security and Reliability

Ad hoc networks are not secure always. Various schemes of authentication should be applied to provide secure communication. Some nodes may not be reliable and may cause hazards to the adhoc network. So, checking the node's reliability is very important.

4.4. Power Consumption

For most of the light-weight mobile devices, the power consumption is an important factor to be considered. Power conservation and power-aware routing must be used for optimal functioning of the network.

V. SECURITY

The following are some security criteria and attacks that occur in Manet:

5.1. Security Criteria

5.1.1. Availability

The term Availability means that all the assigned services should be provided by the node in any condition. This security criterion is violated mainly during the denial-of-service attacks. In the denial-of-service attack, the selfish nodes deny some of the network services.

5.1.2. Authentication

This guarantees that all the nodes participating in communication are genuine and not impersonators. It is necessary that all communication entities should prove their identities. The attacker could act as a beginning node if authentication mechanism is not used in the network. The attacker can thus get rights to see the confidential information. The attacker can also insert some bogus messages and collapse the normal network operations.

5.1.3. Confidentiality

Information is confidential only if the authorized members can get the access. All other entities which does not have authorization, cannot use the confidential data. All the data in the network should be kept confidential.

5.1.4. Non-repudiation

The sender and the receiver of a message cannot refuse the transmission or reception of message. Non-repudiation is used when there is a need to differentiate a node with some abnormal behavior. A node can notify an abnormal behavior node with the evidence of the erroneous message received

5.1.5. Integrity

Message being transmitted should be real. Integrity is spoiled by two ways. One is malicious altering and the other is accidental altering. In malicious altering, the message is changed or dropped repeatedly by an attacker. In accidental altering, link failure in the network may lead alteration in the message or sometimes loss of message.

5.1.6 *Attacks using Fabrication*

False routing messages are generated and transmitted to the nodes which require routes. Such types of attacks are difficult to detect.

5.2. Attacks on Manet

5.2.1. Location Disclosure

Location disclosure is an attack where a compromise is done in the private information of an ad hoc network. An analysis is done on the traffic generated by the network in order to find a node's location and also the network's structure.

5.2.2. Black Hole

In a black hole attack, whenever the source sends route requests, a malicious node gives false route replies to the route requests. Black hole node declares that it is having the shortest path to a destination. Believing these false route replies, the source transmits data packets to the malicious node. The malicious node captures the data packets and drops them instead of transmitting them to destination.

5.2.3. Replay

Another attack that heavily attacks the performance of MANET is replay attack. The valid signed messages are captured and retransmitted by the replay attacker. The transmitter and the receiver nodes use timestamp for validating the signed messages. The freshness of routes is affected by this attack.

5.2.4. Wormhole

The wormhole attack is one of the possible severe attacks. In this attack, two malicious nodes that are involved in the network cooperate to execute this attack. Wormhole nodes fake a route that is shorter than the original route, Wormhole node can easily attack the network without knowing about the network. The two attackers take the control of the wormhole link between the two nodes.

5.2.5. Denial of Service

The routing operation and also the entire operation of the network is affected by the denial of service attack. The resources of the communicating nodes are consumed by the routing table overflow attack. The malicious node floods the network with fake route creation and stops the creation of legal routes.

5.2.6. Masquerading

During the neighbor acquisition process, an outside intruder compromises the authentication system and joins to the existing communication link and masquerades an IS. The danger of masquerading is the same as that of a compromised IS.

5.2.7. Impersonation

The attacker creates a fake belief that it is a friend of the genuine node if there is no authentication mechanism prevailing in the network. The malicious nodes can then join the network as the normal nodes. The malicious nodes start their attack by propagating fake routing information and gets inappropriate access to the confidential information.

5.2.8. Eavesdropping

Eavesdropping attack obtains the confidential information from the nodes that should not be shared to any others during the communication. The information is made confidential by use of various keys like public key, private key, location and passwords of the nodes. The unauthorized nodes cannot get access to the confidential information.

VI. RELATED WORK

In [3], author focuses on grey hole attack. Grey hole attack affects the routing services provided by the network. Adhoc-on-demand (AODV) protocol is used for routing of data packets. This paper discusses the security issues and also the layered architecture of Manet. This paper also gives

the various applications of Manet. It also briefs the various work done in the area of adhoc network.

In [5], author proposes real time monitoring system AODV (RTMAODV). Real time monitoring method is used by the neighbor node to detect and prevent grey hole. Source sends Route request RREQ. On receiving RREQ, some nodes reply to those RREQs. These nodes are monitored in promiscuous mode. This is done by neighbors of the nodes who send RREP to detect the malicious behavior.

In [6], author proposes Trust Based Secure On Demand Routing protocol called "TSDRP". This proposed routing protocol can use for increased size of network. TSDRP protocol transmits data packets to the destination nodes even in the presence of malicious node. Performance analysis is done by comparing the proposed TSDRP and AODV protocol by measuring various parameters.

In [8], author put forward a scheme "BLACK HOLE AODV". Implementing this protocol, black hole is identified and its effect is nullified. This paper also gives the consequences of black hole attack. The performance of the network with and without black hole is analyzed.

In [9], author uses a second-best route for the destination to find the malicious behavior. Source broadcasts route request RREQ to get the route to destination. When the route reply RREP is received by the source, it transmits the confirmation packet using the second-best route to the destination. Source confirms that the destination has a route to the node which generates the RREP or to the Next_Hop_Node of the node that generates RREP. If the destination has no route to these nodes, both the node which creates RREP and its Next_Hop_Node will be assumed to be malicious nodes. The source node can detect cooperative malicious nodes by using this scheme. But in the case of more than two cooperative malicious nodes, this approach is not useful.

In [10], author proposed a scheme which identifies the malicious nodes by using aggregate signature algorithm. It associates three algorithms.
(1) The proof creating algorithm: Whenever the nodes involved in a communication receive a message, they create a proof that is based on aggregate signature algorithm.
(2) The checkup algorithm: This algorithm is called when the source node suspects that the transmitted packets are dropped. If the destination reports that it does not receive all transmitted packets, it will invoke this algorithm to detect the malicious node.
(3) The diagnosis algorithm works with the results of check up algorithm. Simulation is done in ns2 simulator. Using this proposed method, overhead is reduced and packet delivery ratio is improved.

In [11], AODV routing protocol is used to reduce the effect of gray hole attack. The proposed method first set the waiting time for the source node to receive the RREQ coming from other nodes. This waiting time is then added to the current time. RR-table stores the replies with high destination sequence number as the first entry in the table. Then the first destination sequence number is compared with the source node sequence number. The entry in the RR-table is removed when the differences between them are high. The next node id that has the higher destination sequence number is selected. The content of RR-table is sorted according to the DSEQ-NO column.

In [13], authors proposed an intrusion detection system named Enhanced Adaptive Acknowledge (EAACK) . Two encryption techniques DSA and RSA are used in EAACK and their performances are compared in MANET. DSA scheme generates less overhead than RSA. EAACK prevent attackers from initiating forged acknowledgment attack

In [15], author proposes Black hole Avoidance Protocol for wireless network (BAAP). Adhoc on demand multipath distance vector (AOMDV) is used in this proposed method. Each and every mode in this protocol makes cooperation with their neighbor nodes to form the reliable path to destination node. Performance metrics are measured which shows that packet loss is less than AODV. Packet Loss increases as mobility increases. In route discovery process, an intermediate node will try to create a route and this route should not contain a node whose legitimacy ratio is lesser than the lower threshold level.

In [18], author proposed a black hole avoidance scheme. An enhancement is made in the AODV routing protocol to eliminate the black hole. The source first sends the route request and waits for responses from all neighboring nodes with which it gets a reliable route. According to this proposed scheme the source node should not send data packets immediately after receiving the first reply.
"Timer Expired Table" is used to set timer after the reception of first reply. This table stores the sequence number of the packet. "Collect Route Reply Table" is used to store arrival time. Node's waiting time depends on the distance. Entries in the table help to identify malicious node.

In [19], author presented a black hole detection scheme. In this method, when the source node receives RREP packets, it generates a new RREQ. RREQ has the highest sequence number and it is unicast through the route in which the RREP packet was received. Malicious node generates a RREP with highest sequence number on receiving RREQ. Malicious node sends the fake RREP packet to the source node. Now source identifies the malicious node. This method has very less overhead.

In [20], author analyses all the security issues in the mobile ad hoc networks, which is a great hindrance to the working of Manet. Intrusion detection techniques and cluster based intrusion detection techniques are clearly explained. Misbehavior detection through cross layer analyses is also briefed.

In [21], author gives a thorough study on detection of misbehavior links and malicious nodes. The routing protocols used by Manets are also explained. The paper also tells how to protect the connection between the mobile

nodes in a multi hop network. The security issues are analyzed and the state-of-the-art security proposals that protect the MANET link are detailed.

In [22], author gives a brief introduction on Manets. A review is done on the previous research work done on the Manet to provide a complete security solution for efficient communication.

VII. Conclusions

Characteristics of Manet, challenges faced and the various security issues are discussed in this paper. Because of uncertainty in the wireless environment, Mobile adhoc networks needs protection from the vulnerabilities caused by attackers. This paper put forward the research works done in the Manets to provide security. All the research works aims at providing better quality of service in the adverse environment nullifying the attack of intruders.

References

[1] Jian-Ming Chang, Po-Chun Tsou, Isaac Woungang,Han-Chieh, Chao and Chin-Feng, "Defending Against Collaborative Attacks by Malicious Nodes in MANETs: A Cooperative Bait Detection Approach," in IEEE Systems Journal VOL 9. NO.1.Marrch 2015,pp.65-75

[2] Hitender Gupta and Harsh Aggarwal,"Simulation to detect and removal of black hole in Manet", SSRG Intenational Journal of Electronics and Communication Engineering, April 2015,pp.35-39

[3] Rakesh Ranjan, Nirnemesh Kumar Singh, Ajay Singh, Security Issues of Grey Hole Attacks in MANET" nternational Conference on Computing, Communication nd Automation (ICCCA 2015).

[4] Tao Shu and Marwan Krunz," Privacy-Preserving and Truthful Detection of Packet Dropping Attacks in Wireles Ad Hoc Networks", IEEE Transactions On Mobile Computing, Vol 14,No.4,April 2015, Pp.813-828.

[5] Anishi Gupta, "Mitigation Algorithm against Grey Hole Attack Using Real Time Monitoring for AODV Routing Protocol in MANET" IEEE 2015 2nd International Conference on Computing for Sustainable Global Development (INDIACom).

[6] Hongmei Deng, Wei Li, and Dharma P. Agrawal, "Routing Security in Wireless Ad Hoc Network," IEEE Communications Magzine, vol. 40, no. 10, October 2002.

[7] S. Marti et al., "Mitigating Routing Misbehavior in Mobile Ad Hoc Networks," 6th Int'l. Conference Mobile Comp. Net., pp. 255-265, August 2000.

[8] Semih Dokurer, Y.M.Erten and Can Erkin Acar, "Performance analysis of ad-hoc networks under black hole attacks" IEEE conference Procedings,March 2007.

[9] N-W. Lo and F.-L. Liu, "A Secure Routing Protocol to Prevent Cooperative Black Hole Attack in MANET," in Intelligent Technologies and Engineering Systems. vol. 234, ed: Springer New York,2013, pp. 59-65.

[10] G. Xiaopeng and C. Wei "A Novel Gray Hole Attack Detection Scheme for Mobile Ad-Hoc Networks" IFIP International Conference on Network and Parallel Computing, 2007.

[11] Mr.ChetanS.Dhamande and H.R.Deshmukh, "A Efficient way To Minimize the Impact of Gray Hole Attack in AdhocNetwork ", International Journal of Emerging Technology and Advanced Engineering, Volume 2, February 2012.

[12] P. Agrawal, R. K. Ghosh, and S. K. Das, "Cooperative black and gray hole attacks in mobile ad hoc networks," in Proceedings of the 2nd International Conference on Ubiquitous Information Management and Communication 310–314.

[13] Elhadi M. Shakshuki, Nan Kang, and Tarek R. Sheltami, "EAACK—A Secure Intrusion-Detection System for MANETs", IEEE Transactions On Industrial Electronics, Vol. 60, No. 3, March 2013.

[14] Y. Zhang, W. Lee, "Intrusion Detection in Wireless Ad Hoc Networks," 6th Int'l. Conference Mobile Comp. Net., Mobicom 2000, pp. 275-283, August 2000.

[15] Saurabh Gupta, Subrat Kar, S.Dharmaraj, "BAAP:Black hole Attack Avoidence Protocol For Wireless Network",International Conference on Computer and Communication Technology (ICCCT)-2011.

[16] S. Kurosawa, H. Nakayama, N. Kato, A. Jamalipour, and Y. Nemoto, "Detecting blackhole attack on aodv-based mobile ad hoc networks by dynamic learning method," International conference on wireless networks vol. 5, no. 3, pp. 338–346, Nov. 2007.

[17] S. Ramaswamy, H. Fu, M. Sreekantaradhya, J. Dixon, and K. Nygard, "Prevention of cooperative black hole attack in wireless ad hoc networks," in International Conference (ICWN'03), Las Vegas, Nevada, USA, 2003.

[18] LathaTamilselvan and Dr. V Sankaranarayanan, "Prevention of Blackhole Attack in MANET", 2nd International Conference on Wireless Broadband and Ultra Wideband Communications (AusWireless 2007), IEEE

[19] S. Banerjee, M. Sardar, and K. Majumder, "AODV Based Black-Hole Attack Mitigation in MANET," in Proceedings of the International Conference on Frontiers of Intelligent Computing: Theory and Applications (FICTA) 2013. vol. 247,

[20] Pradeep Rai and Shubha Singh, "A Review of 'MANET's Security Aspects and Challenges" IJCA Special Issue on "Mobile Ad-hoc Networks" MANETs, 2010.

[21] Rashmi Mahajan and S. M. Patil, "A Review of 'MANET's Security Aspect and Challenges with Comprehensive Study of SIDS for Discovering Malicious Nodes" International Journal of Innovative Science,Engineering & Technology, Vol. 1 Issue 6 August 2014.

[22] Komal Khedkar and Shubham Josh, "A Review on Secure Routing Protocols in MANET", International Journal of Innovative Research in Computer and Communication Engineering, Vol. 2, Issue 11, November 2014.

Color Recognition System for Visually Impaired Persons

L. Dhamini[1] and D. Bhanuprakash[2]
[1]M. Tech student, CVR College of Engineering/ECE Department, Hyderabad, India
Email: dhamini94@gmail.com
[2]Assoc. Professor, CVR College of Engineering/ECE Department, Hyderabad, India
Email: pbhanududi@gmail.com

***Abstract*: This paper focuses on assisting tools for visually impaired persons. There is an ongoing research on the Human-Computer-Interaction (HCI) which focuses mainly on the use of computer technology, especially on the interaction between the people and the computer. Visually impaired persons are facing many problems in their day-to-day life as everything around us is encoded visually. This paper aims to propose a camera-based system to identify different colors of clothes. This system integrates a camera, a computer and audio output device for the description of clothing colors. The clothing colors are described verbally to visually impaired person.**

***Index Terms*: Camera, Audio Output Device, Visually Impaired.**

I. Introduction

This paper aims at designing and developing a device for visually impaired person's individuals as from past few years we can see a rapid growth of them among our population. Even though there is an increase in the many aspects of this technology, but the society is not much interested in designing and developing the applications for such group of people [1]. Many better tools can be developed which are helpful for visually impaired persons and make their life easy to go. Traditionally, such tools which are in the market are heavy and very expensive. For which visually impaired individuals have to be dependent on others for handling the device. In order to reduce this problem, we need to develop on-board capability device and which can also be used for several applications.

Apart from many other assistive tools, this paper aims to develop a color recognition system which gives benefits to the visually impaired person through which they can recognize the color of the clothes [2] and they can decide whether this color of clothes can be worn together or not, according to the norms of color matching [2]. In this system, camera is mounted on the system, for capture the image using some image processing techniques [3].

An Audio output module will be used to give the information about the color of cloth. This is independent and cost-effective assistive system. In this system single board computer systems like Raspberry pi is used for processing the color of the cloth. This scheme is very useful for the people who are visually impaired as well as elderly to make their life more accessible.

A. Block Diagram

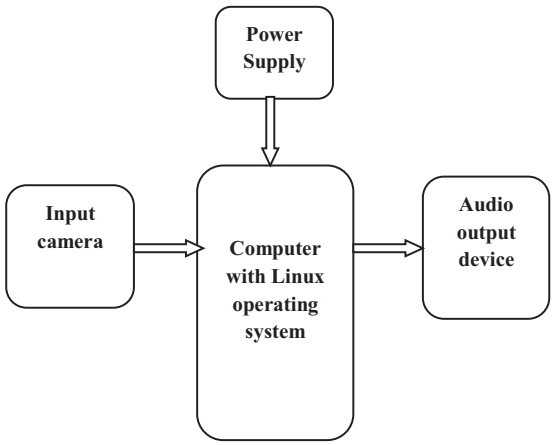

Figure 1. Block Diagram of color recognition system.

USB Camera

USB camera [4] is capable of capturing the high-resolution image of cloth and which will be sent to recognizing the color [5].

Audio Output Device

LCD display can also be used to display the output but this scheme develops a device which is especially useful for visually impaired persons. So, In order to communicate with them, an audio output device plays an important role, which will act as a control surface, Human Interface Device (HID) which allows the user to control a digital audio or other digital audio application. Generally, this will contain one or more controls that can be assigned to the software, allowing control of the software. As digital audio software is complex and which can play a number of functions in the audio chain.

II. Methodology Of Color Recognition System

In this methodology, two types of classification are performed. The first type of classification is the computation of features and the second type of classification is to extract the features using suitable classifiers. In general, all the images used for this experiment are taken in natural light and then resized.

A. Model Conversion

Color [6] is the most important feature of human eyes. By representation, this feature act as the overall of image content when it is used as a "global" feature. Space is defined as a model representing in terms depending on the values of intensity color space is defined as different models. Such as RGB, Lab, HSV, HSI, YCbCr, etc [7]. Though there are different color spaces each has its own benefits and drawbacks. In this paper, the input image has to be converted from one space to another. As all the images are in RGB model space, they should be changed into the suitable space. Among which HSV and L* a* b are much likely to be used. The drawbacks that occur in RGB model is eliminated by using L*a*b, HSV, HSI and YCbCr space models.

*B. RGB to L*a*b model conversion*

According to the international standards, l*a*b is used for measurements, which has been used by the Commission International d'Eclairage (CIE) [8]. By using this model we can generate the image which consists of "L" is the luminance or lightness component, which ranges from 0 to 100, and as the parameters "a" (from green to red) and "b"(from blue to yellow) are the two chromatic components, which range from -120 to 120.

Figure 2. RGB additive primary model (RGB model)

C. Identification of colors of clothes

This is done based on the color histogram, the main theme of this is quantized the pixels of the image based on the relation between the l*a*b array of color space. If the camera-based [9] captured, input image has more colors then the dominant color is given as output.

D. Color histogram

This will give us information that how the colors are distributed in the image based on the pixel values. Pixels are arranged in RGB channels and this is represented by using the numerical values ranges from 0-255.Based on the count of pixel value each color is defined [10].

Let us consider an example of pure purple color image,

In the image every color has RGB channels; in the same way, this purple color has the value of RGB channel as shown in figure 3.

Figure 3. Purple [R G B] = [118 52 149]

For the original image Figure 3 Purple (a), when the luminance scales of each RGB channels is increased by 30. Then the color is transformed as shown in figure 4.

Figure 4. Purple [R G B] = [148 82 179]

For the original image Figure 3 Purple (a), when the luminance scales of each RGB channels is increased by 40. Then the color is transformed as shown in figure 5.

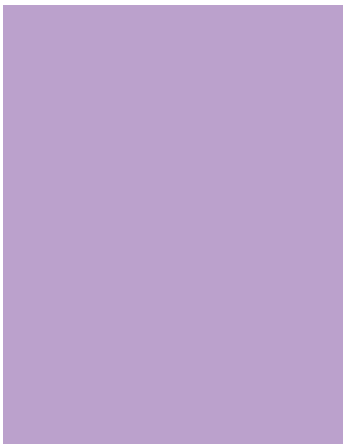

Figure 5. Purple [R G B] = [188 62 219]

For the original image Figure 3 purple (a), when the luminance scales of each RGB channels is decreased by 10. Then the color is transformed as shown in figure 6.

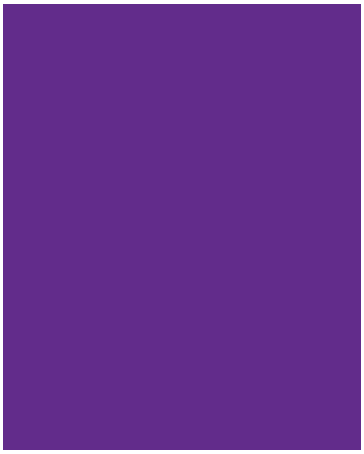

Figure 6. Purple [R G B] = [98 42 139]

For the original image Figure 3 purple (a), When the luminance scale of each RGB channels is decreased by i.e., if only G channel is made as 0. Then the color is transformed as shown in figure 7.

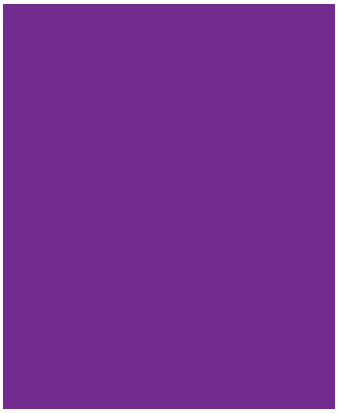

Figure 7. Purple [R G B] = [118 0 149]

Figure 8. Different shades of purple

Above figure gives us the information about the different shades of purple color which can be obtained by changing RGB channel values.

E. Color Labeler

Color labeler program is used to tag image regions with a text label of a color. The first step in this paper is to create a python class that can be used to label shapes in an image with their associated color [3][11] to do this, defines a class named color labeler in the color labeler.py file:

"red": (255, 0, 0),

"green": (0, 255, 0),

"blue": (0, 0, 255),

"pink": (255, 20, 147),

"purple": (90, 40, 200),

To start this, color dictionary is used to the mapping of the color name (the key to the dictionary) to the RGB tuple (the value of the dictionary). From there, system allocate to memory to store these colors, followed by initializing the list of color names. The next step is to loop over the colors dictionary.

RGB channel of the input image is compared with color labeler and according to this; it gives the name of the color in the form of the text and then finally converted into speech [7].

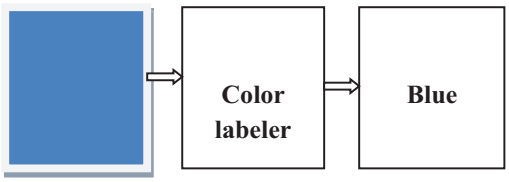

Figure 9. Output of color labeler

D. Software Used

Open CV (Open Source Computer Vision) is a library of programming functions mainly aimed at real-time computer vision. It has C++, C, Python and Java interfaces and supports Windows, Linux, Mac OS, ios, and Android.

Linux is one of the popular versions of UNIX Operating System. It is open source and easy to use. The Linux was designed considering UNIX compatibility. Its functionality list is quite similar to that of UNIX.

Python is a widely used high-level programming language for general purpose programming. Python has a design philosophy that emphasizes code readability, and a syntax that allows programmers to express concepts in fewer lines of code that might be used in languages such as C++ or Java. The language provides constructs intended to enable writing clear programs on both a small and large scale. Python interpreters are available for many operating systems, allowing Python code to run on a wide variety of systems. Python, the reference implementation of Python, is open source software and has a community-based development model, as nearly all of its variant implementations.

III. Working

This paper consist of three major steps which are as follows

1. Capture the image by using camera and saved it for further use.
2. Processing of saved image according to the algorithm and finding the color of the clothes. In this paper processing element is desktop computer or a portable computer like Raspberry.
3. Then the results are given to audio output device. By which the information i.e., about the colors of clothes is given to the visually impaired persons.

A. Flowchart for Color Recognition

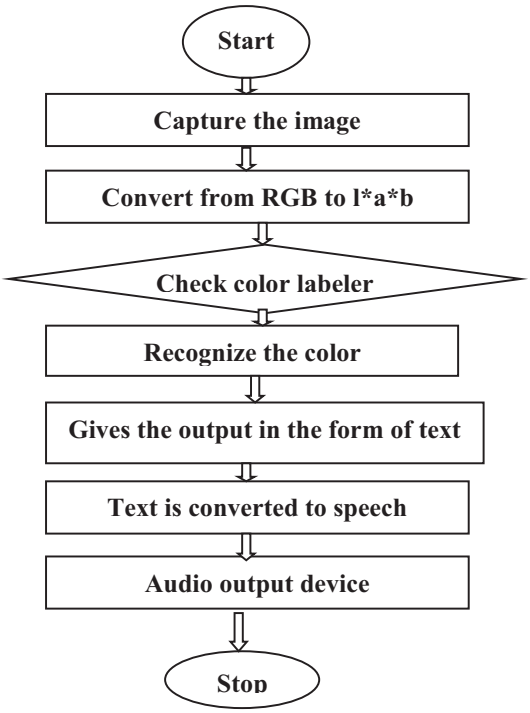

Figure 10. Flowchart for Color Recognition

IV. Results

The color [3] recognition device is used for identifying the colors of clothes and this will be useful for the visually impaired person. This device is developed by using open CV techniques along with some other methods. This will give the output in the form of audio. Here the below table will show the results through this device i.e., the color of clothes.

TABLE I.
RESULTS OF COLOR RECOGNITION SYSTEM

CLOTHES	OUTPUT AS SPEECH (COLOR)
	PINK
	PURPLE
	RED
	GREEN
	BLUE

A. Advantages

1. Low power consumption.
2. Fully automatic, fast response and user-friendly.
3. Low cost to design the circuit.
4. Efficient design.
5. Easy to operate.

This work can be extended by

1) Adding the feature of detecting and recognizing more types of indoor objects and icons on signage.

2) By using high-resolution cameras [12] and Bluetooth earphones can also be used for a clear and noise-free output to assist visually impaired persons to become independent.

V. CONCLUSIONS

This paper "Color recognition system for visually impaired persons" is proposed by using open CV on Linux Processor for identifying the colors of clothes. The paper is mainly intended for visually impaired persons as they are facing many problems in everyday life as everything is encoded visually. This research paper is a small contribution towards the task of bringing the visually impaired people into the environment by providing an independent device to them.

REFERENCES

[1] Mr.Shashi kumar, Mr. Mohamed zakir, Mr. Nikhil kumar. Sai Vidya Institute of Technology, Bangalore "Assistive clothing pattern recognition for visually impaired people" Project reference No:38S0161.

[2] Sameer Antania, Rangachar Kasturia; Ramesh Jain "A survey on the use of pattern recognition methods for Abstraction, indexing and retrieval of images and video", Pattern Recognition 35 (2002) 945–965.

[3] Xiaodong Yang, Shuai Yuan, andyinglitian, "Assistive Clothing Pattern Recognition for Visually Impaired People," IEEE transactions on human machine systems, vol. 44, NO. 2, APRIL 2014.

[4] S. Liu, J. Feng, Z. Song, T. Zhang, H. Lu, C. Xu, and S. Yuan, in Proc. "Hi, magic closet, tell me what to wear," ACM Multimedia, 2012.

[5] Irati Rasines1, Pedro Iriondo2, and Ibai Díez, K. Miesenberger et al. (Eds.):"Real - Time Display Recognition System for Visually Impaired" ICCHP 2012, Part II, LNCS 7383, pp. 623–629, 2012. © Springer-verlagberlin Heidelberg 2012.

[6] N Durga Rao, Dr. G Sudhavani, P Balakrishna, Dr. K Gouthami, "Cloth Pattern Recognition With Four Features (RSSM)", 978-1-4673-6708-0/15/©2015 IEEE.

[7] Ibrahim Patel, Jagdish Goud "Color Recognition for Blind and Color Blind People". International Journal of Engineering and Innovative Technology (IJEIT) Volume 2, Issue 6, December 2012.

[8] Shruti Bharadwaj, Sharath H.K., Praveena M.B.,Ajay Shetty,Shivarudraiah B."Clothing Color and Pattern Recognition for Visually Impaired People". International Journal of Engineering, Management & Sciences (IJEMS) ISSN-2348–3733, Volume-2, Issue-5, May 2015.

[9] Honey Mishra "The Survey Paper on Clothing Pattern and color recognition for Visually Impaired People", ,IJSRD - International Journal for Scientific Research & Development| Vol. 3, Issue 09, 2015 | ISSN(online): 2321-0613.

[10] Thogaricheti Ashwini, Mrs. Anuradha.S.G. "Assistive clothing Pattern Recognition for Impaired people". International Journal of Advanced Research in Computer and Communication Engineering Vol. 5, Issue 4, April 2016

[11] J. Zhang, M. Marszalek, S.Lazebnik, and C. Schmid, "Local features and kernels for classification of texture and object categories: A comprehensive study," Int. J. Computer. Vis., vol. 73, no. 2, pp. 213–238, 2007.

[12] Rakhil k s , Asha s, "Improved fabric defect detection and pattern Classification using radon transform" International journal of innovative research in Science, engineering and technology, vol. 4, issue 7, July 2015.

An Iterative Graph-based Image Restoration using Data-Adaptive Objective Function

P. Hema Sree
Assoc. Professor, CVR College of Engineering/ ECE Department, Hyderabad, India.
Email: phemasree1@yahoo.co.in

Abstract: **An image is defined as a function of weighted graph encoded with Laplacian matrices and its associated kernel similarities. An Iterative Graph (IG)-based Image Restoration with data-adaptive objective function is used to deblur the images that are degraded due to unconstrained conditions. From a normalized graph Laplacian, cost function is defined with a new regularization term and new data fidelity term. From the fast symmetry preserving balancing matrix, the normalizing coefficients are derived. This results in determining the spectral properties like symmetric, positive semi-definite and returning zero vector when applied to a constant Image. This algorithm has inner and outer iterations. In the inner conjugate gradient iterations, an updated objective function is minimized and the similarity weights are recalculated with earlier estimate in each outer iterations. The performance of this method is more effective for various restoration problems like sharpening, deblurring and denoising. Experimental results show that IG-based algorithm performs more powerfully in terms of objective criteria and visual quality.**

Index Terms: **Balancing matrix, Graph Laplacian, Conjugate Gradient, Deblurring, Kernel similarity matrix, Normalizing coefficients.**

I. INTRODUCTION

Many of the real world pictures or images are degraded in some sense due to variation in environmental conditions, camera setting, relative motion between camera and subject, etc. The purpose of restoration algorithm is to undo the undesirable distortions like noise, blur from a degraded image. This paper concentrates mainly on the distortions caused by blurring. The blurring process in linear shift invariant Point Spread Function (PSFs) is represented by a linear model as

$$y = Af + n \quad (1)$$

where, y is N x N ordered vector representation of a input blurred and noisy image, latent image in vector form is represented as f, n is the noise vector which is independent and equivalently distributed zero mean noise with standard deviation σ. Based on PSFs and type of assumptions, Blurring matrix A of size N^2 x N^2 is constructed.

Frequently used deblurring methods depend on optimizing the cost function which is expressed in the form

$$E(f) = ||y-Af||^2 + \eta R(f) \quad (2)$$

with respect to unknown image vector f. The first term in above equation is 'data fidelity term' and the second term is 'prior term' which is used for regularizing the ill-posed problem. The amount of regularization is controlled by parameter η. Based on nature of blurs and type of regularization parameter, many deblurring algorithms are classified. Most of the deblurring algorithms are based on Total Variation (TV)-type regularization [1]. Specific definition of TV term is varied and suitable optimization methods are chosen to define the cost function. Nonlocal differential operator as regularization term with different norms is used in other methods [2]. Example-based manifold priors are used for regularization in [3]. The prior term is added to estimate a gradient distribution in [4]. Hessian norm regularization is used to solve deblurring problem in biomedical applications [5]. BM3D method is one of the most recent algorithm uses generalized Nash equilibrium approach [6], which balances the objective functions for denoising and deblurring. This algorithm is best deblurring method for symmetric blurs like Out-of-focus and Gaussian blurs. A hyper-Laplacian [7], is based on statistics is used for motion deblurring applications. In [8] a progressive inter-scale, intra-scale approach is used for non-blind deconvolution. Different derivative terms are used as cost function for motion deblurring [9]. The proposed approach is kernel similarity-based image deblurring with novel data adaptive objective function. This approach can also be used for image denoising and sharpening.

The block diagram of the proposed iterative deblurring method is shown in Fig. 1. This method consists of outer and inner iterations. In each outer iteration k, an updated objective function is minimized and corresponding estimate f'(k) is obtained in inner iterations using Conjugate Gradient (CG).

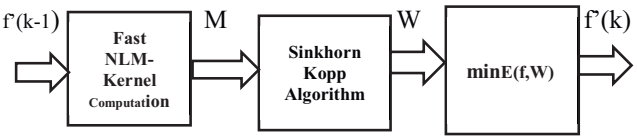

Figure 1. Block diagram of Iterative Graph (IG)-based Image Restoration method

The cost function used in the proposed method is based on new interpretation of a normalized graph Laplacian. It contains a normalized regularization term and data fidelity term. Fast symmetry preserving matrix balancing algorithm is used to extract the Normalizing coefficients [10], which results in spectral properties (symmetric, positive semi-definite) for the graph Laplacian. As the cost function is considered in quadratic form, the filtering operation of the objective function represents the spectral analysis for the restoration algorithm. This results in effective implementation of the algorithm using Conjugate Gradient

(CG) and fast sparse matrix-vector products. Kernel similarity values are initially computed differently by considering blurry image and denoised form of the noisy input. The contribution of ringing and noise articrafts is avoided. Inner CG iterations are stopped when the denoised image is exploited as plug-in estimator of blurred clean image ***Af.*** This is used in Prediction of Mean Squared Error (PMSE) measure. Performance of this algorithm is improved by updating the weights during the outer iterations. These are computed from similarity weights of the input image through outer iterations from their enhanced versions. Denoising and Sharpening methods are used as a special case in this proposed cost function. This approach can handle different varieties of Motion and symmetric blur PSFs.

The paper is organized as follows: Section II discusses on how to derive filtering and symmetric kernel similarity matrices, which are basic building blocks of the algorithm. Further the spectral properties of normalized Laplacian matrix are discussed. Section III presents the objective function and proposed procedure to optimize it for final estimate. Section IV focuses on the implementation details. Experimental evaluation for Gaussian, motion and out-of-focus PSFs are presented in section V. Section VI is devoted to conclusion and discussion on future directions.

II. Derivation of Basic Building Block Matrices

Kernel similarity matrix M and doubly stochastic symmetric matrix W are the main building blocks in the algorithm. A normalized Laplacian matrix is defined from these matrices whose spectral properties are significant for analyzing the nature of the algorithm.

A. Kernel Similarity Matrix (M) and Filtering Matrix (W)

From the valid kernel similarity function in [11], each (i,j)th element of the kernel similarity matrix M is calculated using non-local means (NLM) as [12]

$$M(i,j) = exp\left(-\frac{\|(f'_i - f'_j)\|^2}{k^2}\right) \quad (3)$$

where f'_i and f'_j are strip patches around the pixels i and j of a image f' and k is called smoothing parameter. From the estimate of previous iteration, kernel similarity weights (M) in each outer iteration are recomputed. The resultant M is a symmetric non-negative matrix. M matrix is sparse, as it computes the similarity between each patch and neighborhood patches around it (window size is 9 x 9). The Sinkhorn matrix balancing procedure [13] is applied to matrix M that results in doubly stochastic filtering matrix W, where $W = L^{-1/2}ML^{-1/2}$ (L= diagonal scaling matrix. As W is symmetric, it can be decomposed with orthonormal matrix O as $W= OSO^T$. The columns of O are Eigen vectors of W and S is a diagonal matrix that consists of Eigen values of W as its diagonal matrix, S= diag $\{\lambda_1, \lambda_2, \lambda_3, \ldots \lambda_N\}$. Applying W to a signal, preserves the DC component of the signal, as the largest Eigen value is equal to 1 exactly with corresponding DC vector. This property is more important in filtering operations and the spectral analysis of W matrix reveals its explicit low pass nature.

B. Normalized Graph Laplacian matrix

The normalized graph Laplacian matrix for image filters is defined as

$$I - W = I - L^{\frac{-1}{2}} \quad (4)$$

The set of Eigen vectors of I-W are considered as basis function of the graph and its Eigen values are treated as graph frequencies. Basically the Laplacian of I-W is high pass in nature and it can be interpreted as data adaptive Laplacian filter when applied to an image [14]. Based on the type of application, it integrates different filters in data term which is attached with regularized term. From the concept of Marcov chains, element (i,j) of $D^{-1}M$ represents the probability of shifting from one node i to node j of the graph in one step [15]. In Image deblurring applications, they provide fast methods in solving large linear system of equations when optimizing with CG methods. The linear equations are symmetric and positive definite. This normalized graph Laplacian I-W provides better performance than with un-normalized graph Laplacian.

The difference operator to the proposed normalized graph Laplacian is represented as

$$df(i,j) = \sqrt{M(i,j)}\left(\frac{f(j)}{\sqrt{L(j,j)}} - \frac{f(i)}{\sqrt{L(i,i)}}\right) \quad (5)$$

where L(i,i) and L(j,j) corresponds to ith and jth elements of the diagonal matrix L, derived from Sinkhorn matrix balancing algorithm [13]. Considering the divergence operator [16] with Laplace operator, the normalized Laplacian $I\text{-}L^{-1/2}ML^{-1/2}$ is represented as

$$\Delta f(i) = \frac{1}{\sqrt{L(i,i)}}\sum_{j,j\sim i} M(i,j)\left(\frac{f(i)}{\sqrt{L(i,i)}} - \frac{f(j)}{\sqrt{L(j,j)}}\right) \quad (6)$$

Thus the resultant regularization term is obtained a

$$R(f) = \frac{1}{2}\sum_{i=0}^{N}\sum_{j=i} M(i,j)\left(\frac{f(i)}{\sqrt{L(i,i)}} - \frac{f(j)}{\sqrt{L(j,j)}}\right)^2$$

$$R(f) = f^T(I - W)f \quad (7)$$

The Laplace operator in equation (6) is a second order derivative operator, which represents the effect of normalized laplacian at each pixel i, when applied to an input vector **f.**

III. Deblurring Method

This algorithm consists of inner and outer iterations. Data adaptive matrix M is computed to estimate the unknown image initially and it is gradually improved though iterations. The matrix W is estimated in each iteration and used to minimize the given objective with unknown image **f**

$$E(f) = (y - Af)^T\big(I + \beta(I - W)\big)(y - Af) + \eta z^T(I - W)f \quad (8)$$

where $\beta > -1$ and $\eta > 0$ are parameters related to noise and blur. First term determines the blurred and filtered version of Input **y**. Frequency selectivity is defined by β, based on amount of blur and noise. Second term is adaptive-data difference term which is based on normalized Laplacian matrix I-W. The filtering process of the cost function in [17] is more influenced on the objective function as

$$E(f) = \|\{I + \beta(I - W)\}^{1/2}(y - Af)\| + \eta\|(I - W)^{1/2}f\| \quad (9)$$

the term $I+ \beta(I\text{-}W) = O\Lambda O^T$ is semi-definite and symmetric matrix. The matrix $\{I+ \beta(I\text{-}W)\}^{1/2}=O\Lambda^{1/2}O^T$ has filtering

nature identical to that of I+β(I-W). From Eigen decomposition of a filtering matrix W, the ith diagonal element (λi) of Λ matrix can be represented as 1+ β(1-λi). I+ β(I-W) behaves as sharpening filter on **y**-A**f** residuals where I-W is high pass filter with β>0. The fidelity term undergoes different derivatives of the residuals to avoid deblurring problems in real images. Similar analysis is adapted to second term in equation (9) that forms adaptive high pass filters. This results in avoiding unpleasant artifacts due to noise, ringing artifacts, etc and maintains finest details in the restored image with best solution. Its gradient is set to zero by minimizing the cost function at each step

$$\nabla E(f) = -2A^T\big(I+\beta(I-W)\big)(y-Af) + 2\eta(I-W)f = 0 \quad (10)$$

which is symmetric and positive definite system of linear equations.

$$\Big(A^T\big(I+\beta(I-W)\big)A+\eta(I-W)\Big)f = A^T(I+\beta(I-W))y \quad (11)$$

Further Conjugate Gradient is used and A and A^T are interpreted as blurring with their power spectral functions. Experiments are carried out in three outer iterations to get expected deblurred output in many cases.

A. Spectral Analysis

The minimized cost function in equation (9) is represented as

$$f' = F(A,W)A^T\big(I+\beta(I-W)\big)y \quad (12)$$

The significance of equation 12 is that y is filter by I+ β(I-W), and it is multiplied by transpose of a blurring matrix A through back projection and applied to a symmetric matrix F(A,W). The spectral decomposition of symmetric matrix F(A,W) is represented as $\Theta\Upsilon\Theta^T$. The spectral filtering analysis of the corresponding deblurring result at each outer step is represented by the columns of a matrix Θ, which serves as orthonormal basis to filter the vector $A^T(I+\beta(I-W))y$. The basis Eigen vectors in Θ with their corresponding four largest Eigen values of F(A,W) are shown in figure 3. This reveals the data-adaptive character of the filter.

(a) (b) (c) (d) (e)

Figure 2. (a) Original 61 × 61 image, (b), (c), (d) and (e) are the Eigenvectors of *F(A,W)* that corresponds to four largest Eigen values for $\beta = 0.7$ and $\eta = 0.2$.

B. Image Denoising

With A=I in equation 8, image denoising problem is reduced. Based on SURE-based estimated MSE approach [17], optimal value of regularization parameter η is selected. Further improvement can be obtained by iterative approach with some existing kernel based denoising algorithms.

C. Image Sharpening

Set A=I and η = 0, then the cost function in equation 8 becomes as

$$E(f) = (y-f)^T\big(I+\beta(I-W)\big)(y-f) \quad (13)$$

Simple steepest decent method is used to optimize the above objective function

$$f' = f' - 1 + \mu\big(I+\beta(I-W)\big)(y-f'-1) \quad (14)$$

By selecting zero initialization with $f'_0=0$ and assigning step size with μ=1, the first iteration is in the form

$$f'_1 = \big(I+\beta(I-W)\big)y \quad (15)$$

Some part of high pass filtered version of the input image is added adaptively with β>0. W consists of some amount of information of the original image and also about the nature of blurring process. Therefore, data-adaptive sharpening technique was implemented in equation 15.

IV. Implementation Details

Initially calculate kernel similarity matrix M, from final estimate of the preceding step, i.e from f'^{M-1} for each outer iteration. For all the test images, the regularization parameter values η and β are kept fixed and these values are chosen based on blurring and noise variance. The parameters η and β are selected between [0, 0.4] and [0, 1]. Based on the amount of noise and severity of blurring, these values are chosen accordingly. Each step is initialized with suitable estimate from earlier step so that this iterative algorithm converges very quickly. Based on the amount of degradation, the maximum number of outer and inner iterations is set in advance. The iterations will be stopped according to the estimate of Predicted Mean Square Error (PMSE) which is represented as

$$\widehat{PSME}(q,k) = \frac{||\widehat{Af}-Af'^{(q)}_k||^2}{n^2} \quad (16)$$

where *Af'*is the required deblurred image. The Conjugate Gradient Iterations can be stopped when the following condition is satisfied.

$$\widehat{PSME}(q,k+1) > \widehat{PSME}(q,k) \quad (17)$$

V. Results

The effectiveness of this algorithm is verified with some number of experiments. Experiments are set up for Gaussian, nonlinear camera motion and out-of-focus blur. To get the final estimate for color image, this algorithm is applied separately to R, G and B channels. These experiments are implemented using MATLAB functions. Structurally Similarity (SSIM) index and PSNR in dB are used for comparison purposes. A 25 x 25 Gaussian blur with standard deviation σ =1.6 is convolved with a set of color images. A disk function with radius r= 5 is used to produce Out-of-focus blur and based on [18] motion blur images are generated. These blurred images are added with white Gaussian noise with variance equal to 0.2 and 1 respectively. The experiment is performed by considering i) Patch size of 5x5, ii) Number of outer iterations as 3, iii) Search neighborhood size as 11x11 and iv) Number of inner iterations as 30. Table I summarizes h, η, β parameter values and maximum number of inner CG iterations that are used for Gaussian and out-of-focus blur images.

TABLE I.
DIFFERENT SET OF PARAMETERS IN COLOR IMAGE DEBLURRING METHOD

Experiment	η	β	h	Inner CG iterations
Gaussian (σ2 = 0.2)	0.003	0.23	5.3	100
Gaussian (σ2 =1)	0.0078	0.001	7.7	100
Motion Blur (σ2 = 0.2)	0.005	0.41	6.2	100
Motion Blur (σ2 = 1)	0.01	0.01	6.6	80

This method runs four times faster than implemented on IDDBM3D algorithm on a 2.8GHz Intel Core i7 processor. The two-step IDDBM3D algorithm decouples deblurring and denoising process. It depends on suitable estimate from other deblurring algorithm in its grouping phase. But Iterative Graph based method relies on initial denoising and it handles noise amplification issues in much better way. Table II and III summarizes the numerical deblurring results for the images degraded with Gaussian and out-of-focus blur. This method is compared with IDDBM3D algorithm with $\sigma^2 = 0.2$ and $\sigma^2 = 1$. Images of Book-Shelf, Brain Tumor, Human Face, Satellite Image and Scenery are collected. Figure 3 shows the deblurring results for the images degraded with Gaussian blur. The original images are in first row. Gaussian blur images are in second row and third row shows deblurred images. Figure 4 shows Out-of-focus blurred and deblurred images. This algorithm performs better visual quality which can be noticed in smooth face parts of an image. Table IV illustrates the significant results in case of motion deblurring. These are compared with Hyper-Laplacian Method. Figure 5 shows motion blurred and deblurred images. It is observed that Iterative Graph (IG)-based Image Restoration method produces high quality outputs.

TABLE II.
PSNR AND SSIM PERFORMANCE OF AN ITERATIVE GRAPH (IG) BASED METHOD AND IDDBM3D WITH KERNEL SIZE OF 25 X 25 AND WITH STANDARD DEVIATION 1.6 FOR GAUSSIAN BLUR

Blur/Images	Gaussian ($\sigma^2 = 0.2$)				Gaussian ($\sigma^2 =1$)			
	Iterative Graph-based method		IDDBM3D method		Iterative Graph-based method		IDDBM3D method	
	PSNR	SSIM	PSNR	SSIM	PSNR	SSIM	PSNR	SSIM
Scenery	28.99	0.9793	28.57	0.9726	28.62	0.9683	27.89	0.9576
Human Face	33.84	0.9756	33.18	0.9693	32.94	0.9630	32.34	0.9522
Brain Tumor Image	28.80	0.9732	27.88	0.9677	28.34	0.9677	28.29	0.9624
Satellite Image	28.36	0.9791	27.56	0.9760	27.22	0.9675	26.24	0.9623
Book-Shelf	27.25	0.9827	28.25	0.9841	26.27	0.9717	27.31	0.9787

TABLE III.
PSNR AND SSIM PERFORMANCE OF AN ITERATIVE GRAPH (IG) BASED METHOD AND IDDBM3D WITH DISK FUNCTION OF RADIUS 7 FOR OUT-OF-FOCUS BLUR GENERATED IMAGES

Blur/Images	Out-of-focus($\sigma^2 = 0.2$)				Out-of-focus ($\sigma^2 =1$)			
	Iterative Graph-based method		IDDBM3D method		Iterative Graph-based method		IDDBM3D method	
	PSNR	SSIM	PSNR	SSIM	PSNR	SSIM	PSNR	SSIM
Scenery	28.64	0.9542	28.44	0.9511	27.80	0.9369	26.90	0.9178
Human Face	33.06	0.9489	32.28	0.9609	31.42	0.9201	30.85	0.9058
Brain Tumor Image	29.71	0.9524	29.35	0.9514	27.13	0.9050	27.09	0.9003
Satellite Image	28.08	0.9609	26.92	0.9542	25.75	0.9177	24.04	0.8974
Book-Shelf	27.60	0.9711	28.19	0.9709	25.63	0.9405	24.64	0.9337

TABLE IV.
PSNR AND SSIM PERFORMANCE OF AN ITERATIVE GRAPH BASED METHOD AND HYPER-LAPLACIAN METHOD FOR CAMERA MOTION BLUR

Blur/Images	Motion ($\sigma^2 = 0.2$)				Motion ($\sigma^2 = 1$)			
	Iterative Graph-based method		Hyper-Laplacian Method		Iterative Graph-based method		Hyper-Laplacian Method	
	PSNR	SSIM	PSNR	SSIM	PSNR	SSIM	PSNR	SSIM
Scenery	29.47	0.9741	29.74	0.9732	28.48	0.9521	28.43	0.9507
Human Face	33.54	0.9636	33.53	0.9624	32.15	0.9354	31.99	0.9351
Brain Tumor Image	31.11	0.9791	31.01	0.9766	29.75	0.9507	20.21	0.9354
Satellite Image	29.47	0.9743	29.37	0.9734	28.45	0.9525	28.42	0.9507
Book-Shelf	28.81	0.9857	29.24	0.9839	27.31	0.9711	27.61	0.9680

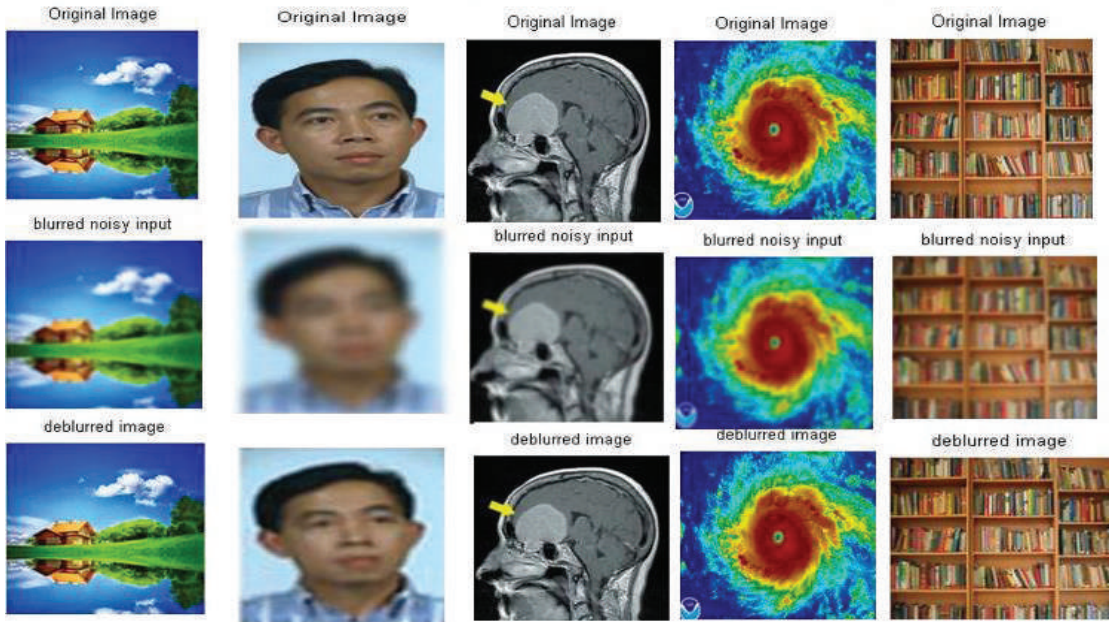

Figure 3. Deblurring example for different Images: First row is Oiginal Image, second row is Gaussian blur Image and third row is deblurred output image

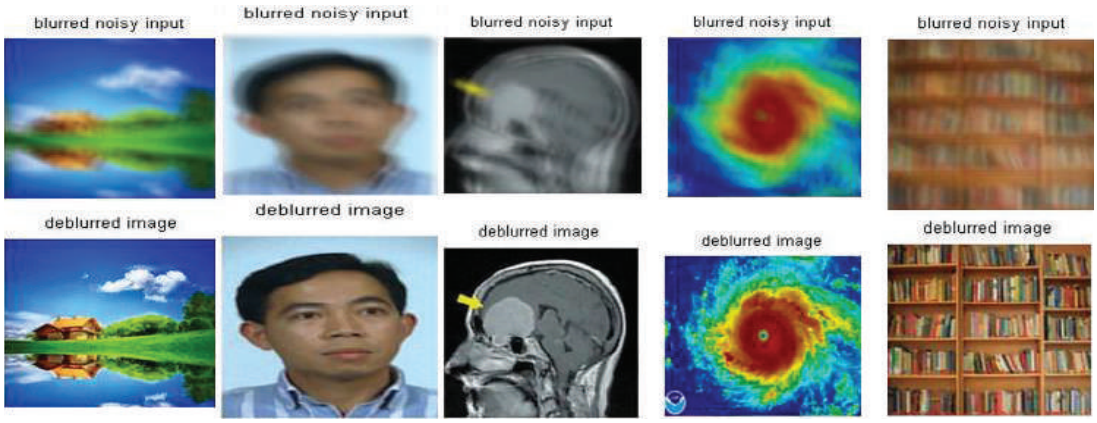

Figure 4. Deblurring examples for Motion Blur: First row are Motion blur Images and second row are deblurred output images

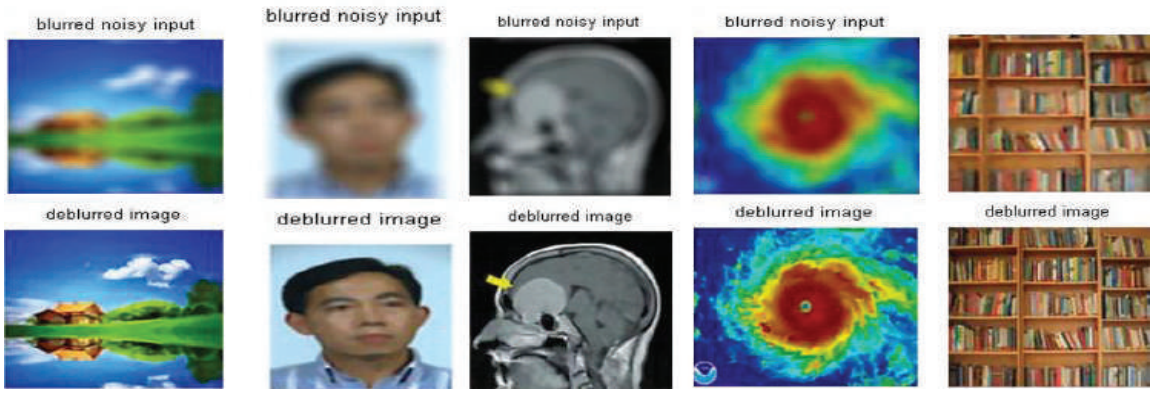

Figure 5. Deblurring examples for Out-of-focus: First row are Out-of-focus blur Images and second row are deblurred output images.

VI. Conclusions

A wide framework for an Iterative graph based image restoration method has been implemented. An Objective function couples the data and prior terms through Laplacian matrices. The data adaptive approach is improved by graph based filtering approach. This method has been verified for different blurring conditions with some existing state of art algorithms. Based on the appropriate selection of kernel similarity matrix K, many different restoration tasks can be handled. This method can be further extended with blind image deblurring techniques and applied for more complicated non-uniform blurring conditions.

References

[1] G. Chantas, N. P. Galatsanos, R. Molina, and A. K. Katsaggelos,"Variational Bayesian image restoration with a product of spatially weighted total variation image priors," *IEEE Trans. Image Process.*, vol. 19, no. 2, pp. 351–362, Feb. 2010.

[2] W. Dong, L. Zhang, G. Shi, and X. Li, "Nonlocally centralized sparse representation for image restoration," *IEEE Trans. Image Process.*, vol. 22, no. 4, pp. 1620–1630, Apr. 2013.

[3] J. Ni, P. Turaga, V. M. Patel, and R. Chellappa, "Example-driven manifold priors for image deconvolution," *IEEE Trans. Image Process.*, vol. 20, no. 11, pp. 3086–3096, Nov. 2011.

[4] T. S. Cho, C. L. Zitnick, N. Joshi, S. B. Kang, R. Szeliski, and W. T. Freeman, "Image restoration by matching gradient distributions," *IEEE Trans. Pattern Anal. Mach. Intell.*, vol. 34, no. 4, pp. 683–694, Apr. 2012.

[5] S. Lefkimmiatis, A. Bourquard, and M. Unser, "Hessian-based norm regularization for image restoration with biomedical applications," *IEEE Trans. Image Process.*, vol. 21, no. 3, pp. 983–995, Mar. 2012.

[6] Danielyan, V. Katkovnik, and K. Egiazarian, "BM3D frames and variational image deblurring," *IEEE Trans. Image Process.*, vol. 21, no. 4, pp. 1715–1728, Apr. 2012

[7] A.Levin, R. Fergus, F. Durand, and W. T. Freeman, "Image and depth from a conventional camera with a coded aperture," *ACM Trans. Graph.*, vol. 26, no. 3, Jul. 2007, Art. ID 70.

[8] L. Yuan, J. Sun, L. Quan, and H.-Y. Shum, "Progressive inter-scale and intra-scale non-blind image deconvolution," *ACM Trans. Graph.*, vol. 27, no. 3, Aug. 2008, Art. ID

[9] Q. Shan, J. Jia, and A. Agarwala, "High-quality motion deblurring from a single image," *ACM Trans. Graph.*, vol. 27, no. 3, pp. 1–10, Aug. 2008, Art. ID 73.

[10] [P. A. Knight and D. Ruiz, "A fast algorithm for matrix balancing," *IMA J. Numer. Anal.*, vol. 33, pp. 1029–1047, 2013.

[11] T. Hofmann, B. Schölkopf, and A. J. Smola, "Kernel methods in machine learning," *Ann. Statist.*, vol. 36, no. 3, pp. 1171–1220, 2008.

[12] A. Buades, B. Coll, and J. M. Morel, "A review of image denoising algorithms, with a new one," *Multiscale Model. Simul.*, vol. 4, no. 2, pp. 490–530, 2005.

[13] P. Knopp and R. Sinkhorn, "Concerning nonnegative matrices and doubly stochastic matrices," *Pacific J. Math.*, vol. 21, no. 2, pp. 343–348, 1967.

[14] U. Von Luxburg, "A tutorial on spectral clustering", Statistics and computing, vol. 17, no. 4, pp. 395–416, 2007.

[15] P. Milanfar, "A tour of modern image filtering: New insights and methods, both practical and theoretical," *IEEE Signal Process. Mag.*, vol. 30, no. 1, pp. 106–128, Jan. 2013.

[16] S. Bougleux, A. Elmoataz, and M. Melkemi, "Local and nonlocal discrete regularization on weighted graphs for image and mesh processing," *Int. J. Comput. Vis.*, vol. 84, no. 2, pp. 220–236, 2009.

[17] S. Ramani, T. Blu, and M. Unser, "Monte-Carlo SURE: A blackbox optimization of regularization parameters for general denoising algorithms," *IEEE Trans. Image Processing*, vol. 17, no. 9, pp. 1540–1554, Sep. 2008.

[18] Q. Shan, J. Jia, and A. Agarwala, "High-quality motion deblurring from a single image," *ACM Trans. Graph.*, vol. 27, no. 3, pp. 1–10, Aug. 2008, Art. ID 73.

Hybrid Method for PAPR Reduction in SFBC OFDM Systems

Balla Bhavani[1] and Thota Sravanti[2]
[1]M.Tech Student, CVR College of Engineering/ECE Department, Hyderabad, India
Email: bhavani333balla@gmail.com
[2]Asst. Professor, CVR College of Engineering/ECE Department, Hyderabad, India
Email: sravanti23@gmail.com

Abstract*: Orthogonal Frequency Division Multiplexing is an important technique in wireless communication systems. Multiple Input Multiple Output (MIMO)-OFDM with Space Frequency Block Code (SFBC) is a smart technique used due to its capability to support elevated data rates, large capacity and robust to multipath fading. A high peak-to-average-power ratio is one of the disadvantages of OFDM. Many PAPR Reduction techniques have been introduced like Companding and Selective mapping (SLM) techniques. In proposed method, the optimum PAPR can be achieved than above methods by a new hybrid method i.e., combining *SLM* and *Companding techniques.

***Index Terms:* Orthogonal Frequency Division Multiplexing, MIMO-OFDM, SFBC, SLM, Companding**

I. Introduction To MIMO-OFDM

The data which is to be communicated wirelessly has been transferred by analog domain in the earlier days which has been mostly done by digital domain in now a days. To make the process easier, multiple sub-carriers are implemented in the system instead of single carrier.

A. OFDM

According to the challenge of this generation, the need and priority of elevated speed communication evolves into various multicarrier modulation techniques, among these techniques OFDM technique is one. OFDM is the frequency-division multiplexing (FDM) system used as a multi-carrier tone technique. To transmit the information, the huge amount of narrowly spaced orthogonal sub-carriers is used and the data is alienated as similar streams of channels. The sub-carriers are modulated with keying techniques (such as QPSK) at a subtle symbol rate in the same bandwidth.
Applications: Asymmetric Digital Subscriber Line, Digital Audio Video broadcast TV systems etc.,. *Advantages:* Saving of Bandwidth, Protection against Inter-Symbol-Interference, Easy Equalization etc.,. *Disadvantages:* Synchronization and High peak-to-average-power ratio (PAPR) [1] [2].

B. MIMO-OFDM

OFDM system plus MIMO have the ability to transmit huge data. In MIMO system the channel capacity can be enhanced by transmitting the data from several numbers of transmitters side to many numbers of receivers side are efficiently combined. The class of wireless describes three basic parameters namely the transmission rate, the range and reliability. Due to these parameters, this technology stands as major attracting technique in wireless communications and becomes an significant part of modern wireless communication principles such as 3GPP long term evolution, 4G, IEEE 802.11n (Wi-Fi) [3]. According to broadband wireless MIMO-OFDM communication systems initial field tests, it has been exposed that the better coverage area, reliability and capacity are reachable with the support of MIMO techniques.

The foremost techniques concerned in MIMO system are: *Pre-coding* is the ray forming method which is generally implemented at the transmitter part, requires precise information of channel state information (CSI). *Spatial multiplexing* method, the lofty information signal is divided into low data streams and the streams are transmitted with the aid of diverse transmit antennas which are having the similar frequency. *Diversity coding* techniques are used at the transmitter with no channel knowledge. In diversity coding, the single data flow is transmitted with a coding procedure called space-frequency coding.

C. Alamouti Space-Frequency Diversity

Space - Frequency codes are engaged to make sure that the signals transmitted in different antennas are orthogonal to each other so that it is trouble free for the receiver to discern one from another. For Line-of-sight (LOS) contact among two stations dual antenna polarization is used to make certain one robust path. To achieve the benefits offered by MIMO systems, *Alamouti Scheme* can be performed [4]. It is the easy way of acquiring transmit diversity in the task of two transmit antennas (also known as transmission/reception scheme) is easy to implement.

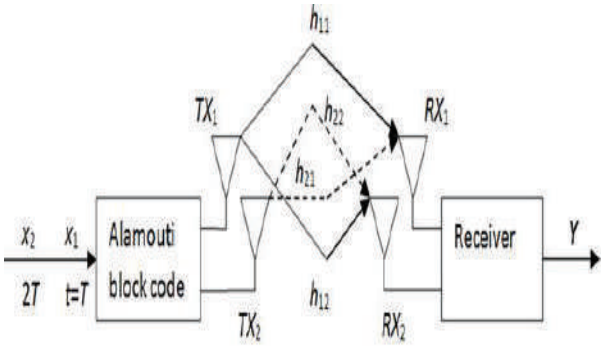

Figure 1. Alamouti Scheme

D. PAPR

The peak to average power ratio of the transmitted signal [4] is:

$$PAPR(x[n]) = \max_{0\le n\le N-1} \frac{|x[n]|^2}{E[|x[n]|^2]}. \quad (1)$$

Expressing in deciblels: *PAPRdB = 10log10 (PAPR)*

E. CDF

The Cumulative Distribution Function (CDF) is used to measure the efficiency and Complementary CDF (CCDF) and is used to compute the probability of any PAPR technique.

F. PAPR Reduction Techniques

PAPR reduction techniques are dependent on various factors and differ according to the needs of the system. Many factors are in use before adopting a PAPR reduction technique [5] like capacity, loss in data rate, increase in power in transmit signal, complexity of computation and bit-error rate performance.

Clipping and Filtering: In this procedure, the threshold value of the amplitude is fixed and the amplitude of the sub-carrier over the threshold is clipped or it is filtered to produce a minimum PAPR[6].

Companding Transform (CT): This transform can be designed to meet excellent transaction between PAPR reduction and BER performance with two inflexion points in order to increase the flexibility of companding [7].

Selective Mapping (SLM): In this process, the representation of information in a group of ample dissimilar information blocks that are similar as the unique data blocks which are selected. Thus, it is suitable for transmission if the selection of data blocks have low PAPR value [8] [9].

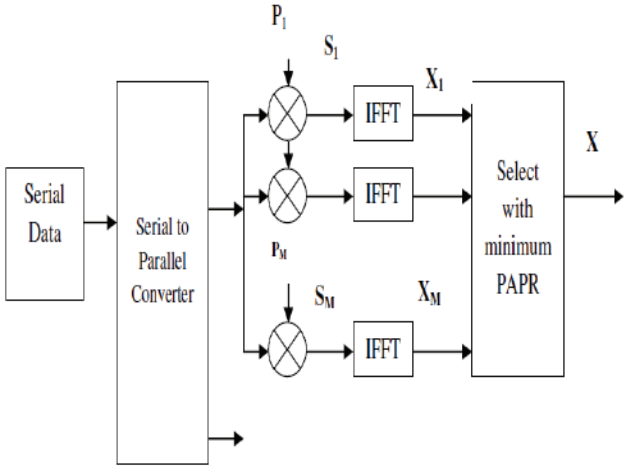

Figure 2. Selective-Mapping Technique

Partial Transmit Sequence (PTS): The information which is to be sent in the signal as a whole is covered by the transmission of only part of the data of varying sub-carrier is called Partial Transmit Sequence Technique [10].

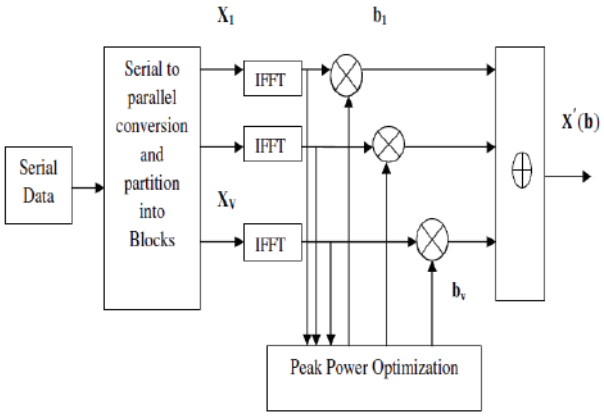

Figure 3. Block Diagram of Partial Transmit Sequence

II. PROPOSED HYBRID METHOD

A. Hybrid Method

The hybrid method comprises of merging the MIMO-OFDM method with SLM method and Companding Mu-law technique. The method is as follows:

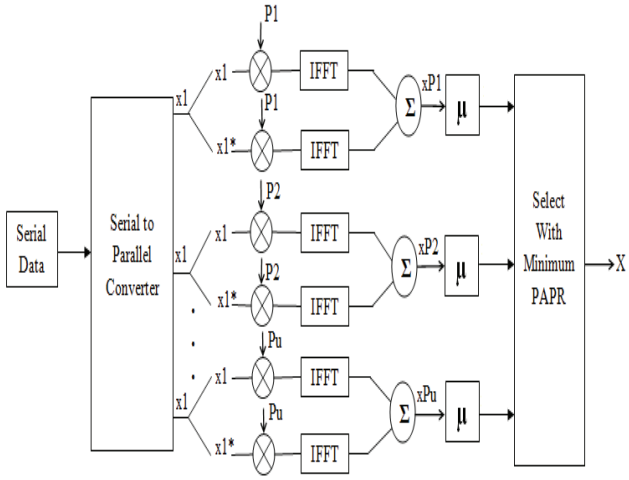

Figure 4. Block Diagram of Hybrid Method

Companding Mu-Law Technique: - It has little complexity despite of the numeral subcarriers in an OFDM signal. In OFDM system, signal will be kept unchanged by taking the suitable companding factors in Companding process [11].

The Mu-law:

$$y(x) = V \frac{\log(1+\mu\frac{|x|}{V})}{\log(1+\mu)} sgn(x) \quad (2)$$

The original OFDM symbol is partitioned into sub-blocks and are computed with phase rotation sequences, then each OFDM symbol is companded using Mu-law technique. By the selection block, the comparatively lowest PAPR can be obtained [12].

The program procedure will be written in the flowchart as follows:

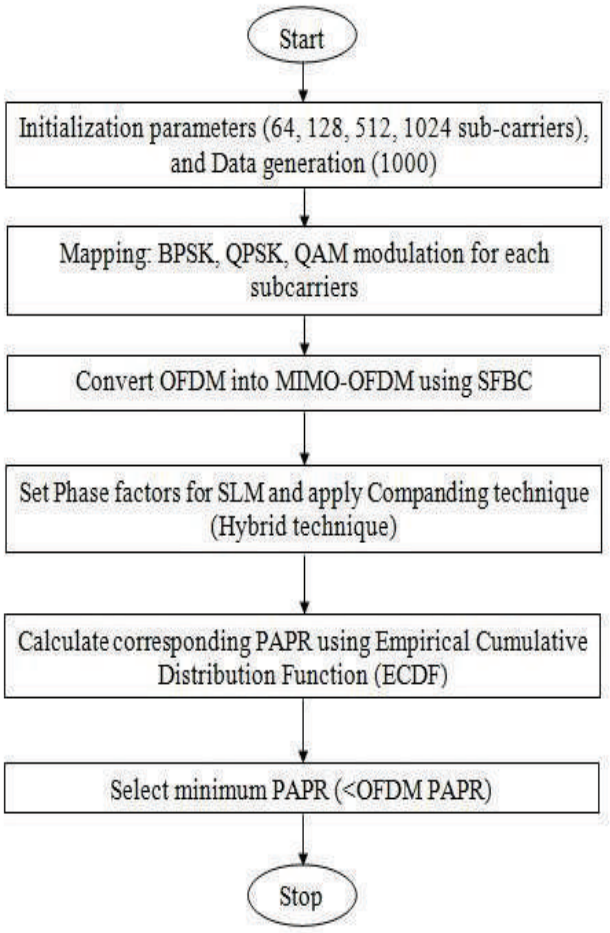

Figure 5. Flow Chart of Hybrid Method

B. Simulation Results

SLM technique is applied to the sub blocks of the input information, and modulated by QPSK technique and phase factors (±1, ±j) are directly transmitted to the receiver through sub block. Complementary Cumulative Distribution Function is used for the performance evolution and it is evaluated for different number of sub-carriers such as 64, 128. The oversampling factor is greater than 4 which is used to increase the resolution of discrete time OFDM signal. The implementation of PAPR reduction in SFBC MIMO OFDM systems has been done with 64, 128 symbols of OFDM generation bits and oversampling is applied to all OFDM symbols [13] [14].

The Figure 6, 7 show the simulation of PAPR reduction of symbol length in MIMO-OFDM by using SLM technique.

The PAPR value of MIMO-SLM method for 1000 symbols when the number of sub-carriers = 64 is 6.8dB.

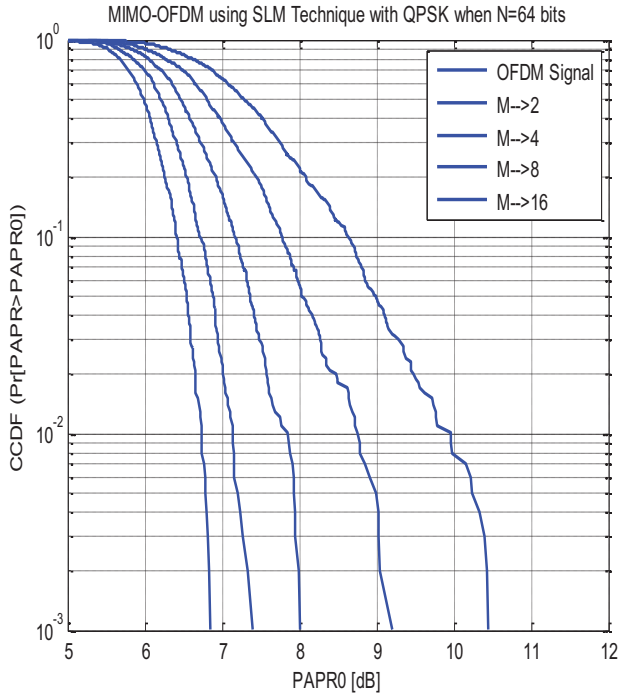

Figure 6. Performance Analysis of the MIMO-SLM Method with QPSK Modulation With N = 64 Bits

The PAPR value of MIMO-SLM method for 1000 symbols when the number of sub-carriers = 128 is 7.6dB.

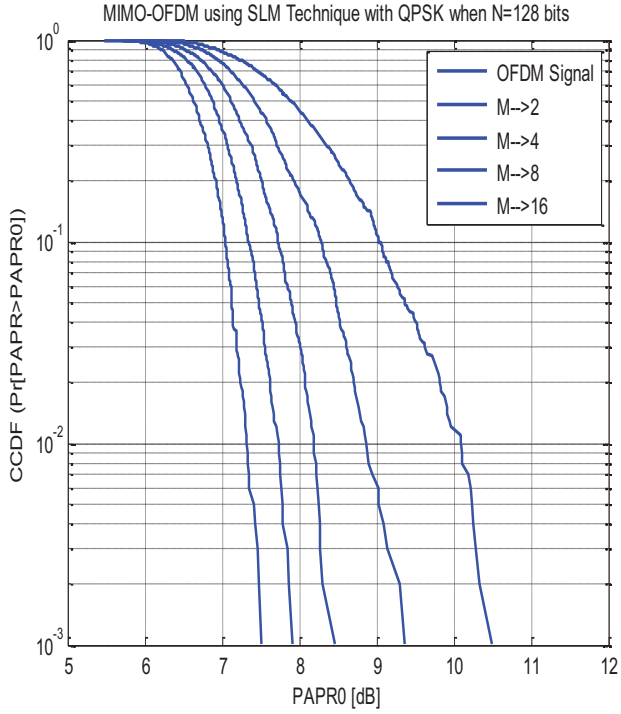

Figure 7. Performance Analysis of the MIMO-SLM Method with QPSK Modulation with N = 128 Bits

The Figure 8, 9 show the simulation of PAPR reduction of symbol length in MIMO-OFDM by using the combination of SLM and Companding Mu-law technique.

The PAPR value of the proposed Hybrid method for 1000 symbols when the number of sub-carriers = 64 is reduced from 6.8dB to 4.9dB.

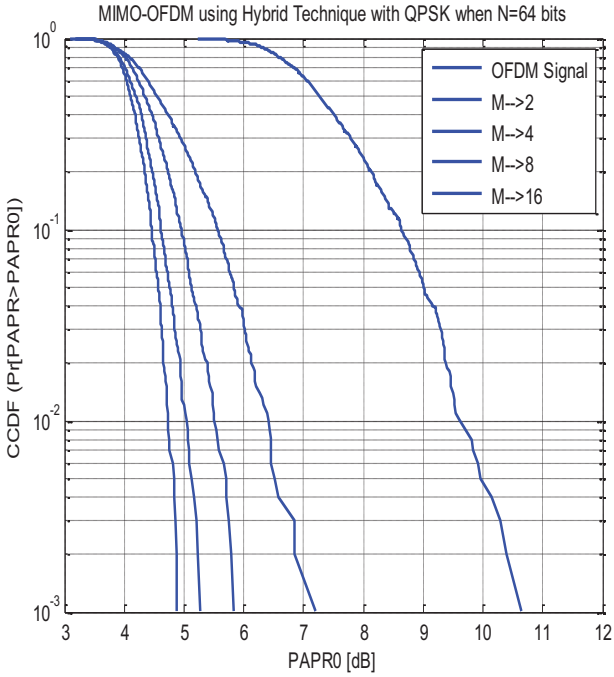

Figure 8. Performance Analysis of the Proposed Hybrid Method with QPSK Modulation With N = 64 Bits

The PAPR value of the proposed Hybrid method for 1000 symbols when the number of sub-carriers = 128 is reduced from 7.6dB to 5.9dB.

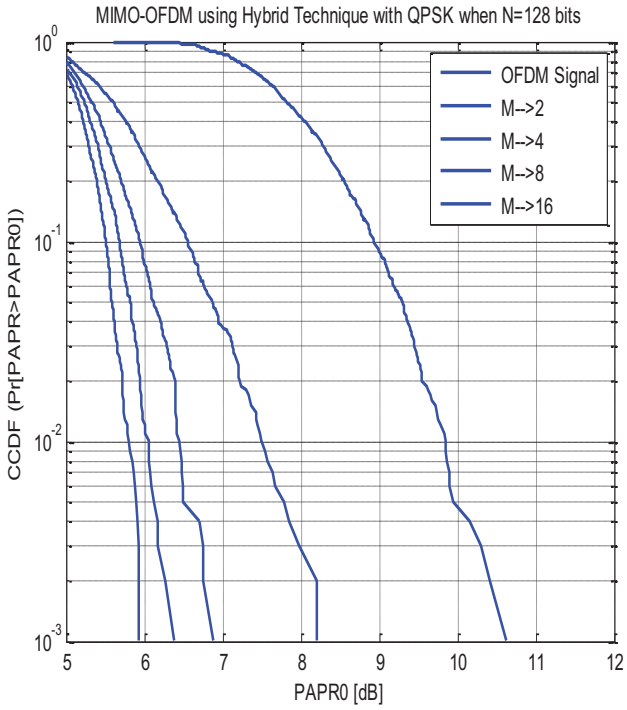

Figure 9. Performance Analysis of the Proposed Hybrid Method with QPSK Modulation With N = 128 Bits

III. Conclusions

For both wired and wireless communications high data rate transmission, OFDM is a spectrally efficient multi-carrier modulation method. MIMO-OFDM suffers with high PAPR and many reduction techniques have been proposed [15]. By comparing these things, the proposed method which is hybrid method has been implemented to reduce PAPR. For N=64, the PAPR of MIMO-OFDM using SLM is 9.2dB. Hence MIMO-OFDM using SLM technique reduced PAPR of about 1dB. In the projected technique the PAPR for N=64 is 7.0dB, thus the PAPR is diminished to 2.2dB than MIMO-OFDM with SLM. In future, the hybrid method can be designed by combining MIMO-OFDM with SLM and any other Companding technique like A-law, Exponential law and Tangent law. Hence hybrid method is a good technique for reducing PAPR and this evaluation can be considered as a valuable research resources.

References

[1] Y.Wu and W. Y. Zou, "Orthogonal frequency division multiplexing: A multi-carrier modulation scheme," IEEE Trans. Consumer Electronics, vol. 41, no. 3, pp. 392–399, Aug. 1995.

[2] E. Telatar, "Capacity of multi-antenna Gaussian channels," European Transactions on Tele-communications, vol. 10, no 3, Dec 1999.

[3] T. S. Rappaport, *"Wireless Communication: Principles and Practice"*: 2nd Edition, Prentice Hall, 2002.

[4] Tolga M. Duman and Ali Ghrayeb, *"Coding for MIMO Communication Systems"*: John Wiley and Sons Ltd, Chichester, England 2007.

[5] S. H. Han, J. H. Lee, "An Overview of Peak – to – Average Power Ratio Reduction Techniques for Multicarrier Transmission", *IEEE Transaction on Wireless Communication,* April 2005.

[6] R. O"Neil, L. B. Lopes, "Envelope Variations and Spectral Splatter in Clipped Multicarrier Signals", *Proc. IEEE PIMRC '95,* Toronto, Canada, September 1995.

[7] Yasir Rahmatallah, Seshadri Mohan, "Peak-To-Average-Power Ratio Reduction in OFDM Systems: A Survey And Taxonomy", *IEEE COMMUNICATIONS SURVEYS & TUTORIALS, VOL. 15, NO. 4, FOURTH QUARTER* 2013.

[8] S. Y. L. Goff, B. K. Khoo, C. C. Tsimenidis, B. S. Sharif, "A Novel Selected Mapping Technique for PAPR Reduction in OFDM Systems", *IEEE Transactions on Communication,* Vol. 56, No. 11, November 2008.

[9] S. Y. L. Goff, S. S. Al – Samahi, B. K. Khoo, C. C. Tsimenidis, B. S. Sharif, "Selected Mapping Without Side Information for PAPR Reduction in OFDM", *IEEE Transactions on Wireless Communications,* Vol. 8, No. 7, July 2009.

[10] S. H. Han, J. H. Lee, "PAPR Reduction of OFDM Signals Using a Reduced Complexity PTS Technique", *IEEE Signal Processing Letters,* Vol. 11, No. 11, November 2004.

[11] T. Deepa, R. kumar, "Performance analysis of mu-law companding & SQRT techniques for M-QAM OFDM systems", *IEEE International Conference ON Emerging Trends in Computing, Communication and Nanotechnology (ICECCN),* 2013.

[12] G. S. Siva Priya, B. Senthil, "An efficient sheme for PAPR reduction in Alamouti MIMO-OFDM systems", *International Conference on Information Communication and Embedded Systems (ICICES2014).*

[13] S. H. Muller, J. B. Huber, "A Comparison of Peak Power Reduction Schemes for OFDM", *Proc. IEEE GLOBECOM '97,* Phoenix, AZ, November 1997.

[14] R. W. Baumi, R. F. H. Fisher, J. B. Huber, "Reducing the Peak – to – Average Power Ratio of Multicarrier Modulation by Selected Mapping", *Elect. Lett.,* Vol. 32, No. 22, October 1996.

[15] Poonam Kundu, Prabhjot Kaur, "Comparision of peak to average power reduction techniques in OFDM", *International Conference on Advances in Computing, Communications and Informatics (ICACCI)*, 2014

Regulation of Frequency and Load Flow Study in a Multi-Area Power System Under Contingencies with the Inclusion of Wind-Generation

K.S.V. Phani Kumar[1], Kalluri Deepika[2], S. Venkateshwarlu[3]
[1]Asst. Professor, CVR college of Engineering /EEE Department, Hyderabad, India
Email: phani5016@gmail.com
[2]Asst. Professor, CVR college of Engineering /EEE Department, Hyderabad, India
Email: deepika.kalluri@gmail.com
[3] Professor, CVR College of Engineering/ EEE Department, Hyderabad, India
Email: svip123@gmail.com

Abstract: **A Sudden loss of a generating station and a sudden switching of heavy loads in the system are the major challenges for a power engineer. Coordinated scheduling of power is necessary to maintain the system parameters under control. In this paper a two-area power system is simulated for contingencies and the frequency deviation is controlled. The load flow studies are also conducted to study the behavior of the system. The results show that the variation of the frequency is within the allowable standards while the system is stable during the period.**

Index Terms: **Frequency Regulation, Wind Generation, Contingency, Multi-area system.**

I. Introduction

A multi area system model has been in practice for a long time [1]. The exchange of power between different areas is based on the balance between the generation and demand in each area. Over the years many advancements happening in the field of renewable energies made it possible to have power generation using sources like wind and solar extensively in MW scales [2-3].

It is a dual problem that the load is not controllable and the power generated by the wind turbines is unpredictable. These two problems are partly addressed in the literature individually [3]. There are advanced topologies available to make the power output of wind to be constant and demand side management makes it easy to control the generation based on generation-scheduling [4].

In each area of power system, the generation should be equal to the load plus the losses incurred in transmission of power [5]. Whenever there is a mismatch, the frequency in the system is varied accordingly. To regulate the frequency, deficit or surplus power should be generated or consumed respectively so that frequency is not deviated out of the limits of ±1%.

The stability of the system is understood when there are contingency studies performed on the system. These include faults, loss of generation units, equipment outages, switching on/off heavy loads etc., which impact the overall system behavior. The stability study includes the frequency deviation, observability and controllability of the system under transient and dynamic states of the system.

In this paper, contingency situation is created like loss of generation during steady state and loss of heavy load on the system, to analyze the system behavior like frequency deviation and load flow study.

The organization of this paper is done as follows: Section II describes the system under investigation. The wind generator model is briefly discussed in section III. Detailed analysis and discussion during contingencies are done with the simulation results in the section IV. The conclusions from the results are given in the section V.

II. System Under Investigation

A two-area power system is considered here in the paper. The description of the two areas considered in the paper is given below.

A. Area-1

Area-1 consists of a synchronous generator connected to a transmission line of 10KM length, which is in turn connected to the distribution system within the area. A wind generator is also connected to a grid via a 25 KM transmission line. The power is generated at a voltage of 575V. This is stepped up to a voltage of 20KV and then to 230KV for transmission. A combination of active and reactive loads is considered and modeled as RLC elements. These loads consume a total active power of 800 MW and a reactive power of 287 MVAR. The total capacity of the synchronous generators is 900MVA, while the rated capacity of the wind generator is 500 MVA. The wind turbine and generators are modeled to have variable wind speeds as input and proportional output can be expected from the stator terminals of the generator.

B. Area-2

The second area considered in the paper consists of a similar system with two generators serving a total active power demand of 100 MW and a total reactive power of 437 MVAR.

Generator-1 having a capacity of 900MVA is connected to the PCC via a step-up transformer (20KV / 230 KV) through a transmission line of 10KM length.

Generator-2 of 900MVA capacity is connected to the PCC through a 25KM line at 230KV using a step-up transformer.

The parameters of the transmission line and the transformer are given in Table-1. The schematic of the

system considered for area-1 and area-2 are shown in Fig. 1 and Fig. 2.

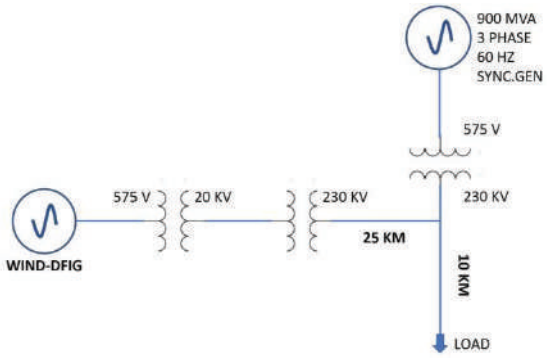

Figure 1. Single line diagram for Area-1.

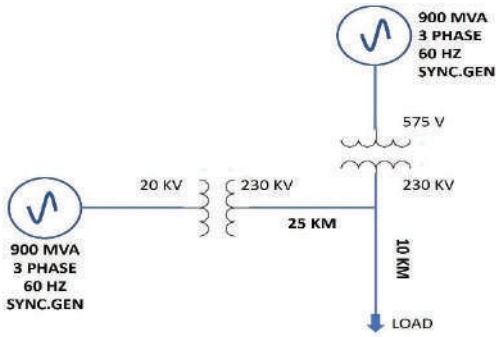

Figure 2. Single line diagram for Area-2.

TABLE I.
TIE LINE TRANSMISSION CONDUCTOR PARAMETERS

Parameter	Value
Resistance per unit length (Ohms/km)	0.0529
Inductance per unit length (H/km)	0.001403
Capacitance per unit length (F/km)	5.014e-9
Line length (km)	220

C. Interconneced System

For power exchange between two neighboring areas, tie-lines are provided [6]. Whenever there is a deficiency of power experienced, a request to buy power can be raised to the neighboring area [7]. Similarly, if there is excess power generation happening in the area, it can be sent to the other areas based on their requests. In this paper a double circuit line is taken between the two areas, separated over 220KM. One of the lines has circuit breakers connected at both ends. The parameters of the tie-line are given in Table II. The overall schematic of the system is shown in Fig. 3.

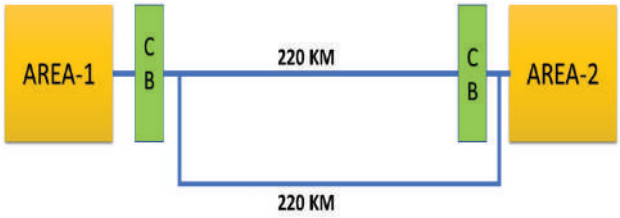

Figure 3. Overall Power System Considered

III. WIND GENERATOR – MODEL CONSIDERED

The wind generator considered in this paper is a doubly fed induction generator suitable for controlling the power output of the generator, as the stator and the rotor are controllable [8]. Here the stator output terminals are tapped and a part of the power generated is used to control the rotor. Maximum energy can be extracted from the varying wind speed energy by electronically interfacing the rotor conductors. The power electronic circuit typically includes AC to DC and DC to AC converters connected back to back. (Less than 25% of the generated power is used for this purpose). The main purpose of this is to convert varying output power to a constant power with controllable frequency and amplitudes. The power factor compensation can also be provided on-board with the electronic circuit with low expenditures. [9-12].

One of these converters is on the grid side and the other is on the machine side. The schematic for voltage control and hence the power factor control is done as shown in the block diagram below. The overall schematic of the doubly-fed induction generator is as shown in Fig. 4. The MATLAB model used in the simulation is considered with the following parameters shown in Table II.

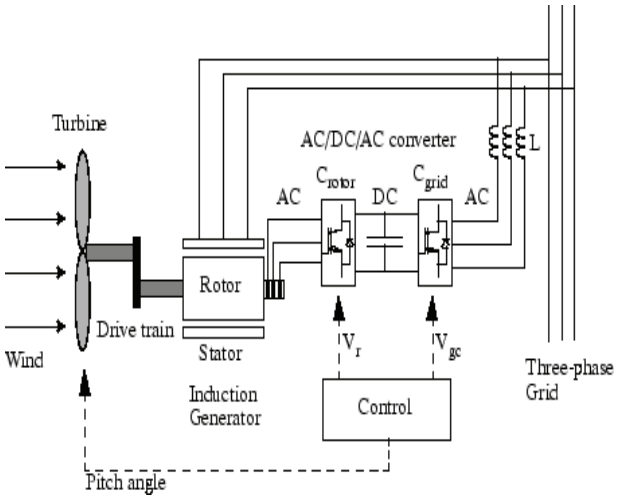

Figure 4. Wind Generator Schematic diagram

IV. Contingency Analysis And Simulation Results

The system described in the Fig. 3 is simulated in MATLAB as shown in Fig. 5.

TABLE II.
WING TURBINE-GENERATOR PARAMETERS

Parameter with units	Value
Nominal power (VA)	6*1.5e6/0.9
line-to-line voltage (Vrms),	575
frequency (Hz)	60
Nominal wind turbine mechanical output power (W):	6*1.5e6
Pitch angle controller gain [Kp]:	500
Converter maximum power (pu):	0.5
Grid-side coupling inductor [L (pu) R (pu)]:	[0.15 0.15/100]
Nominal DC bus voltage (V):	1200
Droop Xs (pu):	0.02
Grid voltage regulator gains: [Kp Ki]	[1.25 300]
Reactive power regulator gains: [Kp Ki]	[0.05 5]
Power regulator gains: [Kp Ki]	[1 100]

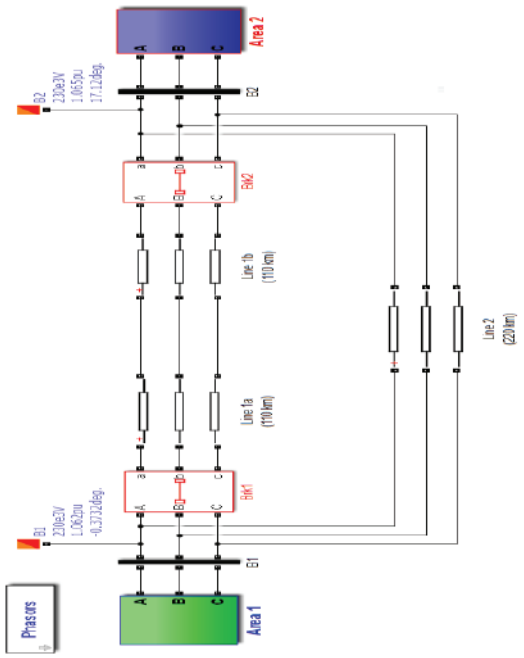

Figure 5. MATLAB model considered for the overall power system

Two different contingency situations are considered here in the paper as discussed in chapter I. They are (i) Loss of heavy load in Area-1, making the generation more than the demand and hence the frequency is expected to shoot up. Secondly, (ii) Loss of generation in Area-1, so that the generation is less than the demand. In this case, the frequency is expected to be less than the nominal.

The behavior of the system under a steady state with no contingencies is analyzed first. The system is simulated from an initial state/zero state. The load flow study is conducted on the system at the buses mentioned in Fig. 5 and the results are given in Table III. The frequency of the system and the power consumption levels are shown in Fig. 6 and 7.

TABLE III .
LOAD FLOW STUDY SCENARIO-1

Appearance		
PARAMETER	P(MW)	Q(Mvar)
Total generation	15.95807	16.40149
Total PQ load	0	0
Total losses	0.538139	15.98149
B1 V= 1.000 pu/230kV -23.67 deg		
PARAMETER	P(MW)	Q(Mvar)
Generation	-134.042	13.06714
PQ Load	0	0
B1	-144.252	12.85714
B2	144.79	3.124345
B2 V= 1.000 pu/230kV 0.00 deg ; Swing bus		
PARAMETER	P(MW)	Q(Mvar)
Generation	-134.042	13.06714
PQ Load	0	0
B1	-144.252	12.85714

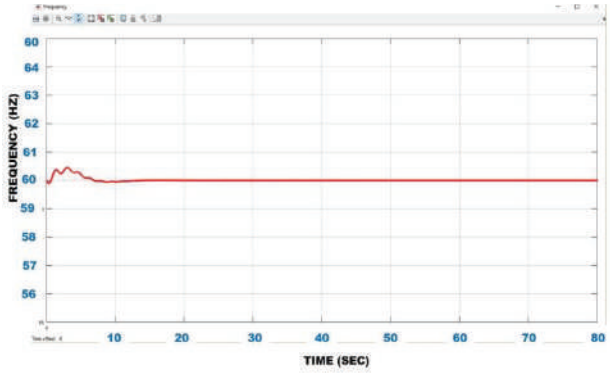

Figure 6. Frequency response under normal conditions

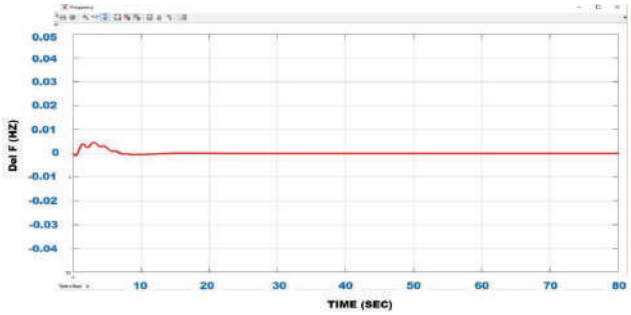

Figure 7. Change in Frequency response under normal conditions

A. Scenario-1 loss of load:

The system is scheduled to expect a loss of heavy load (900 MW) at time t= 40s. Various parameters like frequency, real power and reactive power drawn from the sources, the load sharing at the buses, the voltage profiles at the buses can be analyzed pre and post event using the Table III obtained from the simulation of the system for a time of 80s.

From Fig. 8 and Fig. 9, we can analyze that the system frequency variation after the event has to be controlled and limited to be within the acceptable range of ±1% which is [59.4 60.6]. A maximum excursion of 0.6% is present and it is settled within 10s.

Scenario-2 Loss of Generation:

Due to unexpected lower wind speeds, (speeds less than the cut-in speeds of the turbine), the generator output is not sufficient to be synchronized with the grid. So, there is a loss of generation expected/scheduled at 40s.

Fig. 10 shows the frequency variation in the system during pre and post events. At 40s, there is a disturbance in the frequency, but due to the help of area-2, the frequency is restored. The disturbance caused in the area-2 frequency can also be observed in the figure 10.

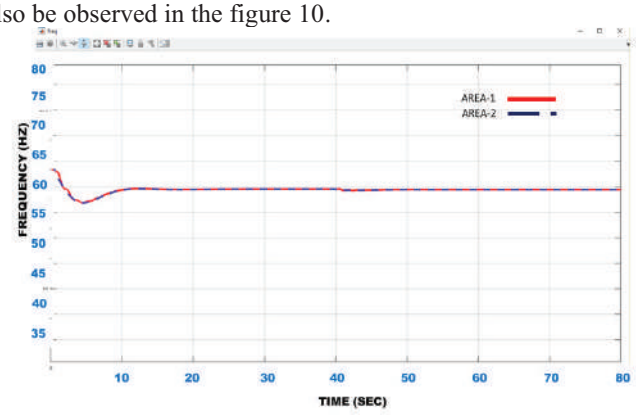

Figure 8. Frequency response under Scenario-1 in Area-1,2

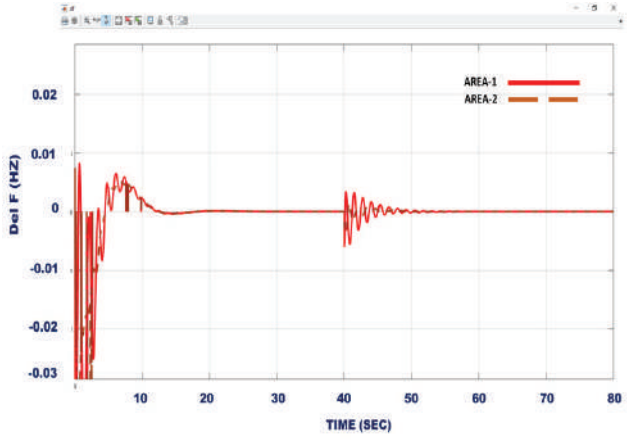

Figure 9. Change in Frequency response under Scenario-1 in Area -1,2

The maximum rate of change of frequency can also be observed from the Fig. 13. The minimum and maximum frequencies during the event are 59.96Hz and 60.04Hz which are limited to the standards of allowable deviation of ±1%.

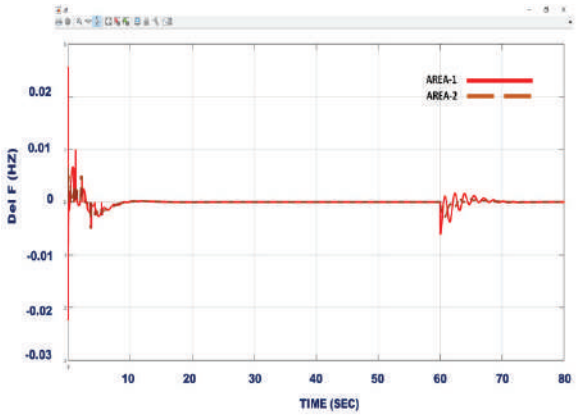

Figure 10. Frequency response under Scenario-2 in Area-1,2

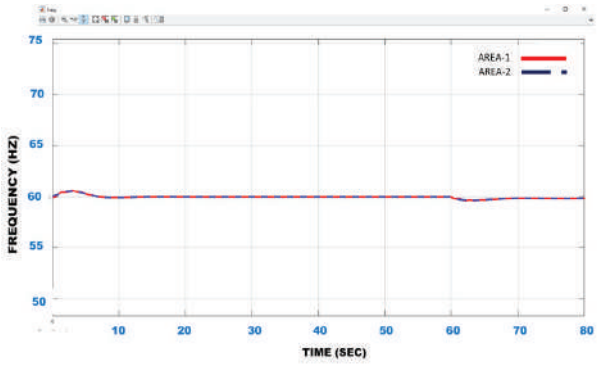

Figure 11. Change in Frequency response under Scenario-2 in Area -1,2

V. CONCLUSIONS

A multi-level power system is considered in the paper with wind-energy generation in area-1. The contingency situations of sudden loss of generation and sudden loss of loads are simulated for a two-area system with one of the areas having Wind-turbine generator. The results show that the frequency deviation and the voltage profiles are within the limits in the two situations.

REFERENCES

[1] I. J Nagrath and D. P Kothari Modern power system analysis-TMH 1993.

[2] Elgerd Ol. Electric energy systems theory- an introduction, 2nd ed.Tata McGrawHill:2000

[3] Elgerd Ol. Fosha C,"Optimal megawatt frequency control of multi area electric energy systems", IEEE Trans Electric Power Apparatus System, vol.PAS-89, pp.556-63, 1970.

[4] K.S.V.Phani Kumar, S.Venkateshwarlu, " A Review on Power Quality in Grid Connected Renewable Energy System", CVR Journal of Science and Technology, pp.84-89, Volume 5, Dec 2013.

[5] Kalluri Deepika, " A Distributed Generation System with Micro Grid for Effective Energy Management", CVR Journal of Science and Technology, pp.65-69, Volume 9, Dec 2016.

[6] Yao Zang, "Load Frequency Control Of Multiple-Area Power Systems" Tsinghua University July, 2007 Master of science in Electrical Engineering.

[7] D. N. Trakas, E. M. Voumvoulakis and N. D. Hatziargyriou, "Decentralized control of power system zones based on

probabilistic constrained load flow," *2014 International Conference on Probabilistic Methods Applied to Power Systems (PMAPS)*, Durham, 2014, pp. 1-6.

[8] K. Siraj, H. Siraj and M. Nasir, "Modeling and control of a doubly fed induction generator for grid integrated wind turbine," *2014 16th International Power Electronics and Motion Control Conference and Exposition*, Antalya, 2014, pp. 901-906.

[9] S. Pati, K. B. Mohanty, A. Choudhury and S. Kar, "Integration and power control of a micro-hydro-PV-wind based hybrid microgrid," *2017 International Conference on Circuit ,Power and Computing Technologies (ICCPCT)*, Kollam, 2017, pp. 1-6.

[10] M. T. L. Gayatri, A. M. Parimi and A. V. P. Kumar, "Utilization of Unified Power Quality Conditioner for voltage sag/swell mitigation in microgrid," *2016 Biennial International Conference on Power and Energy Systems: Towards Sustainable Energy (PESTSE)*, Bangalore, 2016, pp. 1-6.

[11] M. T. L. Gayatri, A. M. Parimi and A. V. P. Kumar, "Application of Dynamic Voltage Restorer in microgrid for voltage sag/swell mitigation," *2015 IEEE Power, Communication and Information Technology Conference (PCITC)*, Bhubaneswar, 2015, pp. 750-755.

[12] M. T. L. Gayatri and A. M. Parimi, "Mitigation of supply & load side disturbances in an AC Microgrid using UPQC," *2016 IEEE 6th International Conference on Power Systems (ICPS)*, New Delhi, 2016, pp. 1-6.

Estimating the Performance Ratio and Degradation Factor of Rooftop Solar PV Plant

Rajesh Kumar Prakhya[1] and Ch.Lokeshwar Reddy [2]
[1]Assoc. Professor, CVR College of Engineering /EEE Department, Hyderabad, India
Email: rajeeecvr@gmail.com
[2]Assoc. Professor, CVR College of Engineering /EEE Department, Hyderabad, India
Email: reddy.lokeshwar@gmail.com

Abstract: **This paper investigates the effect of degradation on the grid connected rooftop solar plant. The effect of degradation and plant performance are evaluated and analyzed for 20kWp SPV plant on rooftop of EEE Block in CVR College of Engineering for the year 2015 and 2016. The above analysis is done manually from the plant data extracted from web-interface. The degradation of the plant is analyzed by first calculating the performance ratio of the plant for two successive years. Later the percentage change in the plant Performance Ratio's are calculated. This investigation reveals that degradation of the plant performance is high in summer season because of increased ambient temperature. The degradation is more during the month of May and less during the month of February. The reasons for this kind of performance are analyzed. After analyzing the results, it is recommended that plant should be maintained and inspected at regular interval for the improved performance.**

Keywords: Degradation factor, Grid Connected Solar PV Plant, Panel degradation, Performance Metrics, Performance Ratio (PR), System Performance.

I. INTRODUCTION

One of the best ways to generate electrical energy from the solar radiation is by Photo-Voltaic effect. In this process the solar radiation is directly converted into DC electrical energy using the Solar Cell. One solar cell can generate only small amount of electrical power. Hence, to generate moderate power, large number of solar cells are connected either in series or parallel to form a Solar array to get the required electrical power from solar energy.

Grid connected PV systems are widely being used because of their own advantages. Power production from these Solar PV plants to be monitored properly for better utilization of plant and available resources [1-4]. The performance of these plants cannot be judged easily by considering the quantity of energy generated from the plant every day. The output of solar plant depends upon the amount of solar irradiation that falls on effective surface area of Solar PV array. This solar radiation is not the same throughout the year and every location. It is good in summer, adequate in winter and moderate in monsoon season. Hence, justifying the performance of the plant based on the amount of electrical energy generated by the plant is not hypothetical. Therefore, to analyze the performance of PV plants, few metrics are essential. Performance Ratio (PR) is the most important metric that is adopted by the solar industry experts to analyze the performance of the plant.

Climatic conditions like high temperature and high humidity have negative influence on performance and consistency of the SPV modules. Besides the module performance, inverter efficiency is also a significant factor which greatly impacts the overall performance of the system and behavior. Besides temperature, many factors that influence the performance of SPV plants are solar insolation, shading effect, effect of climate, wind speed, electrical load matching, dust on panels, accuracy of MPPT operation and various losses that are occurring in the system like array capture losses, soil losses, inverter losses, etc. The solar industry experts need to understand every influencing parameter and its effect on the performance of plant. [5-6].

Performance of the PV module decreases at faster rate compared to other equipment, as modules are exposed to direct weather conditions. The degradation rate is normally high in the first year upon initial exposure to the solar light. Later it stabilizes. Factors affecting the degree of degradation include, quality of the material used in manufacturing, packing of solar cells, process of manufacturing modules and solar cell technology.

Factors for degradation are high winds, soil, dust, snow, fog, discoloration, lamination defects, mechanical stress and cell contact breakdown. Another important factor is breakage of Ethylene Vinyl Acetate (EVA) encapsulation, which is used as a back sheet of the PV module by UV light.

One of the important factors to be considered is that, all the modules will not degrade at same rate. Their degradation rate is different from one module to another module. Proper maintenance and inspection should be done at the site in regular intervals for better performance of the plant over a long time.

In this paper, Section II describes the location of the plant and capacities of the sub-plants located in the site. Section III, clearly discusses the performance analysis of Grid connected plant using Performance Ratio and Degradation Factor in detail. Section IV, systematically analyzes the results and discussion on Plant performance using these parameters followed by conclusion and references.

II. Specifications of Grid Connected SPV Plant

Specifications and design of every grid connected SPV plant depends upon many factors like weather conditions, local load requirements, nature of the loads, maximum demand etc. The geographical coordinates of site/plant determine the seasonal tilt angle of the solar modules.

A. Location of the plant

The grid connected SPV plant for this investigation is located on the rooftop of the CVR College of Engineering, Hyderabad, Telangana state. The global coordinates of the site are Latitude: 17.20^0 N, Longitude: 78.60^0 E. This site location is at an altitude of 545 m. above the sea level.

B. Capacities Of Photo Voltaic Plant

The maximum capacities of various grid connected SPV sub plants on the rooftops of different independent buildings in CVR College of Engineering are tabulated in Table I including the commercial dates of operation of each sub plant with their full name plate ratings.

TABLE I.
Details of Sub Plants, Their Capacities and Date of Commencement of Plant

Name of the Sub Plant	Location of the Plant	Installed Power	Date of Commencement of Plant
CVR PG Block	EEE Block	120 kWp	03-03-2014
Single Axis Tracking	Main Block	40 kWp	18-01-2015
Library	Library Block	20 kWp	23-10-2014
Single Axis Polar Tracking	Main Block	40 kWp	11-03-2015
CVR CS Block	CSE Block	60 kWp	22-10-2015
CVR New	First Year Block	80 kWp	03-03-2016
Overall Plant Capacity		**360 kWp**	**----**

The important electrical apparatus that are required for the grid interactive SPV plants are: Solar PV Modules (Array), DC Solar Cables, Grid tied String Inverters, AC Cables, Junction Boxes, Switchgear Equipment, Net-Metering facility (Bi-directional energy meter), Lighting Arrestors and electrical earthing's at appropriate locations. All the apparatus, components and devices used in this SPV sub-plants are according to the IEC 61724 standards as per the guidelines given by MNRE [7].

String inverter is the power electronic device that converts the DC electricity generated by the Solar Array from incident solar radiation into 3-phase AC electrical energy at PCC. Fig. 1 shows the 20kW grid tied REFU*sol* 008K-020K string inverter used in this 20kW grid connected solar PV plant. Its maximum efficiency is 98.2% at STC conditions. For every 20kW array one independent string inverter is commissioned. Table II. shows the other important inverter data as given by the manufacturer.

The term solar PV array is defined as the interconnection of different solar modules either in series/ parallel depending upon system design, rating and configuration. The modules used in this rooftop SPV plant are supplied by Kohima Energy Pvt. Ltd. The model number of the module is KE-60-M250, with peak DC electrical power rating of 250Wp at STC conditions (25^0C ambient temperature, 1000 W/m^2 Insolation, Air mass ratio is 1.5). The other Specifications of Solar Module -KE-60-M250 are given in Table III. [8].

TABLE II.
Details of Grid Integrated Refusol 020k Solar String Inverter

	REFUsol 020K
DC DATA	
Recommended Max. PV Power, kWp	21.6
MPPT Range	480 V-850 V
DC Start Voltage	350 V
Max. DC Voltage	1000 V
Max. DC Current	41 A
MPP Trackers	1
AC DATA	
Rated AC Power	19.2 kVA
Max. AC Active Power	19.2 kW
Rated Power factor	1
Max. AC current	3 X 29
Distortion factor THD	<1.8 %
Max. efficiency	98.20%
European efficiency	97.80%

Figure 1. String Inverter used in SPV plant on rooftop of EEE Block

As per this design, there are 80 such KE-60-M250 solar modules. These 80 modules are further connected in 4 parallel strings. Each string consists of 20 modules in series. Fig.2 shows the onsite photograph of a 20kW rooftop grid connected plant commissioned on the Library block. Present investigation on performance ratio and degradation factor was performed on the 20kWp grid connected SPV plant commissioned on the rooftop of the library block.

Figure 2. 20kWp Solar PV Plant on EEE Block of CVR College of Engineering

TABLE III.
SPECIFICATIONS OF SOLAR MODULE KOHIMA ENERGY PVT. LTD.

STC–Irradiance of 1000 W/Sq. m at 25°C	KE-60-M250
Maximum Power (P_{max})	250 W
Maximum Power Voltage(V_{mp})	31.44 V
Maximum Power Current(I_{mp})	7.95 A
Open circuit Voltage(V_{oc})	37.86 V
Short Circuit Current(I_{sc})	8.69 A
Fill Factor	75.98%
Module Efficiency(η)	15.40%
Nominal Operating Cell Temperature (NOCT)	45+2
Temperature Coefficient of Isc (α)	0.04 /^{0}C
Temperature Coefficient of Voc (β)	-0.32 /^{0}C
Temperature Coefficient of Pmax (ϒ)	-0.45 /^{0}C
Cells per module	60
Cell type	Multi - Crystalline Silicon
Cell Dimensions	156 m.m X 156 m.m

III. PERFORMANCE ANALYSIS (PR & DEGRADATION)

A. Performance Ratio (PR)

Performance Ratio is one of the most significant metrics that is used for evaluating grid connected SPV plants. The empirical formula to evaluate the PR is as follows.

PR= Actual AC Energy generated by plant / Nominal Energy

Where Nominal Energy =

GHI (in kWh/m^2) X Rated module efficiency X Total Active PV area (in m^2) (1)

The Performance Ratio is generally evaluated for a year to get a complete idea about the plant. PR also can be evaluated on daily, weekly, or monthly basis. Depending on the period of evaluation, corresponding parameters are chosen. In the above empirical formula, the denominator expression consists of GHI, Module efficiency and Active PV area. The value of the Module efficiency is picked from nameplate ratings given by the panel manufacturer. Active area is strictly the area covered by polycrystalline solar cells alone in the entire solar array. Whereas GHI of site or plant location depends upon several factors like ambient temperature, temperature of the cell, soil and losses due to dust, partial shading, weather conditions, etc. Hence calculation of PR takes all the above factors into consideration. Consequently, the influence of all the above parameters will be replicated in the Performance Ratio evaluation. If the evaluated PR value is near 100 %, one can conclude that PV plant is in excellent operating condition.

The manual procedure to evaluate the PR of the SPV plant is as follows:

- Determine the time of analysis (Optimum period is one calendar year).
- Active PV area of the solar array has to be computed by number of modules used in PV array.
- Collect the information about PV module efficiency from the datasheets.
- AC electrical energy output of the Plant from the inverter data.
- By using the irradiance sensor (Pyranometer) gather the values of the measured solar insolation values.

PR is the appropriate performance metric to compare the performance of various SPV plants at different locations independent of weather and climate conditions. Deviations from the expected PR indicate either a fault in the system or a problem within the PV plant itself.

PR is the most accepted global standard to measure the performance of a SPV plant. Periodically few stakeholders and Independent Power Producers (IPP) are very keen to evaluate and compare the PR's of the dissimilar rated solar plants across the globe, which are located at different geographical locations [9-16].

B. Degradation Factor

Degradation is an industry term that is used to describe the decrease in the power output of the solar PV plant over a period of time. The degradation mainly happens in solar modules, inverters and Cables used in the PV plant. All components definitely degrade, but degradation rate is not uniform for all the equipment used in the system. High attention must be paid towards module degradation. Because, solar modules are the critical devices that collect the solar energy from the sun and convert it into DC electricity. If the panels/modules degrade at faster rate, the output power from the modules will decrease day by day resulting in poor energy yield of the plant for life time. Factors affecting the degree of degradation include, quality of the material used in manufacturing, packing of solar cells, and solar cell technology. Other important factor is breakage of Ethylene Vinyl Acetate (EVA) encapsulation, which is used as a back sheet of the PV module by UV light.

IV. RESULTS & DISCUSSIONS

Solar Radiation values of the site are gathered from the data available by the NASA at the nearest location. The table IV demonstrates the monthly solar radiation values at the site for the year 2015 and 2016. Fig.3 shows the graphical representation of the same for the years 2015 and 2016 of the 20kWp SPV plant on rooftop of Library Block.

TABLE IV.
MONTH WISE SOLAR RADIATION VALUES FOR THE YEARS 2016 AND 2015 OF 20KW SPV PLANT

Month & Year	**Solar Radiation 2016**	**Solar Radiation 2015**
January	158.4	154.7
February	169.6	169.9
March	178.9	184.9
April	188.3	197.8
May	201.1	201.7
June	153.2	151.4
July	140.4	169.3
August	150.4	152.4
September	111.6	149.5
October	148.6	155.5
November	139.7	153.2
December	143.2	149.7
Average	156.95	165.83

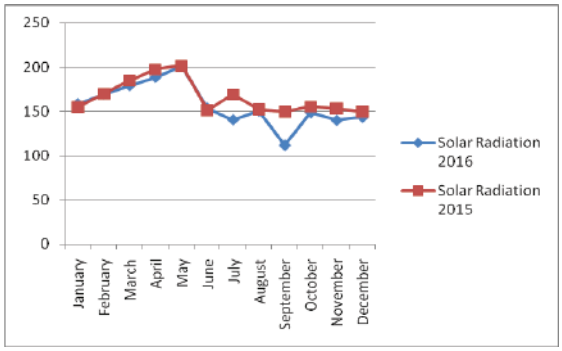

Figure 3. Monthly Solar radiation values for the years 2015&2016 of 20kW$_p$ SPV plant on rooftop of Library Block

A. Calculation of Performance Ratios (at STC)

Table V and Table VI show the calculated monthly nominal Performance Ratios of the plant at STC conditions for the year 2015 & 2016 respectively. All the PR values are calculated by looking at the name plate details of STC conditions (STC conditions are 25° C of ambient temperature, Solar radiation of 1000 W/m^2 and Air-mass ratio of 1.5). The calculated Performance Ratio's at STC conditions are also called as Nominal Performance Ratios. Temperature corrected Performance ratio is getting popular nowadays for better analysis. However, Nominal Performance ratios are used in this work for the analysis of plant performance.

These monthly calculated PR's are compared and analyzed to estimate the degradation of the plant output. The important fact to be understood here is, plant output is always dependent upon solar radiation input to the modules. If the radiation is high, energy output will be high and vice versa. Estimating the degradation rate only using energy output will not give feasible results. For instance, from the Fig. 3, during the months of July and September, solar radiation values are less in the year 2016 compared to 2015. However, corresponding PR's are higher in the year 2015 than in 2016. Hence, it is always better to compare the Performance Ratio's of the plant than comparing the energy output.

TABLE V.
MONTH-WISE AVERAGE ACTUAL AC ENERGY GENERATED, AVERAGE THEORETICAL DC ENERGY COULD GENERATED AT 25°C AND NOMINAL PR OF 20KW SPV PLANT FOR THE YEAR 2015

Month & Year	AC Energy Produced Year 2015	Theoretical DC Energy 2015	PR2015
January	2611.85	2782.92	93.85
February	2787.53	3056.36	91.20
March	2988.03	3326.20	89.83
April	2929.68	3558.26	82.33
May	2973.22	3628.42	81.94
June	2262.63	2723.56	83.08
July	2567.97	3045.57	84.32
August	2365.32	2741.55	86.28
September	2351.52	2689.38	87.44
October	2588.20	2797.32	92.52
November	2581.72	2755.94	93.68
December	2518.12	2692.98	93.51
Average	2627.15	2983.20	88.06

TABLE VI.
MONTH-WISE AVERAGE ACTUAL AC ENERGY GENERATED, AVERAGE THEORETICAL DC ENERGY COULD GENERATED AT 25°C AND NOMINAL PR OF 20KW SPV PLANT FOR THE YEAR 2016

Month & Year	**AC Energy Produced Year 2016**	**Theoretical DC Energy 2016**	**PR2016**
January	2606.70	2849.48	91.48
February	2744.10	3050.96	89.94
March	2791.40	3218.26	86.74
April	2720.00	3387.36	80.30
May	2788.50	3617.62	77.08
June	2207.40	2755.94	80.10
July	2063.50	2525.68	81.70
August	2283.10	2705.57	84.39
September	1720.40	2007.59	85.69
October	2429.60	2673.19	90.89
November	2314.10	2513.09	92.08
December	2355.90	2576.05	91.45
Average	2418.72	2823.40	85.67

B. Calculation of Degradation Factor

Table VII compares the amount of AC energy generated by the plant in the year 2015 & 2016. Fig. 4 shows the graphical comparison of the same. Similarly, Table VIII shows the comparison of the Performance Ratio's of the plant for the year 2015 & 2016. Fig.5 represents the graphical comparison of the same data. From the graphs, it is observed that, the Performance Ratio's of the plant for the year 2015 is slightly higher than the performance Ratio's for the year 2016. This drop in the performance ratio is due to degradation in various components used in the system. If the degradation factor is even 1% per a year, it may result in high payback period. Fig. 6 shows the graphical representation of the month-wise percentage degradation values [17].

TABL VII.
MONTH WISE AC ENERGY PRODUCED FOR THE YEARS 2016 AND 2015 AF 20KW SPV PLANT

Month & Year	AC Energy Produced in Year 2016	AC Energy Produced in Year 2015
January	2606.70	2611.85
February	2744.10	2787.53
March	2791.40	2988.03
April	2720.00	2929.68
May	2788.50	2973.22
June	2207.40	2262.63
July	2063.50	2567.97
August	2283.10	2365.32
September	1720.40	2351.52
October	2429.60	2588.20
November	2314.10	2581.72
December	2355.90	2518.12
Average	2418.72	2627.15

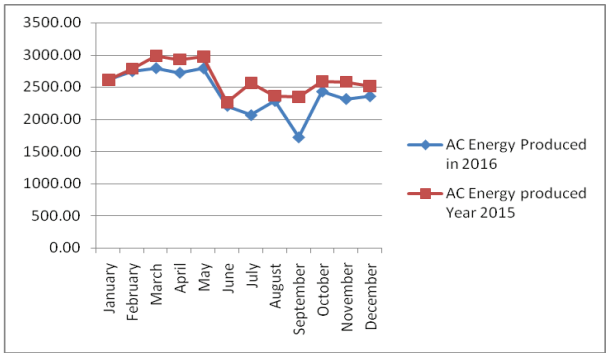

Figure 4. Monthly AC energies produced by the plant for the years 2015&2016 of 20kW$_p$ SPV plant on rooftop of Library Block

TABLE VIII.
MONTH WISE PERFORMANCE RATIO VALUES FOR THE YEARS 2016 AND 2015 OF 20KW SPV PLANT

Month & Year	PR 2016	PR 2015	% Degradation
January	91.48	93.85	2.53
February	89.94	91.20	1.38
March	86.74	89.83	3.45
April	80.30	82.33	2.47
May	77.08	81.94	5.93
June	80.10	83.08	3.59
July	81.70	84.32	3.10
August	84.39	86.28	2.19
September	85.69	87.44	1.99
October	90.89	92.52	1.77
November	92.08	93.68	1.70
December	91.45	93.51	2.20
Average	85.67	88.06	2.72

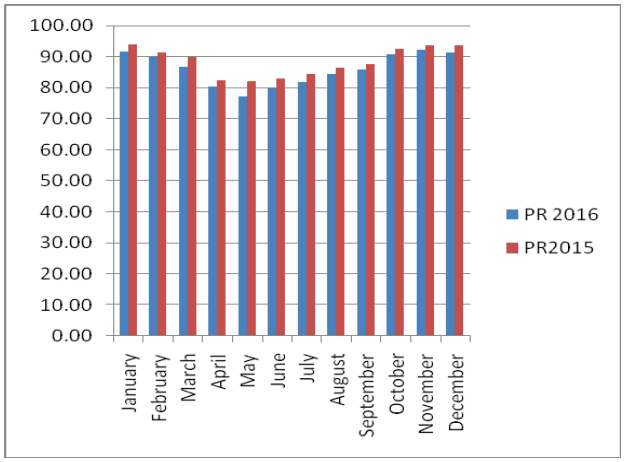

Figure 5. Monthly Performance Ratios of the plant for the years 2015&2016 of 20kW$_p$ SPV plant on rooftop of Library Block

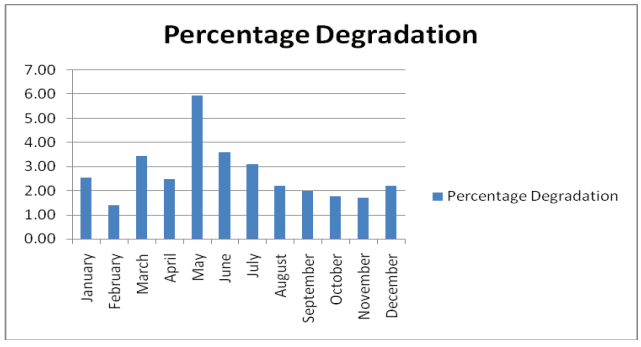

Figure 6. Monthly percentage degradation of 20kW$_p$ SPV plant on rooftop of Library Block from 2015 and 2016 PR data

V. CONCLUSIONS

In this research, the effect of degradation on the Performance of 20kWp grid connected SPV plant on rooftop of Library block was analysed from 2015&2016. During the period March to June, the degradation values are significantly more because of increase in ambient temperature causing more power losses at module level. The

calculated degradation factors were found to be a little higher than expected values. These values should be minimised by taking proper measures for better performance of the solar plant in terms of degradation. It is recommended that modules must be cleaned at regular intervals either before sunrise or after sunset as the main reason for degradation is observed to be dust and soling. The maximum value of the performance ratio is observed in the month of Jan 2015 with 93.85% and minimum value is observed to be in the month of May 2016 with 77.08%. After comparing the PR's of plant for successive years, the maximum degradation is observed to be in the month of May'16 because of high ambient temperature and minimum in the month of February'16 because of clear sky conditions. It is also observed that the overall plant performance is satisfactory as per industry standards.

REFERENCES

[1] Razykov TM, Ferekides CS, Morel D, Stefanakos E, Ullal HS, Upadhyaya HM. Solar photovoltaic electricity: current status and future prospects. Sol Energy 2011; 85: 1580;1608.

[2] Ali Hajiah, T.K., K. Sopian, M. Sebzali1, Performance of grid connected photovoltaic system in two sites in Kuwait, 2013, Kuwait Institute for Scientific Research (KISR): Kuwait. International Journal of Photoenergy Volume 2012 (2012), Article ID 178175, p. 20.

[3] S. Elhodeiby, H. M. B. Metwally, and M. A. Farahat, "Performance Analysis of 3.6 kW Rooftop Grid Connected Photovoltaic System in Egypt," in Proceedings of International Conference on Energy Systems and Technologies (ICEST 2011), Cairo, Egypt, 2011, pp. 151-157.

[4] S. Singh, R. Kumar and V. Vijay, "Performance analysis of 58 kW grid-connected roof-top solar PV system," Power India International Conference (PIICON), 2014 6th IEEE, Delhi, 2014, pp. 1-6.

[5] Yan S, Lai-Cheong C, Lianjie S, Kwok-Leung T. Real-time prediction models for output power and efficiency of grid-connected solar photovoltaic systems. Appl Energ 2012; 93: 319;326.

[6] Al-Sabounchi AM, Yalyali SA, Al-Thani HA. Design and performance evaluation of a photovoltaic grid-connected system in hot weather conditions. Renew Energy 2013; 53: 71;78.

[7] Data sheet of REFUlog Inverters

[8] Data sheet of Kohima Energy Pvt Ltd.

[9] Whitepaper on PR vs. CUF provided by CHROSIS Sustainable Solutions.

[10] Padmavathi K, Daniel SA. Performance analysis of a 3 MWp grid connected solar photovoltaic power plant in India. Energy Sustainable Dev 2013;17:615–25.

[11] B.S.Kumar, K.Sudhakar, Performance of evaluation of 10MW grid connected Photovoltaic power plant in India, Energy Reports 1(2015) 184-192.

[12] Shukla, A.K., Sudhakar, K., Baredar, P., 2016a. Simulation and performance analysis of 110 kWp grid-connected photovoltaic system for residential building in India: A comparative analysis of various PV technology. Energy Rep. 2, 82–88.

[13] Shukla, A.K., Sudhakar, K., Baredar, P., 2016b. Design, simulation and economic analysis of standalone roof top solar PV system in India. Sol. Energy 136, 437–449

[14] Kamal Attari, Ali El Yaakoubi,Adel Asselman Comparative Performance Investigation between Photo-voltaic Systems from two different cities, 10th International conference interdisciplinary in Engineering, Proceedia Engineering 181(2017) 810-817. Elsevier, available on www.sciencedirect.com

[15] P.Rajesh Kumar, D.Koteswara Raju, Rajib Kumar Kar "Performance Metrics of Grid Connected Solar PV Plant on Roof top of CVR College of Engineering- A Case Study" Journal of Green Engineering Vol. 7, 99-128 -July 2017.

[16] "Effect of Ambient temperature on performance of Grid-Connected inverter installed in thailand", komonpan, international journal of photo-energy,volume 2014, hindawi publishing.

[17] Role of performance metrics to identify the Gaps in solar power generation, P.Rajesh Kumar ,4th international conference on electrical energy systems ICEES 2018 Feb 2018

Transmission Line Outage Detection and Identification by Communal Spider Optimization Algorithm

R.Vijay
Assoc. Professor, CVR College of Engineering/ EEE Department, Hyderabad, India
Email: vijai.mtp@cvr.ac.in

Abstract: **The load on the power system network is proliferating along with massive inter-area transfers. Hence it is substantial to have reliable real-time information about the network parameters of the electric power system. To monitor real-time operational reliability, the network model of the system has to be updated continuously in a timely manner to reflect current system conditions. For this continuous data updating, the Phasor Measurement Units (PMUs) are deployed. PMUs measure the phase at very high speed at different locations by different devices and synchronize them with time. In manipulating the arithmetical possessions of voltage phase angle capacities attained from PMUs, this method is formulated. The proposed method detects and identifies the line outages in near real-time. In this method, outage in an unknown line is detected by using Communal Spider Algorithm (CSA) and is verified on Indian utility- 62 bus test system. Using CSA, the system performance of the power network model is optimized and the line outage is reduced.**

Index Terms: **Power system network, Line outage, PMUs, Communal Spider Algorithm.**

I. INTRODUCTION

The operational reliability of electric power system should be maintained indispensably to ensure adequacy and security of the system. As far as India is concerned, ensuring the reliability of the power system plays a significant role to maintain the security of power transmission. The major factor affecting the reliability of the system is line outages. Earlier detection of overloading or outage in transmission line may result in prevention of system blackouts [1]. In order to monitor the operational reliability of the power system, a network exemplary of the structure acquired offline which comprises the power transmission system topology considerations is used. Owing to the point that there is an inadequate simultaneous allocation of SCADA or state estimator statistics in India, these power network topology limitations are not generally conversant.

The fallacious telemetry records of the power system network parameters will contribute to overloading of certain lines and may lead to blackouts ultimately. In order to apprise the exemplary employed in the functional reliability analysis for an appropriate way to replicate current coordination circumstances, the PMUs are deployed. The PMU is a modern, fast transducer that provides coordinated phasor measurements of voltages & currents from extensively spread places of the whole power grid. That measures the voltage and current phasor at precise high speed, typically thirty measurements per second [2]. These measurements are obtained from diverse positions by diverse maneuvers and are time-coordinated [3].

Many approaches to detect line outage by identifying the change in network topology errors by using a state estimation technique have been proposed in [4], [5], [6] and [7]. With the far-flung deployment of PMUs, various techniques like hypothesis testing [8], sparse vector estimation [9] and mixed-integer nonlinear optimization [10] have been developed. These methods consider that the line outage as loss of line is in out of service even after the fault detection. Method of persistent line outage detection with PMUs was developed with Quickest Change Detection (QCD) algorithm [11].

This paper attempts to apply the procedure of Communal spider algorithm (CSA) [12] to detect line outage efficiently and optimize the system performance. Many swarm intelligent algorithms have been proposed mimicking the behavior of insect or animal groups prevailing in nature. CSA is formulated by miming the foraging behavior of communal spiders. In CSA, [13] the searching information is propagated among communal spider species through vibrations by which the loss is attained. Hence they distinguish the vibrations generated by the prey with the ones generated by own species. This quality may contribute to the optimum search in some complex multimodal optimization problems which makes CSA preferable over other swarm intelligent techniques. Also, the statistics produced and proliferated through the vibrations are the existing locations in its place of the preeminent locations that might diverge significantly in their exploration. This distinctive penetrating arrangement and its causal social animal foraging stratagem along with the Information Sharing (IS) foraging typical add the complete enactment of CSA when compared to other evolutionary algorithms.

In this proposed method, the voltage phase angle quantities acquired from PMU's are used to sense and recognize line outages in simultaneous. The incremental change in net power injections at each bus is modeled as independent random variables. Any variations in the probability distribution of these random variables are due to the random fluctuations with the generation and load. Probability distribution of net power injections and voltage angle measurements are related by a linear mapping using incremental small signal power flow model. Whenever an outage occurs in a line, the probability distribution of random variable changes. The objective is to notice this modification in the distribution system as speedy as probable by using the

CSA. In this projected technique the point that line outage is tenacious is too amalgamated.

II. Problem Formulation

A. Power system transmission line model prior to outage

Consider a power system with S nodes, each corresponding to a bus and there exists a transmission line between buses a and b such that a, b ∈ S.

Let $V_i(j)$- Voltage of i^{th} bus

$\emptyset_i(j)$ - Phase angle of the corresponding i^{th} bus

$P_i(j)\&Q_i(j)$ – Injected active & reactive power of i^{th} bus at the time instant τ, where $\tau = j\Delta\tau$; j=0,1,2,...; Δτ>0.

The disparities in both the injected active and reactive power in i^{th} bus amongst braces of successive sampling time jΔτ and (j+1)Δτ is set as $\Delta P_i[j] = P_i[j+1] - P_i[j]$ and $\Delta Q_i[j] = Q_i[j+1] - Q_i[j]$ respectively. Similarly, the variations in voltage and phasor angle in bus i between pairs of consecutive sampling times jΔτ and (j+1)Δτ is given by $\Delta V_i[j] = V_i[j+1] - V_i[j]$ and $\Delta\emptyset_i[j] = \emptyset_i[j+1] - \emptyset_i[j]$ respectively. It is considered that the synchronized voltage phasor measurements in all busses are collected using PMU's each Δτ unit of time. Assuming $\Delta V_i[j]$ and $\Delta\emptyset_i[j]$ are sufficiently small, $\Delta P_i[j]$and $\Delta Q_i[j]$ is approximated with first order Taylor's series expansion as

$$\begin{bmatrix}\Delta P[j]\\ \Delta Q[j]\end{bmatrix} = \begin{bmatrix}J_1[j] & J_2[j]\\ J_3[j] & J_4[j]\end{bmatrix}\begin{bmatrix}\Delta\emptyset[j]\\ \Delta V[j]\end{bmatrix} \quad (1)$$

Normally power transmission lines have high (X/R) ratio, i.e. they are mostly reactive. The change in real power is more sensitive to change in phasor angle and less sensitive to change in voltage. Also change in reactive power is more sensitive to change in voltage and less sensitive to change in angle. Hence $J_2\&J_3=0$ and the equation becomes $\Delta P[j] \approx J_1[j]\Delta\emptyset[j]$. Further the following DC assumptions are considered,

1. The system is taken as lossless.
2. The voltage at all buses, $V_i[j]$=1p.u. for all i∈ S, j
3. The difference in phasor angle of voltage $\emptyset_a[j]$-$\emptyset_b[j] \ll 1$ for all j and a, b ∈ S

In these assumptions, the matrix $J_1[j]$ becomes the negative imaginary part of the considered network admittance matrix created, though abandoning line resistance. Hence $J_1[k] = NP_0$ for all i under the same topology. Therefore

$$\Delta P[j] \approx NP_0\, \Delta\emptyset[j] \quad (2)$$

The items in ΔP[j] are exhibited as self-governing and indistinguishably disseminated with a joint Gaussian probability density function, i.e. $\Delta P[j] \sim \mathcal{N}(0,\Sigma)$. The equation is rewritten as $\Delta\emptyset[j] \approx N_0\Delta P[j]$, where $N_0=NP_0^{-1}$. Thus the distribution of system prior to line outage is given by

$$\Delta\emptyset[j] \sim f_0 \text{ where } f_0 = \mathcal{N}(0, N_0\Sigma N_0^T) \quad (3)$$

B. Power system transmission line outage model

Let at time $\tau = \tau_f$ an outage occurs in line (a, b). In this method it is assumed that line losses would not cause islands to practice in the post-event system. The fundamental graph represents the power system gets connected. Moreover, the line loss is presumed as tenacious event, i.e., line is not reverted to service in the period is considered for line outage detection as in [11].

1) Persistent change detection in phasor angle:

As stated above a persistent outage occurs in line (a,b) at time $\tau = \tau_f$ where $(\beta-1)\Delta\tau \le \tau_f \le \beta\Delta\tau$ for some random time β > 0. Fo rj ≥ β, N_0 matrix changes to$N_{(a,b)}$. Hence the post outage equation is

$$\Delta\emptyset[j] \approx N_{(a,b)}\Delta P[j], \quad \text{for } j \ge \beta b \quad (4)$$

The post-outage matrix $NP_{(a,b)}$ is sum of pre-outage matrix NP_0 and some perturbation matrix$\Delta NP_{(a,b)}$. So $NP_{(a,b)} = NP_0+\Delta NP_{(a,b)}$. The non-zero terms in matrix $\Delta NP_{(a,b)}$ are $\Delta NP_{(a,b)}[a,a] = \Delta NP_{(a,b)}[b,b] = -\Delta NP_{(a,b)}[a,b] = -1/X_{(a,b)}$, where $X_{(a,b)}$ is the imaginary part of the impedance of the outaged line [15]. Hence $\Delta NP_{(a,b)}$ is expressed as $\Delta NP_{(a,b)} = -\frac{1}{X_{(a,b)}} v_{(a,b)} v_{(a,b)}^T$, where $v_{(a,b)}$is a vector then $(a-1)^{th}$ item is taken as 1, $(b-1)^{th}$ item is engaged to -1 and rest other items is articulated to 0. Therefore

$$\Delta\emptyset[j] \approx N_{(a,b)}\Delta P[j], \quad \text{for } j \ge \beta \quad (5)$$

Where $N_{(a,b)} = NP_{(a,b)}^{-1} = N_0+\Delta N_{(a,b)}$.Thus after the outage of line (a,b),

$$\Delta\emptyset[j] \sim f_{(a,b)}^{pc} \quad (6)$$

where $f_{(a,b)}^{pc} = N(0, N_{(a,b)}\, \Sigma\, N_{(a,b)}^T)$ for $j \ge \beta$

If line (a,b) is not restored, this change is persistent. To avoid repeated matrix inversions for each possible line outage matrix inversion lemma is used.

$$\Delta N_{(a,b)} = m1_{(a,b)}\ m2_{(a,b)}\ m2_{(a,b)}^T \quad (7)$$

where $m1_{(a,b)} = 1/(X_{(a,b)} - v_{(a,b)}^T\ NP_0^{-1} v_{(a,b)})$ and $m2_{(a,b)} = NP_0^{-1} v_{(a,b)}$.

2) Instantaneous change detection in phasor angle:

If the line outage occurs at time $\tau=\tau_f$, where $\beta\Delta\tau \le \tau_f < (\beta+1)\Delta\tau$, an instantaneous change that affects only one incremental sample $\Delta\emptyset[\beta]=\emptyset[\beta+1]-\emptyset[\beta]$ is also considered. Since $\emptyset[\beta]$ is got from pre-outage system while $\emptyset[\beta+1]$ is got from post-outage system, the incremental change at j=β, $\Delta\emptyset[\beta]$ is not given in the previous model. Prior to line outage the real power injection in all buses i, i∈ ς, is given by

$$P_i[j] = p_i[j], \quad j \le \beta \quad (8)$$

After outage of line (a,b) and assuming the outage is persistent, the real power equation in post-outage scenario is

$$P_i[j] = p_i'[j], \quad j \ge \beta+1 \quad (9)$$

(3

(2 The incremental variation of whole active power injection amongst the two PMU trials, directly prior to and subsequent line outage, i.e., between j=β and j=β+1 is stated as $\Delta P_i[\beta] =$

$P_i[\beta+1]- P_i[\beta]$. Substituting equations (8) and (9) the equation obtained is $\Delta P_i[\beta] = p_i'[\beta+1]- p_i[\beta]$. Adding and subtracting $p_i[\beta+1]$ to the above equation

$$\Delta P_i[\beta] = \Delta P_i^{ic}[\beta] + \Delta P_i^{pc}[\beta] \quad (10)$$

where $\Delta P_i^{ic}[\beta] = p_i'[\beta+1]- p_i[\beta+1]$ and $\Delta P_i^{pc}[\beta] = p_i[\beta+1]- p_i[\beta]$. As derived previously $\Delta P_i^{pc}[\beta]=p_i[\beta+1]- p_i[\beta]$. ΔP_i^{ic} component is determined next. Using the DC estimates considered above, the line flow through the transmission line (a,b) below the pre-outage network topology is specified as

$$P_{(a,b)}[\beta+1]\approx\frac{1}{X_{(a,b)}}(\emptyset_a[\beta+1]-\emptyset_b[\beta+1]) \quad (11)$$

The line outage is exhibited through accumulating two power instillations to the system, one at every termination of the transmission line to remain plummeted. Hence the outage of line (a,b) is simulated by adding $P_{(a,b)}[\beta+1]$ and $-P_{(a,b)}[\beta+1]$ at buses a and b respectively. Define ΔP^{ic} as an (S-1) dimensional vector, the $(a-1)^{th}$ and $(b-1)^{th}$ entries of which are $P_{(a,b)}[\beta+1]$ and $-P_{(a,b)}[\beta+1]$ respectively, and all other entries are 0. ΔP^{ic} is obtained as

$$\Delta P^{ic}[\beta] = P_{(a,b)}[\beta+1]v_{(a,b)} \quad (12)$$

where $v_{(a,b)}$ is a vector in that $(a-1)^{th}$ item is taken as 1, $(b-1)^{th}$ item is taken as -1 and further items is tends to 0. Combining the expressions for $\Delta P_i^{ic}[\beta]$ and $\Delta P_i^{pc}[\beta]$ and after rearrangement $\Delta\emptyset$ is got as

$$\Delta\emptyset[\beta]\approx N_0(\Delta P[\beta]-P_{(a,b)}[\beta+1]v_{(a,b)}) \quad (13)$$

This indicates that the mean of $\Delta\emptyset[\beta]$ is $-N_0P_{(a,b)}[\beta+1]v_{(a,b)}$ is not simply 0 (as in all sample $j<\beta$). Thus at $j=\beta$,

$$\Delta\emptyset[\beta]\sim f_{(a,b)}^{ic} \quad (14)$$

where $f_{(a,b)}^{ic}=\mathcal{N}(-N_0P_{(a,b)}[\beta+1]v_{(a,b)}, N_0\Sigma N_0^T)$

3) Summary of line outage problem:

Suppose an outage involving line (a,b) occurs at time τ_f between PMU sampling times τ_1 and τ_2 then,

$$\Delta\emptyset[j]\approx\begin{cases}N_0\Delta P[j], & j\le\beta-1\\ N_{(a,b)}\Delta P[j], & j\ge\beta+1\end{cases}$$

Here the probability density function of $\Delta\emptyset[j]$ is

$$\Delta\emptyset[j]\sim\begin{cases}f_0, & j\le\beta-1\\ f_{(a,b)}^{pc}, & j\ge\beta+1\end{cases}$$

At time instant $j=\beta$, two cases are considered depending on τ_1 and τ_2.

(i) If $\tau_1=(\beta-1)\Delta\tau$ and $\tau_2=\beta\Delta\tau$

$$\Delta\emptyset[j]\approx N_{(a,b)}\Delta P[j]$$

(ii) If $\tau_1=\beta\Delta\tau$ and $\tau_2=(\beta+1)\Delta\tau$

$$\Delta\emptyset[\beta]\approx N_0(\Delta P[\beta]-P_{(a,b)}[\beta+1]v_{(a,b)})$$

Here the probability density function of $\Delta\emptyset[\beta]$ is

$$\Delta\emptyset[\beta]\sim\begin{cases}f_{(a,b)}^{pc}, & \tau_1=(\beta-1)\\ f_{(a,b)}^{ic}, & \tau_2=\beta\Delta t\end{cases}$$

4) Probability of false isolation

Probability of false isolation denotes the probability that the outage in transmission line (a, b)is deceptively recognized as outage in next corresponding transmission line. It is used as a metric to device the efficacy of the line outage recognition and considered algorithm.

III. Proposed Line Outage Detection Method Using CSA

A. Spider and vibration

By using CSA for line outage detection, the search space of the problem is formulated as hyper-dimensional spider web *S* as IS model [16]. The web also serves as transmission media of vibrations generated by spiders. Each spider *i* of the population *pop* in the web holds a memory for storing information for parameters used in CSA such as position $P_i(t)$, fitness value $f(P_i(t))$, where *t* is the iteration index and $f(x)$ is the objective function, target vibration V_i^{tar} and dimension mask to guide the movement.

Spiders are extremely sensitive to the vibrations in the web. When a spider travels to a different position, it produces a vibration that disseminated on the web. Every vibration grasps the evidence of lone spider and further the others acquire the evidence upon reception on the vibrations. The spiders generate vibrations at their position using the expression in eqn.15. Two main properties are used to denote a vibration, namely, the source position and the source intensity of the vibration. These two properties are linked to the line outage scenario for identifying the position of outage. The intensity of vibration is obtained by expression

$$I_i= log\left(\frac{1}{f(P_i)-C}+1\right) \quad (15)$$

Where $P_i(t)$ is the position of spider *i* and C is surely a small constant. After a vibration is generated, when propagated over the web it attenuates. Vibration attenuation over distance is given by (16)

$$I_i^D=I_i \times exp\left(-\frac{D}{m_\sigma\times r_a}\right) \quad (16)$$

Where D - distance, m_σ - mean of standard deviation of the spiders location over all dimensions and r_a – rate of attenuation (regulating factor).

B. Computational pattern of CSA

The whole computational pattern of CSA involves three main phases that includes initialization phase, iteration phase and final phase. As the name states, initialization phase involves initialization of the objective function $f(x)$, solution space *S*, population of spiders *pop* and memory and the values for the parameters used in CSA.

Iteration phase is the most notable phase and consists of sub-steps comprises of fitness evaluation, vibration generation, mask changing, random walk and constraint handling. In fitness evaluation the fitness values of all artificial spiders are calculated. For each spider, the iteration

fitness function is evaluated once. Subsequently, every fitness values are assessed; every spider will engender a vibration in its present location by means of eqn.15. The vibrations are disseminated in the spider web which is given in eqn.16 and received by all other spiders. When the strongest vibration is obtained, it is compared with the threshold value. If the constraint is violated, the position from where the strongest vibration is got is reported as the line outage spot.

C. *Pseudocode of modified CSA for line outage detection problem*

Assign the CSA parameters.
Generate the spiders population (pop) & consign reminiscence for each.
Set V_i^{tar} for every pop
for each spider i in pop do
    Evaluate the fitness value
    Generate a vibration at the spider's position
    Calculate the intensity of vibrations
     generated by all spiders
Select the strongest vibration V_i^{stng}
  if $V_i^{stng} \geq V_i^{th}$
      Report the position of strongest
      vibration V_i^{stng}
  end if
end for

IV. Results And Discussion

The CSA algorithm is tested on Indian utility- 62 bus test system and the results obtained are discussed below. The one line diagram of the system is shown in figure 1. This test system contains 62 Bus, 89 Transmission lines, 11 Transformers, 19 Generators and 32 Loads. The system data are taken from the reference [14]. The base is 100 MVA.

The probability of false isolation is a major problem that is encountered in the identification of the line outages in the system. With CSA, which finds solutions based on current values only, this problem is addressed and has been reduced. The table below shows false isolation probability obtained via simulation for single line outages in the test system at a particular hour of the day.

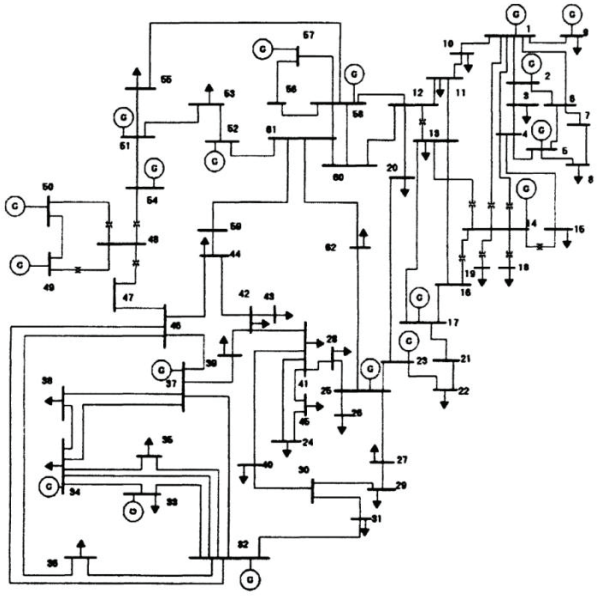

Figure 1. One line diagram of Indian utility- 62 bus test system

MATPOWER [17] simulation tool is used to obtain the voltage angles repeatedly by solving AC power flow, with each step j analogous to artificial power instillation profiles created using $P_i[j] = P_i^0[j] + \sigma\, v[j]$, using $\sigma = 0.03$. Suppose these random variations are non-simultaneous, then, Σrepresents the transverse matrix with every diagonal access taken as 0.0018.

To pretend the most awful circumstance, then the detection delay $\beta = 1$ is preferred. The graph in the figure 2, plots the detection delay time with respect to mean time to false alarm for each four hour a day.

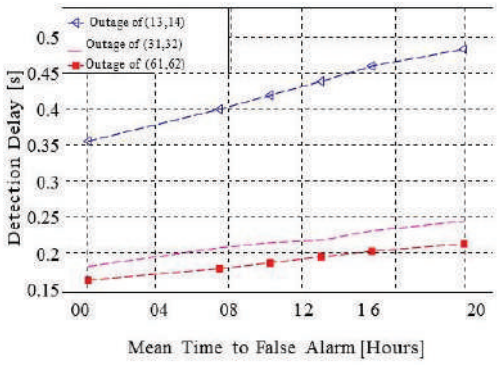

Figure 2. Typical detection delay vs despicable time to initiate false alarm for Indian utility- 62 bus test system.

As it is seen from the Table 1, the probability of false isolation has been considerably reduced. Thus line outage is distinctly identified without much effort and mathematical computations.

TABLE I.
PROBABILITY OF FALSE ISOLATION OBTAINED VIA SIMULATION FOR SINGLE LINE OUTAGE IN INDIAN 62-BUS TEST SYSTEM

Line outage	Time in Hours					
	00	04	08	12	16	20
Line (13, 14)	0.0002	0	0.0023	0.0044	0.0050	0.0088
Line (31, 32)	0	0.0035	0.0010	0	0.0040	0.0055
Line (61, 62)	0	0	0.0035	0	0.0012	0.0020

V. CONCLUSIONS

In this paper a method to detect and identify transmission line outages in near real-time is proposed. The statistical properties of phasor measurements of voltage and current obtained from PMUs are used to formulate the line outage problem. In addition, this paper attempts and introduces the use of CSA in the problem of line outage detection. By using optimization technique, the complex computations are reduced and system performance is improved. The above method assumes PMUs are available at all buses which is practically very difficult. Hence the method has to be modified for PMUs at desired locations and at the same detect the line outage optimally. This method can be extended to identify the double line outages with multiple constraints to optimize the system performance.

REFERENCES

[1] Report on grid disturbance on 30th July and 31st July 2012. Available:http://www.cercind.gov.in/2012/orders/Final_Report_Grid_Disturbance.pdf

[2] Z. Dong and P. Zhang, *Emerging Techniques in Power System Analysis*. Springer-Verlag, 2010.

[3] A.G.Phadke, "Synchronized phasor measurements in power systems," *IEEE Comput. Appl. Power*, vol. 6, no. 2, pp. 10-15,1993.

[4] K. Clements and P. Davis, "Detection and identification of topology errors in electric power systems," *IEEE Transactions on Power Systems*, vol. 3, no. 4, pp. 1748–1753, 1988.

[5] F. Wu and W.-H. Liu, "Detection of topology errors by state estimation [power systems]," *IEEE Transactions on Power Systems*, vol. 4, no. 1, pp. 176–183, 1989.

[6] N. Singh and H. Glavitsch, "Detection and identification of topological errors in online power system analysis," *IEEE Transactions on Power Systems*, vol. 6, no. 1, pp. 324–331, 1991.

[7] F. Alvarado, "Determination of external system topology errors," *IEEE Transactions on Power Apparatus and Systems*, vol. PAS-100, no. 11, pp. 4553–4561, 1981.

[8] J. E. Tate and T. J. Overbye, "Line outage detection using phasor angle measurements," *IEEE Transactions on Power Systems*, vol. 23, no. 4, pp. 1644–1652, 2008.

[9] H. Zhu and G. B. Giannakis, "Sparse overcomplete representations for efficient identification of power line outages," *IEEE Transactions on Power Systems*, vol. 27, no. 4, pp. 2215–2224, 2012.

[10] R. Emami and A. Abur, "External system line outage identification using phasor measurement units," *IEEE Transactions on Power Systems*, vol. 28, no. 2, pp. 1035–1040, 2013.

[11] Chen, Y.C., Banerjee, T., Domínguez-García, A.D. and Veeravalli, V.V., "Quickest line outage detection and identification", *IEEE Transactions on Power Systems*, 31(1), pp.749-758, 2016.

[12] James, J.Q. and Li, V.O., "A social spider algorithm for global optimization," *Applied Soft Computing*, 30, pp.614-627, 2015.

[13] R.Vijay, R. AntrutJaffrin and C. S. Ravichandran. "Optimal placement and sizing of solar constructed DG using SSO technique," *International Journal of Computer Science Trends and Technology*, vol.4, no. 3, pp.333-342, 2016.

[14] R.Vijay and V. Priya. "Anti-Islanding Protection of Distributed Generation Based on Social Spider Optimization," *International Journal of Advanced Engineering Research and Science (IJAERS)*, vol.4, no. 6, 2017.

[15] A. Wood and B. Wollenberg, Power Generation, Operation and Control, New York: Wiley, 1996.

[16] R. Gnanadass, "Optimal Power Dispatch and Pricing for Deregulated Power Industry," Ph.D. Dissertation, Department of Electronics and Communication Engineering, Pondicherry University, India, Mar. 2005, [Accessed Mar. 22, 2015]. [Online]. Available:http://dspace.pondiuni.edu.in/jspui/bitstream/pdy/498/1/T3248.pdf

[17] R. D. Zimmerman, C. E. Murillo-Snchez, and R. J. Thomas, "Matpower: Steady-state operations, planning and analysis tools for power systems research and education," *IEEE Transactions on Power Systems*, vol. 26,no. 1, pp. 12–19, 2011.

Speed Control of BLDC Motor using DRV8312EVM in VisSim Environment

Vardi Satya Kumari[1], R. Anil kumar[2], Syed Sarfaraz Nawaz[3]
[1]M-Tech Student, GRIET/EEE Department, Hyderabad, India
satyavardi@yahoo.com
[2]Asst. Professor, GRIET/EEE Department, Hyderabad, India
rajagiri_anil04@yahoo.co.in
[3]Assoc. Professor, GRIET/EEE Department, Hyderabad, India
sarfaraz86nawaz@gmail.com

Abstract: **The paper presents controlling the Speed of Brushless DC Motor by using VisSim software interfaced with a GUI named InstaSPIN-FOC (Field Oriented Control).VisSim is a software related to Visual Environment for model based exploring the Embedded Systems. It has a highly ingenious diagram-to-code capability, which reduces the complexity of design, time and improves quality of the product. In recent times, Brushless DC Motor has found wide range of Industrial applications for its high reliability, high efficiency, more torque per weight and low maintenance. InstaSPIN-FOC is a complete sensor-less FOC, which provides a solution in on-chip ROM for the selected devices (FAST observer, FOC, speed and current loops), masterfully governs the speed of the Motor without use of any speed sensors.**

This paper provides a basic understanding of DRV8312 and F28069. Simulation using VisSim have been executed. Prior to VisSim, simulation is performed with MATLAB Simulink. The speed waveforms for various gain settings are observed and hence studied the drive response. In this paper, the Speed Control of Brushless DC Motor using DRV8312 evaluation module along with F28069 control card in VisSim environment is been implemented.

Index Terms: **VISSIM, DRV8312EVM, InstaSPIN-FOC, BLDC Motor, FOC,FAST (Flux, Angle, Speed, Torque).**

I. Introduction

Power Electronics devices find numerous options for conducting simulation and analysis. Among those, MATLAB plays a vital role in simulation with an interface of the National Instruments (NI) hardware for conducting experiments. Use of NI fixtures results in high cost. Alternatively other Microcontrollers such as Arduino (Mega) help in reduction of the cost criteria with proper control algorithms, but dynamic simulation is not possible. Concurrently VISSIM overcomes the problems aroused with above discussed Microcontrollers.

VisSim [1] provides a highly efficient environment covering all phases of developing control systems for Electric Drives. Their diagram-to-code capability frees Electric Drive Engineers from manual coding and allows them to concentrate on developing the most optimal control in the shortest time. Enormous list of Motor control blocks set helps in achieving the in-depth motor modeling. And the model based approach gives a clear overview of the designs.

InstaSPIN - support for Motor Identification and efficient Sensor-less Field Oriented Control (FOC) [2,3] even at minimum of 1Hz rates. Industrial applications for the BLDC drive address the challenges of achieving a compact solution with higher efficiency and robust protection features like cycle-by-cycle current limiting during overload and short circuit conditions to protect power devices.

II. Block Diagram For Interfacing BLDC Motor With Vissim

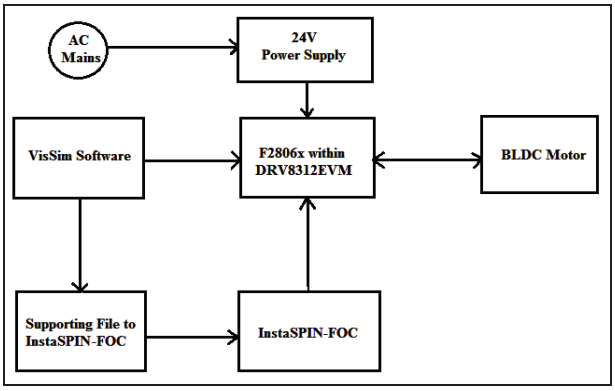

Figure 1. Block diagram of VisSim interfacing with BLDC Motor

Interfacing of BLDC [8] Motor with VisSim using DRV8312 Evaluation Module and InstaSPIN-FOC is shown in Figure 1.The DRV8312 board requires the supply voltage of 24V supplied from AC mains. The code is generated in backend of the VisSim software for designed block diagram, which loads the machine code into the controlCARD (F2806x) placed in the slot provided by the DRV8312 board. The F28069 with DRV8312 and with the supporting files of VisSim initiates InstaSPIN-FOC. InstaSPIN-FOC is sensorless solution which helps in efficient control of BLDC Motor.

III. Modeling And Results Of BLDC Motor For Speed Control In MATLAB

The MATLAB [4] simulation of BLDC motor for controlling the speed in a closed loop to obtain the required target speed is shown in Figure 2 where a reference speed is compared with the achieved target speed in a closed loop.

PI controller is used continuously which calculates the error value and applies a correction based on the

proportional and integral terms depending on the error signal at the input. Controlled voltage source converts the input signal to equivalent voltage source. Inverter used is connected to three phase BLDC Motor. As BLDC Motor needs hall sensors to detect rotor position and decoder converts pin positions to EMF values. And finally position EMF's are converted to gate pulses and fed back to inverter.

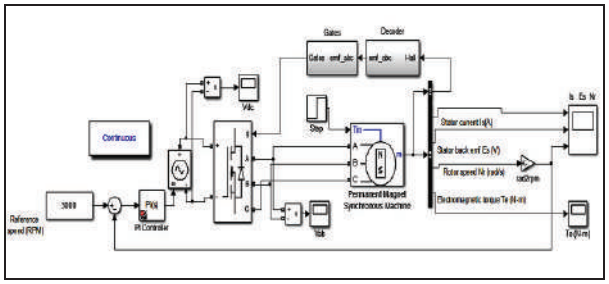

Figure 2. MATLAB simulation scheme of BLDC motor

The Simulation result for Speed Control of BLDC Motor in MATLAB is shown in Figure 3.The graphs represented in the figure indicate Stator current, Stator Back EMF and Speed. From the result shown in graph the set speed is controlled.

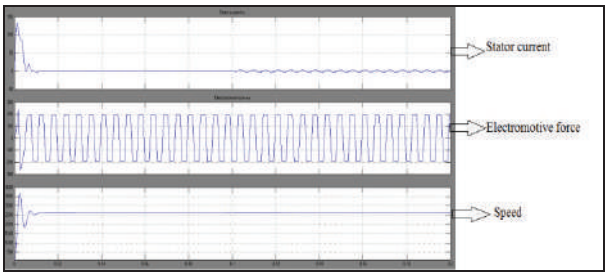

Figure 3. MATLAB simulation results for Stator current, Stator back EMF, Rotor speed

IV. VisSim

VisSim [5] A Visual Environment software for modeling is based on development of Embedded Systems. Its highly efficient diagram-to-code capability reduces the development time and increases quality of the product. By just swapping a small number of blocks, users can change their models from Software to Processor or Hardware in the Loop. VisSim offers full peripheral support for a large family of Microprocessors, thus making hand coding obsolete and the transition to actual Motor control. Models can be simulated and run in hardware in the Loop simultaneously.

VisSim is built with code efficiency being the top priority, so the simulation-only elements and the hardware specific blocks can be disregarded in code generation and simulation respectively. The VisSim/C-Code add-on generates ANSI C code for the model, and generates target specific code for on-chip devices like PWM, ADC, encoder, GPIO, I2C etc. After the behavior of the controller has been simulated, C-code can be generated, compiled and run on the target. For debugging, VisSim supports an interactive JTAG linkage, called "Hotlink", that allows interactive gain change and plotting of on-target variables. The VisSim generated code is efficient and readable, making it well suited for development of Embedded Systems.

V. DRV8312EVM (Evaluation Module)

The Medium Voltage Digital Motor Control (DMC) module (DRV8312) [6], provides a prominent way to learn and experiment with digital control of medium voltage brushless motors for increasing the efficiency of operation. The DRV8312 board with the control card slot for inserting F28069 control card.

The Motor control board is partitioned into functional groups that enable a complete motor drive system. These functional groups are called Macro Blocks and their labeling as shown in Figure 4.

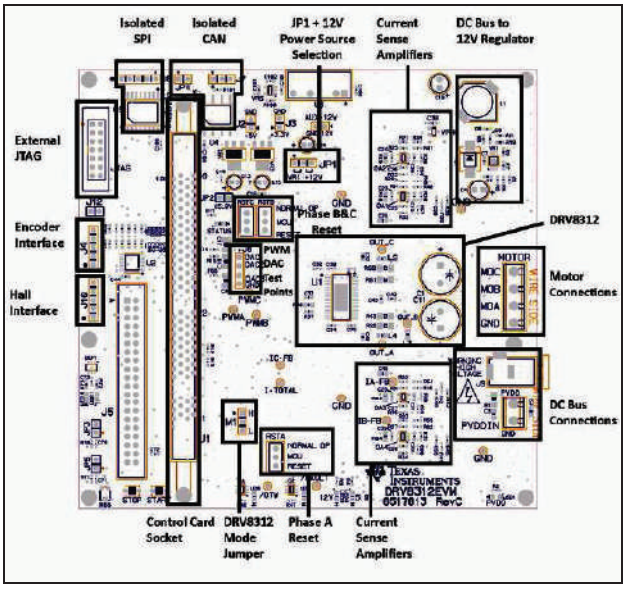

Figure 4. DRV8312 - Evaluation Board Macros

The board is separated into two power domains:

1. The low voltage Controller Power domain powers the controller and the logic circuit present on board
2. The medium voltage supply line that is used to carry the medium voltage and current such as the DC power for the Inverter (also referred to as DC Bus).

A. Controller Power

Comprised of the 12 V, 5 V, and 3.3 V that the board uses to power the controller and the logic and sensing circuit present on the board. This power can be sourced from two places (Jumper JP1 selects between the two)

- **+12V DC control power entry:** Connect an external bench supply with 1A current limit here.
- **On board regulator, VR1:** +12V is regulated from DC bus power via an on-board buck regulator

B. DC Bus Power

Is the medium voltage line up to 52.5V - that provides the voltage to the inverter stage to generate three phases to control the motor. Connect supplied 24 V.

VI. PICCOLO F28069 CONTROL CARD

The F28069 [7] is one of the Piccolo families of microcontroller (MCUs) equipped with the F28069 core and CLA coupled with highly mixed control peripherals in low pin-count devices. An internal voltage regulator, acquiesce for single-rail process. Enhancements have been made to the High-Resolution Pulse Width Modulator (HRPWM) module for enabling dual-edge control (Frequency Modulation). Analog comparators with in-build 10-bit references have been added which can be embedded directly to control the e-PWM outputs. The ADC converts 0 to 3.3V fixed full-scale range and supports ratio-metric VREFHI/VREFLO indications. The ADC interface has been minimized for less complications and inactivity. The device supply voltage is 3.3 V and its clock frequency (system clock) operates between 2MHz - 90MHz.

VII. INSTASPIN-FOC (GRAPHICAL USER INERFACE)

InstaSPIN-FOC [9] is a Graphical User Interface (GUI) with a complete sensor-less FOC solution embedded with on-chip ROM in preferred devices (FAST observer, FOC, speed and current loops). Effectively, it controls the motor without use of any sensors of speed and current.

F2806x peripheral drivers in user code, enable a monitoring InstaSPIN-FOC solution which identify and tune the torque controller resulting in efficiently control the motor within a fraction of time. This complete setup is called InstaSPIN-FOC, which is programmed in ROM.

In case of the F2806x devices, user has an option of working with all FOC functions in user memory (FLASH or RAM), which activates the FAST estimator firmware in ROM. InstaSPIN-FOC is designed for compliance, which accommodate a scope of system software architectures. FAST Estimator module restores the speed control method of motors using mechanical sensors. Field Oriented Control (FOC) of an electric motor propagates-superior torque control, lower torque ripples and improved efficiency when compared with traditional AC control techniques.

For finest dynamic response, rotor flux referenced control algorithms are preferred rather than stator flux referenced techniques. FAST estimator is included to measure rotor flux - magnitude and angle in a sensorless FOC system. The advantage of the FAST estimator is to provide automatic torque or current loop tuning, with preference given for user adjustments. Auto configuration of speed loop gains - K_p and K_i provides stable process for most of the applications. Automatic offset calibration assures quality samples of feedback signals.

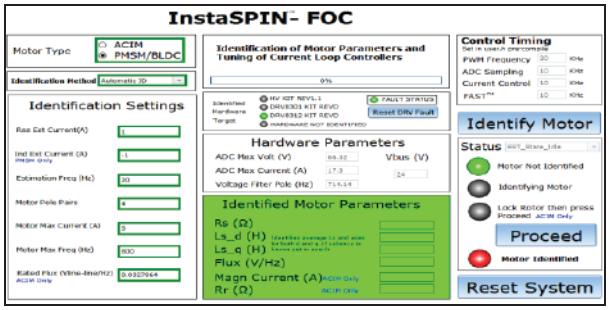

Figure 5. InstaSPIN-FOC initial Identification.

VIII. BLDC DRIVE MODELLING IN VISSIM

The VisSim modeling consists of "F28x Config" block and compound blocks like BLDC as shown below.

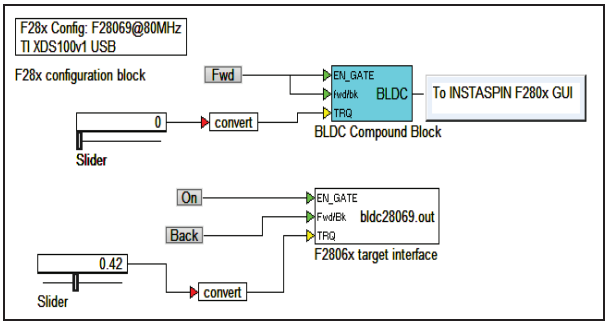

Figure 6. Modeling of BLDC Motor in VisSim.

The "F28x Config" block is used to configure the CPU as "F28069" and JTAG Connection with respective port number is identified. "Fwd" block is used to enable gate of the BLDC [8] motor. The "Slider" block allows the real-time control by moving cursor point in the simulation between lower and upper bounds. The "Convert" block is used to convert data type of input signal to scaled integer.

IX. EVALUATING INSTASPIN-FOC

"InstaSPIN_FOC_F2806xM" [9] is a GUI Composer evolution, that allows to interact with the model developed in VisSim and to evaluate the same using InstaSPIN-FOC.

A. *Hardware Set-up*

1. Verify the board existing has proper settings for all jumpers and switches
2. Install F28069M control CARD into the control CARD slot
3. Check Board Settings for Critical or Diagnostic states

a. TMDSCNCD28069MISO

i. SW1: TOP-TOP
ii. SW2: BOTTOM-BOTTOM
iii. SW3: TOP-TOP

b. DRV8312_REVD

i. JP1: VR1 - Center
ii. JP2: Projected
iii. M1: High-Middle
iv. All three toggle switches in the center (MCU) position
v. Motor Phase Terminals to MOA, MOB, MOC
vi. DC Voltage of 24V to J9/PVDDIN

B. *Launch the GUI*

With low voltage DC power supply, connect USB from PC to J1 on F28069

a. Run: Go to C drive and search for "web apps InstaSPIN_FOC_F2806x.exe" in c://ti/GUI composer location.
The GUI Composer application will start as shown in Figure 7

Figure:7. GUI Composer Start-up

b. After GUI Composer is initialized, connect and then load "vissimbldc.out" into the memory of Piccolo F28069M. The successful GUI interfaced window is displayed in Figure 8.

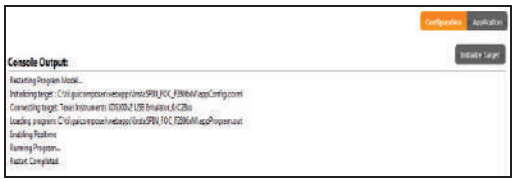

Figure 8. Normal Console Output of a successful GUI Launch

X. SPEED CONTROL OF BLDC WITH INSTASPIN-FOC

A. Motor Identification

Proceed only if the GUI properly diagnose the target hardware that has been used. Here, the Motor Type, Identified Hardware Target, Hardware Parameters and Control Timing values are automatically identified. Identification settings can be enabled as per requirement. Initially, when the application starts the Motor is not identified. It is indicated with a Green Blink and Motor is identified as Red Blink. When the Motor is under identification, Yellow Blink indicates Identifying Motor. When the Motor is completely identified Green blinks indicate Motor Identified.

Click on "Identify Motor" tab for identification of Motor. During identification of motor the indicator at "Identifying Motor" glows to "Yellow". The Status changes to consecutive states while identifying and the percentage will be increasing. If the Motor Identification is successful the indicator turns to "Green". For very low inductance motors, the change of value in "Estimation Frequency" tab of "Identification Settings" between 40 Hz and 60 Hz may result in successful identification. The Start-Up tab for Motor Identification is shown in the Figure 9.

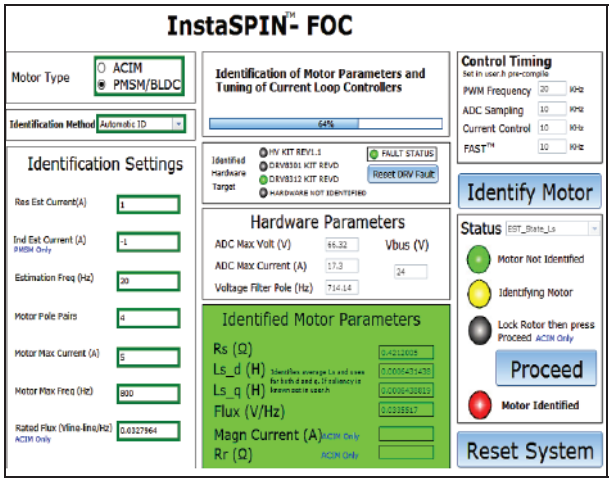

Figure 9. Start-Up Tab : Motor Identification

B. Speed or Torque

In Speed or torque tab, the values of Speed Reference and Max Acceleration have been set. In a short span of time Motor achieves the Target Speed with efficient Control Technique. The Display Panel shows

1. Estimated Speed (RPM) Tab from FAST
2. Target Speed (RPM) connected to the speed controller block
3. Voltage Bus (V)
4. Direction: "Blue" indicator represents clock wise direction and "Yellow" represents anti-clock wise direction

In Figure 10, before starting the Motor set the values of "Speed Reference" and "Max Acceleration" and tune for K_p and K_i values of the "Speed Controller".

The first graph represents the Speed curves for both the "Reference Speed" and the "Estimated Speed", second graph represents the Currents along Direct (d-axis) and Quadrature (q-axis) axes, and third graph represents the Torque produced for the drive operation.

Figure 10. Speed or Torque tab

BLDC Motor operates Stable for K_p value within a range of 6 – 12 and K_i value not greater than 0.10. Default Speed Controller used is the PI, which is included in ROM as part of InstaSPIN-FOC.

The K_p and K_i gains are calculated from "user.h" selected from "Identification Method" drop down list.

• K_p = 0.02 * Motor Max. Freq.*Motor Max.Current (in pu)

• K_i = 2.00 * Motor Max. Freq.*ctrlPeriod_sec*Motor Max.Current (in pu)

The current (I_q and I_d) PI controllers can be altered during execution time also. K_p and K_i settings are obtained from the motor parameters and other scaling parameters can be fetched from user.h. The values are slightly set so that it can give good performance over wide variant types of hardware boards and motors. To stabilize the control of motor, increase the values of K_p and K_i. Further, increase in frequencies (speeds of 1 KHz+) can stiffen the motor control up to multiples of 4x that of the original values.

C. Speed Profiles

The "Speed Profiles" tab shown in Figure 11 is rendered with two different state machine motion profile examples to enable evaluation mode of common variable speed applications. Speed can be positive or negative. "Acceleration" or "Deceleration" mode should always be entered as a positive integer.

Capability is heavily dependent on the motor, design specifications, inertia, power supply, and load. The oscillations in the speed curves is sustainable only for few intervals and can be reduced by proper settings on the Speed Loop tuning block.

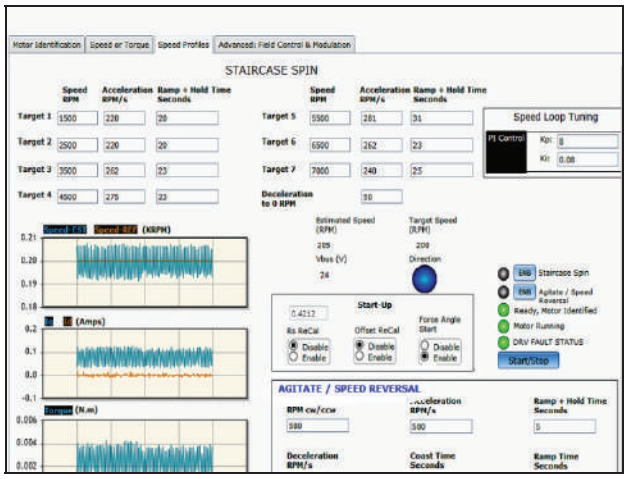

Figure 11. Speed Profiles tab

D. Field Control and Modulation

The tab of "Advanced: Field Control and Modulation" window shown in Figure 12 is used in conjunction with the other tabs, generally Speed and Torque, Staircase Spin (for field weakening), or Torque Mode (for field boosting). High value of $-I_d$ may result in demagnetization of a motor. Insure that

$$\sqrt{(I_d\text{^}2 + I_q\text{^}2)} < I_{rated} \quad (1)$$

Else, motor will demagnetize. Once operating in those modes, this tab can be used for further field control. Improper use of filed weakening mode may result in permanent damage of the motor and/or inverter.

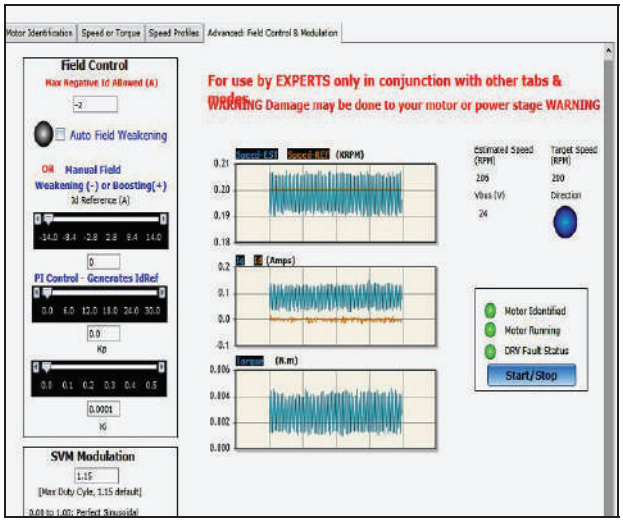

Figure 12. Advanced: Field Control and Modulation tab

XI. Result for The Speed Control of BLDC Motor

Speed control of BLDC Motor with an interface of DRV8312 EVM and InstaSPIN-FOC is shown in the Figure 13.

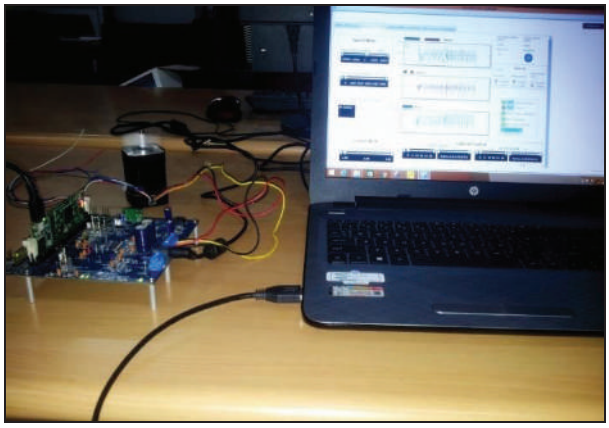

Figure 13. Interface of BLDC Motor with VisSim software

The model designed in VisSim generates a code in the back end and is dumped into the control card F28069 on the DRV8312 Evaluation module. Using the InstaSPIN-FOC GUI, interfacing is done with the BLDC Motor in order to control the speed of Motor. Figure 14 shows the Display panel (Motor tries to reach the target speed both in clockwise and anti clockwise direction.)

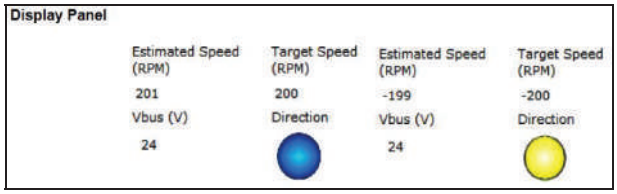

Figure 14. Display panel for Motor Speed Control

XII. CONCLUSIONS

The paper reports modernization on controlling the Speed of Brushless D.C Motor with VisSim software. Using VisSim Software the design concepts involved and computed can be easily understood. The simulation method has been found to be simple and versatile, since governing equations and functions of each power electronics circuit can easily be represented in blocks. This paper would be useful for obtaining the speed performance for numerous power electronic circuits with wide combinations of motors.

The model has been developed and tested in software. VisSim provides a means of testing it with the real world, thereby delaying the need for prototyping still further. VisSim allows a range of ADC and DAC boards which helps in transferring information from signals and forward them to the hardware in a test plant. This means, function blocks within VisSim may be replaced by the real components and thus allowing the real system to be compared with the mathematical model.

The model may be taken a step further by automatically generating ANSI C program code from the VisSim model. This helps in creating an executable model which can be run on any platform including transporters, DSP hardware or programmable controllers.

REFERENCES

[1] . O. Ustun and M. Yilmaz- “Simulation of power electronic circuits using VisSim software : a study on toolbox development” ǁ IEEE Transaction Industrial Electronics. Istanbul Technical University, April2000, pp.183 – 187.

[2] . O.Ustun, “Design of permanent magnet linear brushless D.C. Motor with Printed Circuit Armature”, Ph.D thesis, Istanbul Technical University, April2000.

[3] . Carlo Concari, Fabrizio Troni "Sensorless control of BLDC motors at low speed based on differential BEMF measurement" IEEE Conference Publications.

[4] . MATLAB-Simulink, Math works Incorporated. 2013.

[5] . VisSim User Guide, Visual Solution Inc., 1998.

[6] . DRV8312-C2-KIT Hardware Reference Guide, Texas Instruments Incorporated. 2014.

[7] . TMS320F2806x Piccolo Microcontrollers., Texas Instruments Incorporated., 2016

[8] . Sensorless Trapezoidal Control of BLDC Motors, Texas Instruments Incorporated. 2013.

[9] . InstaSPIN-FOC User guide, Texas Instruments Incorporated., 2013.

Modeling of Potassium Chloride Sensor with Two Dimensional Optical Nanostructure

Santosh Kumar Sahoo
Assoc. Professor, CVR College of Engineering / EIE Department, Hyderabad, India
santosh.kr.sahoo@gmail.com

Abstract: **Presence of potassium chloride concentration in aqueous solution is investigated using optical sensor. Optical sensor is modeled by two dimensional optical nanostructure or photonic crystal structure, which made from silicon materials (background/ substrate) consists of 8×8 air holes containing aqueous potassium chloride solution. Here measurement techniques centered on logarithmic difference of photonic band gap in regard to unlike concentrations of potassium chloride. The photonic band gap is found by means of plane wave expansion scheme. Proposed model is scheduled to quantify the output voltages with respect to same concentrations. Simulation result revealed that potential is measured at photo-detector varies logarithmically with respect to potassium chloride concentration, which leads to an accurate measurement of potassium chloride concentration in aqueous potassium chloride solution.**

Index Terms: **Optical nanostructure, Potassium-chloride, Substrate, Concentration, Photo-detector**

I. INTRODUCTION

Optical nanostructure or photonic crystals (PC) are composed of periodic dielectric nanostructures which affect the motion of photons in the same way as the periodicity of semiconductor crystal affects the motion of electrons [1]. As this structure is a repeatedly sections of high and low dielectric constant so the possibility of photons propagating through this structure depends on wavelength. Wavelength of a stream of photons which are allowed to travel is termed as mode and similarly rejected bands of wavelength photons are termed as band gap (BG_P) [2]. Depending on dielectric structure's dimensions, varieties of photonic crystals are constructed such as 1D, 2D and 3D [3]. We restricted this paper to 2D Optical nanostructure. Insofar as review on optical sensor using PC is concerned, Author in reference [4] covenants with two dimensional PC structure for investigation of Sugar, Salt and Alcohol, again in reference [5] percentage of PAM hydrogel in an aqueous solution is investigated. In the same way in reference [6], author measures glycerol concentration in blood hemoglobin–glycerol solution using three dimensional PC structure. Here glycerol measurement is performed by considering 3x3 air holes on substrate materials. But in the proposed work the concentration of potassium chloride concentration is investigated using two dimensional PC structure consisting of 8x8 air holes on silicon substrate. To obtain such concentration, such as a parameter, photonic band gap of above-mentioned crystal structure plays an important role. The BG_P of two dimensional structure (PCS) can be calculated by plane wave expansion (PWE) [7], Finite difference time domain (FDTD) [8], Order 'N' spectral [9], KRR [10] etc. Among these schemes PWE gives more precise result, because it offers an adequate information for matching boundary conditions in interface problems [11]. So we use the PWE method to calculate the band structure using Eigen values of the Maxwell's equation, henceforth solve Eigen frequencies for each of the propagation direction of the wave vectors. Potassium chloride is a natural compound in mineral, food and sea water which is highly necessary for various body functions like treatment of arterial hypertension [13]. Potassium is very important because it stimulates the kidneys to remove poisonous body wastes [14], for treatment of hypokalemia [15], treatment of animal diseases [16] and manufacturing of fertilizers [17]. The projected work is organized through PWE, discussed in section-2, simulation results along with discussions in section-3 and conclusions narrated in section-4.

II. METHODOLOGY

The proposed structure for investigation of potassium chloride concentration is a square type two dimensional PC structure as shown in figure-1.

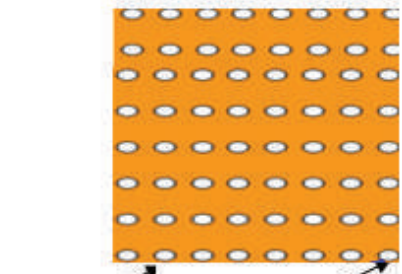

Figure 1. 2D photonic crystal hole with radius 0.42 micrometer and lattice constant 1 micro meter.

Figure-1 denotes a square lattice 2D photonic crystal structure with silicon as substrate, on which 8x8 air holes are etched. The radius of air holes is 0.4µm with lattice constant of 1µm. The BG_P of material changes by dielectric changes in air holes. Besides this, the same can be differs with variation of hole radius, lattice spacing or both. During the course of investigation, the light propagation in 2D photonic structure along Z axis and radiation has TE, then

the Helmoltz equation for the said field can be represented by considering Maxwell's equation as

$$-\left(\frac{\partial}{\partial x}\frac{1}{\in(r_{11})}\frac{\partial}{\partial x}+\frac{\partial}{\partial y}\frac{1}{\in(r_{11})}\frac{\partial}{\partial y}\right)H_z(r)=\frac{\varpi^2}{c^2}H_z(r_{11}) \quad \text{.....(1)}$$

Here r_{11} is a 2D vector in XY plane.

For simulation the BG_P is computed by using the equation-2 which is developed by simplifying the equation-1

$$X(G_{11})=2f\left(\frac{1}{\in_1}-\frac{1}{\in_2}\right)\frac{J_1(G_{r_{11}})}{G_{r_{11}}} \quad \text{.....(2)}$$

$J_1(G_{r_{11}})$ is the Bessel's first order function. Here the limit is varies from $-\pi/T$ ..... π/T, G and G' within $-2\pi N/T$ ..... $2\pi N/T$, Where (2N+1) is the number of plane waves taken into account.

III. Simulation Results Analysis

Here band-gap of 2D photonic crystal structure plays an important role to find out the densities of Potassium chloride in potassium chloride solution. The photonic band-gap of the proposed structure depends on structure types, material background, air hole materials, air hole radius and air hole numbers etc. Table-1 and Table-2 represent the complete figures regarding dielectric constant changes with different potassium chloride concentration [18].

TABLE I.
VARIOUS INPUTS FOR BG_P SIMULATION

STRUCTURE	SQUARE LATTICE
Substrate	Silicon
Air hole radius	0.40 micro meter
Lattice spacing	1.01 micro meter

TABLE II.
DIELECTRIC CONSTANT VERSUS % OF POTASSIUM CHLORIDE

% (gm/ml) KCl in solution	Dielectric constant
2.51	1.8041
5.01	1.8242
7.01	1.8332
10.02	1.8461
16	1.8590
20	1.8730

Considering the information from Table-1 and Table-2, the PWE scheme is followed for computation of BG_P of two dimensional structure having various potassium chloride concentration. The simulation outcomes for the same sample concentration of 2.5 gm/ml (dielectric constant is 1.804) and 20 gm/ml (dielectric constant is 1.873) are shown in figure 2(a) and 2(b).

Figure 2(a) represents the analytical outcome for BG_P of two dimensional PC structure containing 2.5% of Potassium chloride in an aqueous solution.

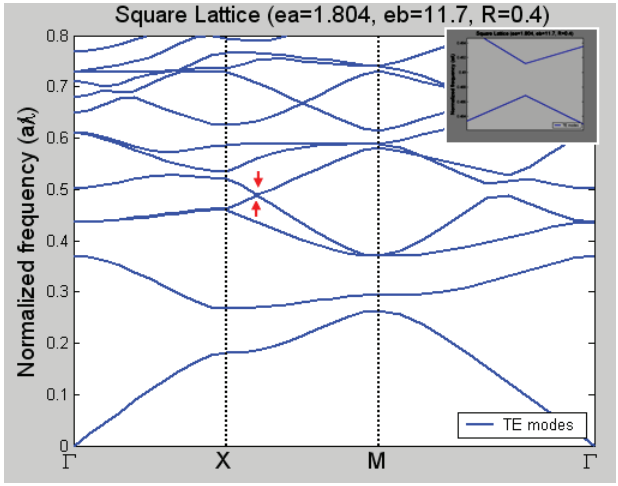

Figure 2. (a). BG_P simulation for 2.5 % potassium chloride concentration

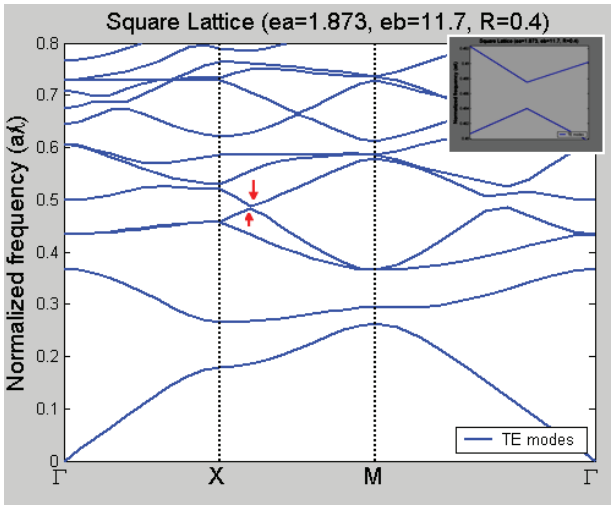

Figure.2 (b). BG_P simulation for 20 % potassium chloride concentration

Figure 2(b) forecasts the effect of BG_P of two dimensional PC structure containing 20% of Potassium chloride in an aqueous solution.

From figure 2(a) and 2(b), normalized frequency is shown between arrow marks and also zoomed. The zoomed figure is insert in each figure. Corresponding each normalized frequency, photonic bandgap is determined. The simulations are also done for other concentrations of potassium chloride such as 5 gm/ml (dielectric constant is 1.824), 7 gm/ml (dielectric constant is 1.833), 10 gm/ml (dielectric constant is 1.846), 16 gm/ml (dielectric constant is 1.859), but these results are not shown here.

On analyzing above photonic band-gap results, it is observed that BG_P declines from 5.5 meV to 4.4 meV as concentration of potassium chloride increases from 2.5 gm/ml to 20 gm/ml.

Graph is plotted between the photonic band gap and a different percentage Potassium chloride solution exposed in figure-3.

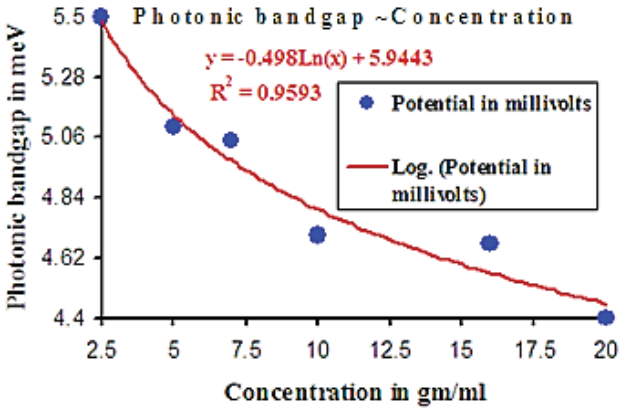

Figure 3. Photonic Band gap versus percentage of potassium chloride solution

From figure 3, it is seen that there is a logarithm variation between photonic band gap and concentration. Apart from this, it is observed that the decreasing variation is well built-in with logarithm trend line. This logarithm variation (R^2 =0.9593) of photonic band gap and concentration gives sensing application for determining the potassium chloride concentration by 2D PC structures. For experimental measurement, Sodium D-lines concentration with wavelength 589 nm is incident at one end of the crystal and the potential is detected at other end. Experimental set up for concentration measurement is shown in figure-4.

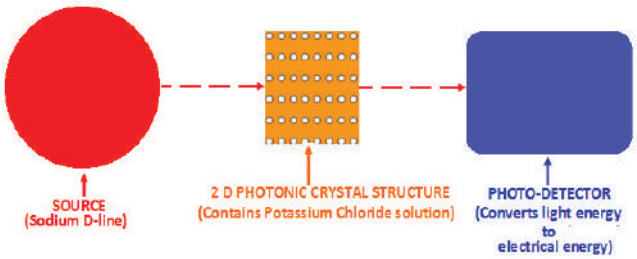

Figure 4. Experimental set up for concentration measurement

In this figure, it is seen that potentials at photo detector are determined with respect to concentration of potassium chloride. Using these results (voltage), a graph is plotted between potassium chloride concentrations along X-axis and voltage in Y-axis which is shown in figure-5.

Form Figure-5 , it is found that potential decreases from 2.045 V to 2.0956 V as potassium chloride concentration increases in the range of 2.5gm/ml to 20gm/ml. Reason for increase of potential with respect to potassium chloride concentartion is that reflectance (photonic bandgap) decreases from 5.5 meV to 4.4 meV. Apart from this , it is observed that the change of output voltage is an remarkably trim with logarithim trendline (R^2=0.985). This outstanding logarithim deviation hints a precise measurement of potossium chloride concentration in aqueous potassium chloride solution.

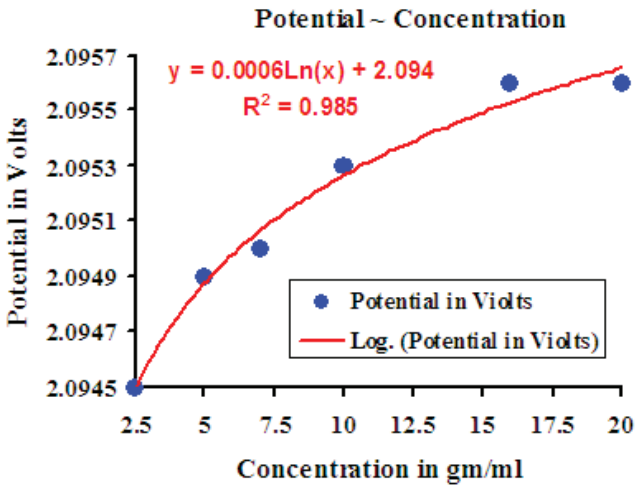

Figure 5. Potential versus concentration of potassium chloride

IV. Conclusions

A Concentration of potassium chloride in their aqueous solution is investigated by using two dimensional photonic crystal structures. The experimental set up is also presented to measure the same concentration. It is found that both photonic band gap of photonic crystal structure and potential at photo detector varies logarithmically with respect to concentration of potassium chloride. Since measurement is carried out at optical frequency, this method can be used for accurate sensing application.

References

1. E.Yablonovitch,“ photonic bandgap structures” : J.Optical Soc. America B 10(2),283-295(1993)
2. V. P. Bykov , “Spontaneous emission from a medium with a band spectrum Quantum Electronics 1975, 4:7, 861–871
3. J.Joannopoulos, Steven G. Johnson, J.Winn, R D. Meade Photonic crystals: Molding the flow of light (Princeton University Press 1995)
4. G.Palai, S.K.Tripathy; A novel method for measurement of concentration using two dimensional photonic crystal structures; Optics Communications, Volume 285, Issues 10–11, 15, Pages 2765-2768 , May 2012.
5. G.Palai, S.K.Tripathy, T.Sahu A novel technique to measure the sucrose concentration in hydrogel sucrose solution using two dimensional photonic crystal structures; Optik – International Journal for Light and Electron Optics; Volume 125, Issue 1,pages: 349-352, January -2014.
6. Measurement of glycerol concentration in B–H–G solution using 3D photonic crystal structure, Optik - International Journal for Light and Electron Optics, Volume 125, Issue 12, June 2014, Pages 2875-2879
7. Xue-liang Kang, Guo-jun Li, and Yong-ping Li , Positive–negative refraction effect based on overlapping bands in a two-dimensional photonic crystal, JOSA B, Vol. 26, Issue 1, pp. 60-63 (2009)

8. Kane Yee, Numerical solution of initial boundary value problems involving Maxwell's equations in isotropic media, IEEE Transactions on Antennas and Propagation 14, 302(1966)
9. P. Ordejon: Order-n tight-binding methods for electronic-structure and molecular dynamics Computational materials science 12, 157(1998).
10. Dunne, J.Lavon : Nutrition Almanac, (McGraw-Hill New York 1990)
11. Young-Chung Hsue, Arthur J. Freeman, and Ben-Yuan Gu ; Extended plane-wave expansion method in three-dimensional anisotropic photonic crystals; Physical Review B; condensed matter and materials physics; Phys. Rev. B 72, 195118 – Published 30 November 2005
12. I.A. Sukhoivanov, I.V. Guryev, Physics and Practical Modeling: Photonic Crystals, Springer, Heidelberg, 2009.
13. W. L. T. Addison, The Use of Sodium Chloride, Potassium Chloride, Sodium Bromide, and Potassium Bromide in Cases of Arterial Hypertension which are Amenable to Potassium Chloride, Can Med Assoc J. Mar 1928; 18(3): 281–285.
14. Material Safety Data Sheet – Potassium Chloride. Sigma–Aldrich. July 2001.
15. Hypokalemia: Treatment & Medication. Emedicine.medscape.com. Retrieved on 2012-02-16
16. http://www.petmd.com/pet-medication/potassium-supplements
17. Lorient, Denis; Linden, G. (1999). New ingredients in food processing: biochemistry and agriculture. Boca Raton: CRC Press. p. 357
18. D.P. Subedi, D.R.Adhikari, U.M.Joshi, H.N.Poudel: Kathmandu Journal of Science, Engineering and Technology 2, 1 (2006)

High Blood Pressure Prediction based on AAA++ using J48 Algorithm

Satyanarayana Nimmala[1] and D.Sujan Kumar[2]
[1]Assoc. Professor, CVR College of Engineering/CSE Department, Hyderabad, India
Email: satyauce234@gmail.com
[2]Assoc. Professor, CVR College of Engineering /CSE Depadrtment, Hyderabad, India
Email: dsujankumar@gmail.com

Abstract: **The heart pumps the blood around the body to supply energy and oxygen for all the tissues of the body. In order to pump the blood, heart pushes the blood against the walls of arteries, which create some pressure inside the arteries, called as blood pressure. If this pressure is more than the desired level we treat it as high blood pressure (HBP). Present days HBP victims are growing in number across the globe. Blood Pressure (BP) may be elevated because of the change in biological or psychological state of a person. In this paper, we considered attributes such as age, anger, and anxiety (AAA) and obesity (+), cholesterol level (+) of a person to predict whether a person is prone to HBP or not. Obesity and cholesterol levels are considered as post-increment of AAA, where obesity as one +, and total blood cholesterol as another + because experimental results reveal that their impact is less comparatively AAA. In our technique, we used different classifiers, where each classifier considers the impact of each A in AAA along with obesity and cholesterol level of a person in predicting the blood pressure. Experimental analysis is done on real-time data set. It consists of 1000 records which are collected from Doctor C, a Medical Diagnostic center, Hyderabad, India. Each record consists of age, anger level, anxiety level, obesity level, total blood cholesterol level and systolic blood pressure (SBP), diastolic blood pressure (DBP) of a person. We used 60% records to train the model, and 40% records to test the model.**

Index Terms: **Blood Pressure, Stress, Age, Anxiety, Anger, Obesity, Blood Cholesterol, Hypertension**

I. Introduction

BP is represented as SBP over DBP. If SBP exceeds 140 mmHg or DBP exceeds 90 mmHg on repeated measurements then it is treated as HBP [3]. Nowadays HBP is one of the prime cause of heart stroke and brain stroke. It may not be a serious problem if it is diagnosed and treated earlier, but undiagnosed HBP may cause a serious health problem. There are many reasons which may elevate the BP, like unhealthy diet, lack of physical exercise, excess bad cholesterol, obesity, age, anger, anxiety etc [5][9]. But in this paper, we focused on the impact of age, anger, anxiety, obesity level and total blood cholesterol levels in elevating the BP. Data is collected from a group of 1000 people aged between 20 and 65. High Blood pressure (HBP) mainly affected by the Cardiac Output (CO) and Total Peripheral Resistance (TPR) [2]. Mathematically, it can be written as

$$BP = CO * TPR \qquad (1)$$

Here, CO is affected by increased venous return or Stroke volume or Heart Rate or Sympathetic activity [1]. Whereas, TPR is affected by the resistance that acts against the blood flow in the arteries [10]. The arteries may show resistance to blood flow because of a blood clot in blood vessels or presence of fat inside the blood vessels or damaged blood vessels. CO affects the SBP, whereas TPR affects the DBP [12].

$$BP = Systolic/\ Diastolic \qquad (2)$$
$$Systolic\ /\ Diastolic = CO\ /\ TPR \qquad (3)$$

TABLE I.
Blood Pressure Range

BP	Low	Normal	Borderline	High
Systolic	<90	90-130	131-140	140
Diastolic	<60	60-80	81-90	>90

We collected age, obesity level, and total blood cholesterol levels of persons from Doctor C, A medical Diagnostic center Hyderabad, India. Although stress, anger, and anxiety may not spike blood pressure for a longer duration of time [1], but uncontrolled anger may affect relationships, career, mental and physical health. Anger and anxiety levels are measured using the response of an individual for the set of predefined questions. For anger measurement, we set 10 predefined questions and for anxiety measurement, we set 20 predefined questions. 1000 people were interviewed and their response is noted on a scale of 0 to 3. The mean value of the response, for all the questions on anger and anxiety, is used in the prediction process along with age, obesity and total blood cholesterol levels. Table I represents the level of Hypertension [3][14].

II. Impact Factors

Blood pressure of a person is elevated because of biological and psychological changes. Biological changes are like age, increase in obesity level and total blood cholesterol. Psychological changes like anger, anxiety, stress, depression, and fear. But the exact influence of each of these factors is left for research. In this paper, we considered AAA to predict whether a person is prone HBP or not. The rest of this section discusses how each A in AAA elevates the BP.

A. Impact of Age

Aging is an inevitable consequence of human beings. Many attributes of human body changes as the person ages[4]. As we age heart muscle cells get degenerated and also become thin, blood vessels show decreased performance,

the ability of the body to process sodium decreases. When we age the elasticity nature of the arteries also decreases as they become stiff [9][11]. In such situation, to pump the blood throughout the body through arteries, the heart has to push the blood using more force. This may, in turn, elevate the blood pressure.

B. Impact of Anger

Anger may be the result of impatience, frustration, irritation and many others. It may be a positive emotion at some point of time but most of the time it is not good for health and state of mind. The way how anger is handled has a significant effect on heart and mind. Frequent explosive anger may lead to serious consequences like elevated blood pressure, and the rise in the heartbeat and pulse rate. When a person gets angry then the fight or flight mode of Sympathetic Nervous System gets activated. As a response, nerves send more blood to muscles and brain, which elevates the blood pressure [12]. Though suppressing and ignoring the anger is not good for health but letting it go is also not good. So everyone should mastery over anger in a way that the impact of it to be as minimal as possible.

Anger Measurement**:** The literature says anger and blood pressure may not associate for a longer period of time. But our experimental results show there is a significant effect of anger along with the anxiety of a person in elevating the blood pressure. Our proposed technique measures the level of anger by using the responses obtained from the predefined questionnaire. Sample questions used for anger measurement are like waiting for anything annoys me, gets angry for the delay in completion of any assignment, gets angry if things won't go on my path, and I find difficult to forgive people who did wrong to me. We used 10 such questions and for each question, the answer is marked as one of the following option a) no, never b) yes, rarely c) yes, often d) yes, most of the time. In the data preprocessing phase option, a is considered as 0, option b is considered as 1, option c is considered as 2 and option d is considered as 3. Based on the mean value of all the answers we considered either floor value or ceil value of mean for experimental analysis.

C. Impact of Anxiety

Stress and anxiety are slightly different, even though represented on the same scale. The active form of stress may be considered as anxiety, and the active form anxiety may be considered as depression. Nowadays stress is one of the key factors that impact the quality of our regular life. If stress is chronic, that happening frequently, it may become anxious. Anxiety response creates specific thought pattern in mind, which gets executed repeatedly. The person, who is a victim of anxiety, thinks again and again about the worst possible outcome of an ambiguous situation, where the possibility of happening best is more. Factors such as negative thinking, fear, insecurity, lack of something compared to others, thinking about a specific thing that may happen in future, lack of confidence, doing wrong things which are not ethical, not getting things right as per his or her perception, expectations from friends, relatives, and closed ones etc., may be the triggering factors for anxiety. When a person is anxious, fight or flight mode of Sympathetic Nervous System gets activated [14][15]. As said earlier it elevates the blood pressure. However, anxiety and long-term HBP may not be linked. The body produces a surge of hormones such as adrenaline and cortical when we are in the anxious situation. This, in turn, may tighten the arteries. Our experimental analysis also reveals that there is a significant impact of anxiety, in raising the blood pressure.

Anxiety Measurement: Our proposed technique measures the level of anxiety by using the responses obtained from the predefined questionnaire. Sample questions used for anxiety measurement are like, the existence of constant fear about something, facing breathing difficulty often, feeling of not having desired things in life, often scared without the clear reason, often aware of the heart beat without doing physical exercise, and sense of dryness in the mouth. We used 20 such questions and for each question, the answer is marked as one of the following option a) no, never b) yes, rarely c) yes, often d) yes, most of the time. In the data preprocessing phase option, a is considered as 0, option b is considered as 1, option c is considered as 2 and option d is considered as 3. Based on the mean value of all the answers we considered either floor value or ceil value of mean for experimental analysis.

D. Impact of Obesity

Body Mass Index (BMI) is used to measure to find where you fall on the scale of obesity. BMI is a measure of weight proportionate to height. If BMI value is in between 18.5 and 24.9 is treated as normal. If BMI value is greater than 25 and less than are equal to 30 is treated as overweight [10]. If the BMI value is more than 30 then person treated as obese. Obesity is considered as increased fatty tissue in the body [7][8][11]. So for the livelihood of increased fatty tissues heart pumps the blood with some additional force to reach newly formed body tissues, which may spike the blood pressure.

E. Impact of Cholesterol

Although for the birth and development of body tissues, cholesterol is needed but too much cholesterol in the body is not good for the wellbeing of human body. Lipoproteins (small packages) are transporters of cholesterol in the human body. Lipoproteins are two types, LDL (low-density lipoprotein) cholesterol which is bad cholesterol and not needed for the body [15]. HDL (high-density lipoprotein) cholesterol is called good cholesterol. Indeed, which is most required cholesterol for the functioning many hormones of the human body. HDL carries cholesterol from all parts of the body back to the liver, where cholesterol is filtered and sent out from the body. If LDL is high, this forms fatty substance inside the arteries. This fatty substance reduces the diameter of arteries and raising the blood pressure.

III. Back Ground Work

This section reveals the existing work carried on each parameter in AAA++, which is the main reason for the elevation of blood pressure. Age: Arteries become stiff and narrowed due to aging and the elasticity nature of arteries gets also decreased [4][13]. Obesity: High BP problems are more common among inpatients with schizophrenia, mainly due to weight gain or obesity [14]. Cholesterol: increase in

cholesterol levels is able to influence BP, at least during sympathetic stimulation [11]. Anger & anxiety: The American Institute of Stress reports that Stress, "Pressure", "Tension", and "Anxiety" are often synonymous. US National Library of Medicine reports that our body produces a surge of hormones when we are in an anxious situation. These hormones increase your blood pressure by causing your heart to beat faster and our blood vessels to narrow. Though several researchers have addressed, how blood pressure is elevated based on physical and psychological factors, but these approaches suffer from the following drawbacks.

- Fail to find the exact risk of age in elevating blood pressure
- Fail to find the exact risk of obesity in elevating blood pressure
- Fail to find the exact risk of total blood cholesterol in elevating blood pressure
- Fail to find the exact risk of the combined effect of age, obesity and total blood cholesterol in elevating blood pressure
- Fail to find the exact risk of psychological factors such as anger and anxiety in elevating blood pressure

In this paper, our focus is on the combined effect of AAA++ in elevating the blood pressure.

IV. Proposed Architecture

Although Anger and Anxiety may elevate the blood pressure temporarily repeated activation of these two may lead to long-term blood pressure also. Different factors which influence blood pressure of a person directly or indirectly are shown in Fig 1. Yellow colour represents that impact AAA is more than the impact of ++ (obesity, total blood cholesterol) in elevating the blood pressure. Fig 1 also represents an increase in blood volume, increase in heart rate, and increase in stroke volume also increases blood pressure. These are normally influenced by sympathetic and parasympathetic nervous system of human body.

V. Proposed Methodology

In this paper, we used a data mining classification technique. Classification is the technique used to predict the class label of a data record or to represent a descriptive analysis of data record for taking effective decisions [2]. It is also called as a supervised approach. The classification model consists of two stages: In stage 1. Training stage, where the model is trained by a set of records, whose class labels are already known. In stage 2. Testing stage, where the model is going to predict class labels of a set of records whose class labels are unknown, also called as test records.

There are various classifiers but for Experimental analysis, we used classifier called as j48 supported by WEKA.

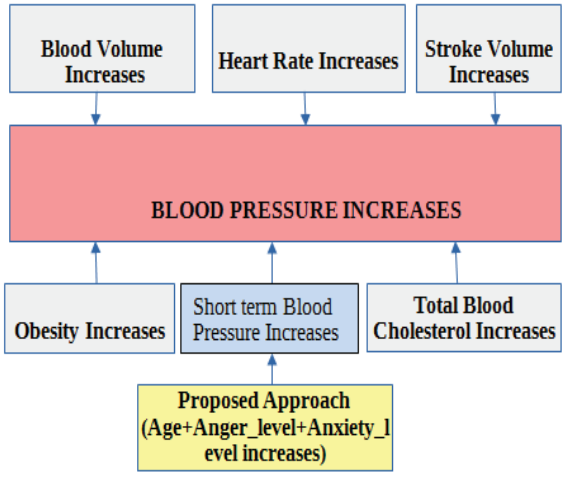

Figure 1. Block Diagram of the proposed approach and different parameters influencing the blood pressures

A. J48 Algorithm

J48 is a Decision tree based WEKA implemented C4.5 classification algorithm. A Decision tree based classifier classifies the input instances by passing it through the tree starting at the top and getting down to the leaf node. Leaf node value represents the predicted output value for a given input instance. Initially, information gain is calculated for each Attribute of input instance. The attribute with highest information gain is selected as splitting attribute. Recursive approach is used to divide the remaining instance at each node. Information gain (IG) of an attribute A is calculated at the selected node using equation 4.

$$Informatio\,nGain(S,A) = Entropy(S) - \sum_{v \in Values(A)} \left(\frac{|S_v|}{|S|} Entropy(S) \right) \quad (4)$$

Here TABLE II represents performance measures used to evaluate classifier performance. Where P is total number of positive records, N is total number of negative records, TP refers to the positive records which are correctly labeled by the classifier, TN is the negative records which are correctly labeled by the classifier, FP is the negative records which are improperly labeled as positive, and FN is the positive records which are incorrectly labeled as negative. In the equation 4,S is the set of instances at that node and $|S|$ is its cardinality, and S_v is the subset of S for which attribute A has value v. The entropy of the set S is calculated using (5).

$$Entropy(S) = \sum_{i=1}^{n} - p_i \log_2 p_i \quad (5)$$

where p_i is the probability of instances in S which belong to the i^{th} class, and 'n' is a number of classes.

TABLE II.
MEASURES AND FORMULA

Classifier Accuracy	$\frac{TP+TN}{(P+N)}$
Classifier Error rate	$\frac{FP+FN}{(P+N)}$
Recall	$\frac{TP}{P}$
Precision	$\frac{TP}{(TP+FP)}$
F-Measure	$\frac{(2\times precision\times recall)}{(precision+ recall)}$

VI. EXPERIMENTAL RESULTS AND ANALYSIS

For the experimental analysis, we have collected real-time data set from 1000 people. Each person data is considered as one record, for each record age of a person, anger level, anxiety level, obesity, blood cholesterol, systolic and diastolic blood pressures are recorded. Based on the systolic and diastolic blood pressure values we calculated class label attribute. If anger level and anxiety level are below 1 we considered their floor value and more than one we considered their ceil value for the better prediction. TABLE I is used to convert systolic and diastolic blood pressure values to get the class label attribute. Performance of classifier [2], the details of the dataset are as shown in TABLE II, III. Data collection is done manually by interacting with the people using questionnaire mentioned in the sections, anger measurement, and anxiety measurement. We have used a data mining tool WEKA (Waikato Environment for Knowledge Analysis) for experimental analysis. It is open source software; consist of many machine learning and data mining algorithms. WEKA processes the input data using ARFF (Attribute file format). So data collected is converted into an arff file, in the data preprocessing phase.

TABLE III.
DETAILS OF ATTRIBUTES

Attribute Number	Attribute	Minimum	Maximum	Mean	Standard Deviation	Attribute Type
1	Age	20	65	37.898	11.021	Numeric
2	Anger level	0	3	1.797	0.618	Numeric
3	Anxiety level	0	3	1.141	0.664	Numeric
4	Obesity level	15.5	37	24.307	3.959	Numeric
5	Cholesterol level	102	258	168.129	31.39	Numeric

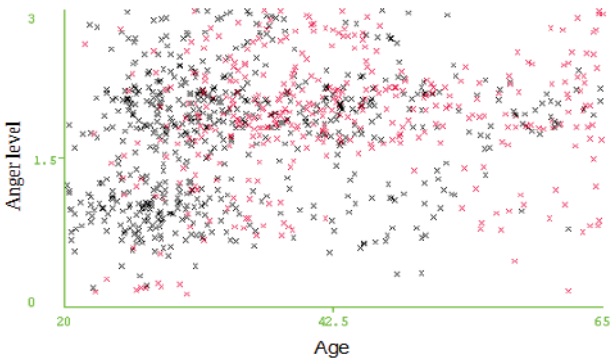

Figure 2. BP prediction using Age and Anger

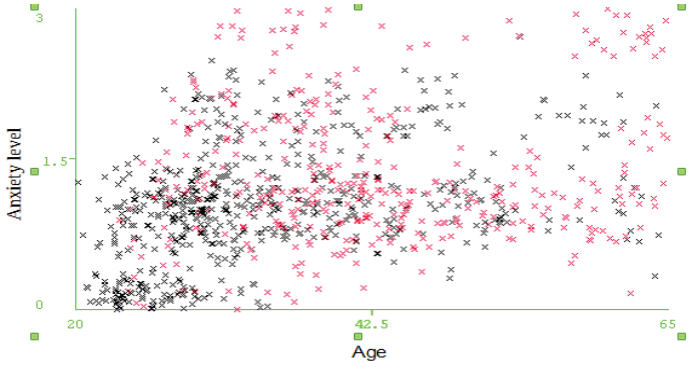

Figure 3. BP prediction using Age and Anxiety

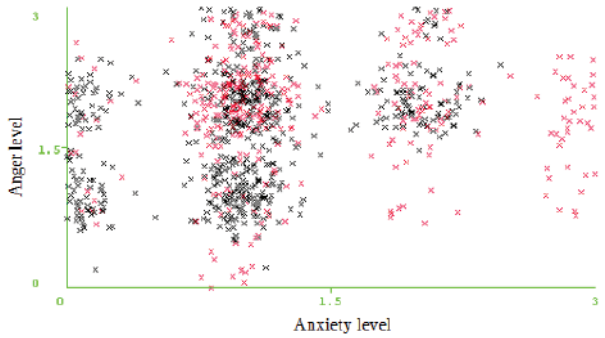

Figure 4. BP prediction using Anxiety and Anger

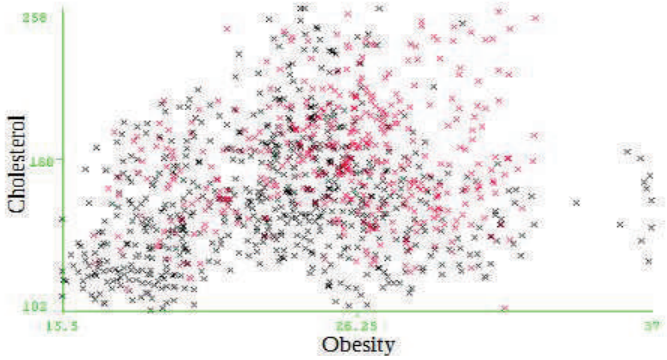

Figure 5. BP prediction using Obesity and cholesterol

Fig. 2 represents age on X-axis, where the minimum age is 20, maximum age is 65. Y-axis represents anger level, where minimum anger level is 0, and maximum anger level is 3. Here red 'x' represents data records which are predicted as YES, black 'x' represents data records which are predicted as NO. Fig. 3 represents age on X-axis, where the minimum age is 20, maximum age is 65. Y-axis represents anxiety level, where minimum anger level is 0, and maximum anxiety level is 3. Here red 'x' represents data records which are predicted as YES, black 'x' represents data records which

are predicted as NO. Fig. 4 represents anxiety level on X-axis, where the minimum age is 0, maximum age is 3. Y-axis represents anger level, where minimum anger level is 0, and maximum anger level is 3. Here red 'x' represents data records which are predicted as YES, black 'x' represents data records which are predicted as NO. Fig. 5 represents Obesity level on X-axis, where the minimum age is 15.5, maximum age is 37. Y-axis represents Cholesterol level, where minimum Cholesterol level is 102 and maximum Cholesterol level is 258. Here red 'x' represents data records which are predicted as YES, black 'x' represents data records which are predicted as NO.

TABLE IV.
CLASSWISE ACCURACY DETAILS USING J48 ALGORITHM

Class	TP Rate	FP Rate	Precision	Recall	F-Measure
YES	0.816	0.154	0.755	0.816	0.784
NO	0.846	0.184	0.888	0.846	0.866

TABLE V.
ACCURACY AND ERROR RATES OF J48 ALGORITHM

S. NUMBER	ALGORITHM	ACCURACY %	MAE	RMSE	RAE %
3	J48 Algorithm	83.5	0.1984	0.3427	41.8241

MAE: Mean absolute error, RMSE: Root mean squared error, RAE: Relative absolute error

VII. CONCLUSIONS

In this paper, we used age, anger, anxiety, obesity and cholesterol levels of a person to predict whether a person is prone to HBP or not. From the experimental analysis we obtained, if the age of a person is greater than 34 and anger, anxiety levels are greater than or equal to two, obesity is more than 30 and cholesterol level is more than 205, then the person is most likely to become a victim of high blood pressure. Results unfold; the influence of anger, anxiety is more than the obesity, cholesterol levels in elevating the blood pressure.

The experiment also reveals that if the person age is greater than fifty irrespective of anger, anxiety, obesity and cholesterol levels, the person is more likely, to become a victim of HBP. Apart from this experimental analysis also unfolds many other interesting correlations, which are not listed here. In future; we would like to consider other attributes such as gender, smoking, alcohol consumption, and job satisfaction, marital status to improve the prediction performance of the classifiers.

REFERENCES

[1] Mikko Peltokangas, Antti Vehkaoja, Jarmo Verho.: "Age Dependence of Arterial Pulse Wave Parameters Extracted from Dynamic blood pressure and Blood Volume Pulse Waves": IEEE journal of biomedical and Health informatics, vol. 21, pp.142-149, 2017.

[2] Satyanarayana, N., Ramalingaswamy, CH., Ramadevi, Y.: "Survey of Classification Techniques in Data mining, International Journal of Innovative Science, Engineering & Technology, vol. 1, pp. 268-278, 2014.

[3] A. Alwan.: "Global status report on noncommunicable diseases 2010", World Health Organization, 2011.

[4] Julie K.K. Vishram., Anders Borglykke., Anne H. Andreasen., Jorgen Jeppesen., Hans Ibsen.: "Impact of Age on the Importance of Systolic and Diastolic Blood Pressures for Stroke Risk", *Hypertension, vol.* 60, pp.1117- 1123, 2012.

[5] Raghupathy Anchala., Nanda K. Kannuri ., Hira Pant .: "Hypertension in India: a systematic review and meta-analysis of prevalence, awareness, and control of hypertension", Journal of Hypertension, Vol. 32, pp.1170-1177, 2014.

[6] World Health Organization Available online at: http://www.who.int/gho/ncd/risk_factors/blood_pressure_prevale_text/en/.

[7] Ilse L. Mertens., Luc F. Van Gaal.: "Overweight, Obesity, and Blood Pressure: The Effects of Modest Weight Reduction: Obesity Research ", vol. 8 ,pp. 270-278, 2000

[8] Richard N. Re.: " Obesity - Related Hypertension", The Ochsner Journal, Vol. 9, pp.133-136, 2009.

[9] Mohamad Forouzanfar., Hilmi R. Dajani., and Mohamad Forouzanfar., Hilmi R. Dajani., Voicu Z. Groza., Miodrag Bolic., Sreeraman Rajan., and Izmail Batkin.: " Oscillometric Blood pressure Estimation: Past, Present, and Future", IEEE reviews in biomedical engineering Engineering, vol. 8, pp.44- 61, 2015.

[10] National Heart, lung and blood institute. Available online at: https://www.nhlbi.nih.gov/health/healthtopics/hbc/Causes.

[11] Meenakshi Kalyan and Shubhangi A. Kanitkar: "Ultrasonographic assessment of abdominal fat and its correlation with blood pressure", International Journal of Biomedical and Advance Research vol. 6, pp. 259-263, 2015.

[12] Gupta V., Lo Gerfo J P., Raingsey PP., Fitzpatrick AL. "The prevalence and associated Factors for Prehpertension and hypertension in Cambodia" , Heart Asia vol.5, pp.253-58, 20 - 13.

[13] K. Takazawa., N.Tanaka, M. Fujita., O.Matsuoka.,T. Saiki,M. Aikawa., S. Tamura.,C. Ibukiyama.: "Assessment of vasoactive agents and vascular aging by the second derivative of photoplethysmogram waveform" , Hypertsion, vol. 32, pp. 365–370, 1998.

[14] S. C. Millasseau., P. R. Kelly., J. M. Ritter.: " The vascular Impact of aging and vasoactive Drugs: comparison of two digital volume pulse measurements", American Journal of HyperTension, vol. 16, pp. 467-471, 2003.

[15] Kanai H., Matsuzawa Y., Kotani K., Keno Y., Kobatake T., Nagai Y.: "Close correlation of intra abdominal fat accumulation to hypertension in obese women", Hypertension, vol. 16, pp.484-490, 1990.

Computer Aided Optical Disc Detection in Fundus Images: A Review

G.N. Balaji[1], S V. Suryanarayana[2], Naresh Babu Kakarla[3]
[1,] Asst. Professor, CVR College of Engineering/IT Department, Hyderabad, India
balaji.gnb@gmail.com,
[2] Assoc. Professor, CVR College of Engineering/IT Department, Hyderabad, India
suryahcu@gmail.com
[3]Asst. Professor, CVR College of Engineering/CSE Department, Hyderabad, India
nareshbabukakarla@gmail.com

Abstract: **Colour fundus images of the human retina are increasingly used in the diagnosis and treatment of several eye related pathologies and in ailments such as arteriosclerosis, diabetes, and hypertension. The effectiveness of treatment for many eye related diseases lies in the early detection through regular screenings. But, screening a large number of patients is a significant problem faced by medical practitioners in populous developing countries like India. In addition, there are extensive influences of human blunders and subjectivity on the consequences of assessment by a human master. This opens up the probability of applying propelled image processing techniques in fundus images to support and improve determination in different ways. Thus, automatic detection of pathologies and computer aided analysis in retinal images play a important role in modern diagnostic procedures and screening systems. Reliable and robust extraction of retinal features like optic disc, macula and vasculature is an essential for ensuing retinal image analysis and handling since these are the overwhelming and most stable structures showing up in the retina. However, automatic segmentation of retinal images is a complicated affair since retinal images are often poorly contrasted noisy, and there are a wide variations in orientation. This paper presents a review on algorithms or methods to detect optic disc automatically.**

Index Terms**: diabetes, hypertension, retina, optical disc and arteriosclerosis.**

I. INTRODUCTION

The human eye is regularly contrasted with a camera. Approaching light reflected from objects is centered around to the retina in the track of passing through cornea, understudy and focal point, which is like the component of a camera. A camera utilizes the photographic film or a CCD board to make a picture, while the eye utilizes a specific layer of cells, called the retina, to create a image. The approaching data is prepared by photoreceptor cells in the retina and transmitted to the mind through optic nerve. The eye's astonishing capacity to concentrate on an extensive variety of articles having distinctive sizes, glow and difference at a rapid is more effective than those of presently accessible cameras.

A fundus camera is used to capture the images of the interior surface of the retina. With its digital imaging capabilities, the images may be enhanced, stored and retrieved more easily than film, and images may be transferred electronically to other sites for a trained optical technician or an expert ophthalmologist to detect or diagnose diseases for a patient at a distant location. In the fundus image of a healthy human subject, features such as optic disc, retinal vasculature and macula are visible as shown in Figure 1.

There are two sorts of value issues in the fundus images: noise pixels and pixels whose color is twisted. Both appear to exist in locales where light has been deficient. Since brightening is normally sufficient in the focal point of the picture, poor picture quality districts are situated close to the edge of the fundus.

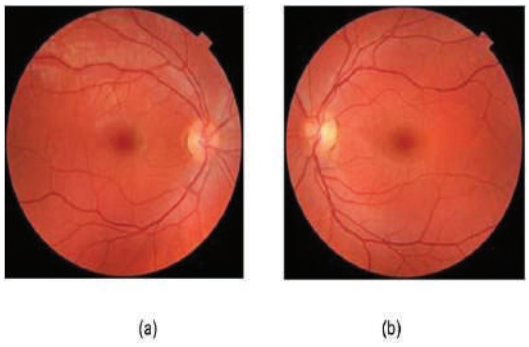

Figure 1. Fundus images of both eyes

Figure 2 demonstrates a solid retinal image with fundamental retinal highlights i.e. veins, macula and optic disk. The color size, shape of optic disk help in discovery and restriction, as it may demonstrate a vast difference.

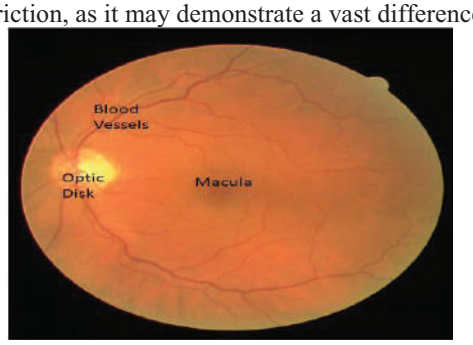

Figure 2. Healthy retinal image with features

Figure 3 indicates cases of a swollen optic nerve, where the circular shape and size are twisted. It likewise

demonstrates a case with a bright circular lesion that seems like optic disk.

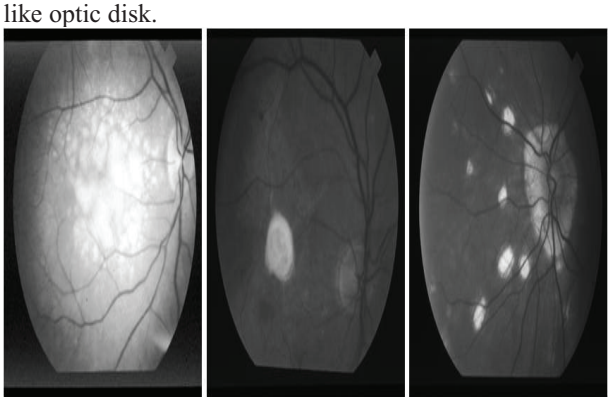

Figure 3. Retinal images with distorted shape of optic disk and lessions.

A. Fundus image preprocessing

Inappropriate scene illumination and in addition non-perfect procurement conditions due to misadjusted imaging framework can introduce serious distortions into the resulting image. These distortions are generally seen as smooth intensity varieties over the image. With such unevenness, the consequent image processing operations like image registration, segmentation, or pattern recognition might be confounded; in this way, the adjustment of illumination in homogeneities is exceedingly alluring. The objective of illumination adjustment is to evacuate uneven illumination of the image caused by sensor defaults, non-uniform illumination of the scene, or introduction of the surface. The known illumination revision techniques in the writing can be classified in the following gatherings: filtering segmentation based, surface fitting, and different strategies [1].

Particular techniques for illumination correction were proposed in the casing work of retinal picture handling and examination. Basic and quick techniques using large-kernel median filter to obtain low-pass correction coefficients were utilized by [2],[3] show the background of a fundus picture as a white Gaussian arbitrary field and utilize Mahalanobis distance for background pixel classification. Contrast normalization using high-pass filtering is utilized as a part of [4] as one stage of microaneurysm detection method. Added substance model of non-uniform illumination is utilized as a part of [5], together with adaptive histogram equalization. In [6-9], the nearby difference improvement strategy is utilized for adjusting uneven illumination in the intensity channel of fundus images. In [10] and [11], a substantial mean channel, vast middle channel, or both are utilized for evaluating the fundus foundation. Illumination variety in a fundus image can be dispensed by subtracting the foundation estimation from the first image or by partitioning the first image by the foundation estimation. Barely any different techniques are likewise displayed in the writing. For instance, in [12], the intensity esteems in dim areas have been expanded. Every illumination equalization strategy has its own points of interest and impediments, yet no method was discovered that would totally take care of the issue of uneven illumination. Illumination correction based on background subtraction is one of the widely accepted methods in fundus image preprocessing. Uneven illumination in a fundus image can be corrected by subtracting the background estimation from the original image or by dividing the original image by an estimated background.

II. Optic Disc Detection

Automatic detection and localization of optic disc is of paramount importance in all image processing applications with fundus images. Current optic disc detection methods available in the literature can be broadly classified in to intensity-based [7] [13-14], template-based [9] [15-21], shape-based [22-23] and vessel-based [5] [24-30] approaches. However most of the existing OD detection methods can be classified as given below.

A. Methods based on Intensity

A variance-based OD-detection method is given by [7]. This method assumes the appearance of the optic disc as a yellowish region typically occupying approximately one seventh of the entire image. The intensity variance of the image should be at its highest within the optic disc because of relatively rapid variation in intensity values. The reason for this variation is the appearance of dark blood vessels besides bright nerve fibers. The variance-based OD-detection method can be divided into three different steps:

- Local contrast enhancement
- Determination of the variance within a running window
- Determination of the average variance within a running window

The authors in [37] have tried optic disk localization and detection system on standard diabetic retinopathy databases. They have utilized four openly accessible datasets, DRIVE, diaretdb1, STARE and diaretdb0. The choice for fruitful localization or fizzled localization depends on human eye perception. Figure 4 represents the optic disk localization occurs for retinal images taken from various databases. Red cross sign demonstrates the optic disk area in each picture. These outcomes bolster the legitimacy of our procedure and demonstrate that our strategy gives great outcomes for localization notwithstanding for those images where it is hard to find optic disk. Similar kind of segmentation techniques are added with mathematical morphological operations and used for segmentation of irregular shapes from echocardiogram images in [39]. This method aided them to classify the basic cardiac views, also acts as an initial stage for computer aided cardiac disease diagnosis system.

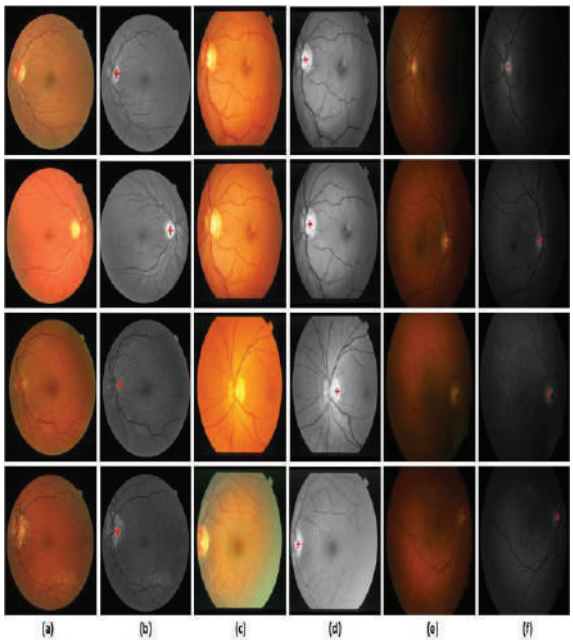

Figure 4. (a) DRIVE database; (b) OD localization in DRIVE (c) STARE database; (d) OD localization in STARE; (e) Diarectdb0 and Diarectdb1 database; (f) results of OD localization.

This method localizes the optic disc merely by means of its high grey level variation. However no method is suggested for the detection of the contours in this work. The techniques reported so far, based on luminosity, however fail on images with severe pathologies. It simply misses to locate the OD where the optic disc is obscured by hemorrhages or with a dark pigmentation. The present approach based on bit plane decomposition and mathematical morphology is an attempt to address the above problem.

B. Methods based on Template Matching

Template matching is a classical way to find the target object in an image [15-19], [31] employed Principal Component Analysis (PCA) to extract features of the optic disc. They first manually cut sub-images around the optic disc region from the training images and then used PCA to obtain the "eigen-discs" that describes the "disc-space". Using a template moving throughout a retinal image, the candidate sub-images were projected onto the disc-space and the candidate sub-image with the smallest reconstruction error was regarded as the optic disc. In their paper [9], [21] proposed to locate the optic disc by using a template matching approach based on a normalized correlation coefficient. The normalization of the colour fundus image is performed by applying histogram specification on each colour plane (R,G & B).Then the optic disc region from 25 normalized images were averaged to produce a template. Finally they used the normalized correlation coefficient to find the most perfect match between the template and all the candidate sub-images.

The authors in the paper [29-30] mentioned that the approach can possibly recognize the area of the OD in retinal images with few or no variations from the norm and the position in the image which is situated amidst the optic circle. To achieve this they utilized k-NN regression to discover the connection between the reliant variable d, speaking to the separation to the optic plate focus, and a feature vector measured around a round layout. The format is round in light of the fact that the optic circle is roughly circular by itself. The round format is put at different areas in the picture and measures the features around the layout. In view of the feature vector the separation of circular layout is utilized and free factors v is measured at the outskirt and under the format. The training set is made putting away separation d to genuine protest focus. The estimated OD Distance d, d can be calculated by:

$$\tilde{d} = \frac{1}{k}\sum_{i=1}^{k} d_i \qquad \text{.....(1)}$$

Where i d is the stored value of d of the i^{th} nearest neighbor of v and d location of object of interest that is get detected.

In [20], the authors Proposed a Hausdorff-based template matching. They estimate the OD contour using Hausdorff-based matching between detected edges and a circular template. In this the OD detection method is primarily based on pyramidal decomposition. First, a multi-resolution processing was employed through pyramidal decomposition. Small bright lesions were eliminated at lower resolutions, which speed up the searching for the optic disc since it reduces the number of false candidates. A confidence value was calculated for all the candidate regions, and then the Canny edge detector [32] was applied on the green channel image regions corresponding to the candidate regions to construct a binary edge map. Finally, the Hausdorff distance was used to match the edge map regions to a circular template of various different radii. It has been reported that this method is not a robust one particularly in images with multiple pathologies and hemorrhages in the vicinity of optic disc.

C. Methods based on the Largest Object

The authors in [14] detected the optic disc as the largest and brightest object in the retina by assuming that all bright lesions are much smaller than the size of the optic disc. In this method of OD-localization a threshold is applied. A straightforward edge is connected to get a twofold picture containing parts of the optic disc and other splendid showing up pathologies like exudates. The biggest associated question inside the thresholded image is relied upon to be a piece of the optic plate. The focal point of this problem is chosen as the focal point of the optic circle. Here, a territory edge is utilized to localize the optic plate and the watershed change to discover its forms. Shape anomalies because of segmentation mistakes, especially with regards to active vessels or in low complexity couldn't have been disposed of. Likewise [33] utilizes a comparative approach. In any case, the calculation comes up short when contrast is too low or when the red channel is soaked.

D. Methods based on Hough Transform

In [22], the author proposes to apply a Hough transform in order to locate the optic disc the Hough transform system can discover geometric shapes in an image. Objects of geometric shapes might be identified by changing over the condition of the protest into a Hough space parameter condition. For instance, a line and a circle can be spoken to in Hough space by:

$$line:\ xi\cos\theta + yi\sin\theta = \rho$$

$$circle:\ (xi-a)^2 + (yi-b)^2 = c^2$$

.....(2)

There are two parameters for line and three parameters for circle in Hough space, center (a, b) and the range c of the circle. The optic circle has a roughly round shape, along these lines the Hough transform can be utilized to recognize the optic plate. With the optic circle span settled in Hough parameter space, the search for a round protest turns into a two-dimensional issue.

This technique finds the round shape with settled span in a thresholded edge image of the fundus. To distinguish edges of every conceivable introduction at every pixel in an image compass edge recognition with a Sobel kernel is connected. The maximal reaction of the Sobel kernel for every introduction is held. On this edge guide of the retinal surface a solitary edge is connected to acquire a paired edge outline. Atlast the Hough transform strategy is connected to the edge pixels in the edge guide to aggregate proof of circles with settled range c in the image. The circle with the highest magnitude of evidence is chosen as the optic disc. The technique used in [34] is again a Hough transform based method to detect the contours of the optic disc. Obviously, some improvements have been made in this, but problems have been stated if the optic disc does not meet the shape conditions (e.g., if it lies on the border of the image) or if contrast is very low.

In [23] It was detected, that the optic disc using the circular Hough transform (CHT). First the retinal vessels were suppressed using a morphological closing operator. Then the Sobel operator was used to extract the edges in the image. Finally the CHT was applied to the edge map, and the optic disc was identified as the largest circle.

E. Methods based on Supervised Learning

In [24], [25] proposed a technique for optic nerve location in view of a calculation called fuzzy convergence. This calculation distinguished the optic nerve as the point of convergence of the vein arrange. Fuzzy convergence utilizes the endpoints of the vein segments to help discover the arrangement. For every partition p it uses the following equation for discriminant statistics as follows:

$$F_P = \frac{(\mu_A - \mu_B)^2}{(\sigma_A^2 + \sigma_B^2)}$$

…….. (3)

Where μ and σ is the mean and standard deviation of each set. The largest value of indicates the best partition. The method used the convergence of the blood vessel network; this method also takes lot of time to execute on single image.

F. Methods based on Vessel model

[24] localized OD by back-tracking the vessels to their origin. It is one of the good methods to localize OD but the system has to rely on the vascular tree segmentation which is time consuming. Grison et al. proposed a technique that depends on a model of the geometrical directional example of the retinal vascular framework. This framework verifiably holds the data on the OD position as the purpose of vessel convergence. Utilizing the vessel focus line focuses and the comparing vessel bearings gave by any vessel ID technique, the model parameters were distinguished by a methods for reducing complexity. These evaluated esteems give the directions of the OD focus. [32] detected OD by phase-portrait analysis. Assuming OD is near the focal point of convergence of retinal vessel. The vasculature network is then extracted by Gabor filter. The ONH is obtained via phase portrait analysis and intensity based condition.

III. MISCELLANEOUS METHODS

Few other schemes for OD detection by Frank ter Har [35] described in the literature. These methods are based on pyramidal decomposition of the vasculature and the green plane, the branch with the most vessels, path convergence with the Hough transform and vasculature fitting on a directional model. The authors observed that the method which performs best is the vasculature fitting on a directional model. This method is found to be better than all other evaluated methods in their own database but it fails in STARE database.

The vasculature fitting on a directional model is described by the author in [35] as follows. This OD-detection method uses the orientation of the vasculature, which can be extracted from a fundus image to locate the optic disk. The idea to use vessel orientations to locate the optic disc was first introduced by the authors in [36]. They used a mathematical model that described the expected vessel orientation for each point in an image with respect to the optic disc. Then the sum of squared differences was used to compare the orientations of a new vasculature with the mathematical model, resulting in the OD-location. Starting at the optic disc, the vessels follow more or less the same divergence pattern in all retinal images. Four or five main vessels move in a vertical direction out of the optic nerve. Two of these main vessels curve away towards the macula and make sure that that part of th111111111111e retina is supplied with blood, while the other main vessels diverge

toward other parts of the retina. Branches of the main vessels are spread around the entire retina.

Branches coming out of the two main vessels near the macula converge toward the macula. The automatic OD-detection method here captures these properties in a directional model. Some of the algorithms discussed above will locate only the centre of optic disc, while another category of algorithms will locate it and encircle the area corresponding to optic disc. Very few algorithms are available in the literature for both localization and extraction of the optic disc pixels. The algorithms used today for optic disc localization and extraction are either computationally intensive or less accurate, particularly in the presence of anomalies like exudates in the human retina. Moreover the methods currently available for OD detection largely depends on a prior knowledge of other retinal features like vasculature for the accurate detection of OD. The authors in [37] presents an OD detection and segmentation methodology which is able to detect the OD center without using any template or prior vascular information. Table 1 shows comparative success rate results of existing methods with different databases.

TABLE I.
COMPARATIVE SUCCESS RATE RESULTS OF EXISTING METHODS WITH DIFFERENT DATABASES

Sr No	OD Detection Methods	Local Database	STARE Database	Drive Database
1.	Template Matching and Matched Filter	100%	98.8%	-
2.	Circular Template Matching and KNN regression	99.9%	-	-
3.	Hausdorff based Template Matching	100%	71.6	-
4.	PCA based Method	99%	-	-
5.	Haar Based DWT	89	70.4	-
6.	Pyramidal Decomposition	93.2	54.3	-
7.	Fuzzy Convergence	97.4	65.4	-
8.	Pyramidal decomposition of both vasculature and green plane	93.2	54.3	-
8.	Gabor filter and Face portrait analysis	-	69	100
9.	Morphology Based	100	58	-
10.	Variation of Intensity	99.1	42	-
12.	Circular Hough transform and grow-cut algorithm Abdullah et al. [37]	100	98.68	100

(-) indicates information is provided in relevant field.

Images of the ocular fundus can convey the retinal, ophthalmic, and even systemic diseases such as diabetes, hypertension, and arteriosclerosis. The use of colour retinal images captured with digital fundus cameras provides a non-invasive way of search and screening for ophthalmic and systemic pathologies. A completely automated segmentation of colour retinal images can greatly help in the management of certain diseases like diabetic retinopathy which require the screening of large populations. But the development of an automated system for this purpose needs a robust system capable of fast segmentation of the normal anatomical features of the retina which is not yet available.

IV. CONCLUSIONS

Unfortunately a large portion of the calculations utilized today for macula localization or fovea detection are computationally concentrated, requires earlier data on OD, and are less exact, especially within the sight of pathologies in the human retina. These downsides can be tended to, and a novel approach based OD can be considered for future work. This will permit to better recognize the framework insufficiencies and to propose arrangements, conceivably by joining existing methodologies.

The most challenging part of OD segmentation is preprocessing as each fundus image taken vary by contrast, color etc. The existing algorithms does not work well for the entire standard databases which are publically available. Circular Hough transform and grow-cut algorithm (GC) is computationally fast in processing, robust to the variation in image contrast and illumination, works well in pathological retinal images and is comparable with state-of-the-art methodologies in terms of quantitative performance metrics. Thus, OD segmentation in medical imaging is the challenging job for the researchers preprocessing the original image before further processing on it is key step in detection of OD. Better preprocessing gives the OD segmentation results up to the mark. Hence there is a need of OD detection algorithms which gives the better performance on noisy databases.

REFERENCES

[1] Kubecka, Libor., Jan, Jiri. and Kolar, Radim. Retrospective Illumination Correction of Retinal Images, International Journal of Biomedical Imaging, 2010.

[2] Niemann, H., Chrastek, R. and Lausen , B. “Towards automated diagnostic evaluation of retina images,” Pattern Recognition and Image Analysis, Vol. 16, No. 4, pp. 671–676, 2006.

[3] Foracchia, M. , Grisan, E. and Ruggeri, A. “Luminosity and contrast normalization in retinal images,” Medical Image Analysis, Vol. 9, No. 3, pp. 179–190, 2005.

[4] Fleming, A. D., Philip, S., Goatman, K. A., Olson, J. A. and Sharp, P. F. “Automated microaneurysm detection using local contrast normalization and local vessel detection,” IEEE Transactions on Medical Imaging, Vol. 25, No. 9, pp. 1223–1232, 2006.

[5] Abdel-Razik Youssif, A.A.H. , Ghalwash, A. Z. and Abdel-Rahman Ghoneim, A. A. S. “Optic disc detection from normalized digital fundus images by means of a vessels’ direction matched filter,” IEEE Transactions on Medical Imaging, Vol. 27, No. 1, pp. 11–18, 2008.

[6] Usher, D., Dumskyj, M., Himaga, M. , Williamson, T. H. , Nussey, S. and Boyce, J., “Automated detection of diabetic retinopathy in digital retinal images: a tool for diabetic

retinopathy screening", Diabetes UK, Diabetic Medicine, Vol. 21, pp.84–90, 2003

[7] Sinthanayothin,C, Boyce, J. F. , Cook, H. L. and Williams, T. H. "Automated localisation of the optic disc, fovea and retinal blood vessels from digital colour fundus images", British J. of Ophthalmology, Vol. 83, No.8, pp. 902–910, Aug 1999

[8] Sinthanayothin,C.,Kongbunkiat, V., Phoojaruenchanachain, S. and Singlavanija, A. "Automated screening system for diabetic retinopathy", Proceedings of the 3rd International Symposium on Image and Signal Processing and Analysis, pp. 915–920, 2003.

[9] Osareh, A. "Automated identification of diabetic retinal exudates and the optic disc," Ph.D. dissertation, Department of Computer Science, Faculty of Engineering, University of Bristol, Bristol, U.K., 2004.

[10] Phillips ,Russell, John, Forrester. and Peter "Sharp. Automated detection and quantification of retinal exudates. Graefe's Archive for Clinical and Experimental Ophthalmology", Vol.231, pp.90–94, 1993.

[11] Bernhard M. Ege, Ole K. Hejlesen, Ole V. Larsen, Karina Moller,Barry Jennings, David Kerr, and David A. Cavan, "Screening for diabetic retinopathy using computer based image analysis and statistical classification", Computer Methods and Programs in Biomedicine, Vol.62, pp.165–175, 2000.

[12] Wang, Huan., Hsu, Wynne., Kheng Guan Goh and Mong Li Lee, "An effective approach to detect lesions in color retinal images", IEEE Conference on Computer Vision and Pattern Recognition (CVPR), South Carolina, USA, pp. 181–187, June 2000.

[13] Sinthanayothin, C. , Boyce, J. F. , Williamson, T. H. , Cook, H. L. , Mensah, E. , Lal, S. and Usher, D. "Automated detection of diabetic retinopathy on digital fundus images", Diabet. Med., Vol. 19, pp. 105–112, 2002.

[14] Walter, T. and Klein, J.C. "Segmentation of color fundus images of the human retina: Detection of the optic disc and the vascular tree using morphological techniques", Proceedings of the 2nd International Symposium on Medical Data Analysis, pp. 282–287, 2001.

[15] Li, H. and Chutatape, O. "Automated Feature Extraction in Color Retinal Images by a Model Based Approach", IEEE Trans. on Medical Imaging, Vol. 51, No.2, pp. 246–254,2004.

[16] Li, H. and Chutatape, O. "A model-based approach for automated feature extraction in fundus images," 9th IEEE Int. Conf. Computer Vision (ICCV'03), Vol. 1, pp. 394–399, 2003.

[17] Li, H. and Chutatape, O. "Boundary detection of optic disk by a modified ASM method", Pattern Recognition 36, pp. 2093-2104, 2003.

[18] Li, H. and Chutatape, O. "Automatic location of optic disc in retinal images," IEEE Int. Conf. Image Process., Vol. 2, pp. 837–840, 2001.

[19] Li, H. and Chutatape, O. "Fundus image features extraction", Proceedings of the 22th annual EMBS International conference,pp. 3071-3073, July 2000.

[20] Lalonde, M., Beaulieu, M. and Gagnon, L. "Fast and robust optic disc detection using pyramidal decomposition and Hausdorff-based template matching", IEEE Transactions on Medical Imaging, Vol.20, No.11, pp.1193–1200, 2001.

[21] Osareh, A., Mirmehdi, M., Thomas, B. and Markham, R. "Classification and localisation of diabetic-related eye disease,"7th Euro. Conf. Computer Vision (ECCV), LNCS, Vol. 2353, pp. 502-516, May 2002.

[22] Barrett, S.F., Naess, E. and Molvik, T. "Employing the Hough transform to locate the optic disk", Biomedical Sciences instrumentation, Vol. 37, pp.81–86, 2001.

[23] Abdel-Ghafar, R., Morris, T., Ritchings, T. and Wood, I. "Detection and characterisation of the optic disc in glaucoma and diabetic retinopathy," Med.Image Understand. Annual. Conf., London, U.K., Sep. 23-24, 2004.

[24] Hoover, A. and Goldbaum, M. "Fuzzy convergence," in Proc. IEEE Computer Soc. Conf. Computer Vis. Pattern Recognit., Santa Barbara, CA, pp. 716-721,1998.

[25] Hoover, A. and Goldbaum, M. "Locating the optic nerve in a retinal image using the fuzzy convergence of the blood vessels" IEEE Transactions on Medical Imaging, Vol.22, No.8, pp.951-958, 2003.

[26] Foracchia, M., Grisan, E. and Ruggeri, A. "Detection of optic disc in retinal images by means of a geometrical model of vessel structure," IEEE Transactions Medical Imaging, Vol. 23, No. 10, pp. 1189–1195, Oct. 2004.

[27] Lowell, J., Hunter, A. , Steel, D. , Basu, A., Ryder, R. , Fletcher, E. and Kennedy, L. "Optic nerve head segmentation," IEEE Transactions on Medical Imaging, Vol. 23, No. 2, pp. 256–264, Feb. 2004

[28] Tobin, K. W. , Chaum, E., Govindasamy, V. P. , Karnowski, T. P. and O. Sezer, "Characterization of the optic disc in retinal imagery using a probabilistic approach," Med. Imag. 2006: Image Process, Vol. 6144, pp. 1088–1097, 2006.

[29] Abràmoff, M. D. and Niemeijer, M. "The automatic detection of the optic disc location in retinal images using optic disc location regression," Proc. IEEE EMBC, pp. 4432–4435, Aug. 2006.

[30] Niemeijer, M. Abràmoff,M.D. "Segmentation of the Optic Disc, Macula and Vascular Arch in Fundus Photographs," IEEE Transactions on Medical Imaging, Vol. 26, No. 1, January 2007.

[31] Gonzales, R. C. , Woods R. E. and Eddins, S.L Digital Image Processing using MATLAB, Reading, Pearson Education Publishing Co., 2002

[32] Canny, J. "A computational approach to edge detection," IEEE Transactions on Pattern Recognition and Machine Intelligence, vol. PAMI-8, pp. 679-698, Nov. 1986.

[33] Walter, T., Klein, J. C. , Massin, P. and Erginay, A. "Detection of Exudates in Color Fundus Images of the Human Retina" IEEE Trans. Med. Imag., Vol. 21, No. 10, pp 1236-1243, October 2002.

[34] Pinz, A., BernÄogger, S., Datlinger, P. and Kruger, A. "Mapping the human retina", IEEE Transactions on Medical Imaging", Vol. 4, pp. 606-619, 2001.

[35] Frank ter Har, "Automatic Localization of Optic Disc in Digital Colour Images of the Human Retina", MS Thesis, Utrecht university, pp. 33-50, 2005

[36] Ruggeri, A., Foracchia, M. and Grisan, E. "Detection of optic disc based on a directional model of vascular network", http://www.cafia.org/cafia2003/cafia-3 abstracts.pdf.

[37] Abdullah et al. (2016), Localization and segmentation of optic disc in retinal images using circular Hough transform and grow-cut algorithm. PeerJ 4:e2003; DOI 10.7717/peerj.2003.

[38] Akram, Usman M., and Shoab A. Khan. "Automated detection of dark and bright lesions in retinal images for early detection of diabetic retinopathy." Journal of medical systems 36.5 (2012): 3151-3162.

[39] Balaji, G. N., T. S. Subashini, and N. Chidambaram. "Cardiac view classification using speed up robust features." Indian Journal of Science and Technology 8 (2015): 1.

A Study Towards Post Hoc Forensic Analysis Using Big Data Analytics

Bipin Bihari Jayasingh
Professor, CVR College of Engineering/ IT Department, Hyderabad, India.
Email: bbjayasingh9@rediffmail.com

Abstract: **The network traffic data of an enterprise is considered to be huge day by day and it gradually becomes big data. The major concern here is how to analyze the data in case of an unusual event occurs and how to draw a conclusion when data is voluminous. The post mortem analysis of traffic data and grabbing the information as evidence is said to be network forensics that can be achieved through big data analytics only. In this paper, the network forensics literature is studied along with how to use big data analytics for accurate analysis of fraud. There is a well understood discussion about the security challenges of big data including big data privacy issues, data provenance problems and visual analytics. Traffic data is used for attack analysis by considering fraud detection methods for the advanced persistent threats in order to correlate large quantities of diverse data to detect an attacker. It is also considered the forensic analysis of an attack in the traffic data to extract the evidence against an attacker. It is more focused on the techniques and associated tools for use of big data analytics for security and use of information security algorithms to protect big data. This rigorous study leads to making use of available tools and techniques of big data analytics in the development of any network forensic system.**

Index Terms**: Network Forensics, Big Data Analytics, Fraud Detection, Advanced Persistent Threats, Privacy Issues, Data Provenance Problems, Visual Analytics.**

I. Introduction

In the cyber environment the data becomes more than the size of petabyte large every day due to network flows (messages, streams, and user actions), user passwords and other information. The fundamental aspect is to analyze the data in order to mitigate the system vulnerabilities and attacks. Big data visualization and analytic techniques are useful to analyze the huge network data available in the storage hub to address cyber security [2, 11]. An other way of analyzing network data after an attack is very important to extract the evidence against the crime which must be through big data analytics tools and visualization [3, 4]. The analysis after the attack is towards a post hoc forensic analysis by using "big data analytics" in the storage hub of an enterprise.

Forensics is an art of discovering and extracting information about a crime suitable to law enforcement agencies as admissible evidence [12]. In the traditional way of expressing, the prevention and detection of network attacks is the network security model that extends to network forensics. Network forensics is the use of scientifically proved techniques to collect and analyze network packets and events for investigative purposes [7]. Network forensics is a branch of digital forensics that focuses on monitoring, capturing, recording and analysis of network traffic includes volatile and dynamic data [7].

However, forensically reconstructing a network attack along with evidence is called network forensic system. The intention behind reconstruction is to prove that the network attack that has been perpetrated by the invader, for whom the evidence is collected. Though the digital evidence is fragile, it must be preserved for future trial. In the internetworking environment, it is difficult to preserve the evidence in the same system as the network traffic is huge and might crash the traffic capture system if left unattended. Hence, the more the network traffic, the harder the network analyzing. Therefore, we need an effective and automated analyzing system for network forensics where data is big.

The remainder of the paper is organized as follows: section 2 specifically discusses the challenges of big data analytics in terms of big data privacy issues, data provenance problems and visual analytics; section 3 focuses more on attack analysis methods considering fraud detection, advanced persistent threats and forensic analysis; section 4 present the use of big data analytics for security and use of security to protect big data with forensic profiles techniques; section 5 provides the concluding remarks.

II. Challenges Of Big Data Analytics

The main challenge is to identify the network attack followed by evidence reconstruction. The information present in the packet header may be crucial evidence for the detection of network level attack. Other way of detecting the network attack is looking at the data fragments carried out by the packet payloads [8]. The detection using big data analytics has a significant promise that must be addressed by the forensic specialist. Data analytics must focus on network traffic and separate the abnormal traffic from the normal flow of traffic. It becomes easy to identify the abnormal pattern in the abnormal traffic

to find the suspected activity. The abnormal pattern may become potential legal evidence of the attack which a network forensic system requires. Another valuable phenomenon called the network forensics, is an investigation process for the network related crimes. In specific, network forensics investigates the problems created by the miscreants in accessing the network devices. It analyzes large amount of network traffic data to find the footprints of network crimes. We consider the big data privacy issues, data provenance problems and visual analytics in this section.

A. Privacy Issues

The privacy issues are viewed in a wider perspective when it relates to data mining and considers various approaches to protect sensitive information [19]. A new knowledge can be extracted through data analytics and aggregated through data processing but not lead to privacy issues of a user [14]. Data analytics has to preserve the privacy of data while extracting and correlating the data. The forensic analysis must ensure to minimize the privacy raids during analysis of data. The data can be used for the purpose for which it has been collected.

Data analytics helps to efficiently process and organize the relevant data. The forensic scientist must examine the data without encroaching the privacy of a person. The system must collect enough metadata consisting of different attributes, to confirm the identity of a person. For example, a facial analysis system should not attempt to identify a person but it must collect enough metadata about a person based on their face like the expressions of a face. The forensic analysis must respect the privacy of data and ensure the security and privacy policies. Any application tools we develop must be allied with principles and recommendations of privacy preservations [2].

B. Data Provenance Problem

Data provenance in big data has been explored recently but it has been studied in database and distributed systems communitie's. It simply refers to the ownership of data or custodian of data and the location of the data where it resides [19]. It is a process of maintaining the origin and creation of data which is useful for validating the data, determining the reliability of data and evaluating the quality of data. The quality of data depends on debugging, transformations, auditing of data objects of various sources [20]. Data provenance can also be used for performance bottleneck analysis.

Big data provenance is another challenge where it allows for expanding data sources and the data can be from any sources. However, the analysts must put proactive effort to secure the abuse of the data sources [2]. The analysts must focus the issues of data provenance discussed hereunder.

- There are various sources of data but access to all sources at a right time is difficult.
- There may be possible access of all data but data analysis probably becomes difficult.
- Generating reports using queries on each source takes longer time to run.
- It is very difficult to share the gained information and useful patterns with others.
- The trustworthiness of data source is hard to maintain to produce accurate results.

There must be some mechanism to identify and mitigate the malicious data in the data source itself like machine learning algorithms. So research is required for innovative methodologies in order to visualize and mine the data provenance [5].

C. Visual Analytics

Visual representations of data is needed for the analysts to interact with data to amplify cognition. This is called information visualization. The visualized information presents graphical models and user interfaces which interactively manipulates the large set of data [12]. The graphical models can transform raw data into proper tables, then turn into visual structure. Visualization of information always considers with small set of data and for the large data set, it will be called as visual analytics.

Human eye has a tendency to look for the summaries or overviews instead of large amounts of unfamiliar data. Analysis of data and getting a decision is a process that makes a sense of the system. This is also referred as visual analytics. The analysis looks for patterns and correlations at a different level of drill down to the data [2]. The aim is to represent the data effectively to convey information to the analyst is called visual analytics [6]. It explores and interacts with data by applying queries and finds the results and interpret the results. It helps the analyst to interpret the results and convey the useful information through effective representation [2]. The simplest example of visual analytics is discovering fraudulent transactions in credit card usage.

III. ATTACK ANALYSIS METHODS

Every day, 2.5 quintillion bytes of data [21] are created and 10 to 100 billion events are generated by a large enterprise [2]. As the events are generated from multiple and heterogeneous sources, the enterprise must deploy more devices, hire more employees and run more software for post hoc forensic analysis. As a result, the overwhelming data volume requires an effective data analysis and prediction platform to achieve the efficacy of such big data. Existing analytical techniques are not sufficient in the large-scale analysis and in the processing of big data events, so the big data analytics has attracted the interest of the security community [6]. There are three ways of doing the attack analysis either through fraud

detection methods, advanced persistent threats or through forensic analysis of the networks.

A.Fraud Detection

The law enforcement agencies attempt to detect fraud becomes harder still due to various factors that lead to fraud. It becomes easier through 'big data analytics' tool which help to anticipate and quickly detect fraud to take immediate action [18]. In order to detect fraud, we must use data mining tools that can search and find patterns on behalf of the analyst. Some such data mining tools are recorded here for the better understanding of the researchers as follows:

- Decision trees
    - Boosting trees
    - Classification trees
    - CHAID
    - Random Forests
- Machine Learning
- Association Rules
- Cluster Analysis
- Neural Networks

There are predictive models which estimate the probability of amount of fraud and focus most efficiently to prevent or recuperate fraud losses.There are some issues which law enforcement agencies must look.

- Fraud detection is a predictive modelling problem that can anticipate a rare event. The model can capture the fraud if the historical data is available along with previously classified verified data. The suggestion for the rare events can be predicted with a best predictor and a validated model that provide a greatest lift to maximize the likelihood of observations associated with fraud.
- Fraud detection is an anomaly detection problem that identifies outliers in multivariate space. This works well even when there is no good training dataset where known fraudulent and non-fraudulent observations are clearly identified. Using Big Data techniques, to analyze and even predict, security incidents [13] are successful.

B. Advanced Persistent Threat (APT)

The advanced persistent threat (APT) is a new breed of insidious threats where hackers can retain control over target systems unnoticed for long periods of time. The adversaries use multiple attack techniques and vectors in order to avoid detection [4]. The traditional defense mechanisms are not sufficient to detect such attacks. The focus should be on developing a depth strategy of defense only after a clear understanding of these attacks. The aim must be constantly to monitor the networks and security control systems to grab possible footsteps of such attacks for post hoc forensic analysis.

APTs occur in such a way where a victim stays oblivious to the happening of insidious crime. It operates itself while it resides in the system and executes for an extended period of time. The detection of such threats requires data from various internal and external data sources to correlate to find posterior information, lead to forensics [2]. In such cases big data tools are useful though it correlates huge amounts of diverse data and performs long term correlation that becomes fundamental for advanced persistent threat (APT) detection and forensics [4, 5]. The techniques may be a pattern analysis or feature extraction that may detect the threat at an early stage.

C. Forensic Analysis of Networks

The analysis of network logs, network flows and system events for an enterprise in order to detect an attack is a major problem in the security and forensic community due to inadequate analytics technology [15]. There are several reasons in practice where voluminous data storage was economically not feasible and retention period for variety of unstructured data is fixed. The traditional management of large data warehouses has become expensive and obsolete. However, the big data tools and techniques along with Hadoop deployment frameworks are suitable for the large scale maintenance of data that are most preferred to process and analyze the data [2].

There are applications that use big data technologies to clean, prepare and query data in heterogeneous, incomplete and noisy formats efficiently. There is also security management software that helps the analyst to do so called clean, prepare and query the data.

There is proposed literature based on Shannon entropy and machine learning techniques for attack detection in network forensics systems [8]. There is also a proposed fuzzy logic based expert system for forensic analysis of computer networks that can analyze the threat and store the digital evidence automatically [9]. There is a possibility of compromise of the system to the network attack. Now, finding the evidence against the attack needs the help of forensic experts where it may lose some useful instant evidence at the time of investigation. So, there must be integrated analysis of the log and audit system and network traffic that can make to an efficient navigation of the traffic. This work discusses the frameworks of distributed agent-based real-time network intrusion forensics system which is deployed in local area network environment [10].

The network forensics objective is to gather evidence of criminal acts in the network infrastructure includes about the perpetrator from any place of the globe. Therefore, software tools, and techniques, that can help with these digital investigations are in great demand. The self-organizing maps (SOM) are presented to analyzing and visualizing network traffic data [11]. The self-organizing map has been widely used in clustering tasks that can enable network clusters to be created and visualized in a manner that makes them immediately more intuitive and understandable.

There is an architecture called trusted Internet forensics (TIF) that collects data from the network for forensics purpose. The architecture consists of network appliances that rely on a trusted computing platform. The architecture allows for the verification of the computational chain so that the data collected in the network could be used as evidence in court [12].

It is more difficult to collect the information for attack analysis though the attackers are trying to remove attack traces such as system logs and related information on the victim systems. Therefore, most of them are focusing on gathering the network packets. There is a network forensics system, Cyber Black box, which is focused on the traffic analysis [13]. Recently, several machine learning techniques have been proposed to automate and develop intelligent network forensics systems. Others adapt recent researches in semantic-web, information architecture, and ontology engineering to design method ontology for network forensics analysis [14].

IV. Security Analysis

Traditional computing methods of security tools and techniques used to process the big data are inadequate due to the involvement of data from different machines and applications. To mine the traffic data and prevent cyber security must be more reactive than proactive. It also creates a large number of false positives, inefficient and distracting from actual threats. Data analytics has to be used to analyze the network traffic, log files and financial transactions. It may be feasible that the data correlations from multiple information sources are represented in a coherent view and possibly identify suspicious activities and anomalies. Data analytics can predict potential cyber security breaches that help to stop cyber-attacks and facilitate post breach cyber forensic analysis.

Security researchers must keep exploring novel ways to find sophisticated attackers though bigdata is not a panacea. The technologies like network monitoring and network forensics become the landscape of security. Keeping in mind the privacy preservation, all must work together to develop some tools for the data analytics [2]. So far, the dominant strategy has been to optimize existing analytical environments that often rely on scripting languages like Python, Spark and R. Therefore, it needs to increase the effort to educate new generation computer scientists and engineers on the value of privacy.

We can use other popular algorithms which are typically available in statistics and machine learning libraries. The typical algorithms include hierarchical clustering and principal component analysis computation and projection methods. We concentrate on using big data analytics for security and forensics, also on protecting the big data through security mechanism by applying suitable advanced data mining algorithms.

A. Big Data Analytics for Security

The data processing using traditional data management tools and techniques to massive, heterogeneous and often unstructured digital content is difficult. The big data refers to the complexity and variety of data and data types whereas real time data collection and processing can be obtained by smart data analytics. Big data analytics in the trade sector provides a better understanding of customer behavior and preferences. It extracts a valuable insight that enables to increase customer satisfaction [3]. In many business and scientific applications, the use of standard advanced data mining tools and techniques that helps to extract information from large and complex datasets to make proper decisions.

The main focus is to analyze the data and find the loopholes of system security then improve the security mechanism to protect the misuse of the data. As the data analytics tools continue to be deployed in enterprise systems, it needs to improve the systems security by introducing new tools, such as Apache's Accumulo, to deal with the unique security problems in big data management [2]. The conventional security mechanisms like integrating Transport Layer Security within Hadoop are not sufficient to justify the security levels. In particular, a better monitoring of macro and micro level data security is essential which help decision makers to catch commercial opportunities i.e. anticipating recessions [4].

B. Security to Protect Big Data

In a security aspect, there are two distinct issues: securing the organization and its customers' information in a Big Data context that means protecting the data as well as data centers. Without the right security and encryption solution in place, however, big data can mean big problems. Big Data breaches will be big too, with the potential for even more serious reputational damage and legal repercussions. Techniques such as attribute based encryption may be necessary to protect sensitive data and apply access controls.

Physically data resides at different locations in a distributed manner when it becomes large volumes using big data technologies. The users have never possessed storage of their data physically. In order to perform data mining, some users hire third party data miners to process their data efficiently and effectively. In the realm of big data, protection of private data focuses on excluding third party access to the original data directly. The solutions rely on some privacy preserving approaches or encryption mechanisms to the source of data. Sometimes data accesses from servers by using virtual disks are avoided due to compromising the user privacy.

To secure the data in the big data store, there are vendors who provide encryption capabilities. It may not secure all the log files and configuration information associated with the big data environment. But the security specialist must

contend for key fragmentation that may helpful for administration of big data stores [5].

One of the solutions for data security is to use vormetric encryption schemes to the diverse data store of an organization. The encryption mechanism follows in two ways:

- Vormetric Transparent Encryption**:** These encryption mechanisms directly handle the file systems to encrypt the data and also control the access to the file system itself. It is very easy to deploy and it will not effect to any changes that are made to any kind of applications.
- Vormetric Application Encryption**:** These encryption mechanisms are encrypting the attributes of the database before it store permanently. It is encrypting the columns of the specific applications before writes to the database. There will be some sensitive field that will remain unreadable due to the column encryption scheme. Also, the same problem remains even after it is imported into, and processed within, the big data environment.

C. Forensic profiles

Data mining techniques are used to discover relevant patterns from large quantities of data. Using those patterns generating forensic profiles is good approach in the big data environment. The forensic profile can be matched to any new data coming to the data source to find the misused data. The evidence can be extracted in the case of misuse or anomaly of data. There are literatures available in the area of extracting and analyzing digital evidence from physical devices such as hard disks. Probably less effort put in the portable storage devices [15]. The forensics on portable devices using data mining is difficult due to the structure and the storage of the data.

There are good number of work that has been done to incorporate the use of decision trees as well as naive Bayesian, a priori, and neural network techniques [16, 19]. Also there are similarity-based machine learning techniques deliver more robust performance than other techniques such as decision trees, ensemble methods and regression-based methods that are to achieve practical efficiency for similarity-based techniques is to sparsely the similarity matrix [1]. Recently proposed architectures also incorporate mechanisms for monitoring process behavior, analyzing trends, and optimizing plant performance [17].

In the data mining perspective, there is a proposed model called big data processing model that is related to HACE theorem. The work characterizes the features of big data revolution that starts with large-volume, heterogeneous, autonomous sources with distributed and centralized control [18]. Data mining algorithms has to perform in such a way that privacy information must be preserved and security of sensitive data must not be compromised [19].

We have proposed a Network Forensic System (NFS) for network related crimes that helps the investigator in finding the attackers associated with crime. The proposed forensic system will combine the best features of existing traditionally framework models and extend them to form a focused investigatory model for networked systems. The forensic system will be classified into three phases shown in fig. 1.

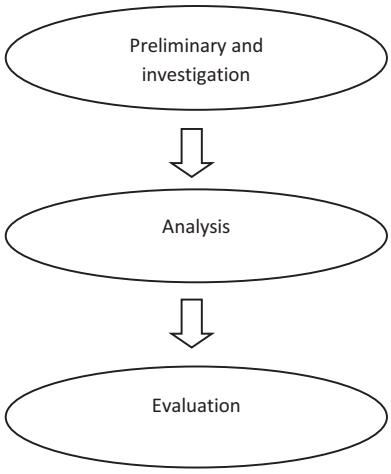

Figure 1. Model of the network forensic system

- Preliminary and investigation

The preliminary process includes the victim of the crime, cyber forensic experts and law enforcement agency. The investigation process will start after the victim's complaint against the crime to the law enforcement agency about the incident that has occurred. The law enforcement deputes the cyber forensic expert to find sufficient evidence against the crime and submit a brief report. This process mainly concerns on validation of the incident and followed by checking requirements for the investigation like human resources, etc. We combined the preliminary and investigation phase that saves the time and money. In this phase, the cyber forensic expert will identify, collect and preserve potential digital evidence that are required to proceed with the investigation. In this process the cyber forensic expert try to find the relation between the culprits and the crime. Any further evidence found will be collected and produced under the court of law or as part of any other relevant legal processes. Once investigation phase is finished, the relevant information will be stored as evidence and will be reported to next step i.e., Analysis phase.

- Analysis

The Analysis phase is the most important part of the model as the investigator needs to verify all the information found is connected to the incident so that it serves as potential legal evidence. The analysis and examination of evidence determines the width and depth of the crime.

Analyzing the suspect's information recorded in the service provider's database is the digital forensic investigation. It is useful to map the relations of the suspects profile with the profiles of other people to obtain constructive evidence. This phase determines if the evidence is genuine or if there is generated evidence to prove the crime.

- Evaluation

In this phase, the investigator will produce all the evidence that are collected about the culprit from the network related crime. This is through appropriate documentation as a report. The investigator needs to present the legal evidence to the law enforcement agency against the crime to fulfill the aim of the investigation.

V. CONCLUSIONS

The study undertakes more emphasis on advanced data mining tools and techniques relating with big data analytics. Though all the information captured or recorded are not useful for analysis, it will be decided by big data analytics. A network forensic system must be developed which can provide an analyzed information to the forensic experts and reduce the time and cost of forensic analysis in case of network attacks. There is a proposed network forensic system in general for the investigators to understand the judiciary process of cybercrime. In the future the analysis of network traffic will be carried out for an attack to show sufficient information as evidence against an unusual event using big data analytics.

REFERENCE

[1] Dorit S. Hochbaum, Philipp Baumann, Sparse Computation for Large-Scale Data Mining, IEEE Transactions on Big Data, Vol. 2, No. 2, April-June 2016, pp. 151-174.

[2] Alvaro A. Cárdenas, Pratyusa K. Manadhata, Sreeranga P. Rajan, Big Data Analytics for Security, IEEE Security & Privacy, 1540-7993/13, 2013 IEEE, pp.74-76.

[3] A. Katal, M. Wazid, R. Goudar. "Big data Issues, challenges, tools and good practices", in the Sixth International Conference on Contemporary Computing, Aug. 2013, pp. 404-409.

[4] D. F. Nettleton, "Commercial Data Mining: Processing Analysis and Modeling for Predictive Analytics Projects", 1st ed. Boston, United states, Morgan Kauffman Publishers-Elsevier, 2014.

[5] Domenico Talia, "Clouds for Scalable Big Data Analytics", IEEE Computer Society, 0018-9162/13, 2013, pp.98-101.

[6] R. Nambiar, R. Bharadwaj, A. Sethi and R. Vargheese."A Look At Challenge And Opportunities In Big Data Analytics In Health Care", In IEEE International Conference In Big Data, Oct. 2013, pp. 17-22.

[7] J. Buric, INsig2 d.o.o., Zagreb, Croatia, D. Delija, Challenges in Network Forensics, IEEE 38th International Convention on Information and Communication Technology, Electronics and Microelectronics (MIPRO), DOI: 10.1109/MIPRO.2015.7160490, 25-29 May 2015, pp. 1382 – 1386.

[8] Khoa Nguyen, Dat Tran , Wanli Ma, Dharmendra Sharma, An Approach to Detect Network Attacks Applied for Network Forensics, IEEE 11th International Conference on Fuzzy Systems and Knowledge Discovery (FSKD), DOI:10.1109/FSKD.2014.6980912 19-21 Aug. 2014, pp. 655 – 660.

[9] Jung-Sun Kim, Chonnam Nat., Dong-Geun Kim, Bong-Nam Noh, A Fuzzy Logic Based Expert System as a Network Forensics, IEEE International Conference on Fuzzy Systems DOI: 10.1109/FUZZY.2004.1375521, Vol. 2, 25-29 July 2004, pp. 879 – 884.

[10] Wei Ren, Wuhan, China, Hai Jin, Distributed Agent-Based Real Time Network Intrusion Forensics System Architecture Design, 19th IEEE International Conference on Advanced Information Networking and Applications (AINA'05), DOI. 10.1109/AINA.2005.164, vol. 1, 28-30 March 2005, pp. 177 – 182.

[11] E. J. Palomo, J. North; D. Elizondo; R. M. Luque, VisualizationOf Network Forensics Traffic Data With A Self-Organizing Map For Qualitative Features, IEEE International Joint Conference on Neural Networks (IJCNN), The 2011, DOI: 10.1109/IJCNN.2011.6033434, July 31 -Aug. 5 2011, pp. 1740 – 1747.

[12] D. Bruschi, M. Monga; E. Rosti, Trusted Internet Forensics: Design of a Network Forensics Appliance, IEEE Workshop of the 1st International Conference on Security and Privacy for Emerging Areas in Communication Networks, 2005, DOI: 10.1109/SECCMW.2005.1588292, 5th -9th Sept. 2005, pp. 33 – 35.

[13] Yangseo Choi, Joo-Young Lee;Sunoh Choi ; Jong-Hyun Kim, Introduction to a Network Forensics System For Cyber Incidents Analysis,18th IEEE International Conference on Advanced Communication Technology(ICACT),DOI: 1109/ICACT.2016.7423270 Jan. 31 2016-Feb. 3 2016, pp. 50 – 55

[14] SherifSaad, IssaTraore, Method Ontology for Intelligent Network Forensics Analysis, Eighth IEEE Annual International Conference on Privacy Security and Trust (PST), DOI: 10.1109/PST.2010.5593235, 17-19 Aug 2010, pp. 7 – 14.

[15] V.H. Bhat, "A Novel Data Generation Approach for Digital Forensic Application in Data Mining," Proc. 2nd Int'l Conf. on Machine Learning and Computing (ICMLC 10) IEEE, 2010, pp. 86-90.

[16] F. Camastra, A. Ciaramella, and A. Staiano, "Machine Learning and Soft Computing for ICT Security: An Overview of Current Trends," J. Ambient Intelligence and Humanized Computing, Oct. 2011; doi:10.1007/s12652-011-0073-z.

[17] T. Kilpatrick et al., "An Architecture for SCADA Network Forensics," Proc. IFIP Int'l Conf. Digital Forensics (IFIP 06), Nat'l Center for Forensic Science, 2006, pp. 273-285.

[18] Xindong Wu, Xingquan Zhu, Gong-Qing Wu, Wei Ding, Data Mining with Big Data, IEEE Transactions on Knowledge and Data Engineering, Vol. 26, No. 1, January 2014, pp. 97-107.

[19] Lei Xu, Chunxiao Jiang, Jian Wang, Jian Yuan,Yong Ren, Information Security In Big Data:Privacy And Data Mining, DOI 10.1109/Access.2014.2362522, IEEE ACCESS, October 20, 2014, Pp. 1149-1176.

[20] Y. L. Simmhan, B. Plale, and D. Gannon, A survey of data provenancein e-science," ACM Sigmod Rec., vol. 34, no. 3, 2005, pp. 31-36.
[21] "IBM What Is Big Data: Bring Big Data to the Enterprise,"http://www-1.ibm.com/software/data/bigdata/, IBM, 2012.

Fully Anonymous Data Access Provision and Attribute based Encryption Scheme for Efficient Cloud Data Privacy

G.V.M.S. Architha[1] and S. Jyothsna[2]
[1]M. Tech Student, CVR College of Engineering/CSE Department, Hyderabad, India
Email: architha.gadi@gmail.com
[2] Asst . Professor, CVR College of Engineering /IT Department, Hyderabad, India
Email: jyothsna.sundaragiri@gmail.com

Abstract: **Cloud computing is a service based distributed computing where the users can access required services on pay per use basis. Cloud enables users to store data and provides on demand accessibility. As the cloud service providers and cloud users are from different trust domains so security concerns rise out of it. Sharing of resources is the key idea behind the cloud which makes access control, a critical issue in cloud computing. Different configurations for attribute based encryption were used for cloud storage security. The work primarily deals with information protection and the access control. The current work is a semi anonymous privilege control scheme called Anony Control which provides identity and data privacy of user. Also Anony Control-F that fully prevents the information leakage of user and achieves the full anonymity has been presented. Here multiple authorities provide attributes in such a way that each authority will know only one attribute. This is called as multi authority cipher text policy attribute based encryption (CP-ABE). Which guarantees the user's personal information privacy and tolerates collusion attacks on attribute authorities.**

Index Terms: **Access control, Anony Control, Privilege control, Semi anonymity, Anony Control-F, CP-ABE**

I. Introduction

Cloud computing enables the people to share their data with others. People can share their information with others through online social networks such as Facebook and Instagram. These services facilitate communication easily but privacy and data security issues will arise. Unauthorized users and their unauthorized accessibility would be threats to cloud data. Providing data security and controlling unauthorized accessibility are the major concerns of this work.

The authorized users can access data based on access control policy. If the data storage server gets compromised, anyone who has access permission can retrieve the data that is not related to them even if they are in encrypted form. So, such kind of unauthorized access and compromise attacks must be controlled. Multiple access control mechanisms with an efficient encryption system are adopted in the cloud computing environment through ABE.

ABE can be classified into two types

- *Key-policy attribute based encryption (KP-ABE)*
- *Cipher text-policy attribute based encryption (CP-ABE).*

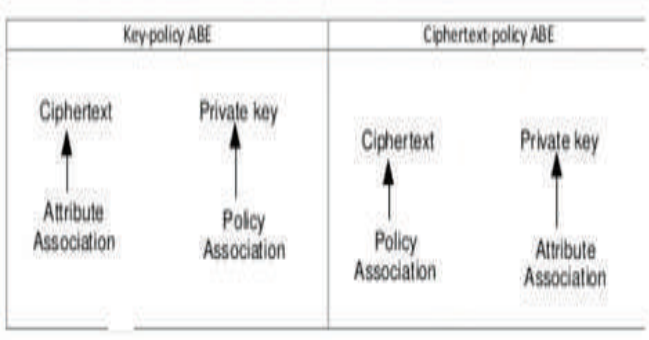

Figure 1. KP-ABE and CP-ABE

In KP-ABE access policy is associated with the private key whereas in CP-ABE, Access policy is associated in cipher text and the data owner will have complete authority about the encryption policy.

II. Related Work

Dfferent attribute based encryption techniques were proposed.

A. *Identity based Encryption*

Initially attribute based encryption called Identity based encryption was presented by "*Shamir*"[9], where the message of a sender indicates an identity and the receiver with a matching identity can only decode it.

B. *Fuzzy based Encryption*

This is a type of public-key encryption in which a cipher text and the private key of a user are based upon attributes. It is also called as attribute based encryption. In ABE algorithm keys and cipher texts are labeled with sets of descriptive attributes and a particular key can decrypt a cipher text only if there is a match between access policy and attribute set.

Anony Control-F prevents completely identity leakage of the user. The proposed scheme of action guarantees user's security against each attribute authority. Partial data is uncovered in the Anony Control scheme and no data is

revealed in Anony Control-F and can tolerate authority collusion. Multi authority based encryption schemes, Anony Control and Anony Control-F are used. The standard servers are not highly secure. To improve the data privacy on the servers, AES algorithm is used. First the data is encrypted using AES algorithm and later it is encrypted using CP-ABE.

III. Design Analysis

The data has to be confidential as the data is stored in semi trusted servers and there are multiple owners and users in cloud computing environment. For data encryption, public key encryption based schemes were used initially. But it was one to one encryption and has high key management overhead. So one-to-many encryption methods like ABE were used. Here the data is encrypted under access policy which enables users to decrypt using the relevant private key. The owner can encrypt the data without knowledge of the access control list. The main feature of ABE is that it prevents user compromise attacks.

This work is implemented using the following modules

- *Setup:* Generates master key and public key.
- *Key Generation:* Generates a private key for a set of attributes for given master key
- *Encryption:* Encrypts a file based on an access policy for a given public key
- *Decryption:* Given a private key, decrypts the file such that only users who has attributes that match the access control policy can decrypt it.

First, data is encrypted using AES and the AES keys are again encrypted and then decrypted using CP-ABE.

A. Advance Encryption Standard

The Advanced Encryption Standard (AES) is a symmetric encryption technique used to secure sensitive data. AES is based on a design principle known as a substitution–permutation network, a combination of both substitution and permutation, and is fast in both software and hardware

The step by step procedure of AES encryption algorithm using 128-bit key is presented in the following flow chart. AES is using shifting of bits and adding in each round. Each round consists of several processing steps, each containing four similar but different stages, including one that depends on the encryption key itself. A set of reverse rounds are applied to transform cipher text back into the original plaintext using the same encryption key.

The symmetric key is generated using AES by following the procedure given in Fig2.

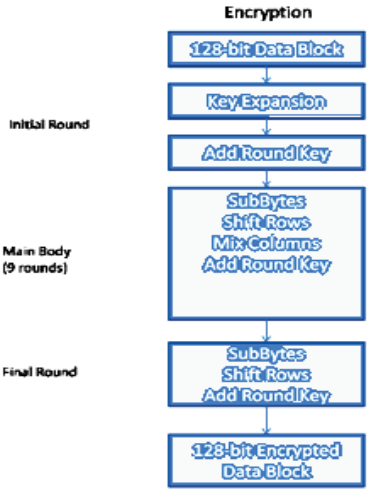

Figure 2. AES process

IV. CP-ABE Algorithm

Cipher text Multi authority ABE (CP-ABE) is used here for data access control in the cloud storage system to prevent centralization of authority. In CP-ABE scheme, user's secret key is tied to a attribute set that represents the user's permissions. A set of attributes is designed for the encryption and the decryption is possible only to the users who have the relevant attributes. Here multi authority CP-ABE is considered i.e. the set of attributes are provided by multiple authorities. Each authority will have a partial set of attributes; with this scheme security can be improved.

The Algorithm followed here is divided into two steps

1. Applied AES for generating symmetric key
2. Applied CP-ABE on the key generated in step 1

CP-ABE does not require a trusted authority like other role-based access control schemes (RBAC) or any form of storage. The encryption itself serves as the RBAC mechanism.

A. Process of Encryption

1. The data owner encrypts the file using AES, this encrypted file called as Data key
2. The above data key is encrypted using attribute set of multiple authorities using multi authority ABE scheme.
3. The encrypted file and access policies are stored in cloud.

B. Process of Decryption

1. The users request the data from the cloud server using the access keys. The user whose attribute set in private key matches the access policy in cipher text can decrypt the file
2. Downloads the decrypted file from the cloud server.

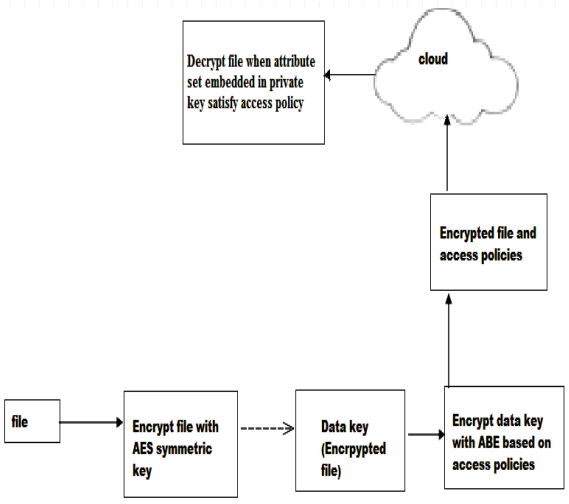

Figure 3. Encrypting data with AES and CP-ABE

V. IMPLEMENTATION

There are four types of entities in this system.

Data Owner: Data Owner encrypts and transfers the file data into the cloud server.

Data Consumer: Data Consumer (user) decrypts and downloads the file from the cloud server.

Attribute Authority: The attribute authorities are the key generators that provide public key to the data owner and private key to the data consumer.

Cloud Server: Cloud server stores the data and provides security.

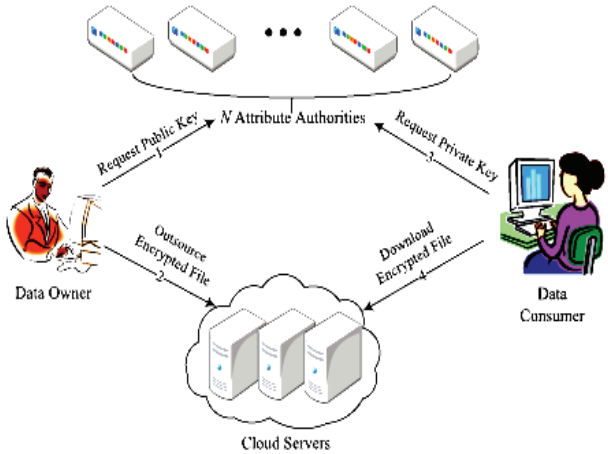

Figure 4. Architectural Flow Diagram

The data owner and the data consumer need to register with the system to access and to perform any operations on files. Central Authority should approve the users and attribute authorities. Attribute authorities provide unique private keys to users only after successful approval. Two attribute authorities are considered to provide private keys to users and these authorities provide keys without knowledge of the user identity information. Thus, anonymity is achieved.

The example considered here is medical data. Attribute authorities generate private keys against user attributes location, experience, specialization and medical degree and presents a cipher text encrypted such that only users with specified attributes able to decrypt it. USER1 have "location" and “specialization” attribute tied to their private keys, and USER2 have "medical degree" and “experience” attribute tied to their private keys. Both groups, therefore, are able to decrypt the encrypted message.

Data owner uploads an encrypted file using a public key generated by attribute authority and adds an access policy such as (India && ENT) && (MD && exp<3). Thus attribute based encryption is achieved.

Users can decrypt the file only if the attributes match the access policy. In the below example, 4 persons with a different attribute set are considered. Two persons have attributes satisfying the access control policy and two others who don’t match the access control policy.

In this example, user 3 and user 4 will not be able to access and decrypt the file and hence these users will get the popup window such as “Sorry the file cannot access by you”, but user1 and user2 can access and decrypt the file as these users can satisfy attributes which are part of access policy. With keys provided by attribute authority the users can access the files in to and from the cloud access.net. Cloud Access provides security-as-a-service from the cloud. It also provides high performance solutions managed from the cloud that meet different business needs and guarantees the protection of cloud services.

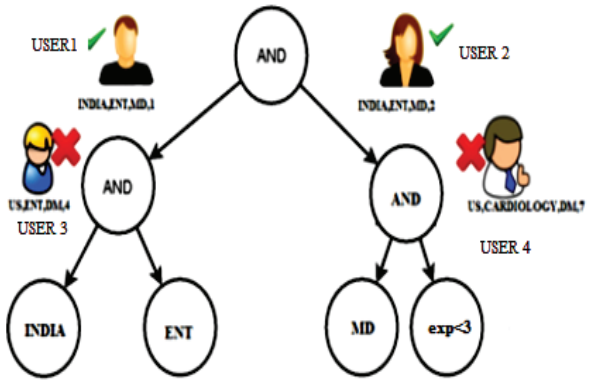

Figure 5. Access Tree

VI. EVALUATION

The performance evaluation of AnonyControl-F and CP-ABE is presented. The below figure displays measurements of private key generation time, encryption time and decryption time produced by running CP-ABE key generation, CP-ABE encryption and CP-ABE decryption on a range of problem sizes.

CP-ABE-key generation runs in time perfectly linear to the number of attributes associated with the key it issues and the running time of CPABE-encryption is almost precisely linear based on the leaf nodes in the access control policy.

The time complexity of CP-ABE key generation and CP-ABE encryption depends on the attributes in a key and the performance of CP-ABE decryption is based on the access policy tree of the cipher text and the attribute set embedded in secret key.

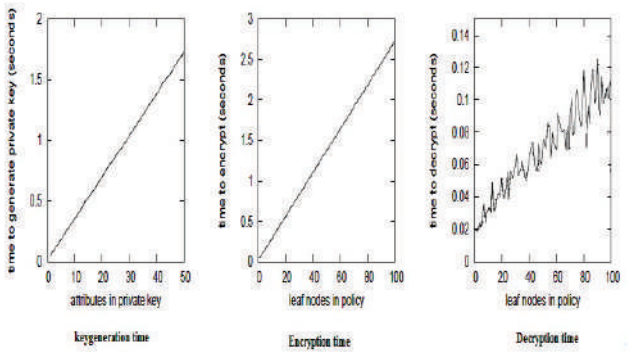

Figure 6. Time Analysis

VII. CONCLUSIONS

The Access control policy in cloud computing is improved using AnonyControl which is a semi-anonymous attribute-based privilege control scheme and AnonyControl-F which is a fully anonymous attribute-based privilege control scheme. Anony Control-F addresses the user privacy problem in a cloud storage server. User's privacy is maintained at each level. Cipher text storage time and cost of encryption are reduced. Every authority can have a partial set of client's attributes that would not be sufficient to identify client's identity. A multi-authority CP-ABE is achieved and guarantees the confidentiality of data consumers' identity information. The system can tolerate authority compromise. The performance and security analysis proves that Anony Control is secure for data storage in cloud. The Anony Control-F inherits the security of the Anony Control.

REFERENCES

[1] J.Bethencourt, A. Sahai, and B. Waters, "Ciphertext-policy attribute based encryption," in *Proc. IEEE SP, May 2007, pp. 321–334.*

[2] M. Chase, "Multi-authority attribute based encryption," in Theory of Cryptography. Berlin, Germany: Springer-Verlag, 2007, pp. 515–534.

[3] M. Chase and S. S. M. Chow, "Improving privacy and security in multi-authority attribute-based encryption," in *Proc. 16th CCS, 2009,* pp. 121–130

[4] S. Müller, S. Katzenbeisser, and C. Eckert, "On multi-authority ciphertext-policy attribute-based encryption," *Bull. Korean Math. Soc.,* vol. 46, no. 4, pp. 803–819, 2009.

[5] Taeho Jung, Xiang-Yang Li, Senior Member, IEEE, Zhiguo Wan, and Meng Wan, Member, "Control Cloud Data Access Privilege and Anonymity With Fully Anonymous Attribute-Based Encryption" IEEE, VOL. 10, NO. 1, JANUARY 2015

[6] M. Li, S. Yu, Y. Zheng, K. Ren, and W. Lou, "Scalable and secure sharing of personal health records in cloud computing using attributebased encryption," IEEE Trans. Parallel Distrib. Syst., vol. 24, no. 1, pp. 131–143, Jan. 2013.

[7] V. Goyal, O. Pandey, A. Sahai, and B. Waters, "Attribute-based encryption for fine-grained access control of encrypted data," in *Proc. 13th CCS, 2006, pp. 89–98.*

[8] M. Chase, "Multi-authority attribute based encryption," in *Theory of Cryptography. Berlin, Germany: Springer-Verlag, 2007, pp. 515–534.*

[9] A. Sahai and B. Waters, "Fuzzy identity-based encryption," in *Advances in Cryptology*. Berlin, Germany: Springer-Verlag, 2005, pp. 457–473.

[10] A. Shamir, "Identity-based cryptosystems and signature schemes,"in *Advances in Cryptology*. Berlin, Germany: Springer-Verlag, 1985,pp. 47–53.

[11] Y. Zhang, X. Chen, J. Li, D. S. Wong, and H. Li, "Anonymous attributebased encryption supporting efficient decryption test," in *Proc. 8th ASIACCS*, 2013, pp. 511–516.

Investigating the Cause of Poor Efficiency in Thermal Power Plant – A Six-Sigma based Case Study

Manjeet Kharub[1], Garuav Sharma[2], Sarat Kumar Sahoo[3]
[1]Asst. Professor, CVR College of Engineering/Mechanical Department, Hyderabad, India
Email: manjeetkharub@gmail.com
[2]Asst. Professor, CVR College of Engineering/ECE Department, Hyderabad, India
Email: ergaurav209@yahoo.co.in
[3]Asst. Professor, CVR College of Engineering/Mechanical Department, Hyderabad, India
Email: saratkumar222@gmail.com

Abstract: **Nowadays, energy in any form has become an essential commodity all over the world. Being a developing country India is facing energy shortage problems. The Indian government is investing into various projects for efficient utilisation of available resources and to improve power plant efficiency. Research scholars and agencies are seeing the quality of thermal power plant is a possible area of improvement. This paper focuses on identifying the causes of capacity waste in a thermal power plant. For this Six-Sigma improvement project, DMAIC (Define-measure-analysis-improve-control) approach has been adopted. The study found low availability of equipment is the primary cause of capacity wastage in a thermal power plant. Various suggestions were provided to reduce equipment availability problem and consequently to improve the plant efficiency.**

Index Terms: **Quality, Six-Sigma Approach, Thermal power plants, Low equipment Availability.**

I. INTRODUCTION

The growth in the Indian economy is accompanied by higher demand in the energy sector, i.e., renewable and non-renewable (3.6 % increase per annum) [1]. To cope with the current situation Indian government is perusing ambitious energy expansion programs [2]. Since 2016, the level of wind power generation capacity has been doubled, and solar power has increased almost 15 fold. Thermal power plants are the primary source of electricity generation in India [3]. At present, the power generation through different sources is uneven as approximately:

- Thermal plants (63%);
- Hydropower contribution (25%);
- Nuclear power (3%);
- Renewable source (9%).

Still, India is not able to meet the growing energy demand from industries, and a gap between supply and demand is continuously increasing [4]. Around ¼ of the total population is still deprived of access to electricity. Currently, the estimated average gap between supply and demand of electricity (peak demand) is about 14% [5]. The power scenario is seeming constant to be wicked indeed the country has geared up to expand power supply to link the large gap. The government has already taken measure to improve the current positions by undertaking power projects [6]. The action plan has been drawn up, which involves short-term, medium-term and long-term measures.

Short term: these projects involve overhaul and maintenance of existing equipment (boilers) and offer optimal operational performance. The short-term plans are employed for the constant increase in Plant Load Factor (PLF).

Medium term: is employed to have a significant improvement in the PLF of a power station. The medium-term project offers proper maintenance planning to the full plant.

Long-term: renovation and moderation programmes can improve the availability factors in old plants.

The common purpose of these programmes (short, medium and large) is to improve the installed capacity of thermal power plants by:

- Adopting supercritical technology
- Providing maintenance policy;
- Reducing the distribution losses;
- Improving the plant availability;
- Modernization and renovation of Power Plant.

The above-stated steps are considered as vital to increasing plant capacity, to minimise cost and maximise profits. The steps are effectively applicable only when they are allying with a systematic approach. Based on discussion Six Sigma can be considered a conventional method [7]. Six Sigma has been adopted by many organisations worldwide with an aim to improve process performance and come out with many success stories [8]. The five steps for improvements under Six Sigma programs are Define-Measure- Analyze-Improve- Control (DMAIC). As shown in Table I and Table II.

TABLE I.
SIGMA AND CORRESPONDING DEFECTED PPM

Sigma Level	Percent Yield	PPM
6 σ	99.9997%	3.4
5 σ	99.98%	233
4 σ	99.4%	6,210
3 σ	93.3%	66,807
2 σ	69.1%	308,537
1 σ	30.9%	691,462

TABLE II.
EXPLAINING DMAIC APPROACH

Define	Measure	Analysis	Improve	Control
• Define customer requirements • Develop problem statement goals and benefits • Develop high-level process mapping, planning and milestone • Assemble and train team	• Define "defect" and opportunity units and metrics • Develop detailed process maps of appropriate areas • Collect data for relevant metrics • Develop process capability baseline • Establish current process sigma level	• Develop "causal" hypothesis • Identify vital few cause • Validate hypothesis • Quantifying the gap and improvement opportunity	• Develop ideas to remove the root cause • Validate potential improvement ideas through pilot studies • Standardize solution • Measure results • Develop improvement plan	• Establish standard measure to monitor performance • Determine process capability continuously • Correct problems and needed • Document best process

Six Sigma is a well-structured program used by various industries to achieve expected performance with continuous improvement [9]. Six Sigma stands for six standard deviation (Sigma is a Greek letter used to represent variation in statistics) from the mean. Six Sigma methodologies provide the tool and technique to improve the performance and minimise the defects in any process. The higher the sigma level, the better will be the process. Table I shows that defective part per million (PPM) opportunities decreases as Sigma level goes high.

II. CAPACITY WASTE IN THERMAL POWER PLANTS

In power generation industry boiler is most crucial equipment particularly for thermal power plants, cements plants, coal plants and paper mills [10]. It is used to heat the water to convert it into steam. The variation in a thermal power plant is only due to the source of boiler fuel (i.e., coal, naphtha, natural gases). Globally, these conventional fuels are going to be exhausted [11]. Organizations are either focusing on non-conventional sources of energy or trying to improve the efficiency of existing systems.

The efficiency of any heating system is defined as the ratio of positive work done to the heat input [12]. As per the study by NTPC, the maximum efficiency is obtained as 35% with a cost of 65% heat losses due to the results of burning of coal in boilers. Plant capacity is defined in three ways:

i. *Design Capacity:* Maximum possible obtainable output. In this case, it is the maximum quantity of steam a boiler can produce minimum fuel consumption.
ii. *Effective Capacity (Expected Variations)*: The maximum capacity obtained with the help of proper plant maintenance.
iii. *Actual Capacity/output:* Rate of production achieved – can't exceed productive capacity. As calculated by the formulas given in Table III.

TABLE III.
THERMAL POWER PLANT EFFICIENCY CALCULATION

Efficiency	=	[(Actual capacity/Output)/(Effective Capacity)] X100 %.
Capacity utilization		[{Actual capacity(AC)/Output}/ {Design capacity (DC)}] X100 %.
So, we can find the capacity waste as		
Capacity waste (C.W.)	=	1 – Capacity utilization (C.U)
	=	1 – [Actual capacity/Design capacity]

It is subject to unplanned disruptions; machine failure, desertion, material deficiency and most importantly the demand. These different types of capacity are beneficial to find the efficiency and plant utilization. The optimum utilisation of above-discussed capacities is essential.

III. SIX SIGMA ROLE IN REDUCING CAPACITY WASTE

Six Sigma is a conventional technique in quality management primarily aimed to eliminate detects, minimise mistakes and failure in any process [7]. The successful implementation of Six-Sigma techniques has been well documented in renowned organisations. From last two decades, organisations are appreciating the positive results obtained from Six-Sigma implementation [13]. In literature, the success of Six Sigma in the automobile industry, food industry, rubber industry, plastic industry, at large and small level, is well documented [14]. However, there is still less documented evidence available for its successful implementation in thermal power plants. Mainly the concept of Six Sigma has been applied in many manufacturing and service industry; still, there is an excellent research gap is available to see the benefits of Six Sigma in process industries. To fill this gap author conducted a case study.

IV. CASE STUDY DESIGN

A case study has been carried in a thermal power plant processing in a northern part of the country. The capacity of plant detail is given below:

CAPACITY	600MW (2*300)
PROJECT COST	2400CRORE
LAND	1107 (ACRE)
DATE OF START CONS	20.08.2005
GENERATING CAPACITY	144 LACS UNIT\DAY

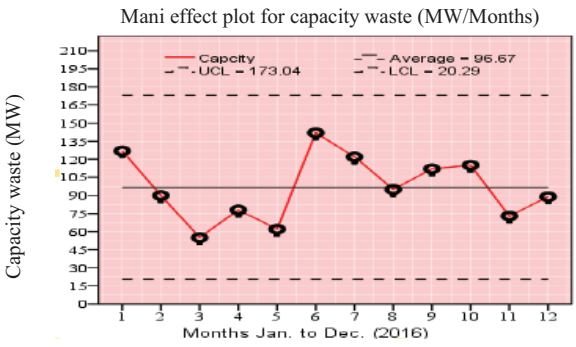

Figure 1. Capacity waste analysis

The plant was operating in two units. In this case study for the application of Six Sigma in process industry unit-II was selected.

Step – I: the Six Sigma steps (define-measure-analysis-improve-control) were applied to define problem relevant to capacity wastage. From previous records, last six months data (i.e., from July - December 2016) was taken and capacity wasted per month was calculated with the help of primary effect analysis. Fig. 1 shows capacity waste analysis. With the help of individual moving charts, sigma levels of capacity wastage were calculated as presented in Table IV.

TABLE IV.
CAPACITY WASTAGE AT DIFFERENT SIGMA LEVELS

Sigma level	UCL	LCL	Process Width	Average
1 σ	122.13	71.21	50.92	96.67
2 σ	147.45	45.75	101.83	96.67
3 σ	173.04	20.29	152.75	96.67
4 σ	198.50	-5.17	203.67	96.67
5 σ	223.96	-30.63	254.59	96.67
6 σ	249.42	-56.09	305.51	96.67
UCL: Upper Control Limit LCL: Lower Control Limit				

From Table IV it is clear that process width is directly proportional to sigma level. In an ideal situation, the process width should be minimum as possible. In another word, the variation in plant's capacity should occur less as possible and for this plants need improvements projects. The average capacity waste was found 96.67 MW/month, which is having a substantial financial and non-financial loss.

Step – II: step one cleared that to improve plant efficiency process width needs to be reduced. So, in step-II, we conducted a brain-storming session with engineers, and supervisors asked the following questions:

Q1: What can be the possible reasons for increased process width or primary cause of this capacity waste?

Q2: How the capacity wastage related to different instruments?

Q3. What is the prime source behind capacity wastage in thermal power plants?

To find out the answers to these questions, based on discussion and available data main reason of capacity wastage were calculated as presented with the help of a pie chart in Fig. 2.

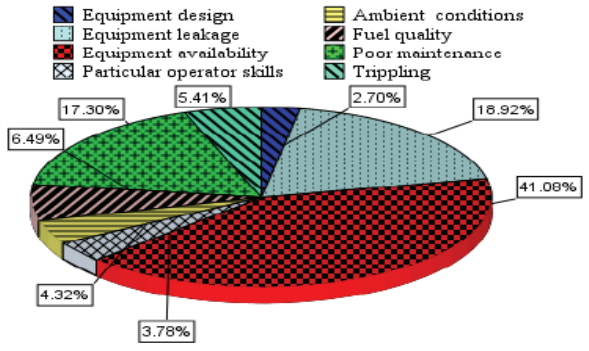

Figure 2. Percent Contribution of different factors

From pie chart, the main reasons were found as:

i. low equipment availability (41.08%);
ii. equipment leakage (18.92%);
iii. reduced maintenance (17.30%);
iv. fuel quality (63.49%);
v. tripling (5.41%);
vi. ambient conditions (4.32%);
vii. operator skills (3.78%); and
viii. equipment design problem (2.70%).

So, it was observed that the most severe cause for capacity waste was low availability.

V. RESEARCH IMPLICATION

- To improve overall availability following suggestion were given:
- Divide the main problem into some small sections. Such as input material (coal) handling system, power generating unit, air system, ash handling, and fuel and condensation system.
- Draw a Pareto analysis chart to deal with few significant problems first.
- Use of simulation and optimisation models to improve equipment availability.
- Calculate the % contribution of different sections based on optimise value.
- To calculate the overall impact of the project in term of finance and plant efficiency.
- Re-design the same project with considering the unusual problem with an aim to improve its sigma level.

VI. CONCLUSIONS

The paper presented a case study for implementing the Six-Sigma concept in a thermal power plant. Pie charts and sigma analysis were used to priorities various problems. Based upon analysis low equipment availability was found the prime cause of capacity waste. It was suggested to sub-divide the system into a different small unit such as fuel section, stream generator, boiler section, evaporator, and superheater, etc. Different modelling and optimisation techniques were suggested to improve equipment availability. It was recommended to involve employees in this type of projects. The study will be useful for managers handling various thermal power plants and for students seeking a new research area in the field of quality engineering. The future investigation can be conducted into other thermal power plants or using other quality improvement techniques with an aim to improve plant efficiency and productivity.

REFERENCES

[1] Pohekar, S.D., Kumar, D. and Ramachandran, M., "Dissemination of cooking energy alternatives in India – a review," *Renewable and Sustainable Energy Reviews*, vol. 9, no. 4, pp. 379-393, 2005.

[2] Ramachandra, T.V. and Shruthi, B.V., "Wind energy potential mapping in Karnataka, India, using GIS," *Energy conversion and management*, vol. 46, no. (9-10), pp. 1561-1578, 2005.

[3] Bhat, I.K. and Prakash, R., "LCA of renewable energy for electricity generation systems—a review," *Renewable and Sustainable Energy Reviews*, vol. 13, no. 5, pp. 1067-1073, 2009.
[4] Asif, M. and Muneer, T., "Energy supply, its demand and security issues for developed and emerging economies", *Renewable and Sustainable Energy Reviews*, vol. 11, no. 7, pp. 1388-1413, 2007.
[5] Ghorashi, A.H. and Rahimi, A., "Renewable and non-renewable energy status in Iran: Art of know-how and technology-gaps", *Renewable and Sustainable Energy Reviews*, vol. 15, no. 1, pp. 729-736, 2011.
[6] Clement, A., McCullen, P., Falcao, A., Fiorentino, A., Gardner, F., Hammarlund, K., Lemonis, G., Lewis, T., Nielsen, K., Petroncini, S. and Pontes, M.T., "Wave energy in Europe: current status and perspectives," *Renewable and sustainable energy reviews*, vol. 6, no. 5, pp. 405-431, 2002.
[7] Chugani, N., Kumar, V., Garza-Reyes, J.A., Rocha-Lona, L. and Upadhyay, A., "Investigating the green impact of Lean, Six Sigma and Lean Six Sigma: A systematic literature review," *International Journal of Lean Six Sigma*, vol. 8, no. 1, pp. 7-32, 2017.
[8] Kharub, M. and Sharma, R., "An integrated structural model of QMPs, QMS and firm's performance for competitive positioning in MSMEs," *Total Quality Management & Business Excellence*, pp. 1-30, 2018.
[9] Lizarelli, F. L. and Alliprandini, D.H., "Comparative analysis of Lean and Six Sigma improvement projects: performance, changes, investment, time and complexity,". *Total Quality Management & Business Excellence*, pp. 1-22, 2018.
[10] Hui, C.W. and Natori, Y., "An industrial application using mixed-integer programming technique: a multi-period utility system model," *Computers & chemical engineering*, vol. 20, pp. S1577-S1582, 1996.
[11] Hoel, M. and Kverndokk, S., "Depletion of fossil fuels and the impacts of global warming," *Resource and energy economics*, vol. 18, no. 2, pp. 115-136, 1996.
[12] Hepbasli, A., "A key review on exergetic analysis and assessment of renewable energy resources for a sustainable future," *Renewable and sustainable energy reviews*, vol. 12, no. 3, pp. 593-661, 2008.
[13] Timans, W., Antony, J., Ahaus, K. and van Solingen, R., "Implementation of Lean Six Sigma in small-and medium-sized manufacturing enterprises in the Netherlands,". *Journal of the Operational Research Society*, vol. 63, no. 3, pp. 339-353, 2012.
[14] Koksal, G., Batmaz, I. and Testik, M.C., "A review of data mining applications for quality improvement in manufacturing industry," *Expert systems with Applications*, vol. 38, no. 10, pp.13448-13467, 2011.

Optimization of Cutting Parameters for Various Work-Tool Combinations in Turning Operation: An Experimental Investigation

G. Bharath Reddy[1] and G. Naveen Kumar[2]
[1]Asst. Professor, CVR College of Engineering/Mechanical Department, Hyderabad, India
Email: gbharathreddys@gmail.com
[2]Assoc. Professor, CVR College of Engineering/Mechanical Department, Hyderabad, India
Email: gnkumarmtech@gmail.com

Abstract: **In the present research work the output responses Material Removal Rate (MRR) and Surface Roughness (SR) are studied and analyzed by varying the turning parameters like cutting speed, feed and depth of cut. The conventional turning of Stainless steel, Normalized steel and Aluminium work materials is carried out by using different cutting tool inserts. The data was compiled into MINITAB ® 17 for analysis. Design of Experiments (DOE) was conducted to analyze the impact of cutting parameters on the Material Removal Rate (MRR) and Surface Roughness (SR) by using Taguchi method. By conducting Analysis of Variance (ANOVA) the results are optimized to determine minimum surface roughness and maximum MRR. Response Surface Optimizer was used for obtaining optimum settings to carry out the machining operations effectively.**

Index Terms: **turning, cutting tool inserts, material removal rate, surface roughness, and optimization**

I. Introduction

Turning is the basic machining operation in which the excess material from the rotated work-piece is removed in the form of chips, by moving a single point cutting tool parallel to the axis of rotation of work-piece, to get exact size and shape of the work-piece. Turning can be done on both the external surface and internal surface of the work part.

To achieve high process performance of turning, it is necessary to choose suitable parameters.

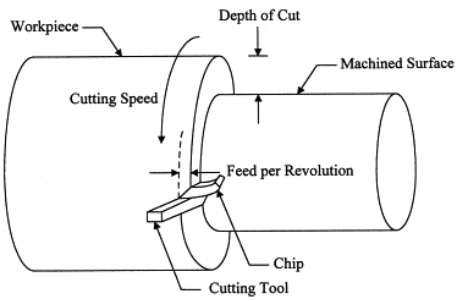

Figure 1. Schematic diagram of turning operation

II. Literature Survey

Singh and Kumar [1] investigated feed force optimization through turning operation of EN24 work piece material by using coated tungsten carbide inserts, varying process parameters.

Ali Riza Motorcu [2] studied the impact of surface roughness during turning of AISI 8660 steel, where the cutting tool used was P.V.D coated ceramic. The results revealed that the feed and depth of cut are more significant parameters.

Adarsh kumar et al. [3] analyzed the effect of surface roughness on EN-8 steel by altering the cutting parameters. The ultimate aim is to correlate and optimize the cutting parameters using multiple regression analysis.

Yong et al. [4] stated that there was excellent increase in life of tool after normal (28.9%), deep (38.6%) treatment of milling inserts treated cryogenically made up of tungsten carbide.

Stewart [5] implemented cryogenically cured C2 WC Co inserts to make out tool wear before and after turning operation of the work piece made of medium density fibre (MDF). The results revealed less tool wear with cryogenically treated tools in comparison to untreated one. He suggested that the cryogenic treatment might have an influence upon the cobalt binder by changing its crystallographic phase.

A lot of work has been done in improving material removal rate and surface modification with Turning Operation. From the literature survey, it is observed that many researchers used High Speed Steels, AISI Steels and composite materials with Carbide and CBN Cutting Tools and examined the various output responses like surface roughness, tool wear rate, material removal rate.

More research is required in field of turning process as there is lackage of few concepts. From the literature review, it is observed that no research work has been carried out on improvement of material removal rate and surface Roughness using Aluminium, normalised steel and Stainless

steel 316. No work has been reported on Carbide and Titanium cutting inserts. All these aspects will be addressed in the research work.

III. Objective of the Project

- To analyze the influence of cutting parameters on the material removal rate and surface roughness while turning of Aluminium, Normalised Steel and Stainless steel-316 by using Carbide and Titanium Cutting inserts.
- To make a comparison between the effects of cutting parameters with different materials (Aluminium, Normalised steel and Stainless steel 316) by using cutting tool inserts (Carbide and Titanium)
- To determine the optimal settings for the work-tool combinations.

IV. Experimental Design

The aim of this research work is to study the influence of cutting parameters on the Material Removal Rate and surface roughness during turning operation of various work materials, using Carbide and Titanium Cutting tool inserts. The designed process variables can be summarized as follows:

- Two types of cutting tool inserts
- Three levels of speed.
- Three levels of feed rate.
- Three levels of depth of cut.
- Three types of work piece materials.

To carry out the Taguchi method of experimental design and an appropriate orthogonal array is to be selected after taking into consideration of the above designed process variables [6]. The influence of each cutting parameter on the concept of surface modification should be studied in order to know its behavior [7]. Thus, it was decided to conduct experiments with each combination of cutting parameters. Out of the above listed designed process variables, the orthogonal array is selected for five design variables which would represent the orthogonal array.

Based on the number of parameters and the levels, an orthogonal array is confirmed by using the array selector.

TABLE I.
Array Selector

	Number of Parameters														
Number of levels		2	3	4	5	6	7	8	9	10	11	12	13	14	15
	2	L4	L4	L8	L8	L8	L8	L12	L12	L12	L12	L16	L16	L16	L16
	3	L9	L9	L9	L18	L18	L18	L18	L27	L27	L27	L27	L27	L36	L36
	4	L16	L16	L16	L16	L32	L32	L32	L32	L32					
	5	L25	L25	L25	L25	L25	L50	L50	L50	L50	L50	L50			

The arrays are generated using Taguchi algorithm; it allows testing of each parameter and settings, equally. MINITAB 17 which is a statistical software was used to assign factors for the present work.

TABLE II.
Machining Parameters And Their Levels

Parameters	Levels		
	1	2	3
Inserts	Carbide	Titanium	--
Speed	280	450	710
Feed	0.2	0.4	0.63
Depth of cut	0.5	1.0	1.5
Work piece	SS316	Normalised steel	Aluminium

TABLE III.
STANDARD L18 ORTHOGONAL ARRAY (TAGUCHI DESIGN)

Exp No.	Parameter 1	Parameter 2	Parameter 3	Parameter 4	Parameter 5
1	1	1	1	1	1
2	1	1	2	2	2
3	1	1	3	3	3
4	1	2	1	1	2
5	1	2	2	2	3
6	1	2	3	3	1
7	1	3	1	2	1
8	1	3	2	3	2
9	1	3	3	1	3
10	2	1	1	3	3
11	2	1	2	1	1
12	2	1	3	2	2
13	2	2	1	2	3
14	2	2	2	3	1
15	2	2	3	1	2
16	2	3	1	3	2
17	2	3	2	1	3
18	2	3	3	2	1

TABLE IV.
EXPERIMENTAL SETTING FOR L18 ORTHOGONAL ARRAY (TAGUCHI DESIGN)

Exp No.	Inserts	Speed (rpm)	Feed (mm/rev)	depth of cut (mm)	Work piece
1	Carbide	280	0.2	0.5	SS 316
2	Carbide	280	0.4	1	Normalised steel
3	Carbide	280	0.63	1.5	Aluminium
4	Carbide	450	0.2	0.5	Normalised steel
5	Carbide	450	0.4	1	Aluminium
6	Carbide	450	0.63	1.5	SS 316
7	Carbide	710	0.2	1	SS 316
8	Carbide	710	0.4	1.5	Normalised steel
9	Carbide	710	0.63	0.5	Aluminium
10	Titanium	280	0.2	1.5	Aluminium
11	Titanium	280	0.4	0.5	SS 316
12	Titanium	280	0.63	1	Normalised steel
13	Titanium	450	0.2	1	Aluminium
14	Titanium	450	0.4	1.5	SS 316
15	Titanium	450	0.63	0.5	Normalised steel
16	Titanium	710	0.2	1.5	Normalised steel
17	Titanium	710	0.4	0.5	Aluminium
18	Titanium	710	0.63	1	SS 316

A. Tools used for experiment:

The single point cutting tool with carbide or titanium insert is used for machining operation. The material of the tool is of high speed steel. After each experiment the cutting tool properly grounded and the same tool geometry is maintained.

TABLE V.
CUTTING TOOL GEOMETRY

S No	Angle	Value
1	Side Rack Angle	7^0
2	Back Rake Angle	9^0
3	Side Cutting Edge Angle	13^0
4	End Cutting Edge Angle	12^0
5	Side Relief Angle	6^0
6	End Relief Angle	8^0

Figure 2. Carbide insert

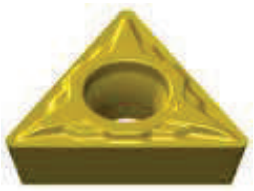

Figure 3. Titanium insert

Figure 4. HSS cutting tool with carbide and Titanium Insert

B. Equipments used for experiment:

Jobber XL CNC horizontal lathe machine was used to perform exepriments for the present work.

Figure 5. Jobber XL CNC lathe (CVR College)

Taly surf was used for measuring surface roughness of work materials

Figure 6. Talysurf (CVR College)

IV. RESULTS AND ANALYSIS

A. Results of material removal rate and Surface Roughness:

The results for rate of material removed were summarized as shown in table 4. The diameter of the work piece before and after machining is determined to evaluate the MRR of each trail. The MRR is given by

$$MRR=1000Vfa$$

Where, V = πdn/1000, is cutting speed in m/min
d is the average diameter of the work piece in mm
n is the spindle speed in rpm
f is feed in mm/rev
a is depth of cut in mm.

Figure 7. Work pieces before machining

Figure 8. Work pieces after machining

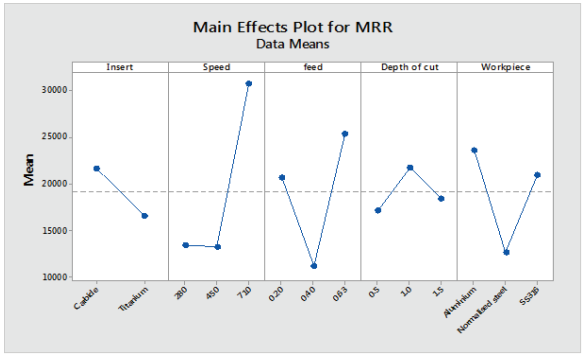

Figure 9. Main effects plot for Material Removal Rate

Fig 9 shows that the Mean material removal rate is higher in case of Carbide insert compared to the Titanium insert. This is perhaps due to the hardness of the insert, high thermal conductivity and higher toughness. As the speed increases the mean of material removal rate decreases first upto some value and then increases. As the feed increases the mean of material removal rate decreases first upto some value and then increases. It is clear that as the depth of cut increases the mean of material removal rate increases first up to some value and then decreases. Among all the the work pieces the maximum mean MRR is for Aluminium.

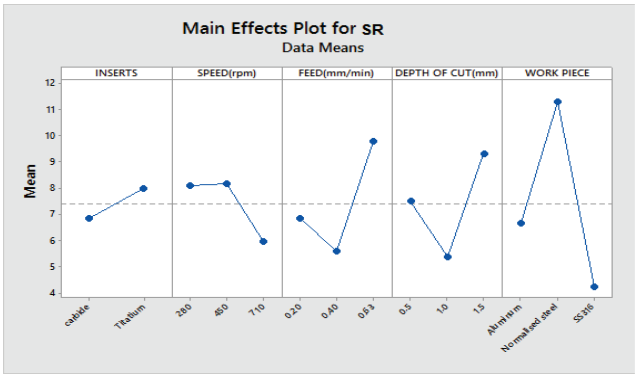

Figure 10. Main effects plot for Surface Roughness

Fig. 10 depicts that the carbide tool insert produces minimum surface roughness as compared to titanium inserts. As the speed increases the surface roughness increases to extent and beyond it decreases. As the feed and depth of cut increases the surface roughness varies similarly. Among all work pieces stainless steel-316 is shows superior surface finish.

TABLE VI.
RESULTS FOR MATERIAL REMOVAL RATE AND SURFACE ROUGHNESS

Exp.No	Inserts	Speed (rpm)	Feed (mm/rev)	Depth of cut (mm)	Work piece	MRR (mm^3/min)	SR (Microns)
1	Carbide	280	0.2	0.5	SS316	3140.3	4.5585
2	Carbide	280	0.4	1.0	Normalised steel	12491.0	7.152
3	Carbide	280	0.63	1.5	Aluminium	29925.1	20.067
4	Carbide	450	0.2	0.5	Normalised steel	18837.1	11.3293
5	Carbide	450	0.4	1.0	Aluminium	4895.0	1.4726
6	Carbide	450	0.63	1.5	SS316	19226.5	2.608
7	Carbide	710	0.2	1.0	SS316	46424.7	2.615
8	Carbide	710	0.4	1.5	Normalised steel	14944.5	7.7156
9	Carbide	710	0.63	0.5	Aluminium	45168.2	3.8616
10	Titanium	280	0.2	1.5	Aluminium	23362.0	2.996
11	Titanium	280	0.4	0.5	SS316	5673.7	2.761
12	Titanium	280	0.63	1.0	Normalised steel	5761.7	10.977
13	Titanium	450	0.2	1.0	Aluminium	18010.8	6.565
14	Titanium	450	0.4	1.5	SS316	8765.0	9.4383
15	Titanium	450	0.63	0.5	Normalised steel	9426.0	17.523
16	Titanium	710	0.2	1.5	Normalised steel	14361.6	13.0116
17	Titanium	710	0.4	0.5	Aluminium	20576.6	4.963
18	Titanium	710	0.63	1	SS316	42859.5	3.5116

B. ANOVA for MRR:

TABLE VII.
ANOVA FOR MATERIAL REMOVAL RATE

Source	DF	Adj SS	Adj MS	F-Value	P-Value
Speed (rpm)	2	1215291804	607645902	6.05	0.025
Inserts	1	118865441	118865441	1.18	0.308
Feed	2	625041621	312520811	3.11	0.100
Depth of cut	2	67639434	33819717	0.34	0.724
Work piece	2	397183879	198591940	1.98	0.201
Error	8	803949257	1000493657		
Total	17	3227971068			

The ANOVA results for MRR reveals that, as P-value for speed is less than standard value (0.05). It concludes that speed is the most significant parameter as compared to other parameters.

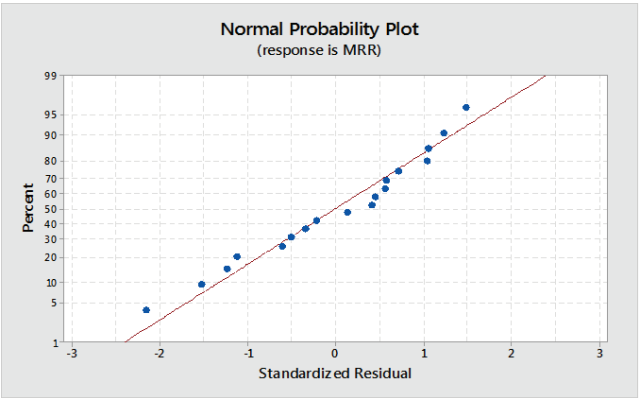

Figure 11. Normal plot of Residual for Material Removal Rate

Fig. 11 depicts that most of the points are nearer to a straight line, which reveals that the errors are normally distributed. Therefore model is satisfactory.

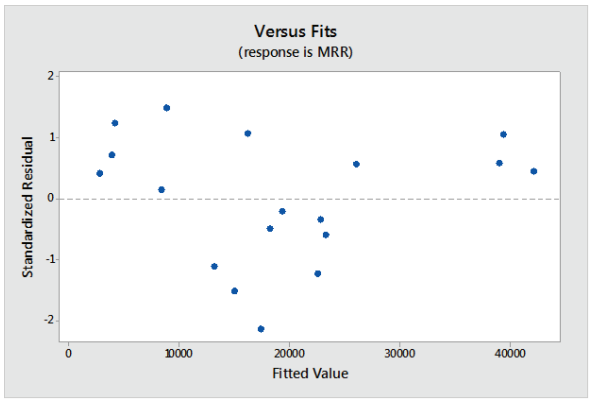

Figure12. Residual vs Fit for Material Removal Rate

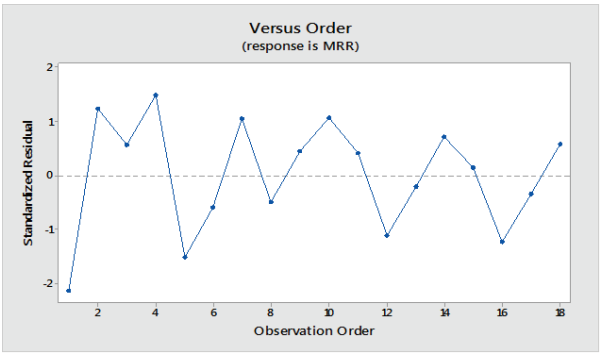

Figure 13. Residual vs Order for Material Removal Rate

Fig. 12 and 13 predicts that the response doesn't have regular structural pattern.

D. ANOVA for Surface Roughness

TABLE VIII.
ANOVA FOR SURFACE ROUGHNESS

Source	DF	Adj SS	Adj MS	F-Value	P-Value
Speed (rpm)	2	18.924	9.462	0.36	0.710
Inserts	1	5.971	5.971	0.23	0.647
Feed (mm/rev)	2	54.996	27.498	1.04	0.396
Depth of cut (mm)	2	46.287	23.144	0.88	0.0453
Work piece	2	153.468	76.734	2.90	0.113
Error	8	211.581	26.448	-	-
Total	17	491.227	-	-	-

The ANOVA results for SR reveals that, as P-value for depth of cut is less than standard value (0.05). It concludes that speed is the most significant parameter as compared with other parameters.

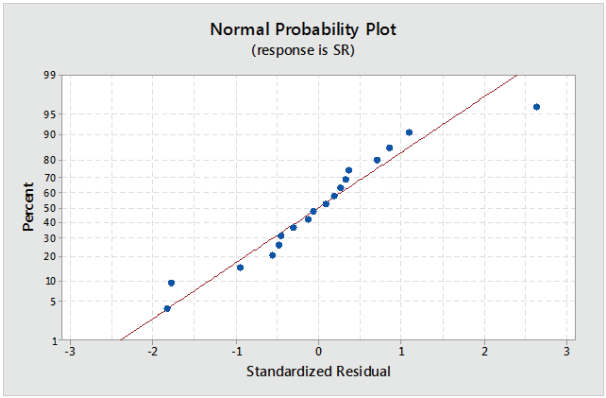

Figure 14. Normal Plot of Residual for Surface Roughness

Fig. 14 depicts that most of the points are nearer to a straight line, which reveals that the errors are normally distributed. Therefore model is satisfactory.

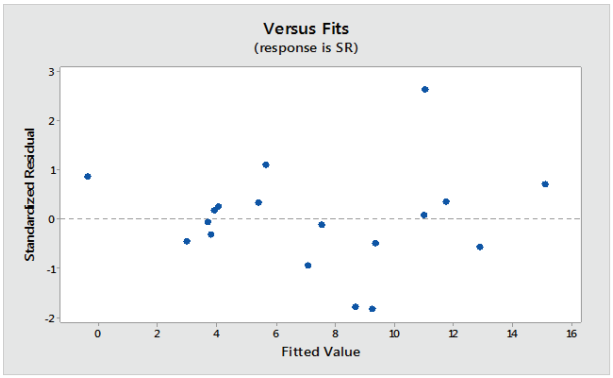

Figure 15. Residual vs Fit for Surface Roughness

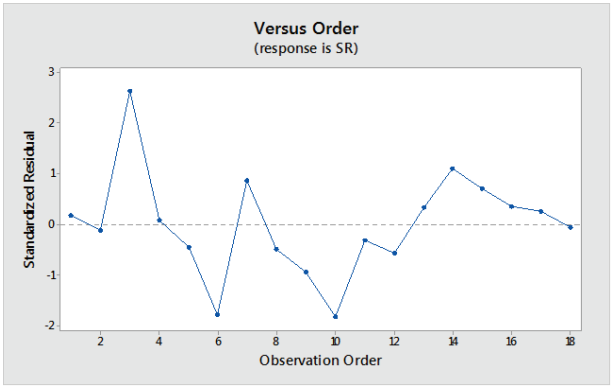

Figure 16. Residual vs order for Surface Roughness

Fig. 15 and 16 predicts that the response doesn't have regular structural pattern.

E. Optimum settings:

The three finest optimum settings shown below are:

TABLE IX.
TOP THREE OPTIMUM SETTINGS

Exp No	Inserts	Speed (rpm)	Feed (mm/rev)	Depth of cut (mm)	Work piece
1	Titanium	710	0.63	1.5	SS316
2	Carbide	710	0.63	1	SS316
3	Carbide	280	0.2	0.5	Aluminum

The optimization plot depicts that, how the required response (surface roughness and Material Removal Rate) alters with the increased speed, feed rate and depth of cut). The optimal setting is assessed by maximum desirability.

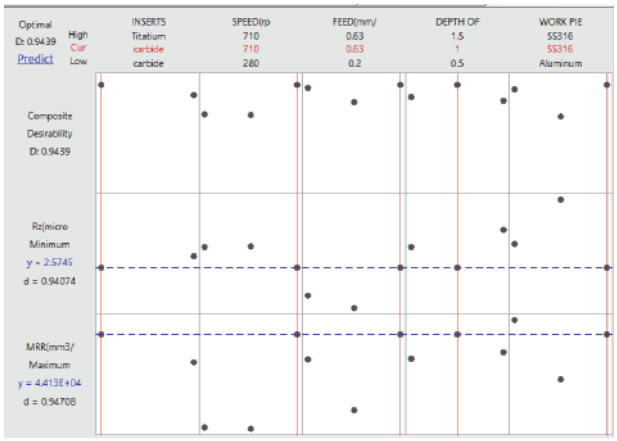

Figure 17. Optimization Plot

V. CONCLUSIONS

1) From the above experiments, it is concluded that the higher material removal rate and lower Surface roughness is possible with the optimum parameters.
2) By determining optimum settings for the machining operation, it is possible to reduce the machining time thereby increasing the productivity.
3) The MRR was maximum for carbide tool insert when compared to the titanium tool insert.
4) The SR was minimum for carbide tool insert when compared to the titanium tool insert.
5) The above results imply that speed has the largest influence on MRR followed by other cutting parameters.
6) The above results imply that depth of cut has the largest influence on SR followed by other cutting parameters.

REFERENCES

[1] Singh H. and Kumar P., "Optimizing Feed Force for Turned Parts through the Taguchi Technique", Sadhana, Volume 31, Number 6, pp. 671–681. (2006).
[2] Ali Riza Motorcu " The optimisation of machining parameters using the Taguchi method for surface roughness of AISI 8660 hardened alloy steel" Journal of mechanical Engineering 566, 391-401, (2010).
[3] Adarsh kumar et.al, "Optimization Of Surface Roughness In Face Turning Operation In Machining Of EN-8" International Journal Of Engineering Science & Advanced Technology Volume-2, Issue-4, 807 – 812
[4] Yong A, Seah K, Rahman M. Performance of cryogenically treated tungsten car-bide tools in milling operations. Int J Adv Manuf Technol, 32 (7-8):638–43, 2007.
[5] Stewart HA. Cryogenic treatment of tungsten carbide reduces tool wear whenmachining medium density fiberboard. For Prod J;54 (2):53, 2004.
[6] Design of Experiments Using the Taguchi Approach: 16 Steps to Product and Process Improvement by Ranjith K. Roy.
[7] Taguchi's quality engineering hand book by Subir Chowdhury.

The Effect of Ball Diameter on Performance of Wet Scrubber with PVC Balls-Mesh Packing Material

Pathan Yasin[1], Animalla Ramesh[2], M.V Ramana[3] and V.Rahul[4]
[1]Asst. Professor, CVR College of Engineering/ Mechanical Department, Hyderabad, India
Email: p.yasin339@gmail.com,
[2]Asst. Professor, CVR College of Engineering/ Mechanical Department, Hyderabad, India
Email: ramesh.animalla@gmail.com
[3] Professor, CVR College of Engineering/ Mechanical Department, Hyderabad, India
Email: ramlalith@rediffmail.com
[4]Asst. Professor, CVR College of Engineering/ Mechanical Department, Hyderabad, India
Email: vudarahul@gmail.com

Abstract: **Toxic pollutants and harmful flue gases resulting from combustion of fossil fuels in several industries are adversely effecting human and his environment. Packed towers, especially with wire mesh type mist eliminator pads are widely used to entrap these flue gas emissions before they enter into the atmosphere. But clogging of pads during the operation became a big problem which needs replacement with new one every time. The present work motivation is to develop and test, a exhaust fume-wet scrubber with new (PVC) balls-mesh replacing traditional packing material in which the spherical surfaces are going to make only point contact between them. Water (PH Value = 8.7) and lime water (PH Value = 12.3) sprinkled finely in modified air cooler body with 72 nozzles of 1mm in diameter and re-circulated for 100 minutes to purify stationary four stroke diesel engine exhaust. The diameter of the balls used, are varied such as 10cm, 5cm and 2.5cms and drain water samples, for every 20 minutes are collected to check PH values.**

Key words**: Packed towers, PVC balls-mesh, lime water, PH Value**

I. INTRODUCTION

Man, and his environment can be affected by the combustion of fossil fuel. The emissions of fossil fuel include the pollutants such as fly ash, sulphur oxides nitrogen oxides, and volatile organic compounds. Combustion of fossil fuels are resources of generation of sulfuric, carbonic, and nitric acids, which falls to earth as acid rains, causes global warming, pollutes natural areas and corrodes buildings. When it comes to human beings, they can cause impaired lung function, shortness of breath, wheezing, asthma attacks and premature death [1,2]. So it is necessary to entrap these pollutants before they enter into the atmosphere. Air pollution reduction involves the control of particulate matter and gas. Electrostatic precipitators, cyclone separators and fabric filters are used for the former and scrubbers, incineration and carbon capture techniques are used for the later one. Out of these, scrubbers are widely used due to its ease of construction and affordability of few types of scrubbers. Based on type of working fluid, scrubbers are classified as air scrubbers, wet scrubbers, and gas scrubbers. Wet scrubbing system is very popular where one can expect satisfaction in terms of efficiency and initial investment maintenance costs [3,4].

Post combustion technique is widely employed to purify petrol and diesel engine exhaust pollutants. Several experimentation results showed that, the capturing of pollutants is almost around 90% of particulate matter, when perfect set up is made. So, care should be taken in order to design the wet scrubber. In addition to engineering aspects to design the wet scrubber, cost is going to be the primary characteristic that should be kept in mind [5,6].

An analogue to human body, the blood of the wet scrubber is its working fluid. Working fluids used to confine the pollutants would have greater impact over the performance of a wet type scrubber. Parameters to be considered for the selection of working fluid mainly depend upon availability and its hardness. The most common working fluid used in scrubber is bore or ground water. In addition to this, lime water is widely employed to catch the pollutants. Base can easily blend with acid solution. This is the reason why nowadays in industries, lime water is used as working fluid in wet scrubbers as blending of lime with water reduces the hardness of water [7,8]. Using working fluids as liquids has an additional advantage that they drops greatly the exhaust emissions temperature [9].

The effectiveness of wet scrubber by closely acquainting the gas stream with working liquid stream. Tubes, weirs and spraying nozzles are widely recruited to distribute the working liquids in wet scrubbers. The need to be fine enough to scrub the pollutants. Impaction, diffusion, direct interception and electrostatic attraction are the four mechanisms to collect the particulate matter in wet scrubbers. Several experiments are conducted to know which mechanism has more impact over the collection of solid pollutants. Results revealed that, the geometric mean diameter of aerosol particle 1.0µm in the diffusion-dominant region increased, whereas it decreases in the impaction-dominant region [10].

Bashir Ahmed Danzomo et al. [11] developed a analytical method to improve the particle removal efficiency. They have focused to catch the particulate matter from cement industry whose diameter are 1µm, 5µm and 10µm and sprayed with droplet sizes of 500µm, 1000µm, 1500µm and 2000µm with a wet scrubbing system. Results revealed that the maximum collection efficiency could be with 500µm sized droplets to collect 5µm and 10µm dust particles.

Seymour Calvert [12] investigated the scrubber capability for the collection of submicron particles. In his investigation, he considered the collection of particles is by diffusion type mechanism for several scrubber types namely venture, plate and packed column spraying tower and established a new relationship between particle cut diameter and scrubber pressure drop.

The flow arrangement to intimately contact the emissions with liquid medium are of two types. One is concurrent and counter current. The later one technique is extensively adopted due to the disadvantage of pressure drop with the former one. H. Krockta et al. [13] reported the selection parameters to fabricate a wet scrubber. They have suggested to consider economic factors, environmental factors, engineering factors in order to design an effective wet scrubber and reported the information required to specify wet Scrubber. In addition to these, they have presented the information required for scrubber at the time of operation and the information for maintenance of a scrubber.

The blood of the wet scrubber is working fluid whereas the heart is its packing material. It is a kind of surface which makes gas stream and liquid stream interacts. The commonly used packing materials are pall ring, intalox metal, berl saddle, tellerette, tri-packs and raschig ring. Initially these packings are made up of stoneware, porcelain or metal but presently they are fabricated with high-density thermo-plastics. The parameters associated in selecting a packing material are its cost, resistance to corrosion, pressure drops in chamber, specific area covered, minimum structural strength and design flexibility [14,15]. Nowadays, wire mesh, fiber bed and baffle type mist eliminators are popular and each type has its pros and cons. The main disadvantage of wire mesh type and fiber bed type are clogging of pollutants, whereas the baffle type mist eliminator Could not remove droplets smaller than 3mm in diameter [16]. The present work is an attempt, to fabricate a new ball mesh type mist eliminator for pollution control. A new method has been employed to check whether the ball mesh type mist eliminator is worthy or not.

II. Materials And Methods

A waste air cooler body has taken and its three sides are covered with single glass fiber reinforced polyester layer and remaining side is fastened with a transparent door to visualize the trapping of pollutants inside the scrubber. Fan along with duct, transport (push or pull) exhaust gases through ducts to and from the scrubber. A heavy duty fan with a speed of 1350rpm and power supply 78W, has been used to escape partially purified gases. Abrasion and corrosion are common problems of chimneys. Abrasion is generally more severe on ductwork leading into the scrubber, while corrosion affects ductwork leaving the scrubber. Duct is made up of thick aluminum sheet upon which single glass fibre reinforced plastic layer has been applied to prevent both abrasion and corrosion as shown in Figure 1(a). Initially, a thick aluminum sheet with required dimension is taken and then 12 inches height and 14 inches diameter cylinder has made. This cylinder is joined with truncated cone shaped aluminum sheet of smaller diameter 14 inches and bigger diameter 24 inches and then single FRP layer has applied. This chimney has fixed to the main body of scrubber and then exhaust fan has fixed inside the chimney.

A perforated tube liquid distributor is made up of a cast iron pipe with a diameter 0.5 inches is bended in a circular form by using tube bender and welded the edges to produce smooth circle shape. After that holes are made by using drilling machine for placing the studs, the studs are welded by using gas welding process. The schematic of a nozzle having diameter of 1mm with 3 ports, which are attached to the studs, is shown in Figure 1(b). A total of 24 nozzles are fixed to the sprinkler and tested as shown in Figure 1(c). Packing media is vital portion of body where the scrubbing mechanism takes place. Packing media is shown in Figure 1(d), made up of rectangular mild steel mesh of 22×22×12 inches, is filled with PVC balls of different diameters such as 2.5cm, 5cm and 10cm.

Precise assembly ensures no leakage of both working fluid and flue gases which in turn results for greater efficiency. The chimney with fan, is attached at the top surface of the body by means of single glass fibre reinforced polyester layer. Sprinkler having two pipe ends, one end is closed another end is connected to water inlet. It is fixed inside the body at top portion, with support of pipe. Packing media is held inside the body at a height of 13 inches from bottom surface with the help of clamps. A transparent fibre plate as a door is fastened on front side of the body, supported with hinges. A pipe of diameter 6.35cm and 275cm in length is screwed between four stroke diesel engine exhaust pipe and inlet pipe to the body to pass the exhaust gases into the scrubber

100L of ground water is taken in container. The water pumped to the sprinkler by means of 1 hp motor with delivery rate of 2000 liters per hour. The sprinkler sprinkles the water with fine amount of spray. When the exhaust gases are entered in to the scrubber the water absorbs the pollutants in the gas. The drain water is re-circulated by using immiscible pump with 0.5hp motor. The sample of drain water is taken for every twenty minutes of time interval for testing the changed PH value with a digital PH meter.

TABLE I.
PVC Balls And Working Fluids Used To Purify The Smoke Of Stationary Four Stroke Diesel Engine

Diameter of the PVC ball (cm)	Number of balls used	Working fluid	PH Value
10	130	Ground water	8.7
5	500	Ground water	8.7
2.5	1300	Ground water	8.7
2.5	1300	Lime water	12.3

III. Results And Discussion

100L of ground water whose concentration is 1108 mg/L, used as working fluid and continuously re-circulated for 100 minutes. At the end of experimentation, the amount of water

Figure 1. (a) 1mm diameter nozzles with 3-ports; (b) 1mm diameter nozzles with 3-ports; (c) testing the sprinkler; (d) packing media of the scrubber ; (e) water before experimentation; (f) water after experimentation.

left is only 65 litres which means 35 litres of water was evaporated. Figures 1(e) & 1(f) clearly indicates change in colour of water before and after experimentation.

The sample of drain water is taken for every five minutes of time interval for testing of change in PH value of water with a digital meter. Bar graph is plotted between PH value vs time interval are shown in Figures from 2 to 5. Results

$CO_2 + H_2O \rightarrow H_2CO_3$ (1)

When 100L of lime water (PH Value=12.3) were sprinkled and re-circulated for 100 minutes, then PH value of the final sample found to be 8.7 and the aqueous solution found to be calcium bicarbonate. Very less, almost no solid pollutants are visible to the naked eye, as the carbon dioxide percent by volume in exhaust is much higher than the other constituents, the collected solution found to be calcium bicarbonate [17].

$CaCO_3 + H2O + CO_2 \rightarrow Ca(HCO3)_2$ (2)

TABLE II.
PH VALUES WITH RESPECT TO TIME

		PH values – Time in minutes					
Ball Dia.(cm)	Fluid	0	20	40	60	80	100
10	Water	8.7	8.2	7.4	7.1	6.8	6.5
5	Water	8.7	8.2	7.8	7.4	7.1	6.8
2.5	Water	8.7	8.3	7.9	7.7	7.3	7.1
2.5	Lime water	12.3	12	11.6	10.5	8.7	8.1

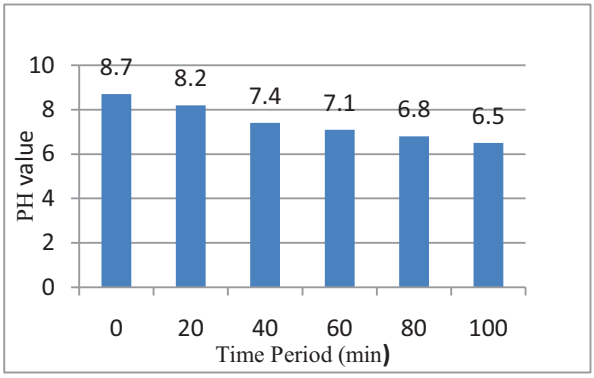

Figure 2. PVC Ball diameter 10cm-ground water.

indicated that, the gradual decrease in PH value with respect to time. It is evident from the graph, acidity of water is increased non linearly with respected to time. The samples were tested and found that final sample is diluted carbonic acid. When the carbon dioxide dissolves in water it exists in chemical equilibrium by producing carbonic acid.

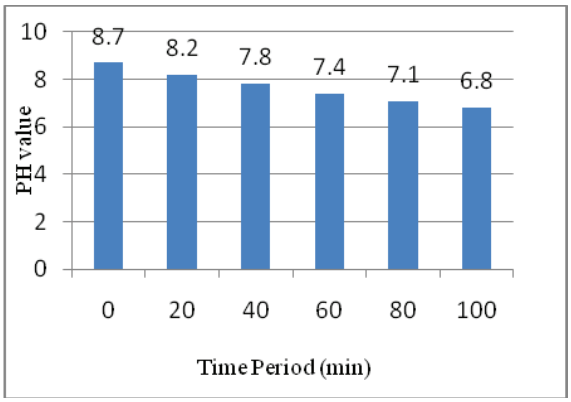

Figure 3. Diameter of the ball 5cm-ground water.

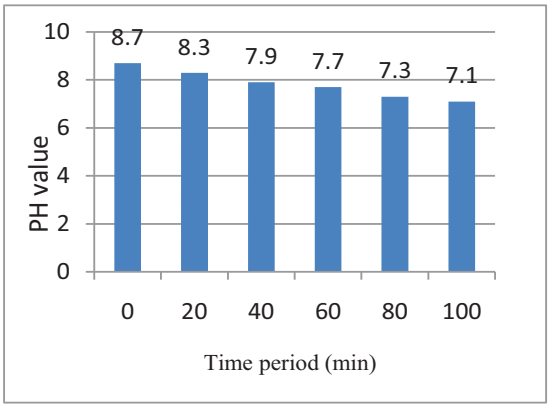

Figure 4. Diameter of the ball 2.5cm-ground water.

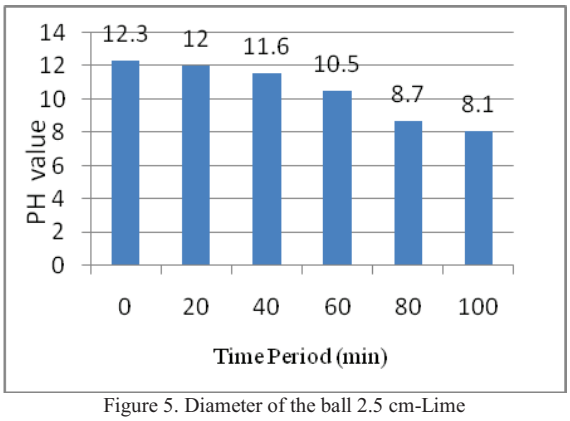

Figure 5. Diameter of the ball 2.5 cm-Lime water

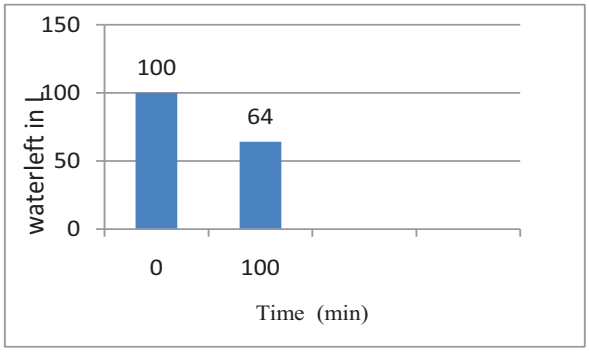

Figure 6. Water left in lit after 100 minutes of circulation

IV. Conclusions

Though wide variety of scrubbers are available both gas & solid pollutants and working fluid mixing phase i.e., packing media going to play vital role in all types of wet scrubbers. The main problem with few traditional mist eliminators is to replacing them every time when they gets clogged. Major conclusions drawn from the study are as follows:

I. Body set up made up of glass fabric reinforced plastics for purifying exhaust, where the temperatures raises up to 350^0C can be promising.

II. New Ball-Mesh can be successfully used as a packing material.

III. Ball diameter is going to effect the exhaust gas scrubbing.

IV. The performance of wet scrubbers can be evaluated by means of checking the PH values-this method employed prosperously.

V. When lime water is used as a working fluid, the samples collected, even the final sample collected was not a milky one and hence confirms again that most of diesel engine exhaust's composition is carbon dioxide.

References

[1] Helena Ribeiro Interactions: Energy/Environment-Fossil Fuel Energy Impacts On Health encyclopedia of life support systems (ELOSS).

[2] A.G.Chmielewski Interactions: Energy / Environment - Environmental Effects Of Fossil Fuel Combustion" Encyclopedia of life support systems (ELOSS).

[3] Bethea, R. M. Air Pollution Control Technology: An Engineering Analysis Point of View. New York: Van Nostrand Reinhold 1978.

[4] H. Tejima, K. Nakazato, I. Nakagawa, M. Nishigaki "PCDDs, PCDFs Emission Control By Dry Scrubbing System" Volume 20, Issues 10–12, 1990, Pages 1899-1905.

[5] Gauravkhandelwal , Ishnathjha, Amitmandal, Hari Singh Use of Scrubber in Petrol and Diesel Engines Vol. 2 Issue 1 January 2013, International Journal of Latest Trends in Engineering and Technology (IJLTET).

[6] Daniel Mussatti , Paula Hemmer Wet Scrubbers for Particulate Matter - US Environmental Protection Agency. EPA/452/B-02-001.

[7] A. Seidell, W. F. Linke, Van Nostrand Solubility of Inorganic and Metalorganic Compounds - A Compilation of Solubility Data from the Periodical Literature.

[8] Ronald Reed The Nature and Making of Parchment. Elmets press, 1st edition 1975.

[9] Makkinejad N. Temperature Profile in Countercurrent/concurrent Spray Towers International Journal of Heat and Mass Transfer. 44: 429-442.

[10] H. T. Kim,C. H. Jung,S. N. Oh, K. W. Lee Particle Removal Efficiency of Gravitational Wet Scrubber Considering Diffusion, Interception, and Impaction Environmental Engineering Science Volume 18, Number 2, 2001 Mary Ann Liebert, Inc.

[11] Bashir Ahmed Danzomo, Momoh-Jimoh E. Salami SaniJibrin,Md. R. Khan and Iskandar M. Nor Performance Evaluation Of Wet Scrubber System For Industrial Air Pollution Control ARPN Journal of Engineering and Applied Sciences Vol. 7, No. 12, December 2012

[12] Seymour Calvert Engineering Design of Fine Particle Scrubbers Journal of the Air Pollution Control Association October 1974 Volume 24, No. 10.

[13] H. Krockta& R.L. Lucas Information Required for the Selection and Performance Evaluation of Wet Scrubbers Journal of the Air Pollution Control Association Volume 22, No. 6 June 1972 Taylor and Francis.

[14] McIlvaine Company. 1974. The Wet Scrubber Handbook. Northbrook, IL: McIlvaine Company.

[15] Richards, J. R. 1995. Control of Particulate Emissions (APTI Course 413). U.S. Environmental Protection Agency.

[16] Encyclopedia of Chemical engineering equipment Mist Eliminators.

[17] Martin A. Elliott, Gerge J. Nebel And Fred G. Rounds "The Composition of Exhaust Gases from Diesel, Gasoline and Propane Powered Motor Coaches" Journal of the Air Pollution Control

Design Methodology and Analysis of Double Cavity Metal-Plastic-Insert Injection Molding Die for Push Board Pin

Neeraj Kumar Jha[1] and P. V. Ramana[2]
[1]Assoc. Professor, CVR College of Engineering/ Mechanical Department, Hyderabad, India
Email: neerajjha.me@gmail.com
[2]Assoc. Professor, CVR College of Engineering/ Mechanical Department, Hyderabad, India
Email: pvramana1964@gmail.com

Abstract: **Properties like high strength, light weight and moldability grants vital use of plastics in manufacturing industries, especially for mass production of products. Injection molding dies are often called plastic molds, are one of the tools for processing plastics to desired shape. It is very easy to understand and perform processes like injection molding to obtain plastic products. But dies developed by correct design steps only can produce defect free products. Insert injection molding is a type of injection molding process in which metal inserts are incorporated in process of injection molding and later they becomes part of product. The purpose of this paper is to discuss the methodology involved with design and development of injection molding die for Push Board Pin. Software used for modeling of parts is UG Nx 8.0 and that for the simulation of process parameters is Autodesk Moldflow Adviser.**

Index Terms: **Moldability, Mass Production, Tool, Plastic Mold, Die, Insert Injection Molding, UG Nx 8.0, Autodesk Moldflow Adviser**

I. INTRODUCTION

Injection molding is essentially the same process as hot chamber die casting. Similar to the process of extrusion, the barrel (cylinder) is heated to promote melting. The pallets or granules are fed into the heated cylinder, and the melt is forced into a split-die chamber, either by hydraulic plunger or by the rotating screw system of an extruder [1]. This split-die is often termed as plastic mold and is obtained by following correct design steps. After the die or mold cavity is filled, it is allowed to cool or cure, then the molds are opened and the solidified part is ejected. The molds are then closed and the process is repeated. Because the material is injected into the mold in molten state, complex shape with good dimensional accuracy can be obtained.

Metallic components such as screws, pins and strips can be placed in the mold cavity and becomes an integral part of the injection molding product, such type of injection molding is referred as Insert Injection Molding. The most common examples of such combinations are electrical components [1]. The process is employed preferably to take advantage of different property of different parts in a single product. For example, in case of an insert injection molded electrical component there can be utilization of conductivity of copper insert and insulation as well as appearance of plastic part molded over it. In another example it could be strength and durability of metallic insert with noncorrosive artistic layer of plastics molded over it.

Push board pins are another example for insert injection molding process. They are also referred as push pin and drawing board pin. These comprise two parts viz. metallic body and plastic head. Its body is a pointed metallic pin and head is usually molded with plastic to achieve various decorative shape and sizes. By holding its plastic head, the pin is inserted against a surface. Usage of such pins is preferably for holding paper against a board or pointing any location on a map.

For obtaining such pins, die (mold) cavity is made according to expected shape and size of head. This cavity usually consists of provision or space to accommodate pre formed pin. First pin is placed in die cavity as insert. Then the die is closed and molten plastic is injected with pressure to occupy shape of head. During solidification, plastic sticks around the projected part of pin in the cavity. The die is then opened and the component is taken out.

Though the process appears simple, it is difficult to obtain a quality product without following the correct methodology of injection mold design. The correct methodology for a plastic mold design is briefly shown in Figure 1 [2].

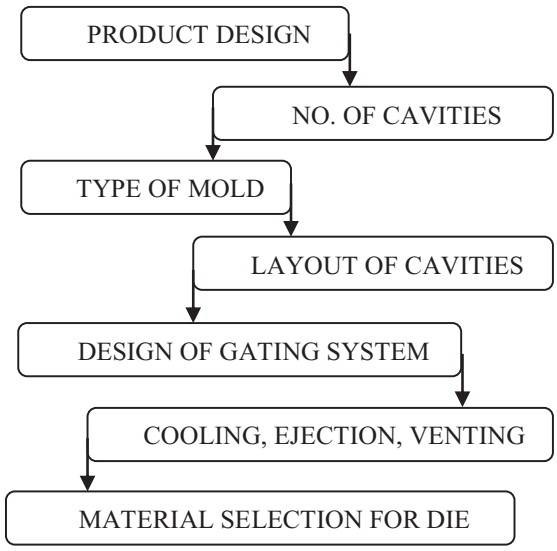

Figure 1. Design Methodology for Plastic Mold

II. Product Design

Figure 2. View of Product, Finalized for Further Analysis

In the phase of product design a product is observed for its manufacturability by a particular process of manufacturing. The finalized product for this research work is different from the existing one, as shown in Figure 2.

TABLE I.
Product Specification

Part Name	Push board pin
Material	Polypropylene head, Steel insert
Part Volume	465 mm^3 (excluding insert)
Surface Area	480 mm^2 (excluding insert)
Mass	0.5gm (excluding insert)

Table I represents few specifications related to the designed product. The designed product for this research work has to serve the same purpose as the existing one. But its design is improved for advantages like increase in grip area as well as in area for contact with paper. Simple design and sufficient space for personalized engraving are other advantages. Simple design leads to ease in design and manufacturing of mold. Engraving on flat face increases complexity of design but the same acts as means of extra material deposition to overcome shrinkages. Therefore, the achieved design of product is unique and profitable technically.

Material selection for molding process is another important aspect to decide in design phase. Polypropylene is selected for this purpose due to its own advantages. Few of the important characteristics of polypropylene (PP) are enlisted in Table II.

TABLE II.
Material Specification
Polypropylene (PP)

Density	946 kg/m^3
Melting Point	160 °C
Formula	$(C_3H_6)_n$
Type	Thermoplastic
Melting Point	171 °C
Flexural Strength	40 N/mm^2
Shrinkage	1-2.5% mm/mm
Tensile Strength	32 N/mm^2
Injection Temperature	32-36 °C
Heat Deflection Temperature	100 °C
Specific Gravity	0.91

Figure 3 shows dimensions of various profiles for head of finalized product, on which design of mold will be based. The design is based on prototyped and observed dimension. It is modeled and drafted using UG Nx 8.0

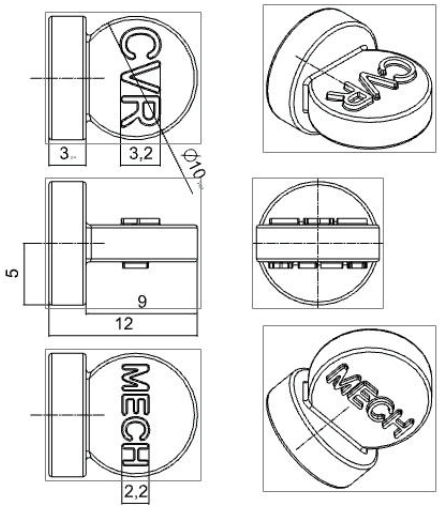

Figure 3. Drafting of Part (All dimensions are in mm)

III. Design Calculations and Tool Design

Once the part design is finalized, one can proceed with design procedure of tool.

A. Number of Cavity

Decision of number of cavity in the mold is first and foremost step of this procedure. The decision gets direct influence from number of component to be produced according to the order as well as from specifications or capacity of molding machine available with the manufacturer. Less number of cavity in the mold refers to longer lead time and the same time more number of cavity can be responsible for defective products. Table III represents common specification of an injection molding machine.

TABLE III.
Machine Specification
(TEXPLASST 1HD, PT LAB, CVRCE)

Shot Capacity	2 – 45 gms / shot
Plunger Diameter	25 mm
Stroke Lenght	450mm
Clamping Capacity	6.0 Tons
Injection Pressure	80 kg/cm^2
Heating Capacity	1.5 kw
Total Installed Power	3.7 kw
Total Shut Height	100 - 450mm

Therefore, the reasonable number of cavity must be calculated for a mold. Out of various methods, Number of cavity based on shot capacity can be obtained as shown in equation 1 [2],

$$Ns = \frac{0.85Ms - Rw}{Cw} \quad (1)$$

Where,

Ns = No. of cavity based on shot capacity
(Based on 85% of rated shot capacity)
Ms = Rated shot capacity of machine (gm/shot)
Rw = Weight of all sprues and runners (gm)
Cw = Component weight per cavity (gm)

$$Ns = \frac{0.85X5 - 2.5}{0.5} = 3.5$$

Therefore, the possible number of cavity is 3.5, but for simplicity of mold design, two cavities in mold can be accepted. Two cavities ensure easy balancing of mold as well as mold manufacturing also becomes simple to much extent.

B. Type of Mold

By seeing draft analysis of part as in Figure 4, it appears clearly that for the component two plate molds with symmetric parting line is the most feasible solution. Figure 5 indicates parting plane, along which splitting of cope half and drag half can be done for the design of two plate mold.

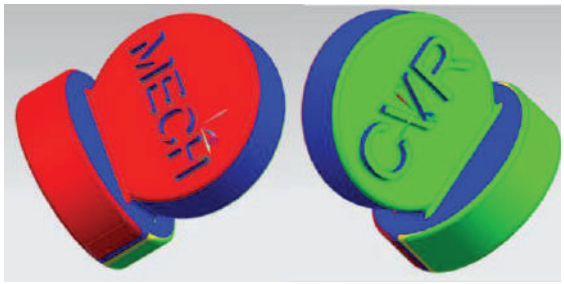

Figure 4. Draft analysis
(Red: Cope half, Green: Drag half)

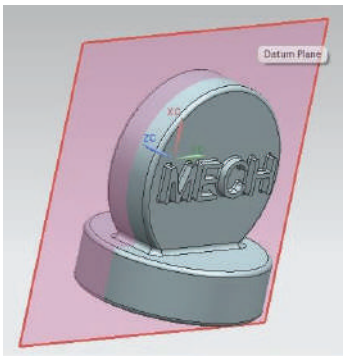

Figure 5. Parting Plane

C. Layout of Cavities

Based on above facts, layout of cavities can be represented as shown in Figure 6. But design of flow path plays a vital role here. Flow path is the channel made in mold, through which molten material enters into the mold cavity.

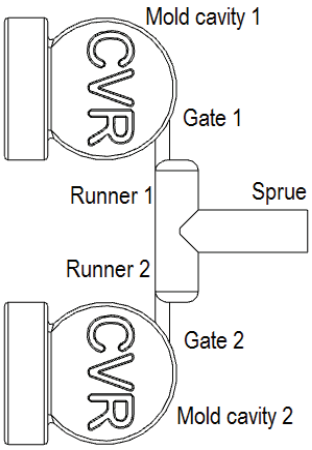

Figure 6. Layout of Two Cavity Symmetrical Arrangement

Sprue is the first element of flow path and its diameter used to be usually 0.5 to 1mm bigger than machine nozzle diameter. Bigger sprue dimension may contribute to higher shot volume. Therefore, the length of sprue must be kept as less as possible. The runner is second part of flow path that connects sprue to the gate. Its diameter can be calculated as shown in equation 2 [3],

$$D = \sqrt{W} X \sqrt[4]{L} / 3.7 \quad (2)$$

Where,

D = Runner Diameter (mm)
W = Weight of the component (gm)
L = Runner length (mm)

$$D = \sqrt{1} X \sqrt[4]{40} / 3.7$$

= 1.45mm

This small value has arrived due to less weight of component as well as due to less number of cavities. The runner should not be below 2mm or above 12mm diameter [2]. Therefore, 3mm runner diameter is considered for flow path design.

The gate is of smallest cross section in the flow path. Through gate molten material enters into the mold cavity. By considering cylindrical cross section of sprue and runner, the gate diameter can be taken as one third of the runner diameter i.e. 1mm.

D. Shot Volume

Shot volume is volume of material sufficient enough to fill all the cavities of the die for one shot [3].

$$Sv = Vs + Vr + Vg + Vc \quad (3)$$

Where,

Sv= shot volume (mm^3)
Vs = volume of sprue (mm^3)
Vr = volume of runner (mm^3)
Vg = volume of gate (mm^3)
Vc = volume of mold cavity (mm^3)

All these values can be easily obtained with help of modeled parts.

$$Sv = 41 + 62 + 24 + 930$$

$=1057mm^3$

D. Clamping capacity Calculation

Clamping capacity allows the mold plates to stick with each other at the time of injection. It actually overcomes the injection pressure. It can be calculated by equation 4 [3].

$$Cf = PPA \; X \; \frac{1}{3} (IP) \qquad (4)$$

Where,

Cf = Clamping Capacity (kg)
PPA = Plan Projected Area Of Mold (cm^2)
IP = Injection Pressure(kg/cm^2)

$$Cf = 2.4 \; X \; \frac{1}{3} (80) = 64kg$$

IV. PROCESS SIMULATION

Autodesk Moldflow Adviser is a simulation tool. It provides details regarding feasibility of designed mold for producing a quality component. By this way we get correct manufacturability guidance for a mold. Using the same software design aspects like cooling or venting requirements can be estimated in our die, as for smaller cavities such entities are difficult to estimate numerically.

A. Gating Stability

When checked about proper gating position, the result obtained as shown in Figure 7 indicates that except engravings any other position is suitable for material flow into the cavity i.e. to be assumed as gate position.

This actually approves our approach of taking parting line along periphery of component. Therefore, the gate is arranged along parting line for ease of manufacturing of mold.

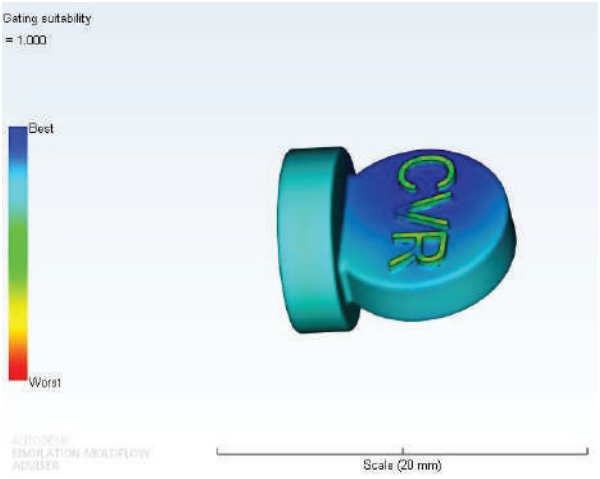

Figure 7. Gating Position All Over the Surface except Engravings

B. Gating Stability

Some values were taken from standards rather than accepting values obtained by imperial relations. Part and flow path were modeled according to these values. Then the model including flow path was taken for analysis. After analysis the result was displayed in Figure 8. It indicates high possibility of filling of mold cavity. This clearly indicates that the values considered from standards were acceptable.

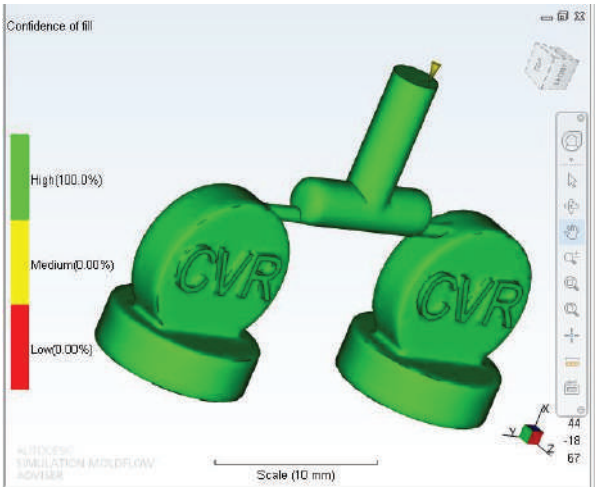

Figure 8. Confidence of Filling

C. Fill Time

Fill time of mold directly affects cycle time of the process. Higher fill time indicates slow flow of material, which can cause cold shut and improper filling of cavity. Actually a slow moving flow front may lose its temperature to become solid, thereby hindering further flow of material. As indicated in Figure 9, result of fill time is also acceptable. Uniformity of filling of both the cavities can also be observed.

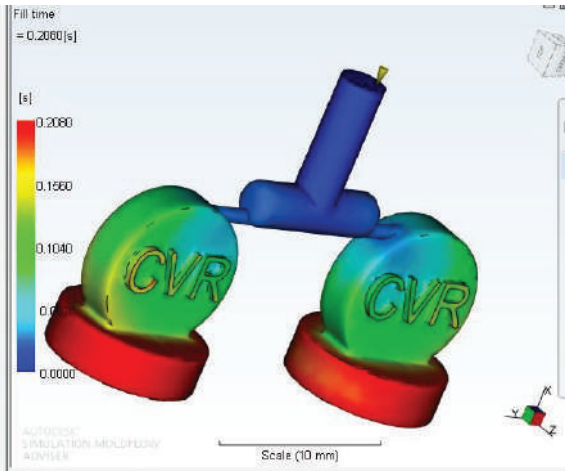

Figure 9. Low Fill Time Contributes to Optimum Cycle Time

D. Temperature Variance

Figure 10 shows analysis result of temperature variance. It is observable that the maximum temperature is at junction of both the circular profiles, which is acceptable. In actual practice this place will be accompanied by a metallic pin. The pin will act as internal chill to drag temperature from molten plastic and no shrink cavities will appear at this place. Estimation of temperature available at junction and

amount of temperature dragged by metal insert can be scope of further research.

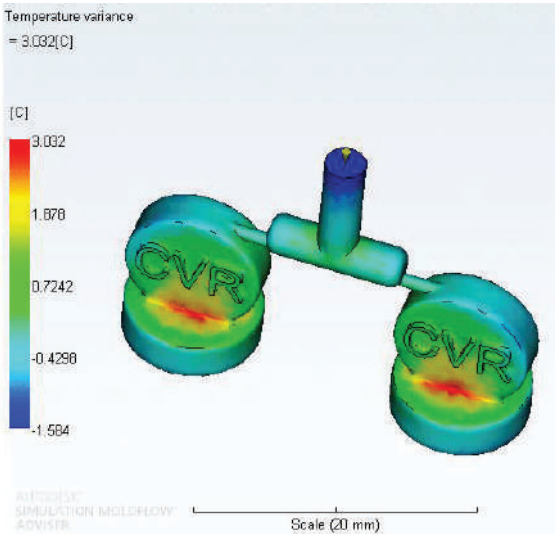

Figure 10. Temperature Variance Result

Low temperature at junction could have been a problem because the pin may cause temperature drop of flow front resulting cold shut or improper filling of mold cavity.

E. Observation And Remeady of Air Trap

Minute amount of air trap is observable in air traps result, the same is shown in Figure 11. The amount of trapped air is not excess. But trapping at mold wall interface can cause unfilled section and bad appearance of the product.

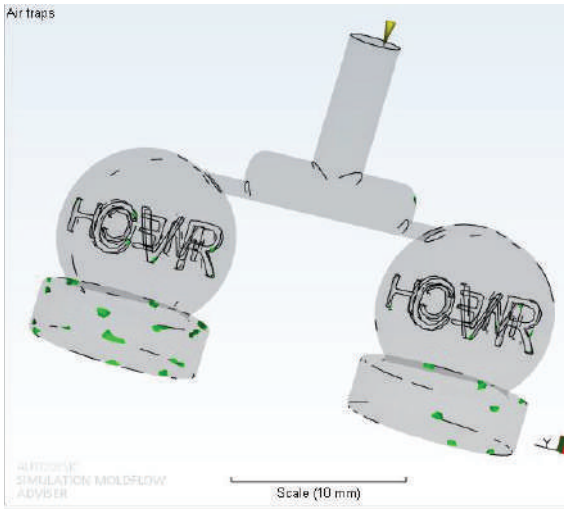

Figure 11. Air Entrapment Result

Air entrapment clearly indicates need of vents. As it is discussed that in the die there will be provision of placement of metallic insert prior to molding, the same provision can easily act as air vent. It is explained with the help of Figure 12 and Figure 13.

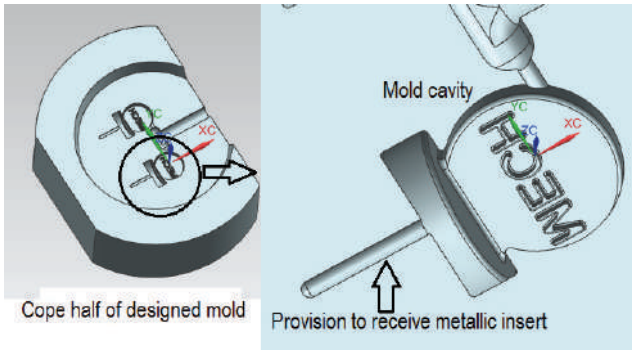

Figure 12. Remedy for Air Entrapment

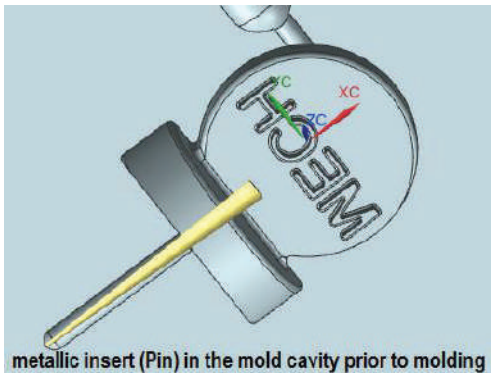

Figure 13. Placement of Insert in Mold Cavity

After placement of insert in the slot, the clearance at the insert- mold cavity interface is big enough to allow passage of trapped air and small enough to block the passage of molten material. In this small passage little amount of material may enter. But this very small volume of material will quickly lose its temperature to solidify, thereby preventing further flow of material through that passage.

Based on results obtained empirically and analyzed by simulation, the designed double cavity metal-plastic-insert injection molding die is shown in Figure 14 to Figure 16.

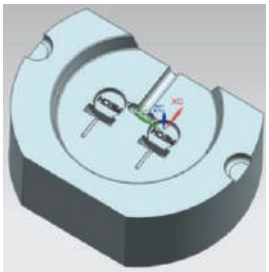

Figure 14. Cope Half of Designed Mold

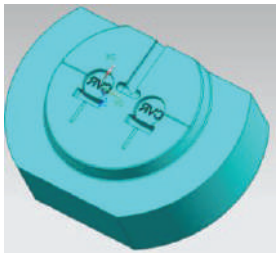

Figure 15. Drag Half of Designed Mold

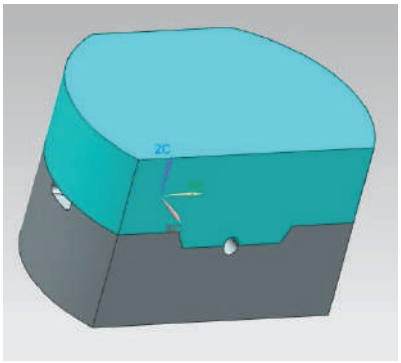

Figure 16. Die Assembly

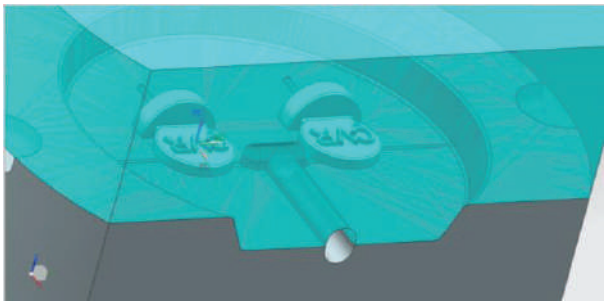

Figure 17. Visibility of Component in the Die

F. Tool Material Selection

It is well known that without proper mold material proper tooling cannot be achieved. A wide range of mould materials are used for fabrication of moulds and dies for plastics which include alloy steel, carbon steel, case hardened steel etc. Mold material selection will have to be carried out based on the requirements from product designer and mold maker [2].

V. CONCLUSIONS

High tooling cost and large required lead time are two major disadvantages of injection molding process. It is task of tool designer to overcome these drawbacks with his innovation and experience. Use of simple profiles may contribute to decrease in manufacturing time and cost. Complex profiles lead to high manufacturing and maintenance cost of tool. The tool discussed in this report can be designed for even higher number of cavities to produce more number of components in given amounts of time. But by increasing number of cavities, placement of inserts in mold cavity prior to molding can be a complex issue. This situation can be handled by using inserts with magnetic property.

Ultimately, it is the task of a designer to achieve profitability in design phase itself.

REFERENCES

[1] Kalpakjian S. and Steven R. Schmid, "*Manufacturing Engineering and Technology*". Pearsion Education, 4th edition, pp. 564, 1995.

[2] Technical committee, *Technical Directory on Design and Tooling for Plastics*, Central Institute of Plastic Engineering & Technology. pp. 43-64, 1970.

[3] Engineers Tooling Service Input ETSI, *Tool Engineering Parameters*, Series 1, ISTE, pp. 24-34, 1970.

Design and Finite Element Analysis of Domestic LPG Cylinder using ANSYS Workbench

C. Sai Kiran[1] and J. Sruthi[2]
[1]Asst. Professor, CVR College of Engineering/Mechanical Department, Hyderabad, India
Email: csaikiran001@gmail.com
[2] Asst. Professor, CVR College of Engineering/ Mechanical Department, Hyderabad, India
Email: sruthij02@gmail.com

Abstract: **In this paper, domestic LPG cylinder was designed and analyzed, which can be used for storing the fluids at a higher pressure. LPG cylinder is one of the kind of pressure vessel that stores pressurised gases. LPG cylinder material should have high tensile and compressive strength for withstanding the high pressure of the gases. The purpose of this work is to design the LPG cylinder for safe, easy operation and able to resist the burst pressure or different loading conditions by studying the total deformation and von-mises stress of the cylinder, which are useful for assessing the safety and life prediction of the LPG cylinder. A detailed finite element analysis of LPG cylinder is performed using ANSYS and these analyses helps to predict the burst pressure of the LPG cylinder when an internal load acts on it.**

Index Terms: **LPG cylinder, Pressure vessel, Von-mises stress, ANSYS.**

I. INTRODUCTION

Abbreviation of LPG is liquefied petroleum gas. LPG consists of hydrocarbons, butane and propane. The LPG is extracted from refining of the crude oil. It is called as liquefied petroleum gas because this gas liquefy under moderate pressure and it is readily vaporize upon the release of pressure. LPG exists in gaseous state at normal atmospheric pressure and at normal room temperature. LPG is a colorless, non-toxic and odorless gas. Therefore, a stench agent like ethyl mercaptan is added to the gas for leak detection. Ethyl mercaptan is selected because it has same boiling point as LPG, non-corrosive and has low Sulphur content. LPG is stored in a cylinder as it is a flammable gas and which can be used as cooking gas in household. The average weight of the cylinder is 14.2 kgs.

Alok et al. [1] has created the LPG model in CATIA VR R20 software and performed a finite element analysis of LPG cylinder which is subjected to an internal pressure, by taking three different materials from ANSYS software. The values estimated by ANSYS are compared with the classical mathematical formulations. The LPG cylinder calculations are performed to determine the cylinder weight and the material with the least weight is selected for new LPG cylinder.

Bandhavi et al. [2] has performed a finite element analysis of LPG cylinders made of steel and fibre reinforced plastic to reduce the weight of the LPG cylinder using ANSYS software, which is subjected to the internal pressure. Stress and deformations inside the LPG cylinders are observed due to internal pressure. The results of deformations and stress on the LPG cylinders are compared with the analytical solutions for validating the software and the created model. The obtained values are within the limits.

Moketla et al. [3] has designed a LPG cylinder and performed a burst pressure test for 3Mpa. The thickness of 3.5 mm in the LPG cylinder has been established by using Abaqus software based finite element analysis. The LPG modelling and finite element simulations were carried out by using Abaqus software. The von-mises stress contour plot of LPG cylinder is generated after static finite element analysis. The maximum operating pressure of the LPG cylinder is 1.3 Mpa and the burst pressure test was performed at 3 Mpa by considering a factor of safety.

Somaiah et al. [4] has elaborated the design procedure of LPG cylinder by alternative materials used for manufacturing. The reduction of weight in the conventional LPG cylinder is done by replacing the material with glass fibre reinforced plastic composites. A glass fibre reinforced polymer material is used as the material for the LPG cylinder because it doesn't explode due to porosity formation in the material. Steel cylinders are manufactured with the welded joint, but the composite cylinders manufacturing has a single joint because they are manufactured by using filament winding technique. The factor of safety for the composite cylinder is considered as 2.5 and the internal pressure is 0.3 Mpa. The design stress values are within the limits and the life time of Fibre reinforced plastic cylinder is double than that of the steel cylinder because of lesser corrosion rate. The developed stress is within the safe limits and a weight saving of 75% is achieved when compared to metallic cylinders. Therefore, the material selected for the LPG cylinder is cost effective and safe in operation.

Gopi et al. [5] has designed and performed the finite element analysis of LPG cylinders which are made up of steel and glass fibre reinforcement plastic. The longitudinal stress, hoop stress and von-mises stress are calculated manually and are compared with the analytical method to know the error percentage for validating the software and LPG model. The optimum thickness of the cylinder is calculated by varying the thickness as 1.5, 1.53 and 1.54 mm and the optimum value for the thickness is 1.53 mm based on the von-mises stress contour plot values.

Krishna et al. [6] has designed a LPG cylinder and performed finite element analysis on the LPG cylinder by using three different materials. The total displacement and von-mises stress values for different LPG cylinder materials is compared and best suited material is selected.

Ashok et al. [7] has modelled a LPG cylinder and performed a finite element analysis of LPG cylinder, which is subjected to an internal pressure. The total displacement and von-mises stress values are compared with the different LPG cylinders. The finite element method and the analytical method values compared with each other and the values of the stress and deformations are found to be within the limits.

Laxmikant et al. [8] has designed a LPG cylinder using PROE software and finite element analysis is performed using ANSYS software by applying boundary and loading conditions on the LPG cylinder. The total deformation and von-mises stress values are observed to determine the burst pressure of the LPG cylinder. The manual calculations are compared with finite element analysis values obtained from ANSYS software.

A. Liquefied Petroleum Gas (LPG) Cylinders

LPG is supplied in pressurized cylinders to keep it liquefied. LP gas inside the cylinder is in two states of matter i.e, liquid and vapour. The liquid is in the bottom portion of the cylinder and the vapour is in the uppermost part of the cylinder. At normal room temperature for withdrawing of the gas, when we open the valve, the pressure inside the cylinder is dropped and the liquid reverts to gas. Therefore, the LPG cylinder must be capable to withstand the internal pressure of the fluid for longer time. The LPG cylinder must be as per IS 3169 standards to withstand the internal pressure of the fluid.

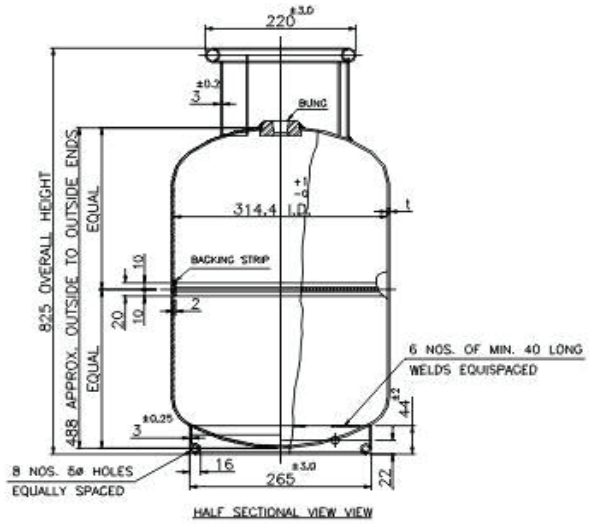

Figure 1. LPG cylinder as per IS 3196 standards

The different parts of the LPG cylinder are represented in Fig.2. The main parts of a LPG cylinder are given below:

1. Collar/Valve Protection Ring.
2. Cylinder Valve.
3. Cylinder Bung or Valve Pad.
4. Top dome.
5. Cylindrical body.
6. Bottom Dome.
7. Base Ring or Foot Ring.

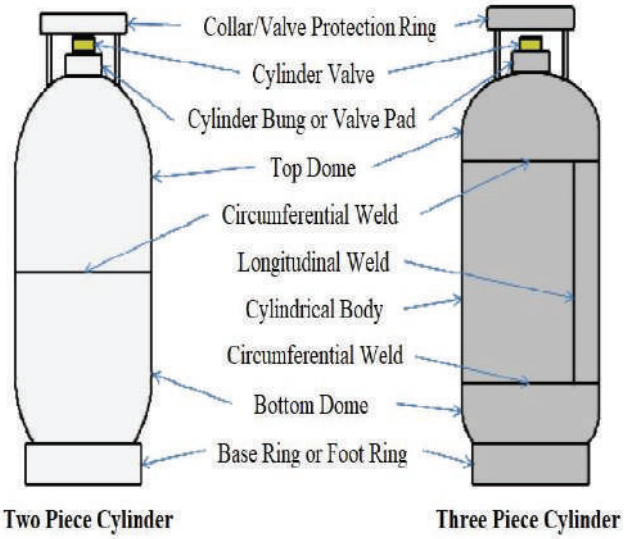

Figure 2. Different parts of the LPG cylinder

B. Manufacturing of LPG Cylinder

The manufacturing of domestic LPG cylinder is done either in two-piece construction or three-piece construction. In the two-piece construction, the fabrication of the cylinders is done by welding of the two domes circumferentially with the circumferential weld. In the three-piece construction, the two half's of the cylindrical body is joined by longitudinal weld and the two dome ends are joined together by circumferential weld. The different types of dome ends are tori-spherical, semi-ellipsoidal and hemi-spherical as shown in Fig.3.

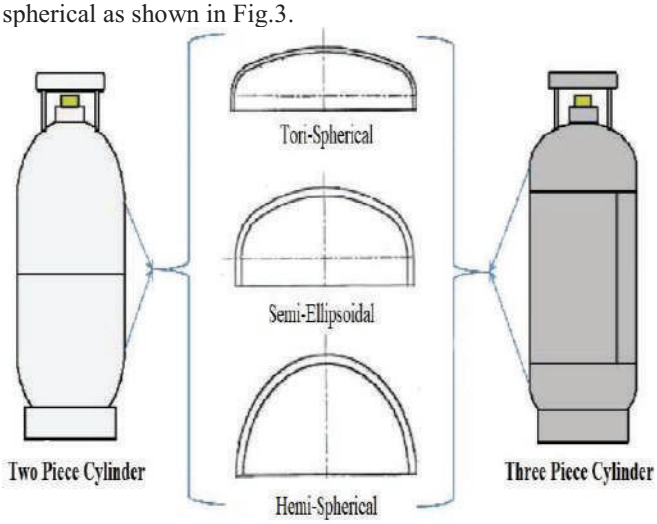

Figure 3. Different dome shapes of the LPG cylinder

C. LPG Cylinder Material

LPG cylinders are usually made of materials that are very strong and are suitable for withstanding the internal pressure. Therefore, low carbon steel is selected as material for LPG cylinder because of its life durability, light weight and safe operations. The material properties of the low carbon steel are shown in the Table I.

TABLE I.
MATERIAL PROPERTIES OF LOW CARBON STEEL

S. No	Properties	Steel
1.	Density (Kg/m^3)	7,800
2.	Young's Modulus (Mpa)	210000
3.	Yield Strength (Mpa)	240
4.	Tensile Ultimate Strength (Mpa)	420
5.	Poisson's Ratio	0.3

II. STRESSES AND DEFORMATION CALCULATIONS OF LPG CYLINDER

By Considering the LPG gas cylinder IS 3196, the von-mises stress and deformation are calculated manually based on the thin cylinder pressure vessel equations of deformation, circumferential, longitudinal and von-mises stress with the internal pressure, thickness and diameter of the cylinder.

Let,

P = Internal pressure of the LPG cylinder = 2.5 Mpa

t = Thickness of the LPG cylinder = 2.5 mm

d = Inner diameter of the LPG cylinder = 300 mm

A. Circumferential Stress of LPG Cylinder

$$\sigma_1 = \frac{Pd}{2t}. \quad (1)$$

$$\sigma_1 = \frac{2.5 \times 300}{2 \times 2.5} = 150 Mpa$$

B. Longitudinal Stress of LPG Cylinder

$$\sigma_2 = \frac{Pd}{4t}. \quad (2)$$

$$\sigma_2 = \frac{2.5 \times 300}{4 \times 2.5} = 75 Mpa$$

C. Deformation of LPG Cylinder

$$\delta = \frac{\Pr^2 (1-\upsilon)}{4Et}. \quad (3)$$

$$\delta = \frac{2.5 \times 150^2 \times (1-0.3)}{4 \times 210000 \times 2.5} = 0.01875 mm$$

By using above calculations, the values of the equations are used for comparing with the finite element values of ANSYS, for validating the software.

III. MODELLING AND FINITE ELEMENT ANALYSIS

A. LPG Cylinder Model

By considering IS 3196 LPG cylinder, all the different parts of the LPG cylinder are modelled in the SOLIDWORKS software by using different commands and all the individual parts of the LPG cylinder are assembled in the SOLIDWORKS software as shown in Fig. 4

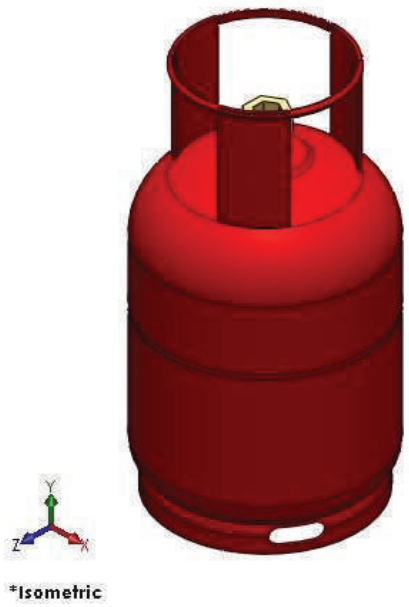

Figure 4. Assembled model of the LPG cylinder

B. Elememt Type

The element type used is SOLID 186. SOLID 186 is a higher order 3-D with 20-node having three degrees of freedom per node, solid element that exhibits quadratic displacement behavior. This element supports large deflections, plasticity, large strain capabilities, hyper elasticity, stress stiffening and creep.

C. Meshing

After assigning element type to the LPG cylinder, the created solid model is converted into IGES format and imported into ANSYS Workbench. Meshing is an important process of an analysis and it should be performed on the LPG cylinder model. Meshing is the process of dividing the created model in number of divisions or elements which consists of nodes. An automated mesh generation is as shown in Fig. 5.

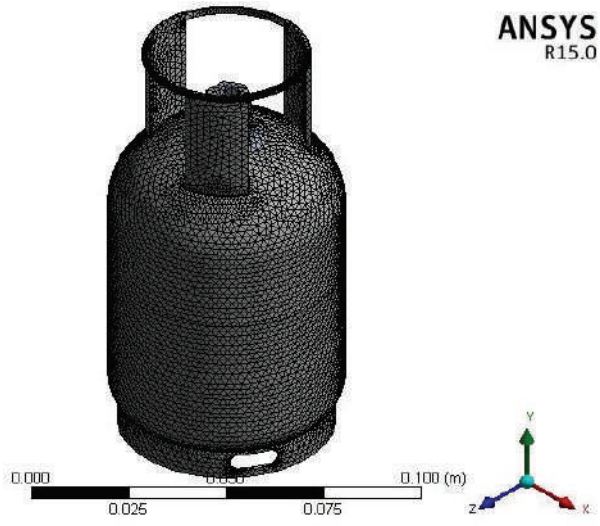

Figure 5. Meshing of LPG cylinder

Meshing is applied by using automatic mesh. Under the mesh sizing, the meshing was set to fine mesh for accurate and precise results. Rather than using a fine mesh all over the components, coarse mesh was used on larger area and fine mesh was used at the area of stress concentration.

D. Applying Loads

In the analysis setting, fixed support is assigned to the base ring or foot ring of the LPG Cylinder, by assigning the fixed support the base ring is constrained in all degrees of freedom and it would withstand the forces acting on the LPG cylinder as shown in Fig. 6.

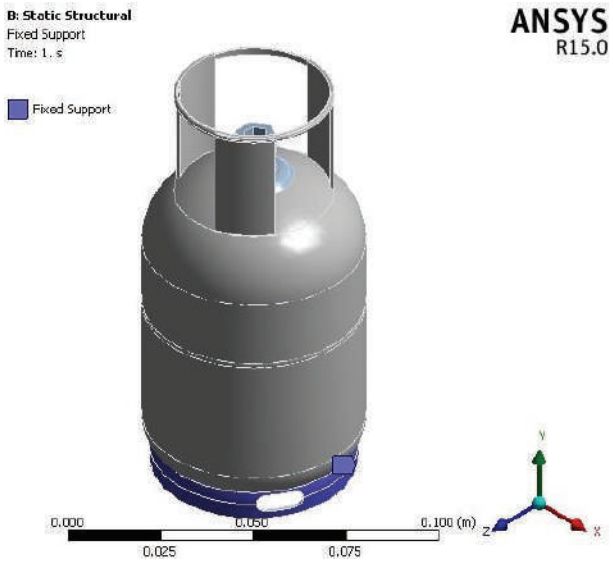

Figure 6. Fixing the base of LPG cylinder

The internal pressure of the fluid inside the LPG cylinder is greater than the atmospheric pressure. Average internal pressure inside the LPG cylinder is calculated. The internal pressure of 2.5 Mpa is applied on the different internal parts of the LPG cylinder as shown in Fig. 7.

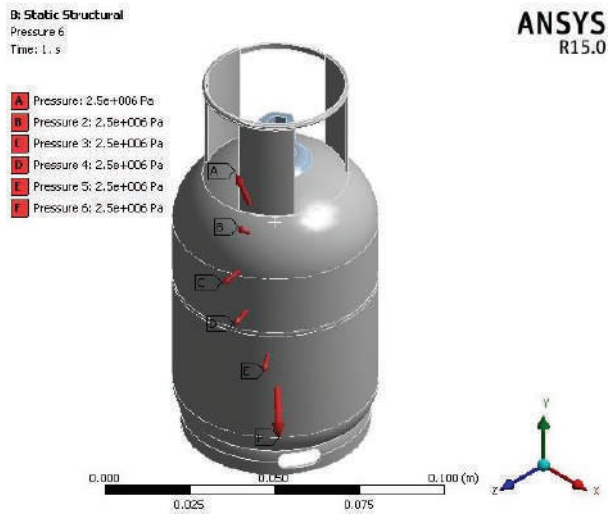

Figure 7. Applying internal pressure on LPG cylinder

IV. Results and Discussions

After fixing the base ring and applying the internal pressure of 2.5 Mpa on the LPG cylinder in the ANSYS software. The following results were observed in the finite element analysis.

A. Total Deformation of LPG Cylinder

After performing the finite element analysis on the LPG cylinder model by applying the internal pressure on it, maximum total deformation of 0.0102 mm is observed from the Fig. 8.

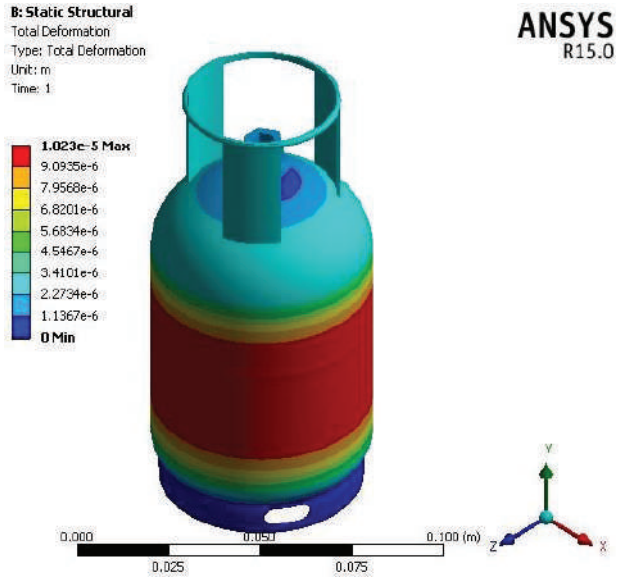

Figure 8. Total deformation of LPG cylinder

B. Von-mises Stress of LPG Cylinder

After performing finite element analysis on the LPG cylinder by applying the internal pressure on it, maximum von-mises stress of 74.96 Mpa is observed in the LPG cylinder from the Fig. 9.

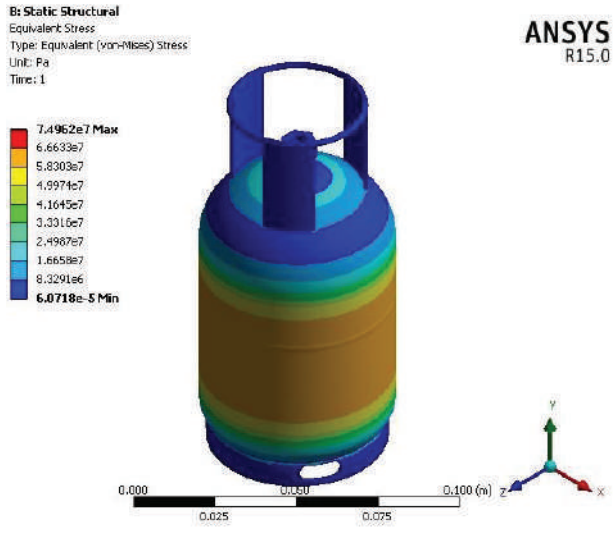

Figure 9. Von-mises stress of LPG cylinder

For validating the finite element values, it is compared with the references. In reference [8], the LPG cylinder is subjected to internal pressure only on the top dome of the cylinder, so it is not considered.

TABLE II.
COMPARISON OF FE VALUES WITH HAND CALCULATIONS

Name	Finite Element Values	Hand Calculation Values	Reference [1]
Von-mises Stress (Mpa)	74.96	75	75.45
Total Deformation (mm)	0.0102	0.0187	0.02

The comparison of finite element values and the manual calculations of the domestic LPG cylinder with the reference [1] are shown in the Table II. The values of the LPG cylinder are under safe limits.

V. CONCLUSIONS

In this paper, a LPG cylinder which is used for storing the fluids is modelled in SOLIDWORKS software and a finite element analysis of a LPG cylinder with an internal pressure of 2.5 Mpa is performed by using ANSYS software. The total deformation and von-mises stress of the LPG cylinder are analysed and compared with the thin cylindrical pressure equations for von-mises and deformation values. For validating the software, the finite element results are compared with the thin pressure vessel equations and the reference [1]. From the results, it is observed that the maximum deformation and the von-mises stress of the LPG cylinder are within the safer limits. Therefore, modelled LPG cylinder is safe to use and has long life to resists the internal pressure of the fluid.

REFERENCES

[1] Alok Tom, Geo Mathew Pius, George Joseph, Jacob Jose and Mathew J Joseph, "Design and analysis of LPG cylinder," *International Journal of Engineering and Applied Sciences*, vol. 6, pp. 17–31, 2014.

[2] Ch. Bandhavi, and N. Amar Nageswara Rao, "Design and analysis of LPG cylinder using ANSYS software," *International Journal of Mathematical Sciences, Technology and Humanities*, vol. 58, pp. 635–646, 2012.

[3] Moyahabo Bradely Moketla and Mukul Shukla, "Design and finite element analysis of FRP LPG cylinder," *International Journal of Instrumentation, control and Automation*, vol. 1, pp. 121–124, 2012.

[4] A. Somaiah, G. Sarat Raju and U. S. P. Rao, "Design procedure of composite LPG cylinder," *International Journal of Application or Innovation in Engineering and Management*, vol. 5, pp. 93–99, November 2016.

[5] Remya Gopi and Beena B R, "Finite element analysis of GFRP LPG cylinder," *International Journal of Engineering Development and Research*, vol. 3, pp. 642–649, 2015.

[6] Kattera Sai Krishna, M. Pramod Reddy and P. Sampath Rao, "Modelling and analysis of metal and fiber reinforced polymer LPG cylinder," *International Journal and Magazine of Engineering, Technology, Management and Research*, vol. 3, pp. 164–168, September 2016.

[7] T. Ashok and A. Harikrishna, "Analysis of lpg cylinder using composite material," *IOSR Journal of Mechanical and Civil Engineering*, vol. 9, pp. 33–42, September 2013.

[8] Laxmikant D. Rangari, P. M. Zode and P. G. Mehar, "Stress analysis of lpg cylinder using ansys software," *International Journal of Engineering Research and Applications*, vol. 2, pp. 2278–2281, July 2012.

Response Reduction of Tall Buildings subjected to Seismic Loads by Tuned Mass Damper

M. Umeshchandra[1] and Mrs. J. Sandhya Rani[2]
[1]M. Tech. Student/CVR College of Engineering /Civil Engineering Department, Hyderabad, India
Email: umesh.chandra57@gmail.com
[2]Asst. Professor/CVR College of Engineering /Civil Engineering Department, Hyderabad, India
Email: sandhyajaligama25@gmail.com

Abstract: **High-rise buildings are comparatively flexible with a low damping value having greater possibilities of failure and less serviceable. Failure potential can be minimized by counteracting vibrations. Methods are available to reduce the vibration of the tall buildings. One of the methods is control of vibrations using Tuned Mass Damper. The behaviour of tall buildings is analysed by considering specific time history data along with gravity loads. The structural mass required to resist the lateral loads increase exceedingly as the level of the building goes up if the stiffness of the building is not sufficient to resist the lateral forces. The main aim of the structural engineer is to provide a suitable solution for the effects due to gravity and lateral loads, by proper usage of Lateral Load Resisting System, approximate analysis and preliminary design. In the present study, the analysis of a 25 storey structure has been done to obtain an optimum mass ratio by using passive resistance. Then by using the optimum mass ratio obtained from the analysis of 25 storey structure, the analysis of 35 and 45-stories reinforced concrete tall buildings subjected to seismic loads has been done as per the IS codes of practice. Safety of the structure has been checked against allowable limits prescribed for joint displacements, base shear, inter-storey drifts by implementing Tuned Mass Dampers (TMD). The behaviour of the building for an optimum mass ratio of Tuned Mass Damper with an increase in the height of building is found out.**

Index Terms: **Tall buildings, Lateral Loads, Mass ratio, Tuned Mass Damper (TMD)**

I. Introduction

The number of Tall buildings constructed nowadays has increased. Most of these buildings have a low natural damping. So, there is a need to increase the damping capacity of a structural system in the new generation of tall and super-tall buildings. The control of vibrations induced in the buildings by seismic waves is achieved by modifying rigidities, masses, damping and shape or by providing passive or active counter forces. Some of the methods provide a possibility of improving efficiency. The selection of a vibration control device is based on a number of factors such as efficiency, compactness, weight, capital cost, operating cost, maintenance requirements and safety. Passive energy dissipation systems utilize a number of materials or devices for increasing damping, stiffness and strength. Passive energy dissipation systems are characterized by the efficiency to dissipate energy in a structure. Energy dissipation is achieved by the conversion of kinetic energy into heat or by transferring energy between vibrating modes. The latter method consists of secondary oscillators, which act as dynamic vibration absorbers.

The energy absorbed by the displacement-activated damper is through the relative displacement of the points of connections within the structure. Therefore, the behaviour is independent of the frequency of motion and the damper is in-phase with internal forces generated at the end of each vibration cycle corresponding to the peak deformations of the structure. The energy absorbed by the velocity-activated damper is through the relative velocity between the points of connection. Therefore, the behaviour depends upon the frequency of motion and the damper is out-of-phase with internal forces generated at the end of each vibration cycle corresponding to the peak deformations of the structure. Motion – Activated Dampers are secondary masses that absorb structure's vibration energy through structures' motion. They are tuned to resonate with the main structure, but remain out-of-phase with the structure. These dampers absorb the input energy of a structure and dissipate by introducing extra forces to the structure so that a less amount of energy is stored in the main structure. Table I shows the types of passive energy dampers (Chang, C. H., and Soong, T T 1980).

A. Tuned Mass Dampers

TABLE I.
TYPES OF PASSIVE DAMPERS

Displacement – Activated	Velocity – Activated	Motion - Activated
Metallic Dampers	Viscous Dampers	Tuned Mass Damper
Friction Dampers	Visco elastic Dampers	Tuned Liquid Damper
Self-centering Dampers		Tuned Liquid Column Damper
Visco elastic Dampers		Tuned Sloshing Damper

The concept of Tuned Mass Damper came into existence in the 1940s. The spring and damping elements are secondary masses of the structure which provides a frequency dependent physical phenomenon to increase damping in the primary structure. Nowadays, numerical and experimental studies have been carried out on the effectiveness of Tuned Mass Dampers in reducing the seismic response of structures.

Tuned Mass Damper system is a well-accepted strategy in the area of vibration control of flexible structures particularly for tall buildings. The mechanism of suppressing structural vibrations by attaching a Tuned Mass Damper to the structure is to transfer the vibration energy of the building to the Tuned Mass Damper and to dissipate the energy. In other words, the frequency of the damper is tuned to a particular structural frequency, so that when that frequency is excited, the Tuned Mass Damper will resonate out of phase with the structural motion (Den Hartog, J. P., 1947).

Properly designed tuned mass damper has the following functions:

a) Reduced displacements, accelerations, internal stresses and strains.

b) Increase structural safety. (i.e., the collapse of a building becomes less probable and hence, human life is protected).

c) Improve serviceability of the structure. (i.e., damage and corresponding repair cost in case of seismic events are reduced significantly)

Classification of Tuned Mass Dampers

Tuned Mass Dampers are divided into two groups, i.e., vertically and horizontally working devices. The application depends on the shape of the disturbing mode as well as on the position/direction of the TMD in order to reduce the vibration.

i. Vertically Acting Tuned Mass Dampers

Vertically Acting Tuned Mass Dampers are supported on helical steel springs. The frequency depends on mass and spring stiffness. The spring system is designed as a hanger system so that the springs are loaded in tension and also combined application with tension and compression springs is possible.

ii. Horizontally Acting Tuned Mass Dampers

It consists of a horizontally swinging mass, which is placed between steel springs. A damping element is arranged in parallel to the springs. The horizontal stiffness of the springs as well as the shape of the mass is responsible for the target frequencies. The flexibility is achieved by the horizontal motion of the mass at the bottom of the hanger system. The mass works in one direction only, but it may also work on the horizontal plane.

C. Optimization of Tuned Mass Damper parameters

The basic principles of Tuned Mass Dampers of reducing structural response are well-established, but optimal Tuned Mass Damper configuration is quite a different problem (Richard Lourenco 2011). In the design of any control device for the suppression of undesirable vibrations, the aim would be to provide optimal damper parameters to maximize its effectiveness. A typical tuned mass damper consists of a mass 'm' which moves relative to the building and is attached to it by a spring with a stiffness 'k' and a viscous damper with coefficient 'c'.

A Tuned Mass Damper is characterized by its tuning, mass and damping ratios. The tuning ratio '*f*' *is* defined as the ratio of fundamental frequency of the Tuned Mass Damper 'ω_t' to that of the building 'ω_o'. Thus,

$f = \omega_t / \omega_o$

Mass ratio μ is

$\mu = m / M$

Where,

M is the total mass of a Single Degree of Freedom structure or the generalized mass of a Multi Degree of Freedom structure, computed for a unit modal participation factor.

Damping ratio is given by

$$\xi = c / 2m\omega_t$$

Time History Analysis

The Time history analysis is a step by step procedure to determine the dynamic response of a structure subjected to a specified loading that may vary with time. The analysis carried out in the present study is nonlinear.

II. Mathematical Formulations

A. Equation of Motion for Forced Vibration Analysis of Multi Storey Plane Frame

The equation of motion of the frame structure subjected to external dynamic force p (t):

The dynamic response of the structure to this excitation is defined by the displacement u (t), velocity (t) and acceleration (t) (Ramancharla Pradeep Kumar, NPTEL). The external force is distributed among the three components of the structure.

Thus,

$f_S + f_D + f_I = p(t)$ (1)

f_S is the stiffness component and is associated with displacement u such that

$f_S = ku$ (2)

Where,

k is the stiffness matrix of the structure and is a symmetric matrix (i.e., $k_{ij} = kji$).

f_D is the damping component and is associated with velocity such that

$f_D = c$ (3)

Where c is the damping matrix of the structure

f_I is the mass component is associated with acceleration such that

$f_I = m$ (4)

Substituting equations (2), (3) and (4) in equation (1) gives

Equation of motion:

$m + c + ku = p(t)$ (5)

Where,

m is the global mass matrix of the 2D frame structure

c is the global damping matrix of the frame structure (Assumed to be a zero matrix, as the damping is neglected in the structure)

k is the global stiffness matrix of the 2D frame structure

u is the global nodal displacement vector

p (t) is the external force

is acceleration vector

is velocity vector

u is displacement vector

Natural Frequency of the structure

$w_a = \sqrt{(k/m)} = \sqrt{(\text{stiffness/mass})}$

Time period $T_n = 2\pi/w_n$

Natural Frequency of the damper $w_d = \sqrt{(k_d/m_d)}$
Damping of the structure $=\xi = c/2mw$
Damping of the damper $=\xi_d = c_d/(2m_d w_d)$
Mass ratio $=\gamma = m_d/m$
Frequency ratio $= f = w_d/w$
Amplitude ratio $= g = w_a/w$

B. Optimum Parameters for Undamped Systems

Harmonic main mass excitation:
$f_{opt} = 1/(1+\gamma)$
$\xi_{dopt} = \sqrt{(3\gamma/(8(1+\gamma)))}$
Harmonic base excitation:
$f_{opt} = 1/(1+\gamma)\ \sqrt{((2-\gamma)/2)}$
$\xi_{dopt} = (\sqrt{(3\gamma/(8(1+\gamma)))})(2/(2-\gamma))$
Optimum parameters for damped systems:
$f_{opt} = [\sqrt{((1-0.5\gamma)/(1+\gamma))}+\sqrt{(2-\xi^2)}-1]- (2.375-1.034\sqrt{\gamma}-0.426\gamma)\ \xi\sqrt{\gamma}-(3.73-16.903\sqrt{\gamma}+20.496\gamma)\xi^2\sqrt{\gamma}]$
$\xi_{dopt} = [\sqrt{(3\gamma/(8(1+\gamma)(1-0.5\gamma)))}\ ] + (0.151\gamma-0.17\gamma^2) + (0.163\gamma-0.498\gamma^2)\ \gamma$
Final computations of Stiffness and Damping of Damper are:
Optimum Stiffness $k_{opt} = \gamma k f_{opt}^2$
Optimum Damping $c_{opt} = 2mw\xi_{dopt}\ \gamma$

C. Model

Analytical investigation was carried out using ETABS software for three multi-storied buildings of 25, 35 and 45 storeys are considered. A sample model of 25 storied building is shown in Figure 1.

Details of 25 Storied Symmetric Building:

(i) Material properties

Grade of concrete	M 50
Grade of Steel	Fe 500
Density of concrete	25 kN/m^3

(ii) Geometry

Each storey height = 3 m
Plan dimensions = 8 m x 8 m for each bay
No. of Bays = 10 in X direction
8 in Y direction
(Same for 35 & 45 storey buildings)

(iii) Member Properties

TABLE II.
FRAME SECTION PROPERTIES

Frame sections	25 Storey (dimensions in m)	35 Storey (dimensions in m)	45 Storey (dimensions in m)
Beam	0.6 x 0.4	0.6 x 0.4	0.6 x 0.4
Column	0.85 x 0.85	0.9 x 0.9	1 x 1
	0.8 x 0.8	0.85 x0.85	0.95 x0.95
	0.75 x 0.75	0.8 x 0.8	0.9 x 0.9
	0.7 x 0.7	0.75 x 0.75	0.85 x 0.85
	-	0.7 x 0.7	0.8 x 0.8
	-	-	0.75 x 0.75
Slab (Thickness)	0.18	0.18	0.18

(Note: Embedded I-section in columns of size UKC152x152x37)

D. Loading

(i) Gravity loading

Live Load	= 4 kN/m^2
Floor Finishes	= 2 kN/m^2
Ceiling load	= 0.25 kN/m^2
Ducting Load	= 0.25 kN/m^2
Wall Loads (Exterior)	= 12.5 kN/m
Wall Loads (Interior)	= 6.5 kN/m

(ii) Time history loading

The time history loading is applied from earthquake data functions. Three real earthquakes data are used.

- The Chamba-1995 earthquake data file loading is used in global-X direction with 8 points per line at a time interval 0.02 seconds.
- The Chamoli-1999 earthquake data file loading is used in global-X direction with 8 points per line at a time interval 0.02 seconds.
- The N-Palm-1986 earthquake data file loading is used in global-X direction with 5 points per line at a time interval 0.005 seconds.

Figure 1. Elevation of the building with Tuned Mass Damper placed at centre

III. RESULTS

A. 25 storeyed structure

The 25-storeyed building is analyzed by using Chamba, Chamoli and N-Palm earthquake data's for finding the optimum mass ratio of the TMD So, Displacement v/s Time graphs are shown here for obtaining the optimum condition by placing the position of TMD at centre.

The results of the observations are presented as follows.

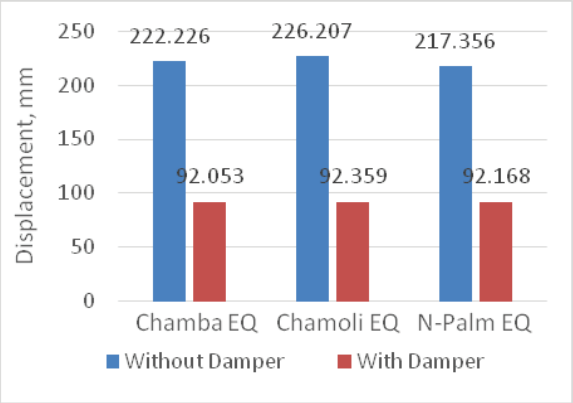

Figure 2. Joint Displacement of 25 storied building with and without Damper

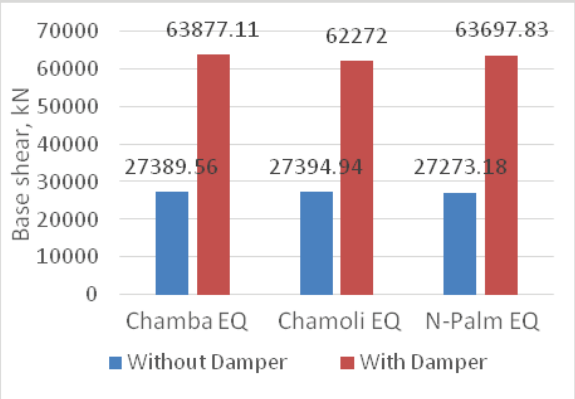

Figure 3. Base shear of 25 storied building with and without Damper

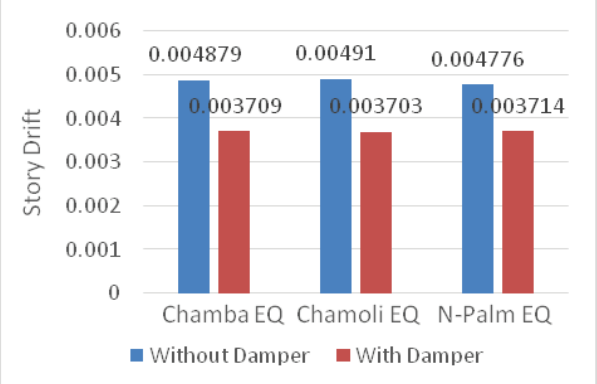

Figure 4. Storey drift of 25 storied building with and without Damper

The maximum reduction is found with 1.2% mass ratio and the storey drift is reduced by 23.98%, 24.65% and 22.23% with Chamba, Chamoli, and N-Palm Earthquake Data's respectively for this specified structure only. The optimum value of storey in seismic response was observed for Tuned Mass Damper is 1.2% mass ratio. So, the base shear graphs are shown for this optimum mass ratio condition by varying height of the structure i.e., for 35 and 45 storey structures with same plan area.

B. 35 and 45 Storeyed Structures

The results of the 35 & 45 storeyed structures are discussed below:

(a) Joint Displacement:

- Max reduction is found when TMD is placed with 1.2% mass ratio.
- The joint displacement is reduced by 60% when the TMD is placed at centre for 35- storeyed structure
- The joint displacement is reduced by 53% when the TMD is placed at centre for 45- storeyed structure.

(b) Base shear:

- For 35 storeyed building, the average increment of Base shear is found with 1.2% mass ratio and the base shear is increased by 57% when the Tuned Mass Damper is placed at centre.
- For 45 storeyed building, the average increment of Base shear is found with 1.2% mass ratio and the base shear is increased by 51% when the Tuned Mass Damper is placed at centre.

(c) Storey Drifts:

- For 35 storeyed building, the maximum reduction is found with 1.2% mass ratio and the storey drift is reduced by 20% when the Tuned Mass Damper is placed at centre.
- For 45 storeyed building, the maximum reduction is found with 1.2% mass ratio and the storey drift is reduced by 5% when the Tuned Mass Damper is placed at centre.

(d) Member Forces:

- For the 35- storeyed structure without Damper, the maximum value of Shear force was observed on the ground floor columns in the outer periphery of the building, and when Tuned Mass Damper is placed with 1.2% mass ratio, the maximum shear force was observed on the columns where the Tuned Mass Damper is placed.
- For the 45- storeyed structure without Damper, the maximum value of Shear force was observed on the ground floor columns in the outer periphery of the building, and when Tuned Mass Damper is placed with 1.2% mass ratio, the maximum shear force was observed on the columns where the Tuned Mass Damper is placed.

IV. CONCLUSIONS

- It is found that Tuned Mass Damper can be successfully implemented as passive TMD to control vibrations of the structure subjected to earthquakes.
- Maximum response reduction was observed for the Tuned Mass Damper of 1.2% mass ratio for 25 storeyed structure. So, the optimum mass ratio of Tuned Mass Damper is 1.2% for this configuration of building.
- For a 25 storeyed building, when the Tuned Mass Damper of mass ratio 1.2% is used, the joint displacement and storey drift are reduced up to 59% and 23% respectively and base shear is increased up to 57%.
- For a 35 storeyed building, when the Tuned Mass Damper of mass ratio 1.2% is used, the joint displacement and storey drift are reduced up to 59% and 20% respectively and base shear is increased up to 57%.

- For a 45 storeyed building, when the Tuned Mass Damper of mass ratio 1.2% is used, the joint displacement and storey drift are reduced up to 53% and 5% respectively and base shear is increased up to 51%.
- The columns on which the Tuned Mass Damper rests should be designed for maximum forces, as the maximum shear forces are found in Tuned Mass Damper columns when the building is subjected to seismic forces.
- The percentage reduction reduces with increase in number of storeys of the structure.
- In the present study, symmetric structures are considered. Therefore, a further scope is to study the problem using Unsymmetrical buildings.
- Behaviour of Tuned Mass Damper was studied for one position only, which provides a further scope of studying the behaviour at various positions on the roof the building.
- Comparative study of response reduction between the Tuned mass damper and Base isolators.
- Study of Fatigue behaviour of Tuned Mass Damper in the building.

REFERENCES

[1] Den Hartog, J. P., "Mechanical vibrations". McGraw-Hill, New York, N.Y., 1947.

[2] Chang, C. H., and Soong, T T, "Structural Control using Active Tuned Mass Dampers", Engineering Mechanics Division, ASCE, 106(6), pp1091-1098, 1980.

[3] Fahim Sadek, Bijan Mohrazt, Andrew W. Taylor and Riley M. Chung, "A Method of Estimating the Parameters of Tuned Mass Dampers for Seismic Applications", Earthquake Engineering and Structural Dynamics, Vol. 26, 617-635, 1997.

[4] Han-Rok Ji, Yeong-Jong Moon, Chun-Ho Kim, In-Won Lee, "Structural Vibration Control using Semiactive Tuned Mass Damper", the eighteenth KKCNN Symposium on civil Engineering – KAIST6, 2005.

[5] Richard Lourenco, "Design, Construction and Testing of an Adaptive Pendulum Tuned Mass Damper", thesis in university of waterloo, 2011.

[6] Ramancharla Pradeep Kumar, "NPTEL ONLINE COURSE Structural Dynamics Tuned Mass Damper" Earthquake Engineering Research Centre, IIT Hyderabad.

Solvent and bio-degradable catalyst for the construction of fully-substituted benzenes

Ramesh Goud Koduri[1], Ramakanth Pagadala[1], Ravi Varala[2]
[1]Asst. Professor, CVR College of Engineering/H&S Department (Chemistry), Hyderabad, India
Email: koduri.rameshgoud@gmail.com
[1]Asst. Professor, CVR College of Engineering/H&S Department (Chemistry), Hyderabad, India
Email: pagadalaramakanth@gmail.com
[2]Professor, RGUKT Basar/Department of Chemistry, Niramal, India
Email: ravivarala@gmail.com

Abstract: **An economical and efficient green chemical method is developed for the synthesis of multi-functionalized benzene derivatives through a natural biopolymer Cellulose Sulfuric Acid (CSA) as a heterogeneous catalytic sequence of Knoevenagal/Michael/Cyclization under solvent-free conditions at 70°C. The metal-free catalytic system under solvent-free condition processes the reactions with a good efficiency. This protocol should be amenable advantages such as simple workup and recoverability of the biopolymer catalyst and reusing several times without significant decrease in catalytic activity.**

Index Terms: **Green synthesis, cellulose sulfuric acid, heterogeneous catalyst, multi-functionalized benzenes.**

I. Introduction

Metal-free catalyst reactions promote more advantageous in chemical transformation since this catalytic reaction forms several bonds from easily available reactants and also reduces the isolated intermediates [1]. In addition, reactions in solvent-free conditions are recognized as unique selectivity, great implements for the synthesis of organic compounds and the products are readily formed in a single step [2].

Multicomponent reaction protocols involving domino processes, which combine multi reactants in a single step, can be powerfully accomplished by employing heterogeneous catalyst [3]. This approach has attracted considerable interest for the formation of multiple bonds that are formed in one-pot process and it addresses the basic principles of synthetic efficacy and reaction strategy arising from minimization of waste, time, energy, and cost [4].

In organic, natural products chemistry and material science Multi-functionalized benzenes holding 2, 6-dicyanoaniline groups are essential class of compounds for asymmetric synthesis [5]. In olden days electrophilic and nucleophilic substitution on existed benzene ring [6], directed to metallation [7], metal-catalyzed cross-couplings of halo-aromatics or aryl triflates [8] were very commonly employed for the synthesis of multi-functionalized benzene derivatives. Various synthetic methods were described for the multi-functionalized benzene derivatives like the reaction between cycloalkylidenemalononitriles and arylmethylenecyanoacetamides in boiling ethanol catalyzed by piperidine [9], NaOH [10], DBU [11], Et_3N [12] and ethane diamine [13]. The reported synthetic protocols have more disadvantages like long reaction time, toxic reagents and prolonged reaction procedure. Moreover the catalysts were not easily regenerated and reused efficiently [14]. In this context it is desirable to develop a convenient and rapid method for the synthesis of multi functionalized benzene derivatives.

However, several research efforts have concentrated on the CSA as heterogeneous catalyst for the synthesis of α-amino nitriles [15], aryl-dibenzo[*a.j*]xanthenes [16], 1,4-dihydropyridines [17], Pechmann condensation [18], thiadiazolobenzimidazoles [19], imidazoazines [20], quinolines [21] and 3,4-dihydropyrimidine-2(1*H*)-ones [22]. These are evident from the literature that CSA supported catalyst has appeal to huge importance as a green catalyst to build carbon-carbon bonds in several organic transformations.

In this regards the synthesis of multi-functionalized benzene derivatives catalyzed by heterogeneous natural biopolymer cellulose sulfuric acid is more attractive [23]. This cellulose biopolymer catalyst is more abundant, biodegradable and renewable natural compounds in the world which has been in the center of attention over the past several decades [24]. The unique property of CSA is more attractive and replaced old organic and inorganic catalytic applications. The additional advantages of CSA are easy regeneration and efficient reuse.

II. Results And Discussion

Primarily, in search of the best solvent system for the synthesis of multi-functionalized benzenes, optimization of various reaction parameters like different temperature, amount of catalyst and solvents were carried out (Table 1). The reaction involves aromatic aldehyde, 2 equivalents of malononitrile and cycloheptanone in the presence of CSA under solvent-free conditions at 70°C (Scheme 1). The scope of this experiment was further demonstrated by studying the reaction of various aromatic aldehydes with malononitrile and cyclic ketone under described reaction conditions (Table 1, entry 10) for the synthesis of multi-functionalized benzenes with good yields.

The comparative study of catalyst was done by performing the experiment with and without catalyst. The desired product was not observed by without catalyst (Table 1; entry 1, 2 and 8). The same reaction was performed in the

presence of catalyst. Impressively, the metal-free catalyst method yielded the target compound selectively in 98% yield.

Reaction performed under various solvents like EtOH, H_2O and solvent free conditions and high conversion (98%) was observed using 20.0 mg CSA in solvent-free at 70°C for 2h. The target compounds were not observed with water as solvent and CSA catalyst under different temperature conditions. The optimum reaction conditions obtained under solvent free conditions with 10.0mg, 20.0mg and 30.0mg of catalyst (CSA), in less reaction period of 2h and at a temperature of 70°C.

A suitable reaction mechanism for the construction of multi-substituted benzenes catalyzed by biodegradable CSA catalyst is shown in Scheme 2. The reaction was anticipated that CSA might preferentially form a Knoevenagel condensation product from aldehyde with malononitrile and followed by Mannich-type reaction with cycloheptanone. Finally, the HCN molecule is eliminated by attacking of another Cyanoacetonitrile molecule.

Heterogeneous catalysis is more attractive due to its profound advantages of straightforward reusable characteristic. The CSA catalyst was recycled and observed through the synthesis of 4a. The crude reaction mixture was dissolved in ethyl acetate after completion of the reaction. It was filtered and then recovered; the recovered catalyst can be reused for five times without loss of its efficiency (Table 2). Due to these positive results, all the reactions were supported out under identical conditions.

The scope of this method was further developed by studying the reaction of various substrates (Table 3) in the presence of 20 mg catalyst in similar reaction conditions, the desired compounds were obtained with good yield. It was found that the substituted aromatic aldehydes with both electron-withdrawing and donating groups, in reaction with other easily available starting materials, had good isolated yields.

III. Experimental

Preparation of Cellulosic Sulfuric acid

Take cellulose (5.00 gm), add n-hexane (20 ml) and magnetically stirred for some period. Then 9 mmol of chlorosulfonic acid (1.0g) was added drop by drop for 2h at 0°C and remove HCl from the vessel. The mixture was then stirred for about 2.5 h at 25°C. The filtered mixture was washed with acetonitrile and dried completely at room temperature. The white color cellulosic sulfuric acid powder was weighed and noted as 5.24g.

Process for the synthesis of multi-functionalized benzene

A mixture of benzaldehyde (1 mmol), malononitrile (2 mmol), cycloheptanone (1mmol) and 20.0 mg of CSA added in sequence, stirred magnetically at 70°C for appropriate time shown in **Table 1**. The reaction progress was checked by TLC (Hexane/EtOAc = 4:1). The reaction mixture was allowed to room temperature and added ethyl acetate after completion of the reaction. The obtained solid was filtered, washed with ethyl ethanoate, dried with anhydrous Na_2SO_4 and the solvent was evaporated. The attained precipitate was re-crystallized from ethyl alcohol to get the pure off white solid objective compound **4a** (98% yield). The recollected catalyst CSA was washed with chloroform, solvent evaporated and the same catalyst reused for the next cycle.

4-phenyl-2-amino-6,7,8,9-tetrahydro-5H-benzo[7]annulene-1,3-dicarbonitrile(4a)

Off white solid: mp 217-218°C; ^{13}C NUCLEAR MAGNETIC RESONANCE SPECTRA δ 26.92, 27.58, 30.27, 31.57, 34.82, 96.06, 97.26, 115.84, 115.87, 128.43, 128.66, 128.92, 132.25, 137.77, 148.75, 149.79, 153.53; ^{1}H NUCLEAR MAGNETIC RESONANCE SPECTRA δ= 1.42-1.83 (6H, m), 2.46 (2H, t, J = 5.4 Hz), 3.08 (2H, t, J = 5.2 Hz), 5.04 (2H, s, NH_2), 7.19-7.50 (5H, m); Mass spectra, m/z = 288 Analytical calculation ($C_{19}H_{17}N_3$): N 14.62 %, C 79.41%, H 5.96%. Found: N 14.63%, C 79.49%, H 5.98%; INFRA RED SPECTRA 3345 (NH_2), 2221 (CN).

4-(4-methoxyphenyl)- 2-amino-6,7,8,9-tetrahydro-5H-benzo[7]annulene-1,3-dicarbonitrile (4b)

Off white solid: mp 199-200°C; ^{13}C NUCLEAR MAGNETIC RESONANCE SPECTRA δ 26.93, 27.63, 30.23, 31.59, 34.82, 55.27, 96.36, 97.03, 114.07, 115.90, 116.08, 129.82, 129.92, 132.61, 148.64, 149.76, 153.41, 159.78; ^{1}H NUCLEAR MAGNETIC RESONANCE SPECTRA δ= 1.44-1.79 (6H, m), 2.51 (2H, t, J = 5.3 Hz), 3.05 (2H, t, J = 5.1 Hz), 3.87 (3H, s, -OCH_3), 5.02 (2H, s, NH_2), 6.98 (2H, d, J = 8.6), 7.11 (2H, d, J = 8.6); Mass spectra, m/z = 318 Analytical calculation ($C_{20}H_{19}N_3O$): N 13.24 %, C 75.69%, H 6.03%. Found: N 13.25%, C 75.77%, H 6.08%; INFRA RED SPECTRA 3346 (NH_2), 2217 (CN).

4-(4-bromophenyl)- 2-amino-6,7,8,9-tetrahydro-5H-benzo[7]annulene-1,3-dicarbonitrile (4c)

Pale yellow solid: mp 228-229°C; ^{13}C NUCLEAR MAGNETIC RESONANCE SPECTRA δ 26.89, 27.56, 30.28, 31.52, 34.83, 95.66, 97.62, 115.69, 115.73, 123.12, 130.18, 131.98, 132.14, 136.61, 147.33, 149.85, 153.79; ^{1}H NUCLEAR MAGNETIC RESONANCE SPECTRA δ= 1.45-1.79 (6H, m), 2.44 (2H, t, J = 5.4 Hz), 3.06 (2H, t, J = 5.3 Hz), 5.09 (2H, s, NH_2), 7.06 (2H, d, J = 8.4), 7.59 (2H, d, J = 8.3); Mass spectra, m/z = 388 ANALYTICAL CALCULATION ($C_{19}H_{16}BrN_3$): N 11.47 %, C 62.31%, H 4.40%. Found: N 11.56%, C 62.26%, H 4.45%; INFRA RED SPECTRA 3347 (NH_2), 2218 (CN).

4-(4-hydroxyphenyl)- 2-amino-6,7,8,9-tetrahydro-5H-benzo[7]annulene-1,3-dicarbonitrile (4d)

Off white solid: mp 240-241°C; ^{13}C NUCLEAR MAGNETIC RESONANCE SPECTRA δ 26.93, 27.62, 30.22, 31.58, 34.83, 96.27, 97.10, 115.62, 115.87, 116.09, 130.02, 131.98, 132.14, 148.57, 149.76, 153.49, 156.01; ^{1}H NUCLEAR MAGNETIC RESONANCE SPECTRA δ= 1.44-1.79 (6H, m), 2.51 (2H, t, J = 5.4 Hz), 3.05 (2H, t, J = 5.3 Hz), 5.02 (2H, s, NH_2), 5.24 (1H, s, -OH), 6.89 (2H, d, J = 8.4), 7.06 (2H, d, J = 8.4); Mass spectra, m/z = 326 ANALYTICAL CALCULATION ($C_{17}H_{17}N_3O$): N 13.85 %, C 75.23%, H 5.65%. Found: N 13.83%, C 75.30%, H 5.68%; INFRA RED SPECTRA 3342 (NH_2), 2204 (CN).

4-(4-(dimethylamino)phenyl)- 2-amino-6,7,8,9-tetrahydro-5H-benzo[7]annulene-1,3-dicarbonitrile (4e)

Pale yellow solid: mp 229-230°C; ^{13}C NUCLEAR MAGNETIC RESONANCE SPECTRA δ 26.98, 27.74, 30.20, 31.66, 34.81, 40.24, 96.48, 96.50, 111.80, 116.14, 116.47, 127.65, 129.60, 132.71, 149.55, 149.84, 150.34, 153.14; ^{1}H NUCLEAR MAGNETIC RESONANCE SPECTRA δ= 1.47-1.79 (6H, m), 2.55 (2H, t, J = 5.4 Hz), 3.02 (6H, s, $(-NCH_3)_2$), 3.06 (2H, t, J = 5.3 Hz), 5.1 (2H, s, NH_2), 6.74 (2H, d, J = 8.7), 7.05 (2H, d, J = 8.7); Mass spectra, m/z = 331 ANALYTICAL CALCULATION ($C_{21}H_{22}N_4$): N 16.96 %, C 76.33%, H 6.71%. Found: N 16.99%, C 76.39%, H 6.78%; INFRA RED SPECTRA 3341 (NH_2), 2211 (CN).

4-(2-chlorophenyl)- 2-amino-6,7,8,9-tetrahydro-5H-benzo[7]annulene-1,3-dicarbonitrile (4f)

Off white solid: mp 236-237°C; ^{13}C NUCLEAR MAGNETIC RESONANCE SPECTRA δ 26.89, 27.17, 30.53, 31.56, 34.94, 95.83, 97.96, 115.32, 115.74, 127.22, 129.93, 130.07, 130.32, 132.51, 132.82, 136.65, 145.72, 149.84, 153.67; ^{1}H NUCLEAR MAGNETIC RESONANCE SPECTRA δ= 1.36-1.78 (6H, m), 2.37-2.43 (2H, m), 3.08 (2H, t, J = 4.9 Hz), 5.09 (2H, s, NH_2), 7.14-7.53 (4H, m); Mass spectra, m/z = 322 ANALYTICAL CALCULATION ($C_{19}H_{16}ClN_3$): N 13.06 %, C 70.91%, H 5.01%. Found: N 13.11%, C 70.98%, H 5.06%; INFRA RED SPECTRA 3245 (NH_2), 2223 (CN).

4-(2-bromophenyl)- 2-amino-6,7,8,9-tetrahydro-5H-benzo[7]annulene-1,3-dicarbonitrile (4g)

Light yellow solid: mp 256-257°C; ^{13}C NUCLEAR MAGNETIC RESONANCE SPECTRA δ 26.87, 27.10, 30.51, 31.57, 34.91, 95.78, 97.96, 115.32, 115.72, 122.66, 127.79, 129.96, 130.38, 132.29, 133.06, 138.72, 147.30, 149.83, 153.75; ^{1}H NUCLEAR MAGNETIC RESONANCE SPECTRA δ= 1.37-1.79 (6H, m), 2.32-2.45 (2H, m), 3.07 (2H, t, J = 4.8 Hz), 5.09 (2H, s, NH_2), 7.14-7.72 (4H, m); Mass spectra, m/z = 366 ANALYTICAL CALCULATION ($C_{19}H_{16}BrN_3$): N 11.47 %, C 62.31%, H 4.40%. Found: N 11.53%, C 62.35%, H 4.46%; INFRA RED SPECTRA 3342 (NH_2), 2225 (CN).

4-(2-methoxyphenyl)- 2-amino-6,7,8,9-tetrahydro-5H-benzo[7]annulene-1,3-dicarbonitrile (4h)

Off white solid: mp 210-211°C; ^{13}C NUCLEAR MAGNETIC RESONANCE SPECTRA δ 26.93, 27.25, 30.61, 31.73, 34.89, 55.45, 96.61, 97.35, 111.10, 115.99, 120.78, 126.45, 130.06, 130.43, 133.11, 145.81, 149.77, 153.04, 156.21; ^{1}H NUCLEAR MAGNETIC RESONANCE SPECTRA δ= 1.42-1.76 (6H, m), 2.42 (2H, t, J = 5.2 Hz), 3.05 (2H, t, J = 5.3 Hz), 3.78 (3H, s, $-OCH_3$), 4.9 (2H, s, NH_2), 6.98-7.43 (4H, m); Mass spectra, m/z = 318 ANALYTICAL CALCULATION ($C_{20}H_{19}N_3O$): N 13.24 %, C 75.69%, H 6.03%,. Found: N 13.27%, C 75.75%, H 6.04%; INFRA RED SPECTRA 3350 (NH_2), 2219 (CN).

TABLE I.
OPTIMIZED REACTION CONDITIONS FOR THE SYNTHESIS OF FULLY SUBSTITUTED BENZENE DERIVATIVES

Entry	Compound	Catalyst	Quantity	Solvent	Temperature (°C)	Time (h)	Yield [a](%)
1	4a	-	-	EtOH	Room temperature	12.0	b
2	4a	-	-	EtOH	70	12.0	b
3	4a	CSA	10.0mg	EtOH	Room temperature	6.0	40
4	4a	CSA	10.0mg	EtOH	60	5.0	56
5	4a	CSA	10.0mg	H_2O	Room temperature	6.0	b
6	4a	CSA	10.0 mg	H_2O	80	5.0	b
7	4a	CSA	10.0 mg	-	Room temperature	2.5	82
8	4a	-	-	-	70	4.0	b
9	4a	CSA	10.0 mg	-	70	2.0	94
10	4a	CSA	20.0mg	-	70	2.0	98
11	4a	CSA	30.0mg	-	70	2.0	98

[a] Isolated yields.
[b]No products found.

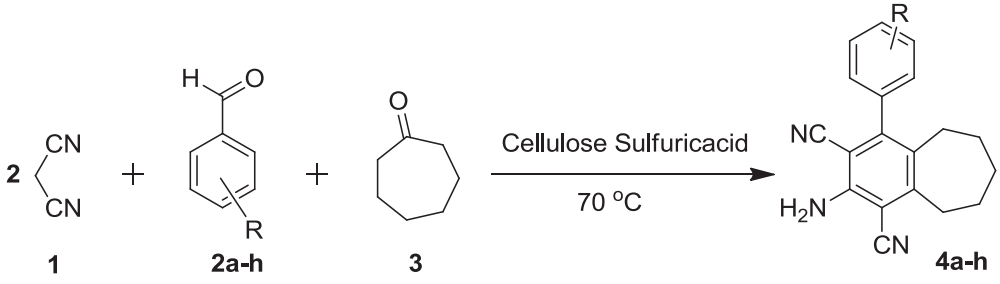

Scheme 1. Cyclo-condnsation reaction for the synthesis of fully-substituted benzenes (4a-h)

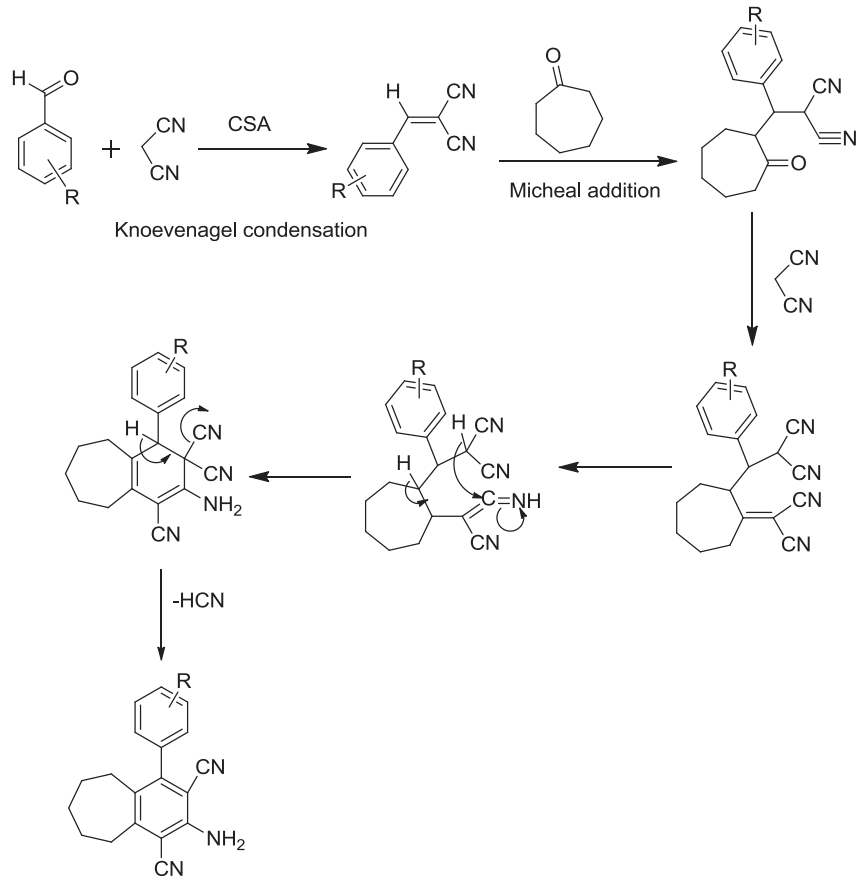

Scheme 2. A plausible reaction mechanism for the formation of fully-substituted benzenes

TABLE II.
REUSABILITY OF CSA CATALYST CONFIRMED FOR COMPOUND (4a)

Entry	Catalyst	Time (h)	Yield [a](%)
1	Fresh	2.0	98.0
2	2nd run	2.0	98.0
3	3rd run	2.0	97.0
4	4th run	2.0	95.0
5	5th run	2.0	94.0

[a] Isolated yields

TABLE III.
CSA CATALYZED SYNTHESIS OF THE FULLY-SUBSTITUTED BENZENE DERIVATIVES (4a-h)

Entry	Product No.	R_1	Time (h)	Yield [a](%)
1	4a	H	2.0	98.0
2	4b	4-OCH_3	2.5	98.0
3	4c	4-Br	2.5	97.0
4	4d	4-OH	2.5	96.0
5	4e	4-$N(CH_3)_2$	2.0	95.0
6	4f	2-Cl	2.0	97.0
7	4g	2-Br	2.0	96.0
8	4h	2-OCH_3	2.5	95.0

[a] Isolated yields.

IV CONCLUSIONS

In conclusion cellulose sulfuric acid was applied in simple and straightforward method for the efficient synthesis of various multi-functionalized benzene derivatives. CSA is an effective, harmless, ecological and environmental friendly solid acid catalyst. This protocol has many advantages such as scale-up, simplicity of experimental process, easy work-up, high yields and green conditions. So far great advances have been developed in research the usage of new CSA catalyst in organic synthesis of pharmaceutical curiosity is obligatory. Further studies in the sustainable applications of this biopolymer catalyst to other organic chemical reactions are continuing in our laboratory.

REFERENCES

[1] (a) K. C. Nicolaou, D. J. Edmonds and P. G. Bulger, *Angew. Chem., Int. Ed.,* 2006, 45, 7134; (b) J. C. Wasilke, S. J. Obrey, R. T. Baker and G. C. Bazan, Chem. Rev., 2005, 105, 1001.

[2] A. Domling and I. Ugi, *Angew. Chem., Int. Ed.,* 2000, 39, 3168.

[3] (a) R. Pagadala, S. Maddila, V. Moodley, W. E. Van Zyl, S. B. Jonnalagadda, *Tetrahedron Lett.,* 2014, 55, 4006; (b) R. Pagadala, S. Maddila, S. Rana, S. B. Jonnalagadda, *RSC Adv.,* 2014, 4, 6602; (c) U. Kusampally, R. Pagadala, K. C. Rajanna; *Tetrahedron Letters* 2017, 58, 3316.

[4] N. G. Shabalala, R. Pagadala, S. B. Jonnalagadda; *Ultrasonics Sonochemistry,* 2015, 27, 423; (b) R. Pagadala, D. R. Kommidi, S. Kankala, S. Maddila, P. Singh, B. Moodley, N. A. Koorbanally, S. B. Jonnalagadda; *Organic and Biomolecular Chemistry* 2015, 13, 1800; (c) R. Pagadala, S. Maddila, S. B. Jonnalagadda; *Journal of Heterocyclic Chemistry* 2015, 52, 1226.

[5] (a) X. S. Wang, M. M. Wang, Q. Li, C. S. Yao, S. J. Tu, *Tetrahedron,* 2007, 63, 5265; (b) F. V. Singh, R. Vatsyayan, U. Roy, A. Goel, *Bioorg. Med. Chem. Lett*., 2006, 16, 2734; (c) F. Dumur, N. Gautier, N. Gallego-Planas, Y. Sahin, E. Levillain, N. Mercier, P. Hudhomme, *J. Org. Chem*., 2004, 69, 2164; (d) Y. Xiao, X. H. Qian, *Tetrahedron Lett*., 2003, 44, 2087; (e) N. J. Long, *Angew. Chem. Int. Ed. Engl*., 1995, 34, 21; (f) N. G. Andersen, S. P. Maddaford, B. A. Keay, *J. Org. Chem*., 1996, 61, 9556; (g) H. Kurreck, M. Huber, *Angew. Chem. Int. Ed. Engl*., 1995, 34, 849.

[6] (a) R. Taylor, Electrophilic Aromatic Substitution; Wiley: Chichester, UK, 1990; (b) J. Miller, Aromatic Nucleophilic Substitution; Elsevier: Amsterdam, 1968.

[7] V. Snieckus, *Chem. Rev.* 1990, 90, 879.

[8] de Meijere, A.; Diederich, F. Metal-Catalyzed Cross-Coupling reactions; Wiley: Weinheim, 2004.

[9] (a) G. E. H. Elgemeie and F. A. Abdelaal, *Heterocycles***,** 1986, 24, 349. (b) G. E. H. Elgemeie and M. M. Ramiz, *Phosphorus Sulfur,* 1989, 46, 95; (c) G. E. H. Elgemeie, H. A. Elfahham and H. Nabey, *Sulfur Lett.,* 1989, 9; (d) A. ***C.*** Cope and K. E. Hoyle, *J. Org. Chem.,* 1941, 63, 733.

[10] (a) L. Rong, H. Han, H. Jiang, S. Tu, *Synth. Commun*., 2008, 38, 3530; (b) H. Han, F. Yang, H. Yao, *Synth. Commun*., 2007, *37*, 3767.

[11] R. Liangce, T. Shimin, X. Sheng, L. Lihua, Y. Shan,S. Yanhui, *Res. Chem. Intermed*., 2012, 38, 1647.

[12] S. L. Cui, X. F. Lin, Y. G. Wang, *J. Org. Chem*., 2005, 70, 2866.

[13] J. Wang, Q. Li, C. Qi, Y. Liu, Z. Ge,R. Li, *Org. Biomol. Chem.*, 2010, 8, 4240.

[14] (a) V. Raghukumar, P. Murugan, V. T. Ramakrishnan, *Synth. Commun*., 2001, 31, 3497; (b) P. J. Victory, J. I. Borrell, A. Vidal-Ferran, *Heterocycles,* 1993, 36, 769; (c) P. Victory, J. I. Borrel, A. Vidal-Ferran, C. Seoane, J. L. Soto, *Tetrahedron Lett*., 1991, 32, 5375.

[15] B. Leroy, I. E. Markó, *Tetrahedron Lett.,* 2001, 42, 8685.

[16] S. Vidal, *Synlett.*, 2001, 1194.

[17] M. D. Carrigan, D. Sarapa, R. C. Smith, L. C. Wieland, R. S. Mohan, *J. Org. Chem.*, 2002, 67, 1027.

[18] M. V. Reddy, S. D. Dindulkar, Y. T. Jeong, *Tetrahedron Lett.,* 2011, 52, 4764.

[19] S. Antoniotti, *Synlett.,* 2003, 1566.

[20] R. Ramachandran, S. Jayanthi, Y. T. Jeong, *Tetrahedron.,* 2012, 68, 363.

[21] M. D. Carrigan, K. J. Eash, M. C. Oswald, R. S. Mohan, *Tetrahedron Lett.*, 2001, 42, 8133.

[22] L. Wu, W. Ma, L. Yang, F. Yan, *Asian J. Chem.,* 2010, 22, 6053.

[23] R. Breslow, *Acc. Chem. Res.,* 1980, 13, 170.

[24] D. Klemm, B. Heublein, H. P. Fink, A. Bohn, *Angew. Chem., Int. Ed.,* 2005**,** 44, 3358.

Microwave Assisted Synthesis of Pyrimidine Carboxamide Catalyzed by Ruthenium Chloride and their Antioxidant Studies

K. Venkatesan
Asst. Professor, CVR College of Engineering/H&S Department (Chemistry), Hyderabad, India
Email: venkippk@gmail.com

Abstract: **A systematic and simple method for the preparation of pyrimidinone compound utilizing RuCl3.2H2O catalyst under traditional and microwave method. The preparation of dihydro pyrimidinone utilizing ruthenium chloride dihydrate had generated lots of interest which includes easy work up, less reaction period and better yields under the usage of CH_3CN as a solvent. The structures of the new substances have been affirmed throgh FT-IR, ^{13}C NMR, ^{1}H NMR and mass spectra. All the new substances were screened for antioxidant nature.**

Index Terms: **Ruthenium chloride, Antioxidant, Microwave, Dihydropyrimidine**

I. Introduction

The multicomponent single step reactions (MCRs) are the most used procedure in medicinal chemistry and organic synthesis. Nitrogen based compounds provides huge range of bio applications. Due to the presence of nitrogen atom it contains a lone pair electron which acts as donor group for building supramolecular blocks. MCRs are important in the field of organic synthesis, that is extensively used to prepare dissimilar target molecules in single step reaction, and in the usage of three or greater number of initial substances. In 1893 Biginelli has describe the new route for the preparation of DHPMs via a simple single step condensation reaction of ethyl acetoacetate, urea and benzaldehyde [1]. The availability is restricted for the natural products which provide interesting goals for total synthesis [2]. The DHPM is the main structure in synthesis of various pharmacological and medicinally used agents like antiviral [3], antibacterial [4], antihypertensive agents [5], antitumor [6], neuropeptic agents [7], antagonists [8], α-1a-antagonists [9] anti-inflammatory and Ca channel blockers [10]. Further, DHPM ring present in alkaloid batzelladine hinder the binding of HIV protein gp-120 to human CD4 cells and the possibility of new substances prepared for AIDS treatment [11-12]. Hence, synthesis of DHPMs shows continuous interest and attraction to organic chemists.

Recent report reveals that mortal kinesin Eg5, plays a crucial part in cellular division by organizing the bipolar group, it has been checked the consideration of drug for the advancement of cancer therapy. Monastrol, the first Biginelli compound, exhibit excellent anticancer activity. The dihyropyrimidinones derived from natural aquatic sources such as Batzelladine A, B [13] is the first low M.Wt products occurs naturally it shows good anti-HIV property and hence DPHM were examined as powerful molecules in AIDS treatment.

Biginelli reaction was carried out by mixing active 1,3-dicarbonyl, different substituted aldehydes, and thiourea or urea is combined with different catalysts like $ZrCl_4$ [14], $Cu(OTf)_2$ [15], AcOH [16], $CdCl_2$[17], Ionic liquids [18], SiO_2/H_2SO_4[19], ion-exchange resin[20], $La(OTf)_3$ [21], LiBr[22],p-TSA[23], $(NH_4)_2Ce(NO_3)_6$ [24], $MgBr_2$[25], $InBr_3$ [26], ultrasound irradiation[27] microwave[28] and solvent-free conditions [29], $ZnCl_2$/TBAB [30]. $Co(NO_3)_2.6H_2O$ [31], $Mn(OAc)_3$ [32]. Microwave reactions have good interest in the last two decades in synthetic organic chemistry because of their low response times and excessive yield and more selectivity.

TABLE I.
Experimental Results And Physical Data Of Arylpyrimidine-5-Carboxamide Derivatives

Compound	R	R_1	X	Reaction time (min.)		Yield (%)[a]		m.p. (°C)
				MW	Con.	MW	Con.	
4a	H	Phenyl	O	16	430	90	78	225-228
4b	H	Phenyl	S	17	440	88	81	214-217
4c	H	3-OEt-4-OH-Ph	O	18	460	87	78	254-256
4d	H	3-OEt-4-OH-Ph	S	21	440	82	76	243-245
4e	H	2,4-Cl-Ph	O	21	460	83	77	207-209
4f	H	2,4-Cl-Ph	S	20	470	83	74	189-191
4g	H	2-C_4H_3S	O	17	400	84	78	191-193
4h	H	2-C_4H_3S	S	17	400	81	73	202-204
4i	H	Ph-4-OH-3-OMe	O	18	410	87	82	231-233
4j	4-Cl	2,4-Cl-Ph	O	16	450	86	80	206-208

A. Experimental procedure

General: All the chemical substances had been bought from SD Fine, Aldrich and Qualigens and utilized without cleaning. The proton NMR spectra was acquired from spectrometer BRUKER AV-400 MHz with DMSO-d6 as the solvent utilizing TMS as the inner standard. The MW experiment was conducted using household MW oven with a turntable was used and the operating frequency was 2200 MHz. Infrared (IR) spectra was recorded at room temperature with potassium bromide (KBr) pellets utilizing

Avatar (330) instrument with DTGS indicator. Mass spectra was obtained from JEOL 1400 HRMS spectrometer. Melting point was obtained using an open capillary tube and the results were uncorrected.

Procedure for the synthesis of pyrimidine-5-carboxamide (**4a-j**):

B. Conventional Method

In a 100 ml RB flask blend of acetoaetanilide (1 milli mol), aldehyde (1 milli mol), thiourea or urea (1.5 milli mol), $RuCl_3.2H_2O$ (5 mole %) and 30 mL CH_3CN have been refluxed according to time interim said in Table 3. The reaction fulfillment was appeared by TLC. After completion, the reaction blend was putting into a pulverized ice, mixed for 25-30 min. The solid product obtained was filtered by using funnel, washed with large amount water and then recrystallization was done using hot ethanol to get pure products 4a-j.

C. Microwave Irradiation

In a small beaker acetoaetanilide (1 milli mol), aldehyde (1 milli mol), thiourea or urea (1.4 milli mol), $RuCl_3.2H_2O$ (5 mol%) and acetonitrile (4 mL) have been taken and the reaction blend were subjected to MW condition at an interim of 5 min at 145 W for around 16-22 min; various time intervals are displayed in Table 3. The reaction completion was observed by using TLC. After completion, the mixture was poured into ice, stirred thoroughly and the separated solid was filtered, air dried and recrystallization was done using hot ethanol to get pure products 4a-j. The physical properties of the prepared compounds are displayed in Table I.

Compound (**4c**): mp. 254-257 ºC; IR (KBr) νmax (cm^{-1}): 3540, 3257, 2975, 2928, 1704, 1663, 1606, 1593, 1584, 1493, 1434, 1412, 1372, 1334, 1284, 1225, 1153, 1120, 1094, 1062, 1040; ^{1}H NMR (400 MHz, ppm, DMSO- d_6,) δ_H 1.18–1.32 (m, CH_3, 3H) , 2.48 (s, CH_3, 3H), 3.77–3.84 (m, OCH_2, 2H), 5.23 (s, CH, 1H), 6.35–7.29 (m, Ph-H, 8H), 7.53 (s, NH, 1H), 8.85 (s, NH & OH, 2H), 9.13 (s, CONH, 1H); ^{13}C NMR (125.757 MHz, ppm, DMSO-d_6,) δ_C = 164.5, 162.3, 151.7, 152.5, 147.8, 146.7, 146.5, 146.4, 143.1, 142.0, 135.9, 131.2, 128.7, 127.3, 126.0, 125.5, 119.3, 118.0, 115.7, 115.5, 112.6, 102.5, 64.2, 64.1, 63.8, 53.1, 37.8, 15.2, 14.9; HRMS: m/z [M^+] calc. 367.1530; obtained: 367.1533.

Compound (**4d**): mp. 243-246 ºC; IR (KBr) νmax (cm^{-1}): 3347, 3190, 2976, 2931, 1670, 1624, 1596, 1571, 1511, 1466, 1434, 1400, 1282, 1234, 1216, 1189, 1148, 1120, 1107, 1084, 1037, 1011; ^{1}H NMR (400 MHz, ppm, DMSO-d_6), δH 1.17–1.34 (m, CH_3, 3H), 2.46 (s, CH_3, 3H), 3.54–3.94 (m, OCH_2, 2H), 5.24 (s, CH, 1H), 6.38–7.26 (m, Ph-H, 8H), 8.88–8.94 (split peak, NH & OH, 2H), 9.51 (s, NH, 1H),10.28 (s, CONH, 1H); HRMS: m/z [M^+] calc. 383.1306; obtained: 383.1304.

Compound (**4e**): mp. 207-210 ºC; IR (KBr) νmax (cm^{-1}): 3398, 3264, 3167, 3084, 3005, 1669, 1628,1593, 1563, 1524, 1498, 1476, 1435, 1380, 1334, 1236, 1176, 1140, 1101, 1073, 1043 cm^{-1}; ^{1}H NMR (400 MHz, DMSO-d6, ppm), δH 2.02 (s, CH_3, 3H), 5.72 (d, J = 2.3 Hz, CH, 1H), 7.02 (t, J = 7.27 Hz, Ph-H, 1H), 7.26 (t, J = 8.2 Hz, Ph-H, 2H), 7.37 (d, J = 8.5 Hz, Ph-H, 1H), 7.51 (d, J = 7.4 Hz, Ph-H, 3H), 7.56 (d, J = 2.6 Hz, m-Ph-H, 1H), 9.36 (s, 1H, NH), 9.86 (s, NH, 1H), 10.11 (s, CONH, 1H); ^{13}C NMR (100.612 MHz, ppm, DMSO-d_6,), δC 173.1, 165.3, 137.3, 136.7, 134.0, 132.0, 131.1, 130.8, 128.7, 127.0, 122.3, 118.4, 105.3, 51.4, 15.2; HRMS: m/z [M^+] calc. 375.0541; obtained: 375.0531.

Compound (**4f**): mp. 189-192 ºC; IR (KBr) νmax (cm^{-1}): 3396, 3275, 3086, 2361, 2340, 1671, 1653, 1628, 1597, 1561, 1541, 1521, 1496, 1471, 1438, 1329, 1233,1202, 1181, 1143, 1103, 1076, 1044; ^{1}H NMR (400 MHz, DMSO-d_6, ppm), δ_H 2.05 (s, CH_3, 3H), 5.75 (d, J = 2.5 Hz, CH, 1H), 7.02 (t, J = 7.26 Hz, p-Ph-H, 1H), 7.24 (t, J = 8.1 Hz, m, m'-Ph-H, 2H), 7.39 (d, J = 8.7 Hz, o'- Ph-H, 1H), 7.51 (d, J = 8.8 Hz, o, o' & m'-Ph-H, 3H), 7.54 (d, J = 2.0 Hz, m-Ph-H, 1H), 9.35 (s, NH, 1H), 9.87 (s, NH, 1H), 10.12 (s, CONH, 1H); HRMS (EI): m/z [M+] calc. 391.0313; obtained: 391.0315.

Compound (**4g**): mp. 193-196 ºC; IR (KBr) νmax (cm^{-1}): 3248, 2360, 1698, 1641, 1590, 1508, 1491, 1451, 1398, 1305, 1287, 1252, 1209, 1146, 1088, 1038, 1010; ^{1}H NMR (400 MHz, DMSO-d_6, ppm), δ_H 2.06 (s, CH_3, 3H), 5.58 (d, J = 3.0 Hz, CH, 1H), 6.91–7.37 (m, Ph-H, 6H),7.57 (d, J = 8.0 Hz, o, o'-Ph-H, 2H), 7.81 (s, NH, 1H), 8.84 (s, NH, 1H), 9.56 (s, CONH, 1H); HRMS (EI): m/z [M^+] calc. 313.0884; obtained: 313.0882.

Compound (**4h**): mp. 202-205 ºC; IR (KBr) νmax cm^{-1}): 3367, 3283, 1677, 1632, 1565, 1547, 1523, 1498, 1476, 1439, 1361, 1326, 1232, 1188, 1116, 1074, 1034; ^{1}H NMR (400 MHz, DMSO-d_6, ppm), δ_H 2.13 (s, CH_3, 3H), 5.64 (d, J = 3.2 Hz, CH, 1H), 6.96–7.68 (m, Ph-H, 8H), 9.63 (s, NH, 1H), 9.72 (s, NH, 1H), 10.11 (s, CONH, 1H),; ^{13}C NMR (100.614 MHz, DMSO-d_6, ppm), δ_C 173.1, 163.5, 147.9, 137.9, 138.6, 127.5, 125.7, 125.6, 123.2, 122.3, 118.7, 106.0, 50.3, 16.5; HRMS: m/z [M^+] calc. 329.0658; obtained: 329.0656.

Compound (**4i**): mp. 231-234 ºC; IR (KBr) νmax (cm^{-1}): 3410, 3284, 2363, 2340, 1683, 1652, 1626, 1597, 1538, 1521, 1486, 1442, 1384, 1330, 1260, 1241, 1163, 1123, 1073, 1032; ^{1}H NMR (300 MHz, DMSO-d_6, ppm), δ_H 2.07 (s, CH_3, 3H), 3.65 (s, OCH_3, 3H), 5.33 (s, CH, 1H), 6.70–7.55 (m, NH & Ph-H, 9H), 8.66 (s, NH, 1H), 8.92 (s, OH, 1H), 9.51 (s, CONH, 1H); ^{13}C NMR (100.614 MHz, DMSO-d_6, ppm), δ_C 164.4, 149.5, 145.3, 144.8, 137.1, 136.8, 135.1, 125.4, 121.0, 118.5, 117.4, 112.2, 110.7, 103.5, 57.4, 54.7, 19.9; HRMS: m/z [M^+] calc. 353.1366; obtained: 353.1363.

Compound (**4j**): mp. 206-209 ºC; IR (KBr) νmax (cm^{-1}): 3396, 3192, 1672, 1633,1598, 1563, 1532, 1467, 1438, 1382, 1233, 1201, 1101, 1043; ^{1}H NMR (400 MHz, DMSO-d_6, ppm), δ_H 2.02 (s, CH_3, 3H) 5.73 (d, J = 2.2 Hz, CH, 1H), 7.26–7.31 (split peak, o' & m'-Ph-H, 2H), 7.43 (d, *J* = 2.1 Hz, m, m'-Ph-H,2H),7.51–7.53 (m, o, o' & m-Ph-H, 3H) 7.57 (s, NH, 1H),8.88 (s, NH, 1H), 9.81 (s, CONH, 1H); HRMS: m/z [M^+] calc. 409.0151; obtained: 409.0141.

D. Screening of Antioxidant Activity

The free radical-scavenging property of prepared derivatives was predicted utilizing the standard ascorbic acid by DPPH radical scavenging method. This

investigation is generally in view of the measurement of the consolidating ability of products towards the radical DPPH.

The extinction of absorbance of buyable radical is estimated using spectrophotometer at 517 nm in a dimethyl sulfoxide (DMSO) solution use of UV/Vis-spectrophotometer underneath thermostatic conditions at 25 ºC. DPPH has a single electron and it has a descent absorption band observed at 517 nm. At the point when the odd electron ends up matched, the absorption band diminishes respectively and the number of atoms becomes paired.

The change in absorbance has been widely used to test the potential of synthesized compounds to act as a radical scavenger. Therefore, faster is the lowering of absorbance; greater is the antioxidant property of the substance.

In a test tube 3.0 mL solution of a newly prepared DPPH of 6.02 x 10^{-5} Molar solution in dimethyl sulfoxide and 100 micro litre of a DMSO solution of each synthesized product was added. After this the test sample was kept at room temperature for 30 min in dull condition and the absorbance of the solution was measured at 517 nm. The control has all reagents except prepared compound. The analysis was done thrice and the average absorbance values are considered. The DPPH scavenging property was expressed in hinderance rate (I %) as depicted by Sokmen *et al.,* 2006[33].

Inhibition percentage (%) = [(control Optical Density– sample Optical Density)/control Optical Density] X 100.

II. Results and Discussion

The one pot three component reaction for the synthesis of 4-aryl pyrimidine-5-carboxamide via reaction between substituted benzaldehyde, actoacetanilide, urea or thiourea using ruthenium(III) chloride dihydrate $RuCl_3.2H_2O$ under traditional heating and microwave irradiation methods were reported (Scheme 1). $RuCl_3.2H_2O$ is a powerful catalyst for the preparation of DHPM, when compared with other catalysts like Lewis acid which are represented in the old report.

SCHEME I
SYNTHETIC PROTOCOL OF COMPOUND 4A-J

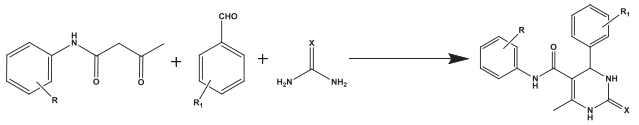

To enhance the reaction condition, the condensation reaction was chosen using acetoacetanilides, benzaldehyde and urea using $RuCl_3.2H_2O$ under traditional and microwave method. The different solvent systems like dichloromethane, chloroform, methanol, ethanol, acetonitrile and different synergist mole percent of catalyst was additionally analyzed and the outcomes were exhibited in Table II & III.

Table one reveals that polar protic solvents like ethanol, methanol and acetonitrile gave high yields. In comparison the nonpolar solvent such as DCM, $CHCl_3$. Results obtained indicate that CH_3CN is a suitable solvent for this conversion.

TABLE II.
EFFECT OF SOLVENT SYSTEM

S. No	Solvents	mol %	Time (min.)	Yield (%)
1	$CHCl_3$	5	25	33
2	DCM	5	25	29
3	C_2H_5OH	5	16	75
4	CH_3OH	5	16	73
5	CH_3CN	5	15	91

The results indicate these reactions proceeded more effectively under microwave condition when compared with that of traditional heating. Further, impact of loading of catalyst was examined. The viable catalyst mole percent is seen to be 5 mol %, while expanding the mole level of catalyst did not display any improvement in the yield rate. After enhancement, the best reaction condition was utilized for preparation of 5-carboxamide dihydropyrimidine utilizing various aldehydes, thiourea or urea and different acetoacetanilide under customary warming and microwave method to produce dihydropyrimidinone substances by $RuCl_3.2H_2O$ as a catalyst. (Table I).

TABLE III.
EFFECT OF CATALYSTS LOADING

S. No	Catalyst	mol %	Reaction Period (min.)	Yield (%)
1	$RuCl_3.2H_2O$	5	15	91
2	$RuCl_3.2H_2O$	10	15	91
3	$RuCl_3.2H_2O$	15	15	91

The catalyst $RuCl_3.2H_2O$ has exceptional solvency in water and is effectively evacuated by washing with water. All the prepared substances were described through spectroscopic techniques.

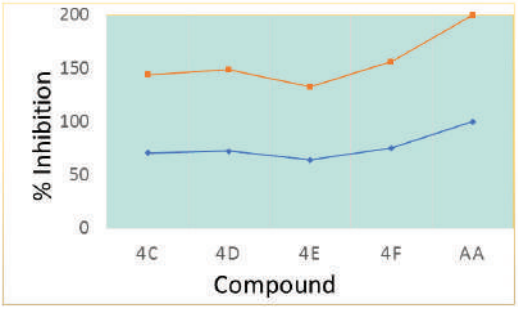

Figure 1. Comparison of antioxidant property of compound 4a-j.

Antioxidant Activity

Antioxidant studies of all the prepared compounds 4(a-j) were accomplished using radical scavenging technique. The antioxidant reports exhibited that compound 4d, 4c, 4e and 4f show acceptable radical scavenging property when compared to that of standard ascorbic acid (100%), while that of compounds 4a, 4b, 4g, 4h, and 4i did not indicate

antioxidant property even at 100 µg/mL and one hour of incubator time.

Radical scavenging properties of the new substances 4(**a-j**) and ascorbic acid at 100 µg/mL after 30 minutes and one hour of incubatory interval in dark at 25 °C are appeared in Figure. 1.

TABLE IV.

ANTIOXIDANT PROPERTY OF SUBSTANCES **4A-J** UTILIZING FREE RADICAL SCAVENGING TECHNIQUE

Incubation for 30 min			Incubation for one hour		
Compound	Absorbance	% Antioxidant activity	Compound.	Absorbance	% Antioxidant activity
4c	2.02	70.68	4c	1.93	73.47
4d	1.98	72.45	4d	1.75	76.13
4e	2.59	64.02	4e	2.26	68.81
4f	1.67	75.34	4f	1.43	80.77
Control	7.00				

The radical scavenging property for dimethyl sulfoxide solutions of new substances **4a-j** are represented in (Table 4) compared with standard ascorbic acid.

III. CONCLUSIONS

Easy and greener technique for the preparation of pyrimidine-5-carboxamide compounds via single step three substance cyclisation reaction of various substituted acetoacetanilides, thiourea or urea and different aldehydes under traditional heating and MW method by utilizing $RuCl_3.2H_2O$ catalyst. The main benefits of this procedure are moderate reaction conditions, shorter response times, easy work-up and excessive yields. The prepared substances **4a-j** have been monitored for antioxidant studies using radical scavenging technique. The products 4c, 4d, 4e and 4f showed acceptable antioxidant property when compared to that of other synthesized compounds.

REFERENCES

[1] P. Biginelli, "The condensation reaction described by Biginelli'' Gazz. Chim. Ital., 23, 1983, pp. 360-416.

[2] J. Kim, C. Park, W. So, M. Jo, M. Seo and Y. Kim, "A novel 3,4-dihydropyrimidin-2(1H)-one: HIV-1 replication inhibitors with improved metabolic stability" Bioorg & Med. Chem. Lett, 22, No. 7, pp. 2522-2526.Bioorg. Med. Chem. Lett. 22, 2012, pp. 2522-2526.

[3] C. O. Kappe, "Recent advances in the Biginelli dihydropyrimidine synthesis. New tricks from an old dog" Acc. Chem. Res, 33, 2000, pp. 879-888.

[4] M.J. Lusch and J.A. Tallarico, "Demonstration of the feasibility of a direct solid-phase split-pool Biginelli synthesis of 3,4-dihydropyrimidinones" Org. Lett, 6, 2004, pp. 3237-3240.

[5] M. Mohammad, A. Mymoona, H. Asif, M. Akranth and H. Rashiduddin, "Anti-inflammatory and antimicrobial activityof 4,5-dihydropyrimidine-5-carbonitrile derivatives: their synthesis and spectral elucidation" Acta. Pol. Pharm. Drug. Res, 69, 2012, pp. 1077-1085.

[6] R.K. Yadlapalli, O.P. Chourasia, K. Vemuri, M. Sritharan, and R.S. Perali, "Synthesis and in vitro anticancer and antitubercular activity of diarylpyrazole ligated dihydropyrimidines possessing lipophilic carbamoyl group" Bioorg. Med. Chem. Lett, 22, 2012, pp. 2708-2711.

[7] L. Zhu, P. Cheng, C. Sheng, C. Zhuang, W. Guo, Y. Zhang, G. Dong, Z. Wang, Z. Miao and W. Zhang, "Synthesis and biological evaluation of novel homocamptothecins conjugating with dihydropyrimidine derivatives as potent topoisomerase I inhibitors" Arch. Pharm, 344, 2011, pp. 726-734.

[8] N. Bhushan, S. Vasant and R. Sanjeev, "Synthesis of novel dihydropyrimidin-2(1H)-ones derivatives using lipase and their antimicrobial activity" Curr. Chem. Lett, 1, 2012, pp. 59-68.

[9] A. D. Patil, A. J. Freyer, P. B. Taylor, B. Carte, and D.J. Faulkner, "Batzelladines F−I, novel alkaloids from the sponge batzella sp.: Inducers of p56lck-CD4 dissociation" J. Org. Chem, 62, 1997, pp. 1814-1819.

[10] S. Z. İnci, S. Selma, C. Semra and E. Kevser, "Synthesis of 4-aryl-3,4-dihydropyrimidin-2(1H)-thione derivatives as potential calcium channel blockers" Bioorg. Med. Chem, 14, 2006, pp. 8582-8589.

[11] B. B. Snider, J. Chen, A. D. Patil and A. Freyer, "Synthesis of the tricyclic portions of batzelladines A, B and D. Revision of the stereochemistry of batzelladines A and D" Tetrahedron Lett, 37, 1996, pp. 6977-6980.

[12] A. V. Rama Rao, M. Gujar and J. Vasudevan, "An enantiospecific synthesis of the tricyclicguanidine segment of the anti-HIV marine alkaloid batzelladine" J. Chem. Soc. Chem. Commun, 1995, 1995, pp. 1369-1370.

[13] A. D. Patil, N. V. Kumar, D. Truneh, J. Faulkner, B. Carte, A. L. Breen, R. P. Hertzberg, R. K. Johnson, J. W. Westley and B.V. Potts, "Novel alkaloids from the sponge batzella sp.: Inhibitors of HIV gp120-human CD4 binding" J. Org. Chem, 60, 1995, pp. 1182-1188.

[14] V. A. Mamedov, L. V. Mustakimova, A. T. Gubaidullin,S. V. Vdovina, I. V. Litvinov and V. S. Reznik "Dichloroacetylaroylmethanes as two-carbon synthons in the Biginelli reaction" Chem. Heterocycl. Comp, 42, 2006, pp. 1229-1232.

[15] C. V. Reddy, M. Mahesh, T. R. Babu and V. N. Reddy, "Zirconium(IV) chloride catalyzed one-pot synthesis of 3,4-dihydropyrimidin-2(1H)-ones" Tetrahedron Lett, 43, 2002, pp. 2657-2659

[16] A. S. Prabhakar, G. K. Dewkar and A. Sudalai, "Cu(OTf)2: a reusable catalyst for high-yield synthesis of 3,4-dihydropyrimidin-2(1H)-ones" Tetrahedron Lett, 44, 2003, pp. 3305-3308.

[17] Y. Ma, C. Qian, L. Wang and M. Yang, "Lanthanide triflate catalyzed Biginelli reaction. One-pot synthesis of dihydropyrimidinones under solvent-free conditions" J. Org. Chem, 65, 2000, pp. 3864-3868.

[18] C. O. Kappe, D. Kumar, and R. S. Varma, "Microwave assisted high speed parallel synthesis of 4-Aryl-3,4-dihydropyrimidin-2(1H)-ones using a solventless Biginelli condensation protocol" Synthesis, 1999, 1999, pp. 1799-1803.

[19] L. Wu, F. Yan and C. Yang, "Silica sulfuric acid promoted one-pot synthesis of benzo[4,5]imidazo[1,2-a]pyrimidine derivatives under solvent-free conditions" Bull. Chem. Soc. Ethiop, 24, 2010, pp. 417-423.

[20] J. Peng and Y. Deng, "Ionic liquids catalyzed Biginelli reaction under solvent-free conditions" Tetrahedron Lett, 42, 2001, pp. 5917-5919.

[21] J. C. Bussolari and P. A. McDonnell, "A new substrate for the Biginelli cyclocondensation: Direct preparation of 5-unsubstituted 3,4-dihydropyrimidin-2(1H)-ones from a β-keto carboxylic Acid" J. Org. Chem, 65, 2000, pp. 6777-6779.

[22] G. Maiti, P. Kundu and C. Guin, "One-pot synthesis of dihydropyrimidinones catalysed by lithium bromide: an

improved procedure for the Biginelli reaction" Tetrahedron Lett, 44, 2003, pp. 2757-2758.
[23] I. T. Phucho, S. Tumtin, A. Nongpiur, R. Nongrum and R.L. Nongkhlaw, "Microwave assisted synthesis of 6-methyl-1,2,3,4-tetrahydro-N-aryl-2-oxo-4-arylpyrimidine-5-carboxamide and 3, 4-dihydropyrimidin- 2(1H)-ones under solvent free conditions" J. Chem. Pharm. Res, 2, 2010, pp. 214-222.
[24] J. S. Yadav, K. B. Reddy, K. S. Raj and A. R. Prasad, "Ultrasound-accelerated synthesis of 3,4-dihydropyrimidin-2(1H)-ones with ceric ammonium nitrate" J. Chem. Soc. Perkin Trans, 2001, 2001, 1939-1941.
[25] H. Salehi and Q. X. Guo, "A facile and efficient one-Pot synthesis of dihydropyrimidinones catalyzed by magnesium bromide under solvent-free conditions" Synn. Comm, 34, 2004, pp. 171-179.
[26] N. Y. Fu, Y. F. Yuan, Z. Cao, J. T. Wang and C. Peppe, "Indium(III) bromide-catalyzed preparation of dihydropyrimidinones: improved protocol conditions for the Biginelli reaction" Tetrahedron, 58, 2002, pp. 4801-4807.
[27] J. T. Li, J. F. Han, J. H. Yang and T. S. Li, "An efficient synthesis of 3,4-dihydropyrimidin-2-ones catalyzed by NH_2SO_3H under ultrasound irradiation" Ultrason. Sonochem, 10, 2003, pp. 119-122.
[28] J. S. Yadav, B. V. S. Reddy, E. J. Reddy and T. Ramalingam, "Microwave-assisted efficient synthesis of dihydro pyrimidines: improved high yielding protocol for the Biginelli reaction" J. Chem. Res, 2000, 2000, 354-355.
[29] K. R. Reddy, C. V. Reddy, M. Mahesh, P. V. K. Raju, "New environmentally friendly solvent free synthesis of dihydropyrimidinones catalysed by N-butyl-N,N-dimethyl-α-phenylethylammonium bromide" Tetrahedron Lett, 44, 2003, pp. 8173-8175
[30] O. Surendranatha Reddy, Ch. Venkata Suryanarayana, N. Sharmila, G. V. Ramana, V. Anuradha and B. Hari Babu, "Synthesis and Cytotoxic Evaluation for Some New Dihydropyrimidinone Derivatives for Anticancer Activity" Lett. Drug. Des. Discov, 10, 2016, pp. 699-705.
[31] M. Nasr-Esfahani, M. Montazerozohori, M. Aghel-Mirrezaee and H. Kashi, "Efficient and green catalytic synthesis of dihydropyrimidinone (thione) derivatives using cobalt nitrate in solvent-free conditions" J. Chil. Chem. Soc, 59, 2014, pp. 2311-2314.
[32] K. A. Kumar, M. Kasthuraiah, C. S. Reddy and C. D. Reddy, "$Mn(OAc)_3 \cdot 2H_2O$-mediated three-component, one-pot, condensation reaction: an efficient synthesis of 4-aryl-substituted 3,4-dihydropyrimidin-2-ones" Tetrahedron Lett, 42, 2001, pp. 7873-7875.
[33] B. Tepe, M. Sokmen, H. A. Akpulat and Sokmen. "Screening of the antioxidant potentials of six Salvia species from Turkey" Food Chem, 95, 2006, pp. 200-204.

In the next issue (Vol 15, December, 2018)

1.	**An Efficient and Automated Classification Scheme for Diagnosing Fatty Liver Disorder using Ultrasonic Images**	*A. Rajesh*
2.	**Design and Structural Analysis of Scissor Jack using ANSYS Workbench**	*C. Sai Kiran* *J. Sruthi*
3.	**The Performance of Solar Powered Agriculture Sprayer: Design & Analysis**	*B.Sravya Reddy* *N.Ankitha* *Abhinay Sai Kothakonda*

Template for the Preparation of Papers for Publication in CVR Journal of Science and Technology

First A. Author[1] and Second B. Author[2]
[1]Designation, Name of Institution/Department, City, Country
Email: first.author@hostname1.org
[2]Designation, Name of Institution/Department, City, Country
Email: second.author@hostname2.org

Abstract: **These instructions give you basic guidelines for preparing camera-ready papers for CVR College journal Publications. Your cooperation in this matter will help in producing a high quality journal.**

Index Terms: **first term, second term, third term, fourth term, fifth term, sixth term**

I. Introduction

Your goal is to simulate the usual appearance of papers in a Journal Publication of the CVR College. We are requesting that you follow these guidelines as closely as possible. It should be original work. Format must be done as per the template specified. Diagrams with good clarity with relevant reference within the text are to be given. References are to be cited within the body of the paper. Number of pages must not be less than five, but not more than eight.

A. Full-Sized Camera-Ready (CR) Copy

Prepare your CR paper in full-size format, on A4 paper (210 x 297 mm, 8.27 x 11.69 in). No header or footer, no page number.

Type sizes and typefaces: Follow the type sizes specified in Table I. As an aid in gauging type size, 1 point is about 0.35 mm. The size of the lowercase letter "j" will give the point size. Times New Roman has to be the font for main text. Paper should be single spaced.

Margins: Top and Bottom = 24.9mm (0.98 in), Left and Right = 16 mm (0.63 in). The column width is 86mm (3.39 in). The space between the two columns is 6mm (0.24 in). Paragraph indentation is 3.7 mm (0.15 in).

Left- and right-justify your columns. Use tables and figures to adjust column length. On the last page of your paper, adjust the lengths of the columns so that they are equal. Use automatic hyphenation and check spelling. Digitize or paste down figures.

For the Title use 24-point Times New Roman font, an initial capital letter for each word. Its paragraph description should be set so that the line spacing is single with 6-point spacing before and 6-point spacing after. Use two additional line spacings of 10 points before the beginning of the double column section, as shown above.

Each major section begins with a Heading in 10 point Times New Roman font centered within the column and numbered using Roman numerals (except for ACKNOWLEDGEMENT and REFERENCES), followed by a period, two spaces, and the title using an initial capital letter for each word. The remaining letters are in SMALL CAPITALS (8 point). The paragraph description of the section heading line should be set for 12 points before and 6 points after.

TABLE I.
TYPE SIZES FOR CAMERA-READY PAPERS

Type size (pts.)	Appearance		
	Regular	Bold	Italic
6	Table caption, table superscripts		
8	Tables, table names, f irst letters in table captions, figure captions, footnotes, text subscripts, and superscripts		
9	References, authors' biographies	Abstra ct	
10	Section titles ,Authors' affiliations, main text, equations, first letters in section titles		Subheading
11	Authors' names		
24	Paper title		

Subheadings should be 10 point, italic, left justified, and numbered with letters (A, B, …), followed by a period, two spaces, and the title using an initial capital letter for each word. The paragraph description of the subheading line should be set for 6 points before and 3 points after.

For main text, paragraph spacing should be single spaced, no space between paragraphs. Paragraph indentation should be 3.7mm/0.21in, but no indentation for abstract & index terms.

II. Helpful Hints

A. Figures and Tables

Position figures and tables at the tops and bottoms of columns. Avoid placing them in the middle of columns. Large figures and tables may span across both columns. Leave sufficient room between the figures/tables and the main text. Figure captions should be centered below the figures; table captions should be centered above. Avoid placing figures and tables before their first mention in the text. Use the abbreviation "Fig. 1," even at the beginning of a sentence.

To figure axis labels, use words rather than symbols. Do not label axes only with units. Do not label axes with a ratio

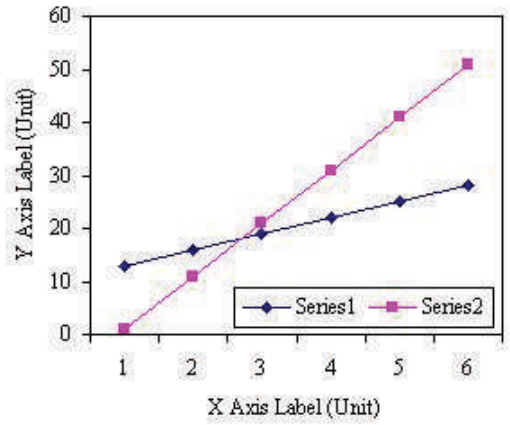

Figure 2. Note how the caption is centered in the column.

of quantities and units. Figure labels should be legible, about 9-point type.

Color figures will be appearing only in online publication. All figures will be black and white graphs in print publication.

B. References

Number citations consecutively in square brackets [1]. Punctuation follows the bracket [2]. Use "Ref. [3]" or "Reference [3]" at the beginning of a sentence:

Give all authors' names; use "et al." if there are six authors or more. Papers that have not been published, even if they have been submitted for publication, should be cited as "unpublished" [4]. Papers that have been accepted for publication should be cited as "in press" [5]. In a paper title, capitalize the first word and all other words except for conjunctions, prepositions less than seven letters, and prepositional phrases. Good number of references must be given.

C. Footnotes

Number footnotes separately in superscripts [1, 2, …]. Place the actual footnote at the bottom of the column in which it was cited, as in this column. See first page footnote as an example.

D. Abbreviations and Acronyms

Define abbreviations and acronyms the first time they are used in the text, even after they have been defined in the abstract. Do not use abbreviations in the title unless they are unavoidable.

E. Equations

Equations should be left justified in the column. The paragraph description of the line containing the equation should be set for 6 points before and 6 points after. Number equations consecutively with equation numbers in parentheses flush with the right margin, as in (1). Italicize Roman symbols for quantities and variables, but not Greek symbols. Punctuate equations with commas or periods when they are part of a sentence, as in

$$a + b = c \ . \qquad (1)$$

Symbols in your equation should be defined before the equation appears or immediately following. Use "(1)," not "Eq. (1)" or "equation (1)," except at the beginning of a sentence: "Equation (1) is ..."

F. Other Recommendations

Use either SI (MKS) or CGS as primary units. (SI units are encouraged.) If your native language is not English, try to get a native English-speaking colleague to proofread your paper. Do not add page numbers.

III. Conclusions

The authors can conclude on the topic discussed and proposed, future enhancement of research work can also be briefed here.

References

[1] G. Eason, B. Noble, and I. N. Sneddon, "On certain integrals of Lipschitz-Hankel type involving products of Bessel functions," Phil. Trans. Roy. Soc. London, vol. A247, pp. 529–551, April 1955.

[2] J. Clerk Maxwell, *A Treatise on Electricity and Magnetism*, 3rd ed., vol. 2. Oxford: Clarendon, 1892, pp.68–73.

[3] I. S. Jacobs and C. P. Bean, "Fine particles, thin films and exchange anisotropy," in *Magnetism*, vol. III, G. T. Rado and H. Suhl, Eds. New York: Academic, 1963, pp. 271–350.

[4] K. Elissa, "Title of paper if known," unpublished.

[5] R. Nicole, "Title of paper with only first word capitalized", *J. Name Stand. Abbrev.*, in press.

[6] Y. Yorozu, M. Hirano, K. Oka, and Y. Tagawa, "Electron spectroscopy studies on magneto-optical media and plastic substrate interface," *IEEE Transl. J. Magn. Japan*, vol. 2, pp. 740–741, August 1987 [Digests 9th Annual Conf. Magnetics Japan, p. 301, 1982].

[7] M. Young, *The Technical Writer's Handbook*. Mill Valley, CA: University Science, 1989.

ABOUT THE COLLEGE

CVR College of Engineering (A UGC Autonomous Institution) was established in the year 2001, and its fourteenth batch of students graduated from the College. This college is on a roll with the recent ***NIRF*** *ranking consecutively for the II year, within the* ***top 3 colleges*** *in the state of* ***Telangana****, followed by record placements.*

The College was the ***first*** *college in Telangana that was promoted by NRI technology professionals resident in the US. The NRI promoters are associated with cutting-edge technologies of the computer and electronics industry. They also have strong associations with other leading NRI professionals working for world-renowned companies like IBM, Intel, Cisco, Facebook, AT&T, Google and Apple who have agreed to associate with the College with a vision and passion to make the College a state-of-the-art engineering institution.*

The college has many accomplishments and to name a few, it obtained ***NBA Tier 1 accreditation for all Seven UG Programs offered by the College, NAAC 'A' grade****,* ***UGC autonomous status****,* ***National Employability Award for*** *seventh year in a row and got a very high rating by several ranking agencies including the most recent Education World ranking of third best college in Telangana and Outlook magazine, rating CVR CE, one among the* ***top 100 colleges in the country.***

The college has been creating records year after year. With more than 90 companies visiting CVR and more than 600 placements for the 2017-18 academic year, it is the highest among the peer group of colleges. The highest offer is Rs. 24 Lakhs and close to 40 students got offers higher than Rs. 7 Lakhs. About 75 offers are higher than Rs. 5 Lakhs. With this, CVR becomes the leading college in entire Telangana in terms of the offers with higher salaries. CVR has made huge progress in a short span of time and is preferred by the students and parents during the EAMCET counseling this year and is among ***the top 3 colleges*** *in the state.*

In keeping with the current global emphasis on green and eco-friendly energy generation, 360kW Solar PV plant has been installed in the campus to meet the power requirements of the college to a significant extent.

CALL FOR PAPERS:

Papers in Engineering, Science and Management disciplines are invited for Publication in our Journal. Authors are requested to mail their contributions to Editor, CVR Journal of Science and Technology (Email Id: journal@cvr.ac.in).

Papers are to be written using a Standard Template, which may be obtained on request from the Editor. It is also available on the college website www.cvr.ac.in under In-House Journal.

CVR JOURNAL OF SCIENCE & TECHNOLOGY

CVR COLLEGE OF ENGINEERING

(UGC Autonomous- Affiliated to JNTU Hyderabad)
Mangalpalli (V), Ibrahimpatnam (M),
R.R. District, Telangana - 501510
http://cvr.ac.in